



# Geological Fieldwork 2022

## A Summary of Field Activities and Current Research



Ministry of  
Energy, Mines and  
Low Carbon Innovation

Paper 2023-01



Ministry of  
Energy, Mines and  
Low Carbon Innovation





Ministry of  
Energy, Mines and  
Low Carbon Innovation



# Geological Fieldwork 2022

A Summary of Field Activities and Current Research

Ministry of Energy, Mines and Low Carbon Innovation  
British Columbia Geological Survey

Paper 2023-01

# Ministry of Energy, Mines and Low Carbon Innovation Mines, Competitiveness, and Authorizations Division British Columbia Geological Survey

Recommended citation format for individual papers:

Schiarizza, P., and Friedman, R.M., 2023. U-Pb zircon dates for rhyolite and sandstone of Cadwallader terrane, lower Chilcotin River area, south-central British Columbia. In: Geological Fieldwork 2022, British Columbia Ministry of Energy, Mines and Low Carbon Innovation, British Columbia Geological Survey Paper 2023-01, pp. 65-84.

## Front Cover:

Examining Stuhini Group strata in the Copper canyon area, looking south. See van Straaten, B.I., Friedman, R.M., and Camacho, A., 2023. Stratigraphy of the Stuhini Group (Upper Triassic) in the Galore Creek area, northwestern British Columbia. In: Geological Fieldwork 2022, British Columbia Ministry of Energy, Mines and Low Carbon Innovation, British Columbia Geological Survey Paper 2023-01, this volume. **Photo by Nate Corcoran.**

## Back Cover:

Contact between orange-yellow weathering volcanosedimentary rocks of the Takla Group (Late Triassic, at left) and grey volcanic rocks of the Hazelton Group (Toodogonne Formation; Early Jurassic, at right). View is to the southwest from the road between the past-producing Baker and Lawyers mines. See Ootes, L., 2023. Did epithermal mineralization in the northern Toodoggonne region develop synchronously with largescale folding? In: Geological Fieldwork 2022, British Columbia Ministry of Energy, Mines and Low Carbon Innovation, British Columbia Geological Survey Paper 2023-01, this volume. **Photo by Luke Ootes.**

This publication is available, free of charge, from the British Columbia Geological Survey website:

<https://www2.gov.bc.ca/gov/content/industry/mineral-exploration-mining/british-columbia-geological-survey/publications>

### British Columbia Cataloguing in Publication Data

Main entry under title:

Geological Fieldwork: - 1974 -

Annual.

Issuing body varies

Vols. for 1978-1996 issued in series: Paper / British Columbia. Ministry of Energy, Mines and Petroleum Resources; vols. for 1997 - 1998, Paper / British Columbia. Ministry of Employment and Investment; vols. for 1999-2004, Paper / British Columbia. Ministry of Energy and Mines; vols. for 2005-2009, Paper / British Columbia. Ministry of Energy, Mines and Petroleum Resources; vols. for 2010, Paper / British Columbia. Ministry of Forests, Mines and Lands; vols. for 2011, Paper / British Columbia. Ministry of Energy and Mines; vols. for 2012- , Paper / British Columbia. Ministry of Energy, Mines and Natural Gas; vols. for 2014- , Paper / British Columbia. Ministry of Energy and Mines; vols. for 2018- , Paper / British Columbia. Ministry of Energy, Mines and Petroleum Resources; vols. for 2021- , Paper / British Columbia. Ministry of Energy, Mines and Low Carbon Innovation.

Includes Bibliographical references.

ISSN 0381-243X=Geological Fieldwork

1. Geology - British Columbia - Periodicals. 2. Mines and mineral resources - British Columbia - Periodicals. 3. Geology - Fieldwork - Periodicals. 4. Geology, Economic - British Columbia - Periodicals. 5. British Columbia. Geological Survey Branch - Periodicals. I. British Columbia. Geological Division. II. British Columbia. Geological Survey Branch. III. British Columbia. Geological Survey Branch. IV. British Columbia. Dept. of Mines and Petroleum Resources. V. British Columbia. Ministry of Energy, Mines and Petroleum Resources. VI. British Columbia. Ministry of Employment and Investment. VII. British Columbia Ministry of Energy and Mines. VIII. Series: Paper (British Columbia. Ministry of Energy, Mines and Petroleum Resources). IX. Series: Paper (British Columbia. Ministry of Employment and Investment). X. Series: Paper (British Columbia Ministry of Energy and Mines). XI. Series: Paper (British Columbia Ministry of Energy, Mines and Petroleum Resources). XII. Series: Paper (British Columbia Ministry of Forests, Mines and Lands). XIII. Series: Paper (British Columbia Ministry of Energy and Mines). XIV. Series: Paper (British Columbia Ministry of Energy, Mines and Natural Gas). XV. Series: Paper (British Columbia Ministry of Energy and Mines). XVI. Series: Paper (British Columbia Ministry of Energy, Mines and Petroleum Resources). XVII. Series: Paper (British Columbia Ministry of Energy, Mines and Low Carbon Innovation).

QE187.46 622.1'09711 C76-083084-3 (Rev.)

Victoria  
British Columbia  
Canada

January 2023

# Preface

## Geological Fieldwork 2022

Geological Fieldwork 2022 is the forty-eighth edition of the annual volume that presents peer-reviewed papers detailing the results of British Columbia Geological Survey (BCGS) geoscience activities. The Survey also publishes other reports, maps, and databases and contributes to peer-reviewed journals and partners publications throughout the year. This work can be accessed for free through the online BCGS Publication Catalogue. BCGS also publishes an annual companion volume, the Provincial Overview of Exploration and Mining in British Columbia.

I would like to acknowledge that BCGS geoscientists work and live on the traditional lands of many First Nations. As the Survey continues to assess the geological history of the province, we look forward to exchanging knowledge with Indigenous communities.

The first paper in the volume, by Wildgust et al., provides an overview of Survey activities in 2022. Ootes investigates the geometric and apparent temporal coincidence between folding, intrusion, and epithermal mineralization in the Toodoggone area of east-central Stikinia. Miller et al. continue with their multi-year project in the Kitsault River area of northwestern British Columbia. This project is focussed on resolving the distribution, age, and affinity of Stuhini and Hazelton group rocks to better understand the metallogeny and mineral potential of the region. Also working in the northwestern part of the province near the Galore Creek porphyry Cu-Au-Ag deposit, van Straaten et al. examine the stratigraphy and depositional setting of units in the Stuhini Group and provide initial geochronologic data and Johnston et al. present preliminary structural analysis of a high-strain zone west of the deposit area. In south-central BC, Schiarizza and Friedman report U-Pb zircon ages from rhyolite and sandstone of the Cadwallader terrane that correlate with Permian to Jurassic rocks in central (Sitlika assemblage) and northern British Columbia (Kutcho assemblage and overlying rocks), forming a fragmented belt that can be traced along the length of the province. Rukhlov et al. report on the provincial Geology Rock Archive, cataloguing efforts that resulted from the relocation of the Archive to its newly constructed home in the basement of Survey headquarters at 1810 Blanshard Street in Victoria.

The BCGS is an organization in transition. The Survey is in a period of renewal because several members have retired or moved on to other opportunities in the last few years. Fortunately, the Survey remains well-supported and has been approved to replace these positions. Additionally, the Survey is filling newly created positions that will service the province as global demand for the geological raw materials that are needed for the transition to a low carbon future increases. Consequently, the Survey is aggressively recruiting new staff and building for the future.

The Government of British Columbia continues to act on climate change. As part of the CleanBC Road Map to 2030, the Survey has been deployed to assess the potential contributions that the province can make supplying critical minerals, the commodities that are essential for diverse modern technologies, electrification, and low-carbon energy. The province is also pursuing a critical mineral strategy that will feature next-generation geoscience directed at better understanding the critical mineral endowment of the province. Our critical minerals initiative is well-aligned with the ongoing mineral potential program, which will provide First Nations and land use policy decision makers with tools to better appreciate mineral opportunities in British Columbia.



Adrian S. Hickin  
Chief Geologist and Executive Director  
British Columbia Geological Survey

# Table of Contents

---

<b>Wildgust, N., Cui, Y., Clarke, G., and Hickin, A.S.:</b> British Columbia Geological Survey annual program review 2022-2023 .....	1
<b>Ootes, L.:</b> Did epithermal mineralization in the northern Toodoggone region develop synchronously with large-scale folding? .....	13
<b>Miller, E.A., van Straaten, B.I., and Hunter, R.C.:</b> Update on bedrock mapping in the Kitsault River area, northwestern British Columbia .....	23
<b>van Straaten, B.I., Friedman, R.M., and Camacho, A.:</b> Stratigraphy of the Stuhini Group (Upper Triassic) in the Galore Creek area, northwestern British Columbia .....	33
<b>Johnston, R., Kennedy, L., and van Straaten, B.I.:</b> Preliminary observations of a high-strain zone along the western flank of the Galore Creek deposit area, northwestern British Columbia .....	51
<b>Schiarizza, P., and Friedman, R.M.:</b> U-Pb zircon dates for rhyolite and sandstone of Cadwallader terrane, lower Chilcotin River area, south-central British Columbia .....	65
<b>Rukhlov, A.S., Coats, B., Van der Vlugt, J., Beaupre- Olsen, I.J., and Zaborniak, K.:</b> British Columbia Geological Survey Sample Archive: An emerging resource for public geoscience .....	85
<b>Appendix:</b> British Columbia Geological Survey Publications 2022, including peer-reviewed external papers co-authored by BCGS staff .....	91

# British Columbia Geological Survey annual program review 2022-2023



Neil Wildgust<sup>1, a</sup>, Yao Cui<sup>1</sup>, Gordon Clarke<sup>2</sup>, and Adrian S. Hickin<sup>1</sup>

<sup>1</sup> British Columbia Geological Survey, Ministry of Energy, Mines and Low Carbon Innovation, Victoria, BC, V8W 9N3

<sup>2</sup> British Columbia Geological Survey, Ministry of Energy, Mines and Low Carbon Innovation, Vancouver, BC, V6Z 2G3

<sup>a</sup> corresponding author: Adrian.Hickin@gov.bc.ca

Recommended citation: Wildgust, N., Cui, Y., Clarke, G., and Hickin, A.S., 2023. British Columbia Geological Survey annual program review 2022-2023. In: *Geological Fieldwork 2022*, Ministry of Energy, Mines and Low Carbon Innovation, British Columbia Geological Survey Paper 2023-01, pp. 1-11.

---

## Executive Summary

This paper provides an overview of current British Columbia Geological Survey (BCGS) geoscience activities, and highlights key findings from 2022 projects. Headquartered in Victoria, the Survey is part of the Mines Competitiveness and Authorizations Division in the British Columbia Ministry of Energy, Mines and Low Carbon Innovation. The Survey generates geoscience knowledge and data to inform land use and resource management decisions, and to support the growth of British Columbia as a competitive jurisdiction for mineral exploration.

The Cordilleran Geoscience Section of the Survey conducts field and office research including bedrock and surficial geology mapping programs, regional geochemical surveys, and targeted mineral deposit studies. The past year has seen further progress of multi-year mapping and applied research across the province. Highlights include detailed mapping in the Kitsault area in the northwest, reconnaissance work in the northern Toodoggone area and the south-central interior, and the deployment of remotely piloted aircraft systems (RPAS) to gather geophysical data in the central and southern parts of the province. Building on an international critical minerals workshop co-hosted by the BCGS in 2021, the Survey embarked on a multi-year study of critical minerals. The initial work of this project included compiling an inventory of critical minerals occurrences across the province. The Cordilleran team has also been kept busy with a major revamp of the provincial Sample Archive, prompted by forced relocation of the facility in late 2022.

Responsible for maintaining and developing provincial geoscience and mineral resource databases, the Resource Information Section disseminates data online through MapPlace geospatial web services. Information managed by the team includes traditional geological maps and reports, geochemical, geophysical, and geological databases, in addition to mineral resource inventory and exploration assessment reports. The databases and webservices are designed to update data, facilitate data mining, and support applications for mineral exploration (particularly for critical minerals), and land-use planning. The team has started projects to modernize information systems and build a geoscience Spatial Data Infrastructure (SDI).

The Mineral Development Office (MDO) is the Vancouver base of the Survey. It provides investment intelligence to government and global business and publishes the annual Provincial Overview of Exploration and Mining in British Columbia volume. The MDO is staffed by a group of Regional Geologists who, stationed in exploration centres across the province, track minerals activities and provide geoscience expertise in their jurisdictions.

---

## 1. Introduction

This paper provides an overview of current British Columbia Geological Survey (BCGS) applied geoscience activities and highlights key findings from 2022 projects. Headquartered in Victoria, the Survey is part of the Mines Competitiveness and Authorizations Division in the British Columbia Ministry of Energy, Mines and Low Carbon Innovation. As the steward of geoscience and mineral resource information in the province, the Survey has an important role in stimulating mineral exploration, attracting investment, informing decisions with technical information, and providing continuous research based on more than a century of corporate memory.

The province has significant endowments of metals, metallurgical coal, and industrial minerals. Many of the metals are considered 'critical' because they are essential for modern technologies and low-carbon emission energy as the world transitions to digital and green economies, and are included in the Canadian list of 31 critical minerals

(Natural Resources Canada, 2022). The provincial minerals endowment is intimately tied to the tectonic evolution of the Canadian Cordillera, which continued from protracted supercontinent breakup starting about 1600 million years ago to accretionary processes that operate today as Pacific Ocean crust slides beneath Vancouver Island. In the northeastern part of the province, the Western Canada Sedimentary Basin hosts significant petroleum hydrocarbon resources.

The Survey is the primary repository for provincial geoscience knowledge. Maps, reports, and databases are freely available online and are public resources for First Nations and stakeholder groups including local communities, the minerals industry, public safety agencies, environmental scientists, research organizations, and government agencies. Current research programs (Fig. 1) continue to define the geological evolution and natural resources of the province, generating knowledge and data to support land use and resource management decisions that balance economic,



**Fig. 1.** British Columbia Geological Survey projects in 2022.

environmental, and community interests. A particular focus is providing public geoscience to support the growth of British Columbia as a competitive jurisdiction for mineral exploration, boosted by the recent attention of policy makers and industry to critical minerals. Providing mineral resource information is essential for informed land-use decisions by government and, increasingly, from communities.

The BCGS consists of three sections: 1) Cordilleran Geoscience; 2) Resource Information; and 3) the Mineral Development Office. The Cordilleran Geoscience Section generates new knowledge through field, laboratory, and office-based research activities including bedrock and surficial geology mapping programs, regional geochemical surveys, and targeted mineral deposit studies. Section team members manage in-house laboratory facilities, curate the provincial sample

archive, and build capacity through contract employment and training of geoscience assistants, typically undergraduate and graduate students. The Resource Information Section is responsible for maintaining and developing provincial geoscience databases and disseminating data online through geospatial web services (MapPlace). The Resource Information Section is also responsible for collecting, evaluating, approving, and archiving mineral and coal exploration assessment reports submitted by industry to maintain titles in good standing. The Mineral Development Office (MDO) is the Vancouver base of the Survey and provides investment intelligence to government and global business. The MDO is staffed by a group of Regional Geologists who, stationed in exploration centres across the province, track minerals activities and provide geoscience expertise in their jurisdictions. The MDO publishes the annual

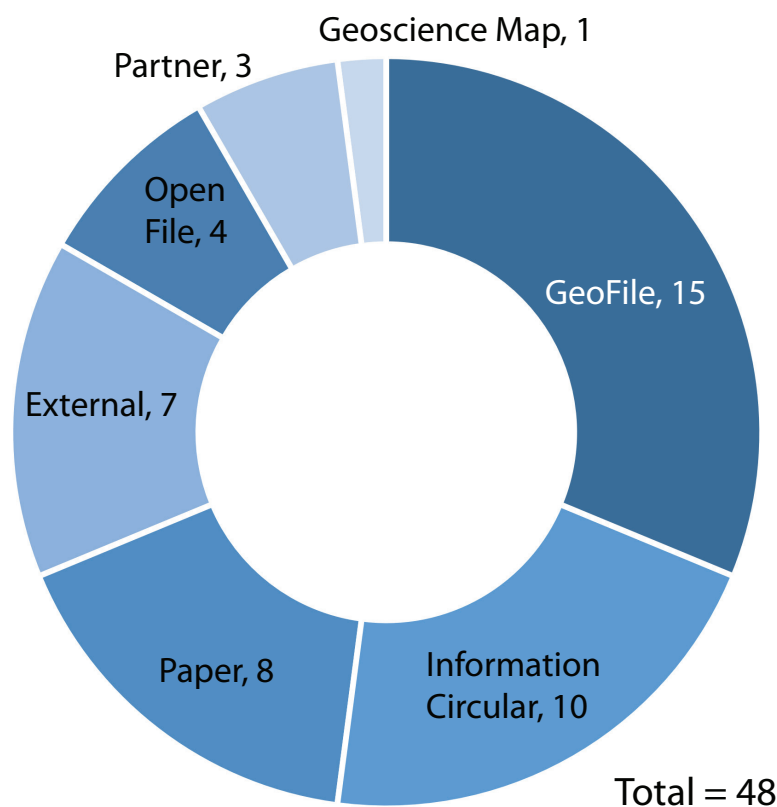
Provincial Overview of Exploration and Mining in British Columbia volume (Clarke et al., 2023).

The global Covid-19 pandemic again affected Survey operations in 2022, despite the relaxation of public health restrictions and resumption of normal working practices. External laboratory services continued to be affected in some cases, leading to delays in analytical testing and processing of

results. Despite these challenges, Survey staff maintained a full workload and publication output (Fig. 2).

## 2. Staffing

Currently staffed by 30 permanent and several term employees (Fig. 3), the Survey endured a challenging year with several retirements and people moving on to new opportunities.



**Papers\*:** This series is reserved for reviews and final thematic or regional works. Geological Fieldwork, our annual review of field activities and current research, is released as the first Paper of each year.

**Geoscience Maps:** This series is the BCGS vehicle for publishing final maps.

**Open Files:** These maps and reports present the interim results of ongoing research, particularly mapping projects.

**GeoFiles:** These publications enable rapid release of extensive data tables from ongoing geochemical, geochronologic, and geophysical work. As such, they serve the same function as data repositories provided by many journals, providing immediate access to raw data from specific projects.

**Information Circulares:** These publications provide accessible geoscience information to a broad audience in government, industry, and the general public. Included in the Information Circular series is the annual Provincial Overview of Exploration and Mining in British Columbia.

**Contributions to partner publications:** This category includes reports, maps, and other products published by another agency such as the Geological Survey of Canada or Geoscience BC, but have received contributions from British Columbia Geological Survey staff.

**External publications:** These are contributions to the peer reviewed literature and published in a recognized national or international scientific journal.

\*The count refers to the total number of articles authored by BCGS personnel in a volume.

**Fig. 2.** Types and numbers of publications produced by the British Columbia Geological Survey in 2022.



**Fig. 3.** British Columbia Geological Survey staff.

Larry Diakow and George Simandl retired after long and successful careers with BCGS; their expertise will be greatly missed. Rebecca Hunter, Holly Arnold, and Neil Wildgust left the Cordilleran team in 2022 for opportunities elsewhere. Emily Miller joined as a permanent staff member, Evan Orovan transferred to the Cordilleran team from the Resource Information Section to lead the critical minerals inventory project, and Wyatt Bain started as a Economic Geologist. The Survey's geomatics team was bolstered by the recruitment of George Nyi, Paulina Marczak, and Kaitlyn McLaren. The Mineral Development Office welcomed Hassan Heidarian as Regional Geologist for the Northeast and North Central regions as Nate Corcoran moved from Prince George to Smithers to support the Northwest region.

Former Director of the Resources Information team Larry Jones, who retired from the Survey in 2021, has been acknowledged with a Special Tribute from the Association for Mineral Exploration (AME) for his leadership in assembling and distributing the British Columbia Geological Survey databases and geospatial datasets and for leading his team in the design, development, and marketing of MapPlace.

The Survey is an organization in transition. Faced with replacing retirements, departures, and the need to fill newly created positions, the Survey began an aggressive hiring program. Capacity building in areas such as critical minerals, field mapping, digital data delivery, geomatics, and mineral potential modelling will continue in 2023. Similarly, capacity building for enhancing engagement with First Nations before, during, and after future field seasons will remain a priority.

### 3. Partnerships

The Survey adopts a collaborative approach to extend the scope and content of public geoscience while minimizing the risk of duplicative work. The Geological Survey of Canada (GSC) is an established partner; 2022 saw multiple discussions between BCGS and the GSC for the Energy and Minerals (GEM)-GeoNorth program, to align research interests and ensure coordinated engagement with First Nations in northern

British Columbia. Active collaboration under GEM-GeoNorth during 2022 focussed on providing BCGS expertise to support assessing the distribution of metallic mineral systems in the northern part of the province.

The Survey signed an agreement with Newcrest Mining Limited in late 2021 to facilitate extensive lithochemical analysis of igneous rock samples collected in the northwestern part of British Columbia and stored in the BCGS Sample Archive. About 950 samples were re-analyzed using modern comprehensive and high-precision analytical methods (Van der Vlugt et al., 2022). This project underscores the value added to geoscience in the province by the archive facility and may provide a blueprint for future collaborative research and public-private partnerships using archived samples.

BCGS hosted a forum in November 2022 focussed on institutional research programs and primarily intended as a networking event, featuring activities at the British Columbia Geological Survey, the Geological Survey of Canada, British Columbia universities, and Geoscience BC. More than 70 participants explored shared, overlapping, and cross-disciplinary research.

### 4. Cordilleran Geoscience Section

Section geologists collect fundamental geoscience data through single and multi-year field-based programs complemented by laboratory and office studies. These programs include regional-scale mapping, mineral deposit studies, and new mineral exploration method development. Expertise encompasses tectonics, structural geology, stratigraphy, petrology, metallogeny, coal deposits, Quaternary and surficial geology, critical minerals, and geochemistry.

Engagement with First Nations communities is a priority for the Survey; as summer field projects are planned early each calendar year, liaison with First Nations is initiated as soon as possible. BCGS is committed to sharing geoscience information with all British Columbians and is expanding efforts to bring geological and mineral science to communities.

The provincial Sample Archive is home to rock, mineral, and geochemical samples collected from across the province in the last several decades by BCGS staff and partner organizations. These collections represent a valuable resource for public geoscience, supporting quality control of published data, re-analysis using modern comprehensive and high-precision analytical methods, and new geoscience initiatives. Following a notice to vacate the historic BCGS storage facility at 254 Belleville Street in downtown Victoria (Fig. 4), systematic sorting, rationalizing, and cataloguing of archived samples was undertaken in anticipation of moving the collection to a new site at 1810 Blanshard Street, Victoria (Rukhlov et al., 2023). Work will continue to make the Archive a modern and reliable resource supporting Cordilleran geoscience with enhanced and accessible digital cataloging.

#### 4.1. Mapping, regional synthesis and compilation

Mapping is a core element of Survey and Cordilleran Section



**Fig. 4.** Heritage 'Stores Building' (ca. 1912) at 254 Belleville Street, Victoria. See Rukhlov et al. (2023).

programs. The Survey delivers two key products: traditional published maps in the form of PDF files with accompanying research papers; and updates to the provincial digital geology database, which ultimately feeds into MapPlace as BC Digital Geology. The digital geology database is an instrumental component of modern mineral potential assessment methods being developed by the Survey to inform land-use planning policies in the provincial government (see section 5.6.).

#### 4.1.1. Northwestern British Columbia

Northwestern British Columbia hosts significant base- and precious-metal mineral deposits, notably in a loosely defined area colloquially referred to as the 'Golden Triangle' between Iskut and Stewart. A multi-year program to expand regional bedrock mapping and better understand the stratigraphic, magmatic, structural, metallogenic, and tectonic framework of northwestern British Columbia is ongoing.

Nelson et al. (2022) continued long-term investigations into the evolution of Stikinia and adjacent terranes in northwestern British Columbia, presenting U-Pb detrital zircon data from the Stuhini and Hazelton groups to reconstruct the uppermost Triassic and Lower Jurassic pre-accretionary arc and early syn-accretionary back arc paleogeography and paleotectonics of the region. Nelson et al. (2022) also examined the relationships between Stikinia, Yukon-Tanana terrane, the Whitehorse trough, Quesnellia, and Cache Creek terrane. New bedrock geology maps were published for the western Skeena arch region (Angen et al., 2022), the Turtle Lake area (Mihalynuk et al., 2022), and a 5,000 km<sup>2</sup> area between the community of Dease Lake and the Stikine River (van Straaten et al. 2022a).

Hunter et al. (2022) reported U-Pb zircon geochronological data as part of a larger study to better establish the ages of the Stuhini and Hazelton groups in the Kitsault River area (Fig. 1). Because the Kitsault River area hosts Ag-rich volcanogenic massive sulphide, Au-rich epithermal, and Cu-Au porphyry systems, resolving the distribution, age, and affinity of prospective host rocks is key to understanding the metallogeny

and mineral potential of the area. Continuing this study, Miller et al. (2023) provide an update on work in the Kitsault River area, presenting a new preliminary map and extended legend for units (Fig. 5) in the northeastern part.

Working in the area of the Galore Creek porphyry Cu-Ag deposit (Fig.1), which is hosted in and broadly coeval with a multi-phase alkalic silica-undersaturated volcano-intrusive complex, van Straaten et al. (2023) examine the stratigraphy and depositional setting of the Stuhini Group (Upper Triassic) and provide initial geochronologic data. van Straaten et al. (2023) recognize a 'lower intermediate to mafic volcano-sedimentary succession' (Fig. 6; at least ~1.2 km thick) that is abruptly overlain by an 'upper alkalic volcanic succession' (at least ~0.8 km thick). Based on high-precision U-Pb zircon titanite geochronology, upper succession alkalic volcanism initiated at  $210.26 \pm 0.17$  Ma, broadly coeval with published ages for mineralogically, texturally, and compositionally similar alkalic silica-undersaturated Galore intrusions. The Galore Creek deposit is bordered to the west near Butte ridge by a 2-3 km wide, >6 km long, poorly understood zone of foliated and folded Stuhini Group rocks that records anomalously high strain relative to elsewhere in the area. Based on preliminary



**Fig. 5.** Parallel- and cross-stratified sandstone and siltstone with a white-weathering tuff layer; upper part of Hazelton Group, unassigned unit (lmJHsv), Kitsault River area. View is to the east. See Miller et al. (2023).



**Fig. 6.** Cobble to boulder conglomerate and pebbly sandstone with light-toned intermediate volcanic clasts and green augite-phyric mafic volcanic clasts; well-developed foliation defined by aligned clasts. Lower succession of the Stuhini Group, conglomeratic unit (uTrSvc), northwest end of Butte ridge, Galore Creek area. See van Straaten et al. (2023).

work, Johnston et al. (2023) interpret that shortening in the Butte ridge area was accommodated by fold and foliation development (Fig. 7) rather than by discrete heterogeneous shear zones and that north-south changes reflect different structural levels.

van Straaten et al. (2022b) released whole rock litho-geochemical data from for 555 Devonian to Quaternary rock samples from northwestern British Columbia, predominantly from Triassic to Jurassic igneous rocks in Stikine terrane and, using modern high-precision techniques, Van der Vlugt, et al. (2022) re-analyzed almost 950 archived igneous samples. Lett et al. (2022) provided historical heavy mineral and geochemical data from stream-sediment, stream-water, and moss-mat sampling.

#### 4.1.2. Central and southern British Columbia

Ootes (2023) examines regional stratigraphic relationships (Fig. 8) in the eastern part of central Stikinia to identify a major synclinorium-anticlinorium pair that extends along strike for more than 100 km into the northern Toodoggone region (Fig. 1) where the hinge zone of the anticlinorium coincides with the Black Lake intrusion (Early Jurassic). Epithermal mineralization (e.g., Baker, Lawyers, Shasta deposits) is distributed along the axial trace of the anticlinorium, which is apparently unique to this part of Stikinia, leading to the hypothesis of a causal relationship between folding, intrusion, and Au-Ag±Cu epithermal mineralization.

Jones et al. (2022) continued generating results from the northern Hogem batholith (Fig. 1) project, releasing in-situ zircon U-Pb, Lu-Hf,  $\delta^{18}\text{O}$ , and trace-element data from intrusive units. Ootes et al. (2022) presented igneous and detrital zircon U-Pb, Lu-Hf, and trace-element data and the first radiolarian ages from the Asitka Group (basement to eastern Stikinia).

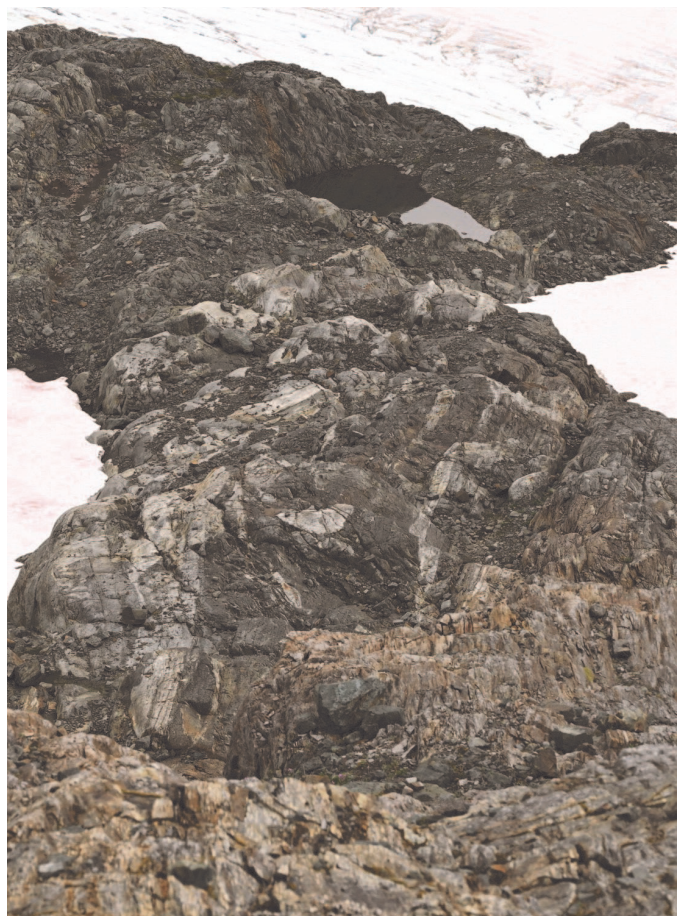


**Fig. 7.** Decametre-scale isoclinal fold in southern part of the ‘Butte ridge deformation zone’ west of the Galore Creek deposit area. The light-toned unit(s) are tuffaceous beds. View to the south. See Johnston et al. (2023).



**Fig. 8.** Contact between orange-yellow weathering volcanosedimentary rocks of the Takla Group (Upper Triassic, at left) and grey volcanic rocks of the Hazelton Group (Toodoggone Formation; Lower Jurassic, at right). View is to the southwest from the road between the past-producing Baker and Lawyers mines. See Ootes (2023).

This work showed that, although an enigmatic older crustal fragment may have been nearby, eastern Stikinia formed on an ocean floor during the Carboniferous to early Permian from entirely juvenile magmatic sources.

Schiarizza (2022) released a 1:50,000 bedrock geology map of the Stump Lake-Salmon River area of the Thompson Plateau. Schiarizza and Friedman (2023) provide new U-Pb geochronologic data from rocks of the Cadwallader terrane that are exposed in a structural window beneath overthrust Cache Creek terrane along the Chilcotin River (Fig. 1). Rhyolites (Fig. 9) from near the top of the Wineglass assemblage returned a crystallization age of  $260.8 \pm 0.3$  Ma, confirming that they are Late Permian. Detrital zircons from the lower part of the Tyaughton Formation, which unconformably overlies the Wineglass assemblage suggest a late Norian or Rhaetian maximum depositional age, and include a population of Late Permian to Middle Triassic grains, probably derived from the underlying Wineglass assemblage and/or related rocks. A second population of Late Triassic zircons are inferred to have been derived from Late Triassic volcanic and plutonic rocks exposed elsewhere in Cadwallader terrane. A sandstone from a higher stratigraphic level in the Tyaughton Formation contains only Late Triassic zircons and suggest a late Norian maximum depositional age. The Permian to Jurassic rocks of the Cadwallader terrane in the Chilcotin River window correlate with rocks in central and northern British Columbia, forming a fragmented belt that can be traced along the length of the province.

A study to investigate the relationships between the Harper Ranch (Devonian-Carboniferous), Slovan Group (Triassic), and Nicola Group (Triassic) and potential affiliations with the Chase Formation (Devonian) started in the Trinity Valley area (Fig. 1). A number of past-producing mines are in the



**Fig. 9.** Quartz and plagioclase-phyric metarhyolite from near the top of the Wineglass assemblage, Cadwallader terrane with a new U-Pb zircon crystallization age of  $260.8 \pm 0.3$  Ma. See Schiarizza and Friedman (2023).

area (mainly placer gold), and questions also remain about the connection between mineralization and bedrock. Mapping of the Lardeau Group in the Kaslo area (Fig. 1) continues, focussed on highly strained and well-metamorphosed rocks of the Index Formation, and its age, stratigraphic position, and tectonic significance. Within graphitic metapelites of the Index Formation are previously unmapped ultramafic layers and pods (now talc and chromian mica schist) with massive sulfide mineralization, the mineral potential of which is also being investigated.

#### 4.2. Province-wide critical minerals assessment

Low-carbon energy technologies demand critical minerals, but the highly globalized supply chain of critical minerals and products is vulnerable to disruption. Furthermore, increased use of green technologies is increasing the demand for many metals, which could lead to shortages in the next few decades. British Columbia is Canada's largest producer of copper and metallurgical coal and only producer of molybdenum, and also produces zinc and manganese. The four metals are elements on Canada's critical minerals list (Natural Resources Canada, 2022), and metallurgical coal is required for high-quality steel. British Columbia has near-term potential to contribute significantly to the production of other critical metals required for a green economy including nickel, rare earth elements, niobium, tantalum, tungsten, and cobalt.

Following from an online international workshop co-hosted by BCGS, (British Columbia Geological Survey, 2021), the Survey has embarked on a multi-year project to assess critical mineral deposits and associated mineral systems across the province. The Survey is preparing an inventory of British Columbia's critical minerals, assessing geological settings most favourable to host deposits, and developing exploration techniques that would enhance discovery of new deposits.

#### 4.3. Targeted deposit studies and exploration methods

Regional mapping programs are complemented by more specific or thematic studies, typically selected to develop public geoscience knowledge and datasets in key topics that support minerals exploration or government land-use policy. Survey geoscientists test new technologies that can support future regional mapping and mineral exploration activities.

This year the Survey finished data collection for its pilot study on the utility of RPAS (remotely piloted aircraft systems)-borne magnetometry and gamma-ray spectrometry to detect dispersal trains in subglacial tills, with test sites at the Mount Polley and Woodjam deposits and in the Guichon Creek batholith area (Fig. 1; Highland Valley deposit). In total, more than 300-line km were flown in 68 individual surveys designed to measure K, eU, eTh (using a Radiation Solutions Inc. RS-530; Fig. 10), and total field magnetics (using GEM Systems DRONEmag potassium magnetometer) over tills derived from contrasting bedrock rock types. Gridded autopilot surveys were flown in cutblocks at 5, 7.5 or 10 m above ground level. A radar altimeter instructed the RPAS flight control systems in



**Fig. 10.** Radiation Solutions Inc. RS-530 gamma-ray spectrometer, mounted to a DJI Matrice 600 Pro, completing a survey north of Merritt above tills derived from Bethsaida phase (Late Triassic) granodiorite, Guichon Creek batholith.

real-time to maintain a constant height above ground, ensuring measured data variation was not related to changes in distance between the geophysical sensors and ground. As part of this final field season, ground radiometrics (using a Radiation Solutions Inc. RS-230BGO) and magnetic susceptibility measurements (using a KT-20 with 3F-32 sensor) were also collected within the survey areas to further validate the RPAS data. In early 2023, processed data from all surveys will be released as a GeoFile (Elia et al., 2023). Interpretations and assessments of the individual datasets will follow in a series of Open File publications (e.g., Ferbey et al., 2023).

## 5. Resource Information Section

The Survey collects, compiles, and disseminates provincial public geoscience information that supports effective mineral exploration, sound land use management, and responsible governance. This public geoscience includes traditional geological maps, reports, and thematic studies, province-wide digital coverage of bedrock geology (BC Digital Geology), and databases including mineral assessment reports (ARIS), mineral inventory (MINFILE), coal information (COALFILE), geochemical and geophysical surveys, and collections of documents donated to the British Columbia Geological Survey since the late 1880s by government, universities, industry, and individuals (Property File). The Survey operates numerous information systems to update these databases and deliver them through web portals and MapPlace, the BCGS geospatial web service.

As part of the Survey's digital transformation efforts, information systems are being re-engineered to build a geoscience Spatial Data Infrastructure (SDI). The Survey carried out a system review with recommendations for an SDI architecture to improve efficiency in operating and updating databases, to further digitalization and analytical-ready geoscience, and to enable interoperable data sharing.

## 5.1. Geoscience Spatial Data Infrastructure

Geoscience data are inherently related in the data lifecycle and need to be managed coherently. However, the Survey currently operates geoscience databases and applications built in the last two decades, mostly in discrete systems of varying legacy or obsolete technologies. Thus, the Survey is now developing a geoscience Spatial Data Infrastructure (SDI) to manage all geological and mineral resource data together as sub-systems in the same environment, using common data and system components and well-defined interface across service boundaries. In early 2022, we commissioned a consultant to conduct a system review of all geoscience databases and applications in the Survey. The review recommended a containerized microservices architecture using Cloud-native technologies and opensource software for our SDI. As a first step on our path to SDI the Survey, completed an upgrade of ARIS (Assessment Report Indexing System) from obsolete technologies with multiple manual steps to a modern and standard-based environment with streamlined and automated processes.

## 5.2. MapPlace

MapPlace is the BCGS geospatial web service to discover, visualize, search, and generate summary reports and maps from province-wide geoscience databases. Easy access to, and analysis of, geoscience maps and data are fundamental to inform decisions on mineral exploration, mining, environmental protection, and land use management. MapPlace provides a platform to facilitate data mining and analysis of geoscience information in the context of all other relevant data such as mineral titles, assessment reports, land ownership, public infrastructure, aquifers, and topographic base maps. Some of the data layers and applications are specifically developed to enable research and analytics for mineral exploration and prospecting.

## 5.3. ARIS assessment reports and database

Results of mineral exploration are submitted by industry as assessment reports to the government in compliance with the Mineral Tenure Act regulations. After a one-year confidentiality period, the assessment reports become freely available to the public. The Survey manages these reports in the Assessment Report Indexing System (ARIS) database with metadata to search the locations, mineral occurrences, commodities, claims, work types, and expenditures as documented in the reports. ARIS contains more than 39,100 reports dating from 1947. All the assessment reports are available online as PDF documents through the ARIS website, and nearly 800 of them contain data (e.g., geochemical analyses and geophysical surveys) in common digital formats that can be readily used. In addition to the search interface on the ARIS website and MapPlace, a copy of the ARIS metadata is available to download in Microsoft Access, with locations in Microsoft Excel and ESRI shapefile format.

### 5.3.1. Assessment report digital submission

Traditionally, assessment reports from mineral exploration have been submitted in hardcopy or as files such as scanned PDF, which render data within the files difficult to extract and use. The BCGS has set up a digital data submission portal to encourage inclusion of digital files such as spreadsheets, databases, GIS maps, and grids. Explorationists will benefit because digital data can be easily retrieved, integrated, and recast for specific needs. Digital submission will also enable the Survey to better maintain province-wide databases and create derivative products that use past results to guide future exploration. Both assessment reports and digital data can be uploaded through the ARIS data submission page. The Survey continues to digitally extract information for our assessment report-sourced surface sediment geochemical database (ARSSG). In 2022, digital extraction was expanded to include drillhole collar and core geochemical data.

### 5.4. Other databases

MINFILE is a database for mineral, coal, and industrial mineral occurrences that includes information for more than 15,800 records. In 2022, more than 400 new occurrences and 2,100 updates were added to the database. COALFILE includes a collection of assessment reports, dating from 1900. Property File is a collection of archived reports, maps, photos, and technical notes documenting mineral exploration activities in British Columbia from the late 1800s. The provincial geochemical databases hold field and geochemical data from multi-media surveys by the Geological Survey of Canada, the BCGS, and Geoscience BC. The databases are updated regularly and contain results from the Regional Geochemical Survey program, till surveys, and lithochemical samples. Accompanying the physical relocation and rationalization of the BCGS Sample Archive in 2022 a modern digital inventory was created for integration with other provincial datasets (Rukhlov et al, 2023).

### 5.5. British Columbia Digital Geology

The BCGS offers province-wide digital coverage of bedrock geology including details from field mapping, with a typical regional compilation at a scale of 1:50,000. A geospatial frame data (GFD) model is used to simplify the compilation and integration of new regional mapping into the BCDigital Geology database (Cui, 2021). Bedrock geology is standardized with consistent stratigraphic coding, ages, and rock types to enable computations, and is available for download in GeoPackage and Esri shapefile formats. Customized bedrock geological maps and legends can be explored, and data downloaded as KML by spatial and non-spatial queries via MapPlace. The BCGS has transformed the digital geology to the GeoSciML Lite schema

and mapped the contents using the vocabularies adopted by the IUGS Commission for the Management and Application of Geoscience Information (CGI). The GeoSciML Lite-compliant digital geology is accessible via the OneGeology portal and open standard-based interface such as Web Mapping Service (WMS) and Web Feature Service (WFS) specification, to enable interoperable data sharing and analytics.

### 5.6. Mineral potential modelling

Modernized mineral potential modelling identifies areas of high prospectivity for key mineral systems. Mineral potential assessment continues as a renewed focus for the Survey, with an emphasis on supporting government, First Nations, and stakeholders in land-use planning and policy development. A pilot study, which produced data-driven mineral potential maps for three mineral systems (VMS, porphyry copper, magmatic nickel), now continues into new areas and will be applied to the Survey's province-wide critical minerals assessment.

## 6. Mineral Development Office

The mining industry contributes greatly to the economy of British Columbia. Particularly important for northern communities and First Nations, the mineral exploration, mining, and related sectors employ more than 30,000 people. For 2022, the forecast value of mine production in British Columbia is \$18.2 billion (Clarke et al., 2023).

Mineral exploration is the backbone of mining and an estimated \$740.4 million was spent on exploration in 2022. More than 200 companies have projects in British Columbia and these projects are monitored by the Mineral Development Office (MDO) and its Regional Geologists. The MDO is the Vancouver base of the British Columbia Geological Survey. It links the more than 1100 exploration and mining companies headquartered in Vancouver to provincial mineral and coal information. The MDO distributes Survey data and provides technical information and expertise about mineral opportunities to the domestic and international investment community. The MDO monitors the activities of the mining and exploration sectors and produces the Provincial Overview of Exploration and Mining in British Columbia, an annual volume that summarizes activities in the different regions of the province (see e.g., Clarke et al., 2023).

The British Columbia Regional Geologists (Table 1) represent the provincial government on geological matters at a regional level, capture information on industry activity in their jurisdictions, and produce reports such as a province-wide review of volcanogenic massive sulphide deposits by Northcote (2022). Within their communities, the Regional Geologists provide information on exploration trends, possible investment opportunities, land use processes, First Nation capacity building, and public outreach.

**Table 1.** British Columbia Regional Geologists.

Regional Geologist	Office	Region
Nate Corcoran	Smithers	Northwest
Hassan Heidarian	Prince George	Northeast and North Central
Vacant	Kamloops	South Central
Fiona Katay	Cranbrook	Southeast
Bruce Northcote	Vancouver	Southwest

### Acknowledgment

We thank George Owsiacki of Total Earth Science Services (Victoria) for the desktop publishing of this volume.

### References cited

- Angen, J.J., Hart, C.J.R., Nelson, J., and Rahimi, M., 2022. Geology and mineral potential of the western Skeena arch: Evolution of an arc-transverse structural corridor, west-central British Columbia. British Columbia Ministry of Energy, Mines and Low Carbon Innovation, British Columbia Geological Survey Open File 2019-09, Geoscience BC Report 2022-09, MDRU Publication 458, 47 p. British Columbia Geological Survey, 2021. Critical minerals: From discovery to supply chain, program with abstracts. British Columbia Ministry of Energy, Mines and Low Carbon Innovation, British Columbia Geological Survey GeoFile 2021-14, 74 p.
- Clarke, G., Northcote, B., Corcoran, N.L., Heidarian, H., and Hancock, K., 2023. Exploration and Mining in British Columbia, 2022: A summary. In: Provincial Overview of Exploration and Mining in British Columbia, 2022. British Columbia Ministry of Energy, Mines and Low Carbon Innovation, British Columbia Geological Survey Information Circular 2023-01, in press.
- Cui, Y., 2021. A geospatial frame data model to simplify digital map compilation and integration. British Columbia Ministry of Energy, Mines and Low Carbon Innovation, British Columbia Geological Survey Paper 2021-03, 20 p.
- Elia, E.A., Ferbey, T., Ward, B.C., Best, M., Shives, R.B.K., and Martin-Burtart, N., 2023. Remotely piloted aircraft systems (RPAS) data for subglacial tills of the Highland Valley and Mount Polley porphyry areas. British Columbia Ministry of Energy, Mines and Low Carbon Innovation, British Columbia Geological Survey GeoFile, in press.
- Ferbey, T., Elia, E.A., Best, M., Shives, R.B.K., Martin-Burtart, N., and Ward, B.C., 2023. Remotely piloted aircraft-borne radiometric data from subglacial tills of the Highland Valley and Mount Polley porphyry areas. British Columbia Ministry of Energy, Mines and Low Carbon Innovation, British Columbia Geological Survey Open File, in press.
- Hunter, R.C., Sebert, C.F.B., Friedman, R., and Wall, C., 2022. Geochronologic data from the Kitsault River area, northwest British Columbia. Ministry of Energy, Mines and Low Carbon Innovation, British Columbia Geological Survey Geofile 2022-13, 4 p.
- Johnston, R., Kennedy, L., and van Straaten, B.I., 2023. Preliminary observations of a high-strain zone along the western flank of the Galore Creek deposit area, northwestern British Columbia. In: Geological Fieldwork 2022, British Columbia Ministry of Energy, Mines and Low Carbon Innovation, British Columbia Geological Survey Paper 2023-01, pp. 51-63.
- Jones, G., Ootes, L., Luo, Y., Stern, R., Vezinet, A., and Pearson, D.G., 2022. In situ zircon U-Pb, Lu-Hf,  $\delta^{18}\text{O}$ , and trace elements from intrusive units in northern Hogen batholith, Quesnel terrane, north-central British Columbia. British Columbia Ministry of Energy, Mines and Low Carbon Innovation, British Columbia Geological Survey GeoFile 2022-09, 19 p.
- Lett, R.E., Friske, P.W.B., and McClenaghan, M.B., 2022. Heavy mineral and geochemical data from detailed stream-sediment, stream-water, and moss-mat sampling in northwestern British Columbia. British Columbia Ministry of Energy, Mines and Low Carbon Innovation, British Columbia Geological Survey GeoFile 2022-10, 7 p.
- Mihalynuk, M.G., Milidragovic, D., Tsekhmistrenko, M., and Zagorevski, A., 2022. Turtle Lake area geology (NTS 104M/16). British Columbia Ministry of Energy, Mines and Resources, British Columbia Geological Survey Open File 2022-02, Geological Survey of Canada Open File 8757, 1:50,000 scale.
- Miller, E.A., van Straaten, B.I., and Hunter, R.C., 2023. Update on bedrock mapping in the Kitsault River area, northwestern British Columbia. In: Geological Fieldwork 2022, British Columbia Ministry of Energy, Mines and Low Carbon Innovation, British Columbia Geological Survey Paper 2023-01, pp. 23-32.
- Natural Resources Canada, 2022. The Canadian Critical Minerals Strategy. <<https://www.canada.ca/en/campaign/critical-minerals-in-canada/canadian-critical-minerals-strategy.html>>
- Nelson, J.L., van Straaten, B., and Friedman, R., 2022. Latest Triassic-Early Jurassic Stikine-Yukon-Tanana terrane collision and the onset of accretion in the Canadian Cordillera: Insights from Hazelton Group detrital zircon provenance and arc-back-arc configuration. *Geosphere*, 18. <<https://doi.org/10.1130/GES02444.1>>
- Northcote, B., 2022. Volcanogenic massive sulphide (VMS) deposits in British Columbia: A review. British Columbia Ministry of Energy, Mines and Low Carbon Innovation, British Columbia Geological Survey GeoFile 2022-11, 30 p.
- Ootes, L., 2023. Did epithermal mineralization in the northern Toadogone region develop synchronously with largescale folding? In: Geological Fieldwork 2022, British Columbia Ministry of Energy, Mines and Low Carbon Innovation, British Columbia Geological Survey Paper 2023-01, pp. 13-21.
- Ootes, L., Milidragovic, D., Friedman, R., Wall, C., Cordey, F., Luo, Y., Jones, G., Pearson, D.G., and Bergen, A., 2022. A juvenile Paleozoic ocean floor origin for eastern Stikinia, Canadian Cordillera. *Geosphere*, 18. <<https://doi.org/10.1130/GES02459.1>>
- Rukhlov, A.S., Coats, B., Van der Vlugt, J., Beaupre-Olsen, I.J., and Zaborniak, K., 2023. British Columbia Geological Survey Sample Archive: An emerging resource for public geoscience. In: Geological Fieldwork 2022, British Columbia Ministry of Energy, Mines and Low Carbon Innovation, British Columbia Geological Survey Paper 2023-01, pp. 85-90.
- Schiarizza, P., 2022. Bedrock geology, Stump Lake-Salmon River, parts of NTS 82L/05 and 92I/08. British Columbia Ministry of Energy, Mines and Resources British Columbia Geological Survey Open File 2022-03, 1:50,000 scale.

- Schiarizza, P., and Friedman, R.M., 2023. U-Pb zircon dates for rhyolite and sandstone of Cadwallader terrane, lower Chilcotin River area, south-central British Columbia. In: Geological Fieldwork 2022, British Columbia Ministry of Energy, Mines and Low Carbon Innovation, British Columbia Geological Survey Paper 2023-01, pp. 65-84.
- Van der Vlugt, J., Rukhlov, A.S., and van Straaten, B.I., 2022. Lithogeochemical re-analysis of British Columbia Geological Survey archived rock samples from northwestern British Columbia. British Columbia Ministry of Energy, Mines and Low Carbon Innovation, British Columbia Geological Survey GeoFile 2022-14, 15 p.
- van Straaten, B.I., Logan, J.M., Nelson, J.L., Moynihan, D.P., Diakow, L.J., Gibson, R., Bichlmaier, S.J., Wearmouth, C.D., Friedman, R.M., Golding, M.L., Miller, E.A. and Poulton, T.P., 2022a. Bedrock geology of the Dease Lake area. British Columbia Ministry of Energy, Mines and Low Carbon Innovation, British Columbia Geological Survey, Geoscience Map 2022-01, 1:100,000 scale.
- van Straaten, B.I., Logan, J.M., Hunter, R.C., Nelson, J.L., and Miller, E.A., 2022b. Igneous lithogeochemistry data for the Dease Lake, Kitsault River, Galore Creek, Telegraph Creek, Foremore, and other areas in northwestern British Columbia. British Columbia Ministry of Energy, Mines and Low Carbon Innovation, British Columbia Geological Survey GeoFile 2022-12, 14 p.
- van Straaten, B.I., Friedman, R.M., and Camacho, A., 2023. Stratigraphy of the Stuhini Group (Upper Triassic) in the Galore Creek area, northwestern British Columbia. In: Geological Fieldwork 2022, British Columbia Ministry of Energy, Mines and Low Carbon Innovation, British Columbia Geological Survey Paper 2023-01, pp. 33-49.



# Did epithermal mineralization in the northern Toodoggone region develop synchronously with large-scale folding?



Luke Ootes<sup>1, a</sup>

<sup>1</sup> British Columbia Geological Survey, Ministry of Energy, Mines and Low Carbon Innovation, Victoria, BC, V8W 9N3

<sup>a</sup> corresponding author: Luke.Ootes@gov.bc.ca

Recommended citation: Ootes, L., 2023. Did epithermal mineralization in the northern Toodoggone region develop synchronously with large-scale folding? In: Geological Fieldwork 2022, British Columbia Ministry of Energy, Mines and Low Carbon Innovation, British Columbia Geological Survey Paper 2023-01, pp. 13-21.

## Abstract

In the eastern part of central Stikinia, regional northwest-plunging, northeast-vergent folds are indicated by stratigraphic relationships. A synclinorium southeast of Sustut Provincial Park is connected to an anticlinorium in the northern Toodoggone region by a long (ca. 100 km) southwest-younging limb. The hinge zone of this anticlinorium coincides with the Black Lake intrusion (Early Jurassic), which cuts volcano-sedimentary rocks that host epithermal Au-Ag±Cu mineralization (e.g., Baker, Lawyers, Shasta deposits). Although intrusion-related porphyry mineralization is common along the length of eastern Stikinia, northern Toodoggone epithermal mineralization, which is distributed along the axial trace of the anticlinorium, appears to be unique. This geometric and apparent temporal coincidence may imply a causal relationship between folding, intrusion, and epithermal mineralization. This hypothesis can be tested with high-precision geochronology.

**Keywords:** Toodoggone, epithermal Au-Ag±Cu, deformation, stratigraphic younging, Black Lake intrusion

## 1. Introduction

The Stikine terrane (Stikinia, Late Triassic to Jurassic) of the Cordilleran orogen (Fig. 1) hosts porphyry Cu-Au, epithermal Au-Ag±Cu, and volcanogenic massive sulphide deposits. In eastern Stikinia (Fig. 2), the Toodoggone region hosts one past-producing porphyry Cu-Au deposit (Kemess) and several epithermal Au-Ag deposits (e.g., Baker, Lawyers, Shasta). Diakow (2001) and Diakow et al. (1993, 2006) mapped the bedrock geology of the Toodoggone region, providing a geological framework for the mineral deposits, and Durning et al. (2009) summarized the age of the host rocks and the timing and thermochemical conditions of mineralization. They showed that the Kemess porphyry mineralization (ca. 200 Ma) in the southern Toodoggone region is slightly older than the epithermal mineralization (<194 Ma) to the north. However, whereas mineralization-host rock relationships are well-established in the northern Toodoggone region, a large-scale structural control may have gone unrecognized.

A field reconnaissance of the northern Toodoggone area, on the traditional lands of the Tsay Keh Dene, Kwadacha, Takla Lake, Kaska Dena, and Tahltan First Nations, combined with published studies in the area (Diakow et al., 1993, 2001) and in the rest of eastern Stikinia (Lord, 1948; Richards, 1976; Diakow, 2001; Legun, 2001; Evenchick et al., 2007; Ootes et al., 2020a, b, 2022), allow regional tracing of stratigraphic younging directions. These define a northwest-plunging, northeast-vergent synclinorium-anticlinorium pair. A synclinorium southeast of Sustut Provincial Park in the south connects to an anticlinorium in the northern Toodoggone region by a long (ca. 100 km) intervening limb (Fig. 3). Coincident with the hinge zone of the anticlinorium is the Black Lake intrusive



Fig. 1. Terrane map of the Cordilleran orogen and location of this study (eastern Stikinia). Modified after Colpron (2020).

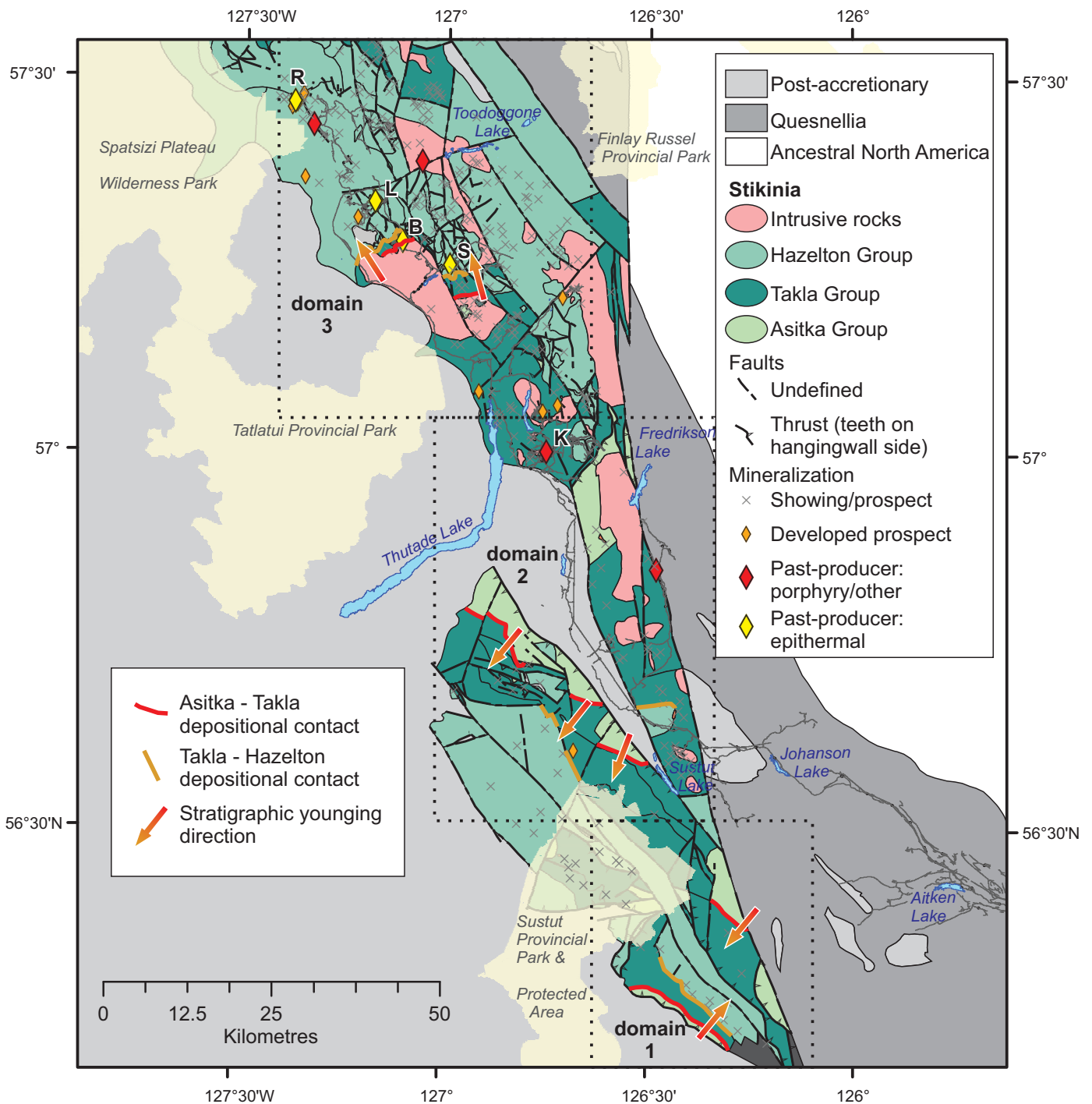


**Fig. 2.** Geology of eastern Stikinia, modified after Lord (1948), Richards (1976), Diakow et al. (1993, 2006), Diakow (2001), Legun (2001), Evenchick et al. (2007), and Ootes et al. (2020a). B-Baker mine; L-Lawyers mine; K-Kemess mine; R-Ranch project (Thesis mine); S-Shasta mine. Informal structural domains 1, 2, 3.

suite, and coincident with the axial trace of the anticlinorium is epithermal mineralization. Although porphyry mineralization is common in the eastern part of central Stikinia, epithermal mineralization is only known in the northern Toodoggone area. Geometric and possible temporal coincidence may indicate a causal link between folding, intrusion, and epithermal mineralization.

## 2. Eastern Stikinia

### 2.1. Stratigraphic framework

Although eastern Stikinia is dismembered by faults, which range from syndepositional and/or volcanic structures to Eocene and younger crustal-scale terrane-bounding structures (Richards, 1976; Diakow et al., 1993, 2006; Diakow, 2001; Legun, 2001; Evenchick et al., 2007; Ootes et al., 2020a),

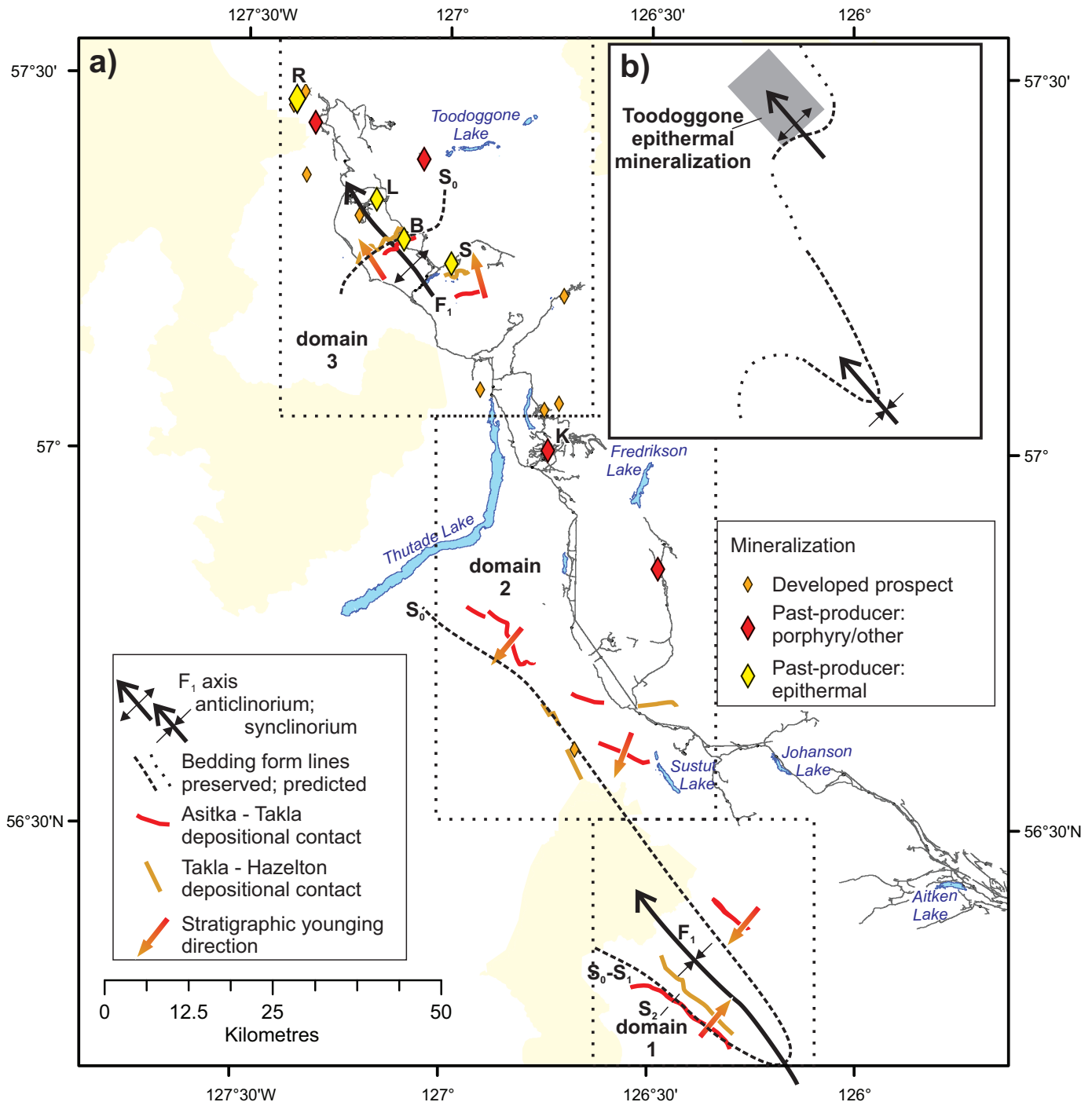


**Fig. 3. a)** Simplified geology from Figure 2 highlighting stratigraphic younging directions with a synclinorium in domain 1 and an anticlinorium in domain 3 (northern Toodoggone area) that are linked by a long southwest-younging limb (domain 2). Stratigraphic younging and structural interpretations in domain 1 are from Ootes et al. (2020a, b), in domain 2 from Richards (1976), Diakow (2001), and Legun (2001), and domain 3 from Diakow et al. (1993, 2006) and this study. B-Baker mine; L-Lawyers mine; K-Kemess mine; R-Ranch project (Thesis mine); S-Shasta mine. **b)** Sketch of fold relationships in eastern Stikinia based on stratigraphic younging directions in 3a, and highlighting the coincidence of the anticlinorium in domain 3 with epithermal Au-Ag±Cu mineralization.

unconformities can be used as form lines to define regional stratigraphic younging (Fig. 2). Eastern Stikinia is underlain by the Asitka Group (Carboniferous-Permian; equivalent to the Stikine assemblage in western Stikinia), the Takla Group (Upper Triassic; equivalent to the Stuhini and Lewes River

Group in western and northern Stikinia), the Hazelton Group (Lower Jurassic), and felsic to mafic intrusions (Late Triassic to Early Jurassic; Fig. 2; Table 1). The eastern exposures of Stikinia are in fault contact with the Quesnel and Cache Creek terranes; to the west, Stikinia is overlain by the Bowser Lake

**Table 1.** Supracrustal units of eastern Stikinia. See Figures 2-3 for informal structural domains.

Supracrustal stratigraphy of eastern Stikinia

Structural domain	Group*	Formation	Stratigraphic age	Stratigraphic age (Stage)	Numerical age Circa (Ma)	Description	Source
3 (northern Toodoggone)	Hazelton	Toodoggone	Lower Jurassic	Sinemurian	198 to 192	felsic-intermediate flows and felsic tuff, conglomerate	3
	Takla	-	Upper Triassic	-	-	mafic volcanic and related sandstone and siltstone	3
	Asitka	-	Late Carboniferous to Lower Permian	-	-	limestone, chert, tuff	3
2 (southeast of Kemess mine area)	Hazelton	Toodoggone	Lower Jurassic	Hettangian to Sinemurian	201 to 190	felsic-intermediate flows and epiclastic sandstone and conglomerate	4
	Takla	-	Upper Triassic	-	-	mafic volcanic and related sandstone and conglomerate, local mudstone	2, 4
	Asitka	-	Middle Pennsylvanian	Moscovian	309	chert, limestone, mafic and intermediate flows, felsic tuff	4
2 (northeast of Sustut Provincial Park)	Hazelton	Telkwa	Lower Jurassic	Sinemurian	-	mudstone, epiclastic sandstone and conglomerate	1, 5
	Takla	Moosevale	Norian	Norian	-	mafic-intermediate sandstone, conglomerate, breccia	2, 5
	Takla	Savage Mountain	Carnian	Carnian	-	mafic volcanic breccia and pillow lava	2, 5
	Takla	Dewar	Carnian	Carnian	-	siltstone, mafic sandstone and conglomerate	2, 5
	Asitka	-	Permian (Cisuralian)	-	-	chert, tuff, shale, volcanic, and carbonate	2, 5
1 (southeast of Sustut Provincial Park)	Hazelton	Telkwa	Lower Jurassic	Sinemurian	196	mudstone, epiclastic sandstone and conglomerate	1, 6
	Takla	±Savage Mountain	Upper Triassic	Carnian	-	mafic volcanic breccia and pillow lava	2
	Takla	Dewar	Upper Triassic	Carnian	-	siltstone, mafic sandstone and conglomerate	2, 6
	Asitka Group	-	Permian (Cisuralian)	Asselian-Sakmarian	290	phyllite, chert, intermediate and felsic volcanic	6

\*Takla Group is considered equivalent to Stuhini and Lewes River groups in other parts of Stikinia

Thick black lines between groups represent unconformities

- 1 - Tipper and Richards, 1976
- 2 - Monger and Church, 1977; Monger, 1977
- 3 - Diakow et al., 1993, 2006
- 4 - Diakow, 2001
- 5 - Legun, 2001
- 6 - Ootes et al., 2022

and Sustut groups (Late Jurassic to Cretaceous; Figs. 1 and 2; Lord, 1948; Monger and Church, 1977; Richards, 1976; Tipper and Richards, 1976; Monger, 1977; Diakow, 2001; Diakow et al., 1993, 2006; Legun, 2001a; Evenchick et al., 2007; Ootes et al., 2020a, b, 2022).

In structural domain 1 southeast of Sustut Provincial Park (Fig. 2; Table 1), the Asitka Group is mostly deep-water mudstones (now phyllites) with lesser chert and minor volcanic rocks that are unconformably overlain by thick bedded mafic clast-bearing sandstones, interbedded argillite, and lesser cobble conglomerates of the Dewar Formation (Takla Group). In that area, rocks of the Dewar Formation are in direct contact with unconformably overlying phyllitic mudstones and epiclastic conglomerates of the Telkwa Formation (Hazelton Group; Ootes et al., 2020a, b, 2022). To the north, in structural domain 2 east of Thutade Lake, intervening Takla Group units (Moosevale and Savage Mountain formations) are variably preserved and overlain by undivided Hazelton Group rocks (Fig. 2; Table 1; Richards, 1976; Diakow, 2001; Legun, 2001). In structural domain 3 in the Toodoggone area (Fig. 2; Table 1), the Asitka Group is predominantly platformal fossiliferous carbonate rocks that are overlain by pyritic siltstones and massive mafic volcanic rocks of the Takla Group. At the base of the Toodoggone Formation is a locally preserved unit of polymitic conglomerate and interbedded sandstone, a few metres thick, that is overlain by massive intermediate volcanic flows and tuffaceous rocks of the Toodoggone Formation (Hazelton Group) and its members (Diakow et al., 1993; 2006). In summary, the Asitka-Takla and Takla-Hazelton depositional contacts are unconformities.

## 2.2. Structural framework

Regional younging directions, from domain 1 in the south to domain 3 in the north, appear to preserve a northwest-striking and plunging, northeast-vergent synclinorium-anticlinorium pair linked through domain 2 by a long (ca. 100 km) northwest-striking, southwest-younging limb (Figs. 2, 3). The dashed lines on Figure 3b are idealized bedding formlines defined by unconformities; the dotted lines are predictions of where the formlines may have continued, but are not readily apparent due to structural dismemberment or from being hidden by overlying stratigraphic units. Notably, the epithermal Au-Ag±Cu mineralization in the northwestern Toodoggone area appears to fall along the axial surface trace of the domain 3 anticlinorium (Figs. 2, 3).

### 2.2.1. Structural domain 1

Large-scale younging defines a synclinorium in structural domain 1, southeast of Sustut Provincial Park (Figs. 2, 3). In the southwestern part, rocks young to the northeast, from lowermost Asitka Group, Takla Group (Dewar Formation), and Hazelton Group (Telkwa Formation; Fig. 2). In the northeastern part, units young to the southwest, from the Asitka Group to the Takla Group; the Takla-Hazelton group contact is interpreted as a thrust fault in this area (Fig. 2). The Asitka Group contains

a strong first-generation foliation ( $S_1$ ) that is parallel to compositional layering, with bedding in less competent layers transposed into the foliation. The Takla and Hazelton groups also contain this  $S_1$  fabric although it is less strongly developed and bedding is better preserved (Ootes et al., 2020b). The  $S_1$  parallels the unconformities as well as the predicted fold axis for domain 1, implying that the synclinorium is a first-generation fold ( $F_1$ ; Fig. 3). The opposite stratigraphic younging directions and the axial planar  $S_1$  indicate that domain 1 records a northwest striking and plunging  $F_1$  synclinorium (Figs. 2, 3). In the same area, a northeast-striking second-generation foliation ( $S_2$ ) is nearly perpendicular to and kinks the  $S_0$ - $S_1$  (Ootes et al., 2020b). It is likely that this  $S_2$  fabric is related to the Cretaceous Skeena fold belt (e.g., Evenchick, 2001).

### 2.2.2. Structural domain 2

Structural domain 2 was not directly investigated in the current reconnaissance and geological contacts and structural measurements were extracted from mapping by Richards (1976), Diakow (2001), and Legun (2001). From the eastern side of the domain 1 north to Thutade Lake, folds are common in each stratigraphic unit but, overall, the stratigraphy youngs to the southwest (Fig. 2). Stratigraphic units include the Asitka Group, Takla Group (Dewar Formation and subdivisions of the Moosevale and Savage Mountain formations), and the Hazelton Group (subdivisions of the Telkwa Formation; Table 1). Farther north, east, and south of the Kemess mine area, Asitka Group and Takla Group are only preserved in structural contact (Diakow, 2001; Legun, 2001).

### 2.2.3. Structural domain 3 (northern Toodoggone region)

Between domains 2 and 3, stratigraphic contacts of major supracrustal units are not exposed. However, in domain 3 near the Lawyers, Baker, and Shasta mines in the northwestern Toodoggone area, the stratigraphic sequence is well-preserved, younging to the north-northwest, from Asitka Group to Stuhini Group to Hazelton Group (Figs. 2-4). The base of the lowest preserved Asitka Group stratigraphic unit is intruded by the Black Lake intrusive suite (Early Jurassic, 200 to 190 Ma; Fig. 4; Diakow et al., 1993, 2006; Bouzari et al., 2019). The Stuhini Group overlies the Asitka Group and is predominantly tan-rust-weathering pyritic siltstone that is ubiquitous throughout the Toodoggone region. Locally preserved basalts with pyroxene phenocrysts provide diagnostic evidence of the Takla Group (Monger, 1977; Monger and Church, 1977; Diakow et al., 1993). Stratigraphically above this is the Hazelton Group (Fig. 4), which is mostly felsic-intermediate flows and felsic tuffs of the Toodoggone Formation (Diakow et al., 1993, 2006). Unlike the domain 1 area to the south, penetrative deformation fabrics are rare.

## 3. Epithermal mineralization and relationship to folds in the northern Toodoggone region

The northern Toodoggone area (domain 3) contains past-producing epithermal Au-Ag±Cu mineralization (e.g., Shasta,

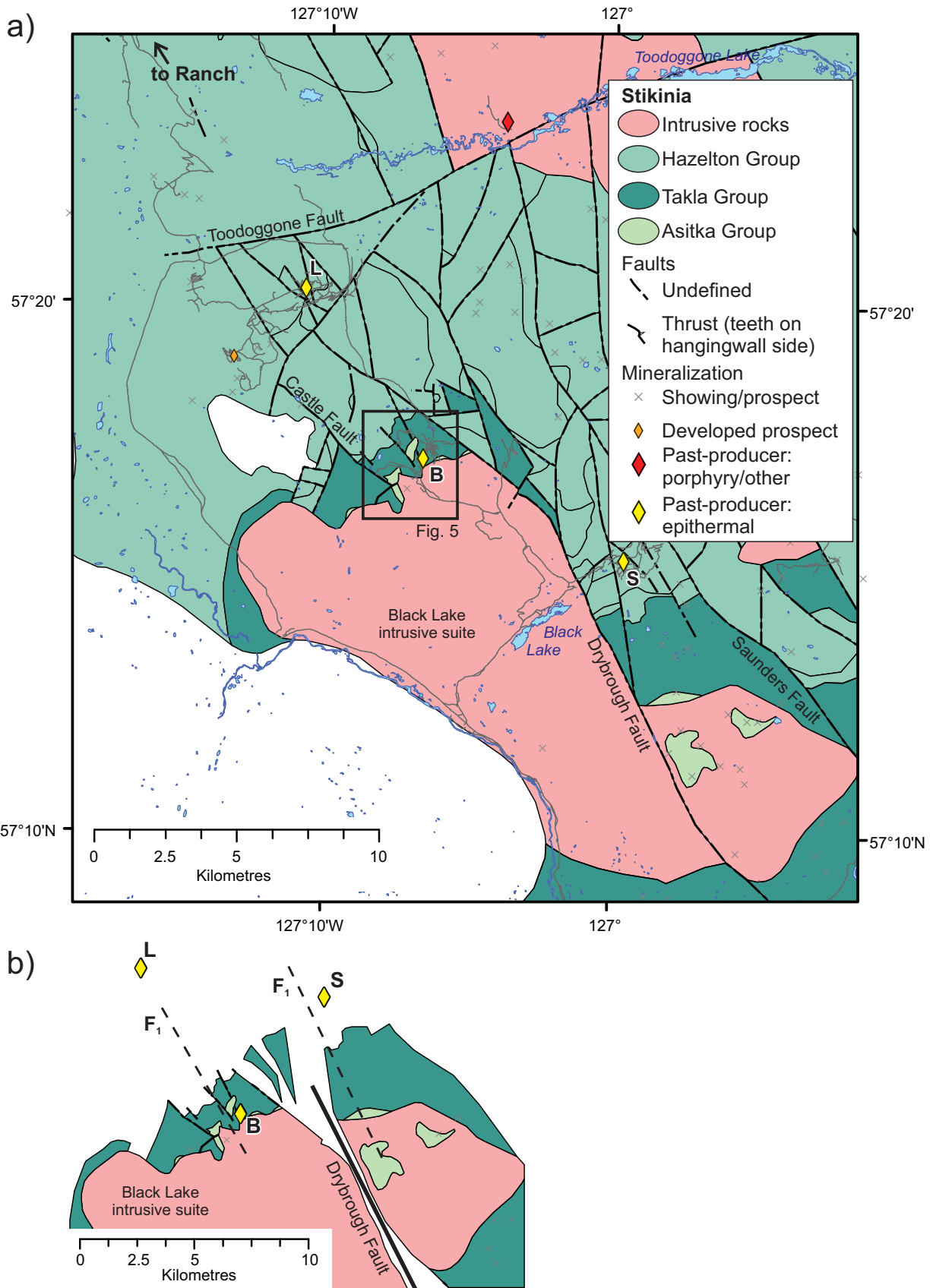


**Fig. 4. a)** Geology of the northern Toadoggone region, simplified after Diakow et al. (1993, 2006). B-Baker mine; L-Lawyers mine; S-Shasta mine. **b)** Simplified reconstruction across the Drybrough fault, showing potential locations of epithermal mineralization before dextral faulting.

Baker, Lawyers) and a number of advanced prospects and showings (Figs. 2, 3). The Baker deposit is hosted in the Asitka and Takla groups close to the contact of the Black Lake intrusive suite, which roughly parallels the overall supracrustal contacts (Figs. 4, 5). The Baker deposit is considered intermediate-sulphidation and has high-fluid temperature ( $>300^{\circ}\text{C}$ ) and salinity characteristics that are consistent with a genetic link to an underlying magmatic system (Duuring et al., 2009; Bouzari et al., 2019). The Shasta and Lawyers deposits are more distal from the intrusions and hosted in the Toodoggone Formation (Hazelton Group; Fig. 4). The Baker and Shasta mines are separated by the Drybrough fault (dextral); reconstructing units along the fault indicates that the Shasta and Lawyers deposits may have formed in similar stratigraphic and structural positions (Fig. 4b). The mineralization at Shasta and Lawyers is considered low-sulphidation, with low mineralization temperatures (ca.  $200^{\circ}\text{C}$ ) and salinities that are most consistent with meteoric or metamorphic fluids (Duuring et al., 2009), possibly a reflection of distance from the Black Lake suite intrusive contact (Fig. 4b).

More detailed aspects of the domain 3 anticlinorium described above are preserved in the Baker mine area where northwest plunging folds are exposed (Fig. 5). Southwest of the mine site, bedding in the Asitka Group strikes southeast and dips west ( $160^{\circ}/50^{\circ}$ ). Adjacent to the mine site, bedding strikes northwest and dips east ( $340^{\circ}/45^{\circ}$ ). East of the mine site, bedding strikes west and dips north ( $260^{\circ}/70^{\circ}$ ). The unconformity with the overlying Takla Group parallels bedding. The Black Lake suite intrusive contact is only preserved in Asitka Group outcrops in the southwest and east on Figure 5, and its trace under surficial cover is speculated (Fig. 5a). In general, the Takla-Hazelton group unconformity parallels Asitka-Takla group relationships (Figs. 2, 3, 4a).

Epithermal mineralization in domain 3 is distributed along the axial trace of the regional anticlinorium (Fig. 3) and in the hinge zone, perpendicular to stratigraphic and intrusive contacts (Fig. 4b). Zones of extension related to folding mechanisms are well-understood (e.g., Cosgrove, 2015), and this hinge location is consistent with zones of dilation and fluid flow for mineralization. This geometry suggests a twofold causal relationship. First, positioned in the hinge zone of the anticlinorium, the Black Lake intrusion may have been emplaced during folding using volume created by extension in the outer arc of the fold. Second, hydrothermal fluids generated by magma exsolution may have migrated into overlying supracrustal units along similar shallow-level space-accommodating brittle faults, precipitating Au-Ag $\pm$ Cu epithermal mineralization at high crustal levels, both in the hinge zone and downplunge along the axial trace. Tied to a unique structure, this hypothesis would explain why epithermal mineralization appears to be unique to the northern Toodoggone area and lacking elsewhere in eastern Stikinia (Figs. 2, 3).

#### 4. A test: Timing of deformation and mineralization

If the relationships between deformation and mineralization

presented above are correct, they should coincide with the crystallization age of at least one phase of the Black Lake intrusive suite. South of the epithermal mineralization, near the Kemess mine (Figs. 2, 3), different intrusive suites and sub-phases are recognized and dated. For example, the phase that hosts the Kemess porphyry deposit is dated at ca. 200 Ma (U-Pb zircon; Re-Os molybdenite; Diakow, 2001; Duuring et al., 2009). In the Baker epithermal mineralization area (Fig. 4), molybdenite in a quartz-feldspar porphyry has yielded a  $194 \pm 0.8$  Ma Re-Os date (Bouzari et al., 2019). Individual intrusive phases of the Black Lake suite have not been separated and the U-Pb zircon ages that have been reported (Diakow et al., 1993; Bouzari et al., 2019) are too imprecise to resolve the relationships between intrusive phases and mineralization. North of the Baker mine and immediately above the Takla Group, Toodoggone Formation volcanic rocks yielded an Ar-Ar age of  $194.2 \pm 0.4$  Ma (Diakow et al., 2006), which improved upon a previously reported  $193 \pm 2.7$  Ma age (K-Ar) from the same location (Diakow et al., 1993). A statistically indistinguishable Ar-Ar age determination of  $193.8 \pm 2.6$  Ma was reported from the Shasta mine area, but was interpreted as a cooling age of the alteration assemblage associated with epithermal mineralization (Diakow et al., 2006). In general, ca. 200 to ca. 185 Ma Ar-Ar and lesser U-Pb zircon volcanic crystallization age determinations are consistent throughout the Toodoggone Formation (Diakow, 2001; Diakow et al., 2006; Duuring et al., 2009). The Lawyers epithermal deposit is hosted in a volcanic unit that is stratigraphically above the Toodoggone Formation flow dated at ca. 194 Ma, thus mineralization at Lawyers has to be younger than ca. 194 Ma.

Duuring et al. (2009) compiled available age data from the entire Toodoggone region and showed that the epithermal mineralization at Lawyers and Shasta may be younger than the Baker mineralization. However, some of the age determinations in that compilation were from outdated techniques (e.g., K-Ar) and the accuracy and precision of these determinations are difficult to assess. Bouzari et al. (2019) presented U-Pb zircon results derived from LA-ICP-MS (laser ablation inductively coupled plasma-mass spectrometry); the reported uncertainties ( $\sim \pm 2$  Ma) are significant underestimates because they are derived from weighted means of single zircons with  $>20$  million year ranges, with individual uncertainties  $\pm 10$  Ma ( $2\sigma$ ). These results are far less precise than U-Pb zircon dating by CA-IDTIMS (chemical abrasion isotope dilution thermal ionization mass spectrometry) that routinely generate dates with uncertainty less than 0.5 Ma ( $2\sigma$ ).

The critical chronological test now rests with new modern U-Pb zircon dates (CA-IDTIMS) from the intrusive phases of the Black Lake suite and Ar-Ar laser step-heating dates from alteration mineral assemblages associated with epithermal mineralization at Baker, Lawyers, Shasta, and other deposits in the area. Because mineralization at Lawyers and Shasta appears to have been deposited from relatively low-temperature fluids (ca.  $200^{\circ}\text{C}$ ; Duuring et al., 2009) and because Ar-Ar laser step-heating dating is only appropriate for higher

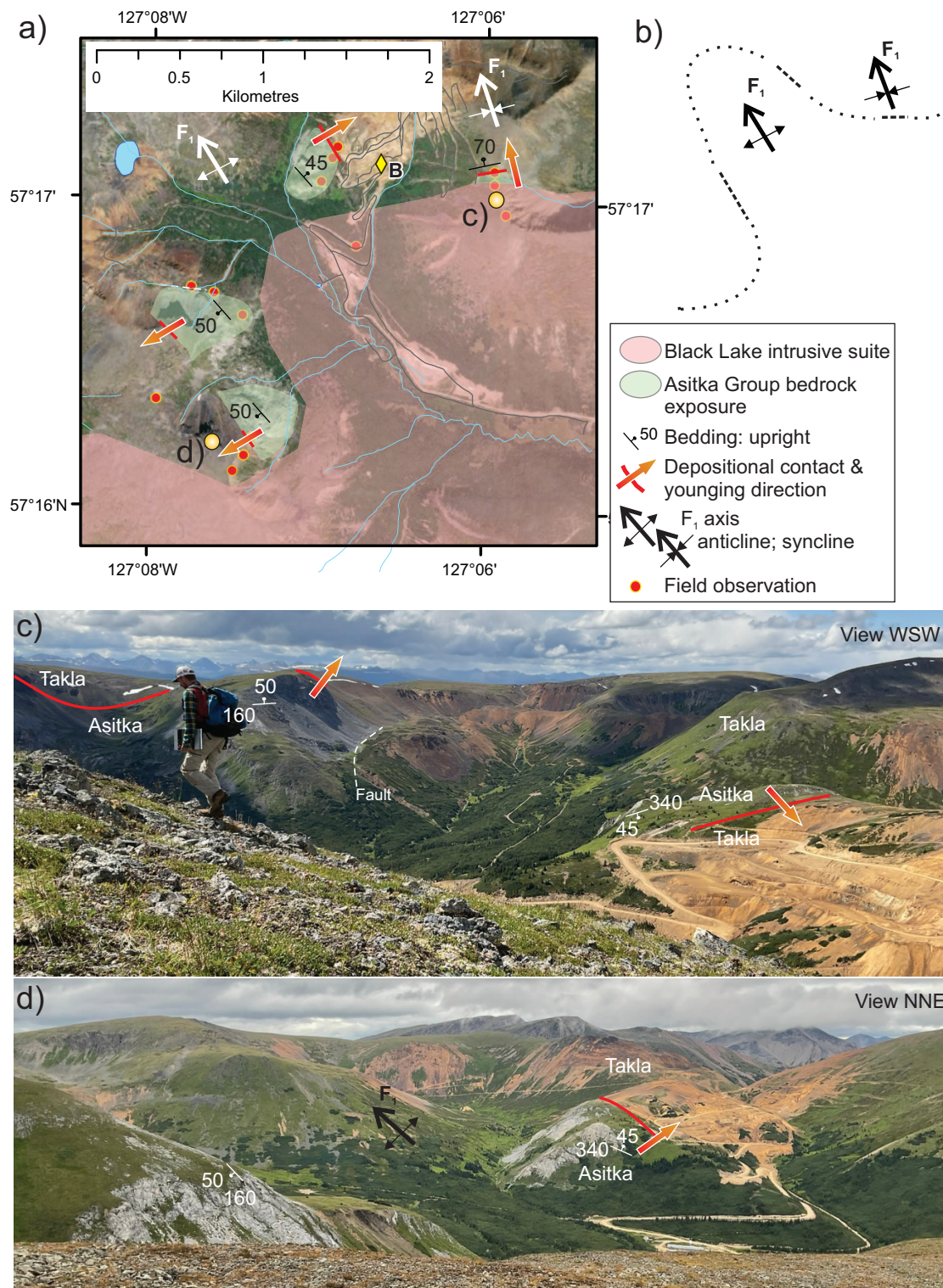


**Fig. 5.** Folds in the northern Toodoggone area from observations near Baker mine (see Fig. 4 for location). **a)** Geology near Baker mine (B) showing Asitka Group outcrops, bedding orientations, and contacts with overlying Takla Group and younging directions. Yellow dots refer to the photograph location in c) and d). **b)** Sketch of fold relationships in the Baker mine area based on bedding in the Asitka Group and younging directions. **c)** Perspective view looking west-southwest toward the Baker mine. Note the possible disruption of stratigraphy where a fault is interpreted in the centre-left of the photograph, preserving Takla Group topographically below Asitka Group exposures. It remains possible that these outcrops are part of the Asitka Group. Bedding in Asitka Group carbonate rocks (grey cliff-forming outcrops) dips in opposite directions on either side of the valley. Younging direction is upright at both locations, indicating that a north-plunging anticline underlies the valley. **d)** Perspective view looking north-northeast showing exposure of Asitka and Takla groups rocks and interpreted northwest striking, north plunging  $F_1$ . Roads and workings in both photographs are part of the past-producing Baker mine.

temperatures  $>350^{\circ}\text{C}$ , low-temperature thermochronological tools (e.g., zircon/apatite fission track and U-Th/He) may be required, while acknowledging that the necessary accuracy and precision may be lacking and the possibility of post-mineralization resetting is high.

## 5. Conclusion

Stratigraphic younging directions in eastern Stikinia reveal a large-scale, northwest-striking and plunging, northeast-vergent synclinorium-anticlinorium pair connected by a long (ca. 100 km) westward-younging limb. The northern Toodoggone region hosts several past-producing epithermal Au-Ag±Cu deposits and numerous prospects, lacking elsewhere in eastern Stikinia. In northern Toodoggone, the Black Lake intrusive suite coincides with the hinge zone of the anticlinorium and epithermal mineralization is aligned along its axial trace. Reconstruction of the Drybrough fault supports that the Lawyers and Shasta mines developed more distant and higher in the stratigraphy than the Black Lake suite intrusive contact, whereas the Baker mine is more proximal. Folding, emplacement of the Black Lake intrusive suite, and epithermal mineralization may be co-genetic, a hypothesis that may explain the uniqueness of epithermal mineralization to the Toodoggone region of eastern Stikinia and that can be tested by high-precision geochronology.

## Acknowledgments

This project benefited from field assistance from Alan West. TDG Gold Corp. provided access to the Baker and Shasta properties and Benchmark Metals provided access to Lawyers and Ranch and provided accommodations and logistical support at Lawyers camp. Emily Laycock and Rob L'Heureux (Apex Geosciences) provided valuable knowledge about the geology and mineralization at Lawyers and vicinity. Constructive reviews and comments by C. Greig and R. Greig helped improve the paper.

## References cited

- Bouzari, F., Bissig, T., Hart, C.J.R., and Leal-Mejia, H., 2019. An exploration framework for porphyry to epithermal transitions in the Toodoggone mineral district (94E). *Geoscience BC Report* 2019-08, 105 p.
- Colpron, M., 2020. Yukon Terranes-A digital atlas of terranes for the northern Cordillera. Yukon Geological Survey. <<https://data.geology.gov.yk.ca/Compilation/2#InfoTab>> (accessed April 2021).
- Cosgrove, J.W., 2015. The association of folds and fractures and the link between folding, fracturing and fluid flow during the evolution of a fold-thrust belt: a brief review. In: Richards, F.L., Richardson, N.J., Rippington, S.J., Wilson, R.W., and Bond, C.E., (Eds.), *Industrial Structural Geology: Principles, Techniques, and Integration*. Geological Society, London, Special Publications, 421. <<http://dx.doi.org/10.1144/SP421.11>>
- Diakow, L.J., 2001. Geology of the southern Toodoggone River and northern McConnell Creek map areas, north-central British Columbia: Parts of NTS 94E/2, 94D/15 and 94D/16. British Columbia Ministry of Energy and Mines, British Columbia Geological Survey Geoscience Map 2001-1, scale 1:50,000.
- Diakow, L.J., Panteleyev, A., and Schroeter, T.G., 1993. Geology of the early Jurassic Toodoggone Formation and gold-silver deposits in the Toodoggone River map area, northern British Columbia. British Columbia Ministry of Energy, Mines and Petroleum Resources, British Columbia Geological Survey Bulletin 86, 72 p.
- Diakow, L.J., Nixon, G.T., Rhodes, R., and van Bui, P., 2006. Geology of the Central Toodoggone River map area, north-central British Columbia (Parts of NTS 94E/2, 6, 7, 10 and 11). British Columbia Ministry of Energy, Mines and Petroleum Resources, British Columbia Geological Survey Geoscience Map 2006-6, scale 1:50,000.
- Duuring, P., Rowins, S.M., McKinley, B.S.M., Dickinson, J.M., Diakow, L.J., Kim, Y.-S., and Creaser, R.A., 2009. Examining potential genetic links between Jurassic porphyry Cu-Au±Mo and epithermal Au±Ag mineralization in the Toodoggone district of North-Central British Columbia, Canada. *Mineralium Deposita*, 44, 463-496.
- Evenchick, C.A., 1991. Structural relationships of the Skeena Fold Belt west of the Bowser Basin, northwest British Columbia. *Canadian Journal of Earth Sciences*, 28, 973-983.
- Evenchick, C.A., 2001. Northeast-trending folds in the western Skeena Fold Belt, northern Canadian Cordillera: A record of Early Cretaceous sinistral plate convergence. *Journal of Structural Geology*, 23, 1123-1140.
- Evenchick, C.A., Mustard, P.S., McMechan, M., Ferri, F., Porter, S., Hadlari, T., and Jakobs, G., 2007. Geology, McConnell Creek, British Columbia. Geological Survey of Canada Open File 5571. British Columbia Ministry of Energy, Mines and Petroleum Resources, Petroleum Geology Open File 2007-10, scale 1:125,000.
- Legun, A.L., 2001. Geology of the southern McConnell Range and Sustut River area, British Columbia, parts of NTS 94D/3, 7, 9, 10, 15, 16. British Columbia Ministry of Energy and Mines, British Columbia Geological Survey Open File Map 2001-18, scale 1:50,000.
- Lord, C.S., 1948. McConnell Creek map-area, Cassiar District, British Columbia. Geological Survey of Canada Memoir 251, 82 p.
- Monger, J.W.H., 1977. The Triassic Takla Group in McConnell Creek map-area, north-central British Columbia. Geological Survey of Canada Paper 76-29, 45 p.
- Monger, J.W.H., and Church, B.N., 1977. Revised stratigraphy of the Takla Group, north-central British Columbia. *Canadian Journal of Earth Sciences*, 14, 318-326.
- Ootes, L., Bergen, A.L., Milidragovic, D., and Jones, G.O., 2020a. Bedrock geology of the northern Hogem batholith and its surroundings, north-central British Columbia. British Columbia Ministry of Energy, Mines and Petroleum Resources, British Columbia Geological Survey Open File 2020-02, scale 1:50,000.
- Ootes, L., Bergen, A.L., Milidragovic, D., Jones, G.O., Camacho, A., and Friedman, R., 2020b. An update on the geology of northern Hogem batholith and its surroundings, north-central British Columbia. In: *Geological Fieldwork 2019*, British Columbia Ministry of Energy, Mines and Petroleum Resources, British Columbia Geological Survey Paper 2020-01, pp. 25-47.
- Ootes, L., Milidragovic, D., Friedman, R., Wall, C., Cordey, F., Luo, Y., Jones, G., Pearson, D.G., and Bergen, A., 2022. A juvenile Paleozoic ocean floor origin for eastern Stikinia, Canadian Cordillera. *Geosphere*, 18. <<https://doi.org/10.1130/GES02459.1>>
- Richards, T.A., 1976. McConnell Creek map-area (94D), east half, British Columbia. Geological Survey of Canada Paper 76-1A, pp. 43-50.
- Tipper, H.W., and Richards, T.A., 1976. Jurassic stratigraphy and history of north-central British Columbia. *Geological Survey of Canada Bulletin* 270, 73 p.



# Update on bedrock mapping in the Kitsault River area, northwestern British Columbia



Emily A. Miller<sup>1,a</sup>, Bram I. van Straaten<sup>1</sup>, and Rebecca C. Hunter<sup>1,2</sup>

<sup>1</sup>British Columbia Geological Survey, Ministry of Energy, Mines and Low Carbon Innovation, Victoria, BC, V8W 9N3

<sup>2</sup>Now at: Forum Energy Metals Corp., Suite 615, 800 West Pender Street, Vancouver, BC, V6C 2V6

<sup>a</sup>corresponding author: Emily.X.Miller@gov.bc.ca

Recommended citation: Miller, E.A., van Straaten, B.I., and Hunter, R.C., 2023. Update on bedrock mapping in the Kitsault River area, northwestern British Columbia. In: Geological Fieldwork 2022, British Columbia Ministry of Energy, Mines and Low Carbon Innovation, British Columbia Geological Survey Paper 2023-01, pp. 23-32.

## Abstract

The Kitsault River area in northwestern British Columbia hosts Ag-rich volcanogenic massive sulphide (VMS), Au-rich epithermal, and Cu-Au porphyry systems. Resolving the distribution, age, and affinity of prospective Stuhini and Hazelton Group host rocks is key to understanding the metallogeny and mineral potential of the area. Geological mapping of the northeastern portion of the Kitsault River area shows that mafic volcanic and sedimentary rocks of the Stuhini Group (Upper Triassic) are conformably overlain by Hazelton Group rocks (uppermost Triassic to Middle Jurassic). The lower part of the Hazelton Group consists mainly of intermediate volcanic rocks, lesser sedimentary rocks, and rare felsic volcanic rocks of the Betty Creek Formation (uppermost Triassic to Lower Jurassic). In the centre of the map area, the basal Hazelton Group comprises conglomerate and megaconglomerate (with clasts up to 120 m) of the Kinskuch unit (Rhaetian), which record deposition in a local syndepositional fault-bounded basin. The Kinskuch unit is overlain by intermediate volcanic rocks of the Betty Creek Formation. The Kinskuch unit and basal Betty Creek Formation are cut by the Big Bulk stock (latest Triassic), which hosts the coeval Big Bulk porphyry Cu-Au prospect. The upper part of the Hazelton Group (Lower to Middle Jurassic) consists of thin Spatsizi Formation sedimentary rocks that are overlain by intermediate, mafic, and felsic volcanic rocks of the Kitsault unit, which host the Dolly Varden Ag-rich VMS deposits. The Kitsault unit is only found in the northern part of the map area and appears to transition eastward to an unnamed sedimentary unit with common tuff beds. Within northwestern British Columbia, the Kitsault unit is prospective for Dolly Varden-style Ag-rich VMS mineralization.

**Keywords:** Kitsault River, Stikinia, Hazelton Group, Stuhini Group, Kinskuch unit, Betty Creek Formation, Spatsizi Formation, Kitsault unit, Quock Formation, Bowser Lake Group, Late Triassic, Jurassic, porphyry, VMS, Golden Triangle, silver, gold, copper

## 1. Introduction

Northwestern British Columbia is host to significant porphyry, epithermal, and volcanogenic massive sulphide (VMS) precious and base metal deposits (Figs. 1, 2), including Schaft Creek, Galore Creek, Red Chris, KSM, Red Mountain, Premier, Snip and Bronson slope. Particularly significant in the metallogeny of the region are latest Triassic to Jurassic volcano-sedimentary rocks of the Hazelton Group and coeval plutonic rocks (Nelson et al., 2013; Logan and Mihalynuk, 2014). Most of the Mesozoic VMS mineralization in Stikinia, including the Eskay Creek and Anyox deposits, is hosted in rift-related rocks of the Iskut River Formation (Lower to Middle Jurassic) in the upper part of the Hazelton Group (Gagnon et al., 2012; Nelson et al., 2013, 2018). Recent geochronological studies in the Kitsault River area have shown that rocks hosting the Dolly Varden VMS deposits are in the upper part of the Hazelton Group and coeval with volcanism in the Eskay rift (Hunter and van Straaten, 2020; Hunter et al., 2022).

As part of a multi-year project, ongoing detailed bedrock mapping in the Kitsault River area is directed at resolving the age and affinity of latest Triassic to Middle Jurassic Hazelton Group rocks and testing regional Hazelton Group correlations. Establishing the stratigraphic, magmatic, structural, and

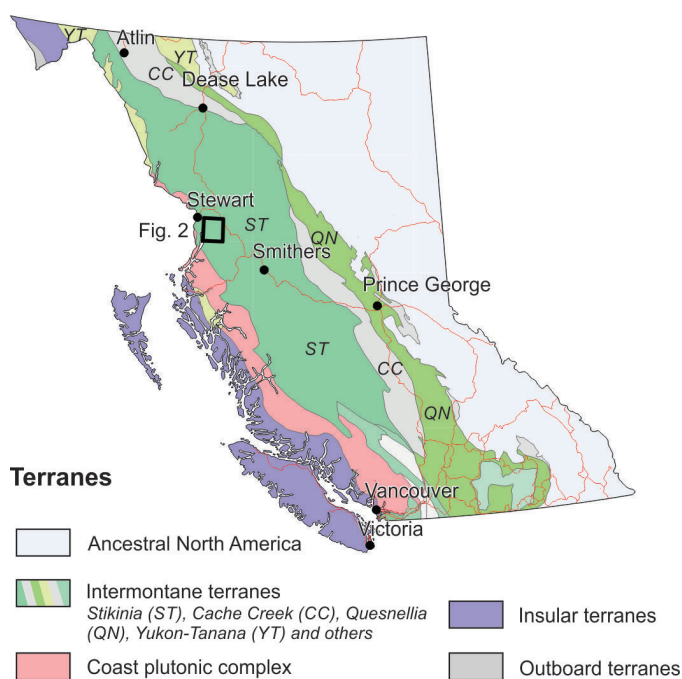


**Fig. 1.** Location of the Kitsault River area with respect to terranes of British Columbia (after Colpron and Nelson, 2011).

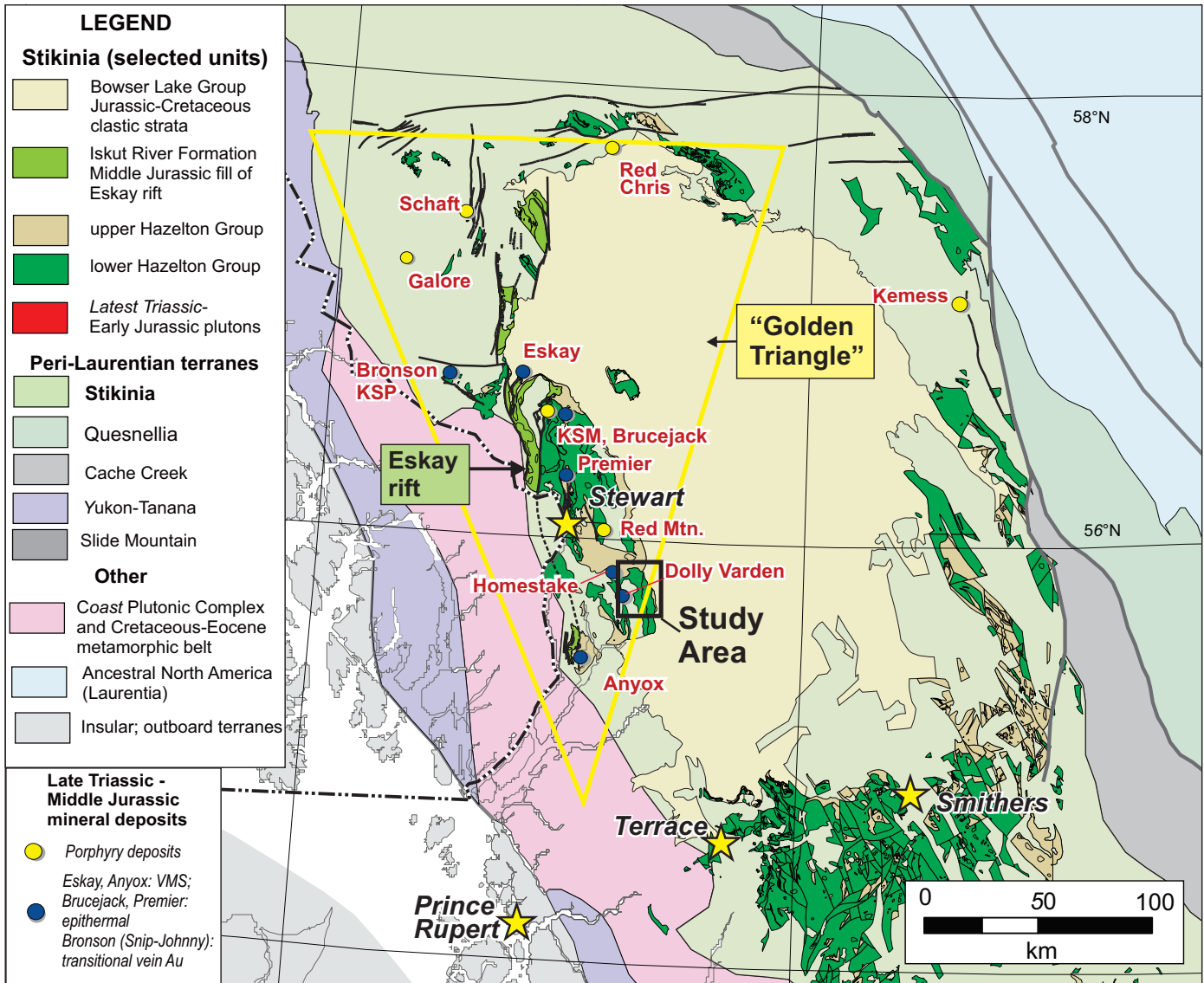


Fig. 2. Regional geological setting (after Alldrick et al., 1986; Greig, 1992; and Colpron and Nelson, 2011), with selected mineral deposits (red dots). After Nelson et al., 2022.

chronological framework of rocks in the Kitsault River area will help in better understanding the distribution of mineral deposits in northwestern British Columbia. Based on fieldwork in 2022, we present a new preliminary map and extended legend of the northeastern part of the Kitsault River area that builds on and incorporates historical mapping by Alldrick et al. (1986), Devlin (1987), Greig et al. (1994), and Evenchick et al. (2008), our previous work (Hunter and van Straaten, 2020; Hunter et al., 2022a, b), detailed mapping of the Kinskuch Lake area (Miller et al., 2020), and property-scale mapping by Dolly Varden Silver Corporation (unpublished data). We recognize a conformable contact between Stuhini Group and overlying Hazelton Group, record the lithological variation in the Hazelton Group, and show that the upper part of the Hazelton Group comprises a local volcanic unit that is prospective for Ag-rich VMS systems.

## 2. Regional geological and metallogenic setting

The Kitsault River area is along the west-central margin of the Stikine terrane (Stikinia), in the Intermontane belt of the Canadian Cordillera (Fig. 1), in the traditional lands of the Nisga'a, Gitanyow, Tsetsaut Skii Km Lax Ha, and Metlakatla First Nations. It is at the southern end of a region popularly referred to as the 'Golden Triangle', which is a loosely defined area that includes most of the major gold, copper, and silver deposits in west central Stikinia (Fig. 2). The region is underlain primarily by arc-related volcano-sedimentary rocks of the Stuhini Group (Late Triassic) and Hazelton Group (Jurassic), which are overlain by the Bowser Lake Group (Middle Jurassic) in the east and bounded by Eocene intrusions of the Coast Plutonic complex (Nelson et al., 2013) in the west.

The Stuhini Group comprises augite-phyric mafic volcanic rocks and sedimentary rocks that are generally unconformably

overlain by the Hazelton Group (e.g., Kyba and Nelson, 2014; Nelson et al., 2018), although in parts of the Kitsault River area the Stuhini to Hazelton Group transition is gradational (see below). Basal rocks in the lower part of the Hazelton Group include sandstones and conglomerates including those of the Jack Formation (Rhaetian to Sinemurian; Nelson et al., 2018) that display evidence of sedimentation controlled by syndepositional faulting (Nelson and Kyba, 2014; Febbo et al., 2019; Miller et al., 2020). These sedimentary rocks are overlain by intermediate volcanic, lesser felsic volcanic and volcanic-derived sedimentary rocks (Rhaetian to Pliensbachian; Betty Creek and Klastline formations; Nelson et al., 2018). The regionally developed Texas Creek plutonic suite (latest Triassic to Early Jurassic) is coeval and comagmatic with volcanic units in the lower part of the Hazelton Group (Nelson et al., 2018). This magmatism is associated with significant latest Triassic to Early Jurassic porphyry copper-gold and related epithermal gold deposits (Fig. 2) including: Red Chris, Red Mountain, Premier, Kerr-Sulphurets-Mitchell-Snowfield-Iron cap and Brucejack. In the Kitsault River map area, the Homestake Ridge deposit (MINFILE 103P 216) is a tabular vein and breccia-hosted Au-Ag-Cu system hosted in Stuhini and Hazelton Group rocks. Mineralization at Homestake Ridge may be coeval with monzonite dikes found to the west of the deposit which returned a  $191.71 \pm 0.20$  Ma U-Pb zircon age (Hunter and van Straaten, 2020).

The upper part of the Hazelton Group (Pliensbachian to Bajocian) contains predominantly post-arc sedimentary rocks of the Spatsizi and Quock formations, felsic volcanic rocks of the Mount Dilworth Formation and local bimodal rift-related volcanic and sedimentary rocks of the Iskut River Formation

(Gagnon et al., 2012; Nelson et al., 2018). Bimodal rift related rocks have not been reported in the Kitsault River study area, but felsic tuffs of roughly equivalent age to the Mount Dilworth Formation ( $173.6 \pm 1.7$  Ma; Cutts et al., 2015) and Iskut River Formation (ca. 179-173 Ma; Nelson et al., 2018 and references therein) have been identified in the Kitsault River valley. The Iskut River Formation is host to several mineral deposits such as VMS-type mineralization at the Au-Ag-rich Eskay Creek and Cu-rich Anyox deposits in the Eskay rift (Fig. 2; Barrett and Sherlock, 1996; Childe, 1996; MacDonald et al., 1996; Roth et al., 1997; Evenchick and McNicoll, 2002). Middle Jurassic to mid-Cretaceous sedimentary rocks of the Bowser Lake Group overlie the Hazelton Group (Evenchick and Thorkelson, 2005; Nelson et al., 2018).

Significant shortening in the Cretaceous resulted in the development of the thin-skinned Skeena fold and thrust belt, which was first recognized and described within the rocks of the Bowser basin (Evenchick, 1991). Northwest- and northeast-trending Skeena folds and thrusts, which display a wide variety of geometries as a function of competency contrast, define the structural style of northern Stikinia (Evenchick, 1991; Evenchick et al., 2007). Initiating in the Late Cretaceous and continuing into the Eocene, significant dextral offset accumulated along large-scale faults that appear to have reactivated pre-existing orogen-parallel structures (Nelson and Kyba, 2014).

### 3. A new geological map of the northeastern Kitsault River area

The oldest rocks exposed in the map area (Fig. 3; Table 1) are part of the Stuhini Group (Upper Triassic). These rocks include

**Table 1.** Summary of U-Pb zircon geochronological data from the northeastern part of the Kitsault River area. See Figure 3 for locations. LA-ICP-MS, laser-ablation inductively coupled plasma mass spectrometry; CA-TIMS, chemical abrasion thermal ionization mass spectrometry; and ID-TIMS, isotope dilution thermal ionization mass spectrometry. References: <sup>1</sup> Mortensen and Kirkham (1992); <sup>2</sup> Greig and Gehrels (1995); <sup>3</sup> Hunter and van Straaten (2020); <sup>4</sup> Miller et al. (2020); and <sup>5</sup> Hunter et al. (2022a, b).

Sample	Age (Ma)	Type	Lithostratigraphic Unit
1	$154.3 \pm 0.9^5$	LA-ICP-MS (detrital)	Bowser Lake Group (muJBs)
2	$168.9 \pm 2.2^3$	LA-ICP-MS (detrital)	Quock Formation (mJHs)
3	$178.1 \pm 2.2^3$	LA-ICP-MS	Kitsault unit (lmJHva)
4	$187.3 \pm 0.8^5$	LA-ICP-MS (detrital)	Spatsizi Formation (lmJHs)
5	$188.1 \pm 0.6^5$	LA-ICP-MS (detrital)	Spatsizi Formation (lmJHs)
6	$193.5 \pm 0.4^1$	ID-TIMS	Betty Creek Formation (lJHvf)
7	$193.93 \pm 0.11^5$	CA-TIMS	Betty Creek Formation (lJHva.xor)
8	$193.98 \pm 0.11^5$	CA-TIMS	Betty Creek Formation (lJHva.xor)
9	$196 +5/-1^2$	ID-TIMS	Betty Creek Formation (lJHvf)
10	$198 +4/-3^2$	ID-TIMS	Betty Creek Formation (lJHva.xor)
11	$198 +8/-7^2$	ID-TIMS	Betty Creek Formation (lJHva)
12	$200.85 \pm 0.15^5$	CA-TIMS	Betty Creek Formation (uTrlJHsv)
13	$204.61 \pm 0.18^4$	CA-TIMS	Texas Creek Plutonic Suite (LTrEJmd)
14	$206.7 \pm 1.9^3$	LA-ICP-MS (detrital)	Betty Creek Formation (uTrlJHva)
15	$228.4 \pm 1.4^3$	LA-ICP-MS (detrital)	Betty Creek Formation (uTrlJHsv)

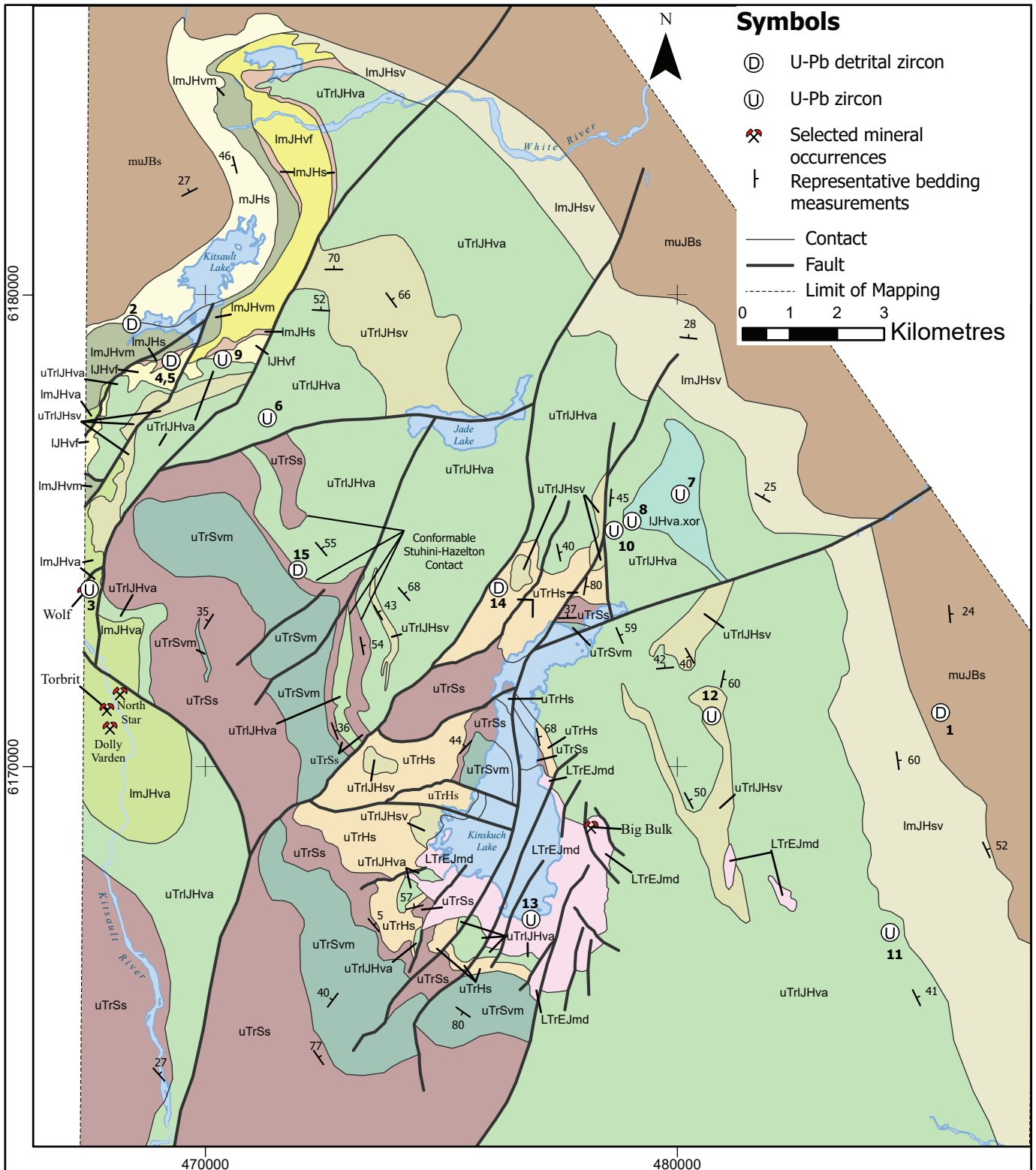


Fig. 3. a) Preliminary geology map of the northeastern part of the Kitsault River area, with locations of geochronological samples listed in Table 1.

**Bowser Lake Group (Middle to Upper Jurassic)**

ImJBS

Grey to brown, well-stratified feldspathic wacke, siltstone and mudstone. Common load casts, flame structures, and mudstone intraclasts. Lesser very thick conglomerate beds locally containing chert granules and pebbles in a coarse sandstone matrix (154.3+/-0.9 Ma U-Pb detrital zircon MDA, Hunter et al., 2022a,b).

**Hazelton Group****upper Hazelton Group****Quock Formation (Middle Jurassic)**

mJHs

Well-stratified dark grey mudstone and siltstone (commonly siliceous) and minor pale-toned tuff laminae. The base of this unit consists of a sandstone interval several m thick containing belemnite casts with 168.9±2.2 Ma U-Pb detrital zircon MDA (Hunter and van Straaten, 2020).

**Unassigned unit (Lower to Middle Jurassic)**

ImJHsv

Mudstone, siltstone, feldspathic wacke, limestone, and fine tuff to lapilli-tuff. Mudstone is commonly siliceous and locally graphitic or carbonaceous. Predominantly laminated to thinly bedded. Locally light brown weathering fine tuff to lapilli-tuff layers, 3-20 cm thick. Rare limestone, sandstone, and conglomerate near the base of the unit in the east.

**Kitsault unit (Lower to Middle Jurassic)**

ImJHvf

Felsic to lesser intermediate volcanic rocks including pale greenish, grey to cream tuff breccia, lapilli-tuff, lapillistone, and crystal tuff. Commonly with plagioclase-phyric volcanic clasts and/or plagioclase crystal-bearing matrix. Locally foliated or with elongate volcanic clasts.

ImJHvm

Mafic volcanic rocks including lapilli-tuff, tuff breccia, and coherent rocks. Volcanic clasts and coherent rocks are augite-plagioclase-phyric. Interstratified with lesser limestone, siltstone, and feldspathic wacke.

ImJHva

Intermediate volcanic rocks including tuff, lapilli-tuff, crystal tuff, and local tuff breccia. Interstratified with volcanic-derived sandstone, reworked tuff, and pebble conglomerate with volcanic and sedimentary clasts. Rare felsic volcanic rocks similar to ImJHvf yielded a 178.1+/-2.2 Ma U-Pb zircon age (Hunter and van Straaten, 2020).

**Spatsizi Formation (Lower to Middle Jurassic)**

ImJHs

Fine- to coarse-grained feldspathic sandstone, pebble wacke, siltstone, and local thin limestone beds (187.3±0.8 and 188.1±0.6 Ma U-Pb detrital zircon MDA, Hunter et al., 2022a, b).

**lower Hazelton Group****Betty Creek Formation (Lower Jurassic)**

JHvf

Light green to grey to maroon-grey felsic lapilli-tuff, crystal tuff and tuff. Locally with quartz, biotite, and K feldspar crystals; rare elongate volcanic clasts or possible flammé up to 2 mm (193.5+/-0.4 Ma U-Pb zircon, Mortensen and Kirkham, 1992; 196+5/-1 Ma U-Pb zircon, Greig and Gehrels, 1995)

JHva\_xor

K feldspar-hornblende-plagioclase-phyric intermediate coherent rocks and K feldspar hornblende plagioclase crystal tuff. K feldspar phenocrysts are commonly aligned along bedding. Interstratified with 100 m-thick lapilli-tuff to tuff breccia intervals with hornblende-plagioclase-phyric volcanic clasts, similar to unit uTrJHva. Local lenticular and discontinuous beds of brown weathering, coarse- to very coarse-grained sandstone (193.93+/-0.11 Ma and 193.98+/-0.11 Ma U-Pb zircon, Hunter et al., 2022a,b; 198+4/-3 Ma, U-Pb zircon; Greig and Gehrels, 1995).

**Texas Creek plutonic suite (Late Triassic to Early Jurassic)****Big Bulk stock**

LTrEJd

Hornblende diorite and lesser biotite-hornblende monzonite stocks and dikes. Hornblende plagioclase porphyritic (1-2 mm) to equigranular (1-5 mm) (204.61+/-0.18 Ma U-Pb zircon, Miller et al., 2020).

**Lower Hazelton Group****Betty Creek Formation (Upper Triassic to Lower Jurassic)**

uTrJHsv

Sedimentary and intermediate volcanic rocks. Well-stratified to locally massive coarse- to fine-grained feldspathic sandstone, siltstone, limestone, and lesser pebble conglomerate. Conglomerate clasts include chert, limestone, and augite-phyric basalt. Intercalated with pale-weathering, well-stratified to locally massive, lapilli-tuff, lapillistone, and tuff breccia with hornblende-plagioclase-phyric volcanic clasts (228.4±1.4 Ma U-Pb detrital zircon MDA; Hunter and van Straaten, 2020; 200.85+/-0.15 Ma U-Pb zircon age, Hunter et al., 2022a, b).

uTrJHva

Intermediate volcanic and coherent rocks. Massive to very thickly bedded (5-100 m) lapilli-tuff, lapillistone, tuff breccia and lesser crystal tuff. With angular to subrounded hornblende-plagioclase-phyric or less common biotite-plagioclase-phyric juvenile volcanic clasts, locally with minor sandstone, limestone, argillite and rare augite-phyric volcanic accessory clasts. Rare, discontinuous, coarse-grained sandstone channels (206.7±1.9 Ma U-Pb detrital zircon MDA from base of unit, Hunter and van Straaten, 2020; 198+8/-7 Ma U-Pb zircon age, Greig and Gehrels, 1995)

**Kinskuch unit (Upper Triassic)**

uTrHs

Massive to poorly stratified conglomerate with rounded to angular pebbles to boulders and local megaclasts (up to at least 120 m). Clast types include sandstone, mudstone, limestone, chert, augite-phyric mafic volcanic, and hornblende-feldspar-phyric intermediate volcanic rock. Locally interstratified with coarse-grained feldspathic sandstone and pebbly sandstone (Constrained to the Rhaetian by cross-cutting Big Bulk stock and conodonts from a limestone megaclast originally assigned a Late Norian age, now considered Rhaetian; Cordey et al., 1992; Golding, pers. comm. 2021.)

**Stuhini Group (Upper Triassic)**

uTrSs

Well-stratified argillite, mudstone, siltstone, wacke, and feldspathic sandstone. Detrital quartz is absent in all rock types. Local graphitic mudstone. Rare conglomerate, pebbly sandstone, and calcite-rich sandstone. Very rare thin limestone and chert beds.

uTrSvm

Mafic coherent rocks and mafic volcanic breccia, coherent rocks and volcanic clasts are augite-phyric, and locally amygdaloidal. Intercalated with lesser well-stratified, monomictic mafic volcanic clast-bearing conglomerate to volcanic-derived sandstone.

Fig. 3b. Legend.

coherent and fragmental augite-phyric mafic volcanic rocks (uTrSvm) and well-stratified siltstone, mudstone, feldspathic wacke, and rare conglomerate (uTrSs). The Stuhini Group is overlain by diverse rock types in the lower part of the Hazelton Group; all are assigned to the Betty Creek Formation except for the Kinskuch unit (Fig. 3, Table 2). Approximately 4 km southwest of Jade Lake, intermediate volcanic rocks of the Betty Creek Formation (uTrlJHva) conformably overlie Stuhini Group sedimentary rocks (uTrSs). Slightly farther southeast, intermediate volcanic rocks of the Betty Creek Formation (uTrlJHva) interfinger with Stuhini Group sedimentary rocks (uTrSs; Figs. 3, 4). These conformable and gradational transitions are in marked contrast to the unconformity between the Stuhini Group and Hazelton Group observed elsewhere in the region (e.g., Greig, 2014; Nelson and Kyba, 2014; Nelson et al., 2018). Close to Kinskuch Lake, basal Hazelton Group strata consist of conglomerates and local megaclast-bearing conglomerates of the Kinskuch unit (uTrHs, Rhaetian; Fig. 5) that are overlain by intermediate volcanic rocks of the Betty

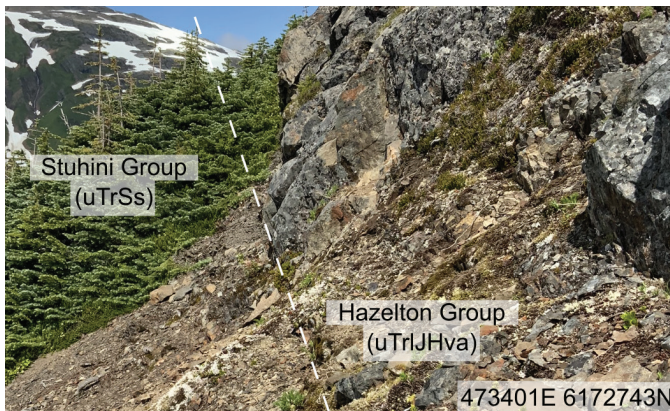


**Fig. 4.** Conformable Stuhini Group-Hazelton Group contact. Stuhini Group (unit uTrSs) consists of recessive-weathering laminated black siltstone with rare reworked plagioclase crystal tuff beds. Hazelton Group (Betty Creek Formation unit uTrlJHva) consists of hornblende-plagioclase crystal tuff that grades up into lapilli tuff with hornblende-plagioclase phyric clasts (473401E, 6172743N, UTM NAD83, Zone 9; looking northeast).



**Fig. 5.** Kinskuch unit (uTrHs) megaclast-bearing conglomerate near the base of the lower part of the Hazelton Group ( $S_0$ =bedding) (475260E, 6170718N, UTM NAD83 Zone 9N; looking northwest).

Creek Formation (uTrlJHva). The Kinskuch unit is considered to represent the fill of a local fault-bounded basin (Miller et al., 2020). The Betty Creek Formation includes intermediate volcanic rocks with hornblende-plagioclase-phyric or biotite-plagioclase-phyric clasts (uTrlJHva; 206.7  $\pm$  1.9 Ma U-Pb detrital zircon maximum depositional age (MDA) from base of unit, 198  $\pm$  8/-7 Ma; U-Pb zircon age from higher up the section; Table 1) that are locally interstratified with medium- to fine-grained feldspathic sandstone, siltstone, lesser mudstone, and rare conglomerate and limestone (uTrlJHsv; 228.4  $\pm$  1.4 Ma U-Pb detrital zircon MDA; 200.85  $\pm$  0.15 Ma U-Pb zircon age; Table 1; Fig. 6). Approximately 3 km northeast of Kinskuch Lake is a distinctive unit of limited areal extent consisting of K-feldspar-phyric volcanic rocks (lJHva.xor; 198  $\pm$  4/-3 Ma, 193.98  $\pm$  0.11 Ma, 193.93  $\pm$  0.11 Ma U-Pb zircon ages; Table 1). South of Kitsault Lake a felsic volcanic rock package (lJHvf; 193.5  $\pm$  0.4 Ma, 196  $\pm$  5/-1 Ma U-Pb zircon ages; Table 1) is at the top of the lower part of the Hazelton Group.

Units in the upper part of the Hazelton Group (Lower to Middle Jurassic) vary significantly from west to east across the map area. In the west and northwest, near Kitsault Lake, the base comprises well-bedded to massive sedimentary rocks of the Spatsizi Formation (lmJHs), including fine- to coarse-grained feldspathic sandstone, pebbly wacke, siltstone, and local thin limestone beds (187.3  $\pm$  0.8 Ma and 188.1  $\pm$  0.6 Ma U-Pb detrital zircon MDA; Table 1). The several million year age gap between the lower and upper parts of the Hazelton Group may suggest the presence of an unconformity, similar to elsewhere in the region (e.g., Gagnon et al., 2012; Nelson et al., 2018). The Spatsizi Formation is overlain by interbedded volcanic rocks, volcanic-derived sandstone, pebble conglomerate, and rare



**Fig. 6.** Betty Creek Formation (uTrlJHsv), interbedded pebbly sandstone with limestone and minor plagioclase-phyric volcanic clasts (top of photo, grey), reworked calcareous crystal tuff, and pale buff siltstone (473514E, 6173208N, UTM NAD83 Zone 9N; looking northeast).

**Table 2.** Comparison of the lithostratigraphic subdivisions used in this study to those used in previous work.

Group	Formation	Hunter et al., 2022	This Study
<b>Bowser Lake Group</b>		Bowser Lake Group	muJBs
	<b>Quock Formation</b>	Facies 6	mJHs
	<b>Unassigned unit</b>	Facies 6	lmJHsv
<b>upper Hazelton Group</b>			lmJHvf
	<b>Kitsault unit</b>	Facies 5 (Kitsault unit)	lmJHvm lmJHva
	<b>Spatsizi Formation</b>		lmJHs
<b>lower Hazelton Group</b>			lJHvf
	<b>Betty Creek Formation</b>	Facies 4a	lJHva.xor
		Facies 2 and 3	uTrlJHsv
		Facies 2, 3 and 4	uTrlJHva
	<b>Kinskuch unit</b>	Facies 1	uTrHs
<b>Stuhini Group</b>			uTrSs uTrSvm

coherent volcanic or subvolcanic rocks of the Kitsault unit. The Kitsault unit contains intermediate volcanic facies (lmJHva; 178.1 ±2.2 Ma U-Pb zircon age; Table 1), mafic volcanic facies (lmJHvm; Fig. 7), and felsic volcanic facies (lmJHvf; Figs. 3, 8). The intermediate volcanic rocks in the Kitsault unit (lmJHva) can be difficult to differentiate from compositionally similar rocks in the Betty Creek Formation (uTrlJHva), particularly in areas where no intervening sedimentary rocks of the Spatsizi Formation (lmJHs) have been identified. The Kitsault unit hosts stratabound to locally vein-hosted Ag-Zn-Pb VMS deposits at Dolly Varden (MINFILE 103P 188), North Star (MINFILE 103P 189), Torbrit (MINFILE 103P 191), and Wolf (MINFILE 103P 198; Hanson, 1922; Black, 1951; Campbell, 1959; Dawson and Alldrick, 1986; Devlin and Godwin, 1986; Devlin, 1987; Pinsent, 2001; Dunne and



**Fig. 7.** Kitsault unit (lmJHvm, upper part of Hazelton Group) mafic tuff breccia with augite-plagioclase phyric clasts (470583E, 6183982N, UTM NAD83 Zone 9N; looking northwest).



**Fig. 8.** Kitsault unit (lmJHvf, upper part of Hazelton Group) foliated felsic tuff breccia to lapilli tuff with medium green plagioclase-phyric clasts (471908E, 6183396N, UTM NAD83 Zone 9N; looking north).

Pinsent, 2002; Higgs, 2015; McCuaig and Seibert, 2017; Hunter and van Straaten, 2020; Hunter et al., 2022a; Fig. 3). The Kitsault unit is overlain by mudstone and siltstone (commonly siliceous) interbedded with felsic tuff laminae of the Quock Formation (mJHs; 168.9 ±2.2 Ma U-Pb zircon MDA at base; Table 1).

In the eastern and northeastern parts of the map area, the upper part of the Hazelton Group consists of well-stratified mudstone, siltstone, sandstone, and limestone with fine tuff to lapilli-tuff beds (unit lmJHsv). This unit was mapped as the Surprise Creek facies of the Salmon River Formation by Evenchick et al. (2008); the formation name was abandoned by Gagnon et al. (2012). Hunter et al. (2022a) tentatively assigned this unit to the Quock Formation but based on the significantly

coarser nature of the siliciclastic and volcanic strata, and a current lack of age constraints, we revert to an unassigned unit (ImJHsv). It may represent the lateral equivalent of the Kitsault unit and correlate regionally with the Spatsizi Formation.

The Quock Formation (in the north) and an unassigned unit (in the northeast and east; Figs. 3, 9) in the upper part of the Hazelton Group are overlain by well-stratified siliciclastic sedimentary rocks of the Bowser Lake Group (muJBs;  $154.3 \pm 0.9$  Ma U-Pb detrital zircon MDA; Table 1). The contact appears to be gradational and conformable and is marked by the disappearance of tuff to lapilli-tuff and appearance of chert clast-bearing pebble conglomerate (Hunter et al., 2022a).



**Fig. 9.** Unassigned unit, (ImJHsv, upper part of Hazelton Group) well-stratified sandstone to siltstone with a white-weathering 10 cm thick tuff layer; younging upright to the east from cross bedding (485093E, 6166413N, UTM NAD83 Zone 9N; looking east).

#### 4. Discussion

Continued mapping combined with geochronological results in the Kitsault River area permit preliminary interpretations that will guide future work and have implications for understanding the geological evolution and metallogeny of the area.

The study area records the early timing ( $206.7 \pm 1.9$  Ma U-Pb detrital zircon MDA; Hunter and van Straaten, 2020) of Hazelton Group volcanism and overlaps with latest Triassic to Early Jurassic ages for the onset of Hazelton Group volcanism (e.g., Nelson et al., 2018). The conformable Stuhini to Hazelton

Group contact in the Kitsault River area is in contrast with the sub-Hazelton Group angular unconformity found elsewhere in the region (e.g., Nelson et al., 2018). Relative to areas farther north, the Kitsault River area preserves a more continuous record from Stuhini Group sedimentation to Hazelton Group volcanism and may have been outside of the area affected by latest Triassic contractional strain (e.g., Nelson and Kyba, 2014; Nelson et al., 2018) recorded regionally. Rocks in the Kitsault River area likely represent a Late Triassic marine back arc (Nelson and van Straaten, 2020) with the Kinskuch unit (Rhaetian; Miller et al., 2020) deposited in a fault bounded pull-apart basin. In the Kinskuch Lake area, these basin-related faults may have exerted control on the emplacement of the Big Bulk porphyry stock, which hosts the Big Bulk Cu-Au porphyry system (Rhaetian;  $204.61 \pm 0.18$  Ma U-Pb zircon; Fig. 3; Miller et al., 2020; MINFILE 103P 016).

Preliminary geochronological data from the upper Hazelton Group in the Kitsault River area ranges from ca.  $<188$  Ma to  $178$  Ma (Hunter and van Straaten, 2021; Hunter et al., 2022a) suggesting that VMS type mineralization in the Kitsault River area may be the same age or slightly older than VMS mineralization in the Eskay rift (ca.  $174$ - $176$  Ma; Childe, 1996; Evenchick et al., 2004; Alldrick et al., 2005; Barresi et al., 2015). Hunter et al. (2022a) noted that the volcanic to epiclastic strata in the upper part of the Hazelton Group in the study area differ significantly from the typical Iskut River Formation and thus introduced the Kitsault unit, which represents deposition outside of the main Eskay rift. The VMS-prospective Kitsault unit was only observed on the northwest side of the map area and appears to transition laterally into an unassigned sedimentary unit found in the northeastern and eastern parts. The Kitsault unit likely formed in local extensional basins much like the broadly coeval Iskut River Formation (Barresi et al., 2005, 2015; Nelson et al., 2018) but without developing into a rift. The unassigned, predominantly sedimentary unit to the east may represent its lateral equivalent, with thin tuff interlayers representing distal volcanic input.

#### 5. Conclusions

Stuhini Group rocks in the Kitsault River area were likely deposited in a Late Triassic marine back arc (Nelson and van Straaten, 2020). In contrast to the sub-Hazelton Group unconformity observed elsewhere in the region, our current mapping in the area suggests a continuous or near-continuous record across the transition from Stuhini Group sedimentation to the onset of Hazelton Group volcanism in the latest Triassic. Therefore, the Kitsault River area may allow for precise determination of the onset of Hazelton Group volcanism, which is significant because coeval and comagmatic intrusions are responsible for the emplacement of most of the porphyry Cu-Au deposits in the region. The Kinskuch unit (Rhaetian; Miller et al., 2020), locally at the base of the Hazelton Group, was deposited in a fault bounded pull-apart basin. The basin-related faults likely exerted control on the emplacement of the Big Bulk porphyry stock, which hosts the Big Bulk Cu-Au

porphyry system (Rhaetian; 204.61 ±0.18 Ma U-Pb zircon; Fig. 3; Miller et al., 2020).

In the study area, volcanic rocks of the Kitsault unit (upper part of the Hazelton Group) host several Ag-rich VMS deposits. The Kitsault unit is distinct from the Iskut River Formation within the Eskay rift, lacking the latter's characteristic bimodal volcanism (Hunter and van Straaten, 2020). The Kitsault unit is interpreted to record local volcanism of a similar or slightly older age than the Iskut River Formation. The volcanic rocks of the Kitsault unit are notably absent in the eastern half of the map area. Here, thin tuff interlayers in a predominantly sedimentary unit may represent distal volcanic input. Future work will focus on better defining the lower contact of the upper part of the Hazelton Group, determine the extent of the Kitsault unit and its relationship to broadly coeval sedimentary rocks, which will be a key step in assessing prospectivity of VMS-style mineralization throughout the region.

### Acknowledgments

We thank Dolly Varden Silver Corporation, in particular Chris Sebert, Rob van Egmond, and Charlie Fleenor for logistical support, their hospitality while staying in the Alice Arm camp, and their generosity in sharing property-scale geological maps and data. Summit Helicopters and their pilots transported us safely throughout the summer. Fantastic field assistance and sample preparation was provided by Ben Coats, Cameron Fielding, and Shannon Murtonen. A thoughtful and insightful review by JoAnne Nelson significantly improved the manuscript.

### References cited

- Alldrick, D.J., Dawson, G.L., Bosher, J.A., and Webster, I.C.L., 1986. Geology of the Kitsault River area (NTS 103P). British Columbia Ministry of Energy, Mines and Petroleum Resources, British Columbia Geological Survey Open File 1986-02, 1:50,000 scale.
- Alldrick, D.J., Nelson, J.L., and Barresi, T., 2005. Geology and mineral occurrences of the upper Iskut River area: Tracking the Eskay rift through northern British Columbia. In: Geological Fieldwork 2004, British Columbia Ministry of Energy and Mines, British Columbia Geological Survey Paper 2005-1, pp. 1-30.
- Barresi, T., Nelson, J.L., Alldrick, D.J., and Dostal, J., 2005. Pillow basalt ridge facies; Detailed mapping of Eskay Creek-equivalent stratigraphy in northwestern British Columbia. In: Geological Fieldwork 2004, British Columbia Ministry of Energy and Mines, British Columbia Geological Survey Paper 2005-1, pp. 31-38.
- Barresi, T., Nelson, J.L., Dostal, J., and Friedman, R., 2015. Evolution of the Hazelton arc near Terrace, British Columbia: Stratigraphic, geochronological, and geochemical constraints on a Late Triassic-Early Jurassic arc and Cu-Au porphyry belt. *Canadian Journal of Earth Sciences*, 52, 466-494. doi: 10.1139/cjes-2014-0155.
- Barrett, T.J., and Sherlock, R.L., 1996. Geology, litho-geochemistry and volcanic setting of the Eskay Creek Au-Ag-Cu-Zn deposit, northwestern British Columbia. *Exploration and Mining Geology*, 5, 339-368.
- Black, J.M., 1951. Geology and mineral occurrences of the Upper Kitsault Valley. In: British Columbia Ministry of Energy, Mines and Petroleum Resources, British Columbia Geological Survey Annual Report, pp. A76-A83.
- Campbell, F.A., 1959. The geology of Torbrit Silver Mine British Columbia. *Economic Geology*, 54, 1461-1495. doi: 10.2113/gsecongeo.54.8.1461.
- Childe, F., 1996. U-Pb geochronology and Nd and Pb isotope characteristics of the Au-Ag-rich Eskay Creek volcanogenic massive sulfide deposit, British Columbia. *Economic Geology*, 91, 1209-1224. doi: 10.2113/gsecongeo.91.7.1209.
- Cordey, F., Greig, C.J., and Orchard, M.J., 1992. Permian, Triassic, and Middle Jurassic microfaunal associations, Stikine terrane, Owegee and Kinskuch areas, northwestern British Columbia. In: Current Research Part E, Geological Survey of Canada Paper 92-1E, pp. 107-116.
- Cutts, J.A., McNicoll, V.J., Zagorevski, A., Anderson, R.G., and Martin, K., 2015. U-Pb geochronology of the Hazelton Group in the McTagg anticlinorium, Iskut River area, northwest British Columbia. In: Geological Fieldwork 2014, British Columbia Ministry of Energy and Mines, British Columbia Geological Survey Paper 2015-1, pp. 87-101.
- Dawson, G.L., and Alldrick, D.J., 1986. Geology and mineral deposits of the Kitsault Valley. In: Geological Fieldwork 1985, British Columbia Ministry of Energy, Mines and Petroleum Resources, British Columbia Geological Survey Paper 1986-1, pp. 219-224.
- Devlin, B.D., 1987. Geology and genesis of the Dolly Varden silver camp, Alice Arm area, northwestern British Columbia. M.Sc. thesis, University of British Columbia, Vancouver, B.C., Canada. <<https://open.library.ubc.ca/cIRcle/collections/ubctheses/831/items/1.0052815> (last accessed November 5, 2015).
- Devlin, B.D., and Godwin, C.I., 1986. Geology of the Dolly Varden camp, Alice Arm area. In: Geological Fieldwork 1985, British Columbia Ministry of Energy, Mines and Petroleum Resources, British Columbia Geological Survey Paper 1986-1, pp. 327-330.
- Dunne, K.P.E., and Pinsent, R.H., 2002. Depositional setting of silver-rich quartz-sulphate-carbonate deposits of the upper Kitsault River area, northwest British Columbia. In: Geological Fieldwork 2001, British Columbia Ministry of Energy, Mines and Petroleum Resources, British Columbia Geological Survey Paper 2002-01, pp. 177-196.
- Evenchick, C.A., 1991. Geometry, evolution, and tectonic framework of the Skeena Fold Belt, north-central British Columbia. *Tectonics*, 10, 527-546. doi: 10.1029/90TC02680.
- Evenchick, C.A., 2001. Northeast-trending folds in the western Skeena Fold Belt, northern Canadian Cordillera: A record of Early Cretaceous sinistral plate convergence. *Journal of Structural Geology*, 23, 1123-1140. doi: 10.1016/S0191-8141(00)00178-4.
- Evenchick, C.A., and McNicoll, V.J., 2002. Stratigraphy, structure, and geochronology of the Anox Pendant, northwest British Columbia, and implications for mineral exploration. *Canadian Journal of Earth Sciences*, 39, 1313-1332. doi: 10.1139/e02-036.
- Evenchick, C.A., and Thorkelson, D.J., 2005. Geology of the Spatsizi River map area, north-central British Columbia. *Geological Survey of Canada Bulletin* 577, 276 p.
- Evenchick, C.A., McNicoll, V.J., and Snyder, L.D., 2004. Stratigraphy, geochronology, and geochemistry of the Georgie River area, northwest British Columbia, and implications for mineral exploration. *Canadian Journal of Earth Sciences*, 41, 199-216. doi: 10.1139/e03-091.
- Evenchick, C.A., McMechan, M.E., McNicoll, V.J., and Carr, S.D., 2007. A synthesis of the Jurassic-Cretaceous tectonic evolution of the central and southeastern Canadian Cordillera: Exploring links across the orogen. In: Sears, J.W., Harms, T.A. and Evenchick, C.A., (Eds.), *Whence the mountains? Inquiries in the Evolution of Orogenic Systems: A volume in honor of Raymond A. Price*, Geological Society of America Special Paper 433, pp. 117-145.
- Evenchick, C.A., Mustard, P.S., Greig, C.J., McMechan, M.E., Ritcey, D.H., Smith, G.T., and Ferri, F., 2008. Geology, Nass

- River, British Columbia. Geological Survey of Canada Open File 5705, 1:125,000 scale.
- Febbo, G.E., Friedman, R.M., Kennedy, L.A., and Nelson, J.L., 2019. U-Pb geochronology of the Mitchell deposit, northwestern British Columbia. British Columbia Ministry of Energy, Mines and Petroleum Resources, GeoFile 2019-03, 8 p.
- Gagnon, J.-F., Barresi, T., Waldron, J.W.F., Nelson, J.L., Poulton, T.P., and Cordey, F., 2012. Stratigraphy of the upper Hazelton Group and the Jurassic evolution of the Stikine terrane, British Columbia. *Canadian Journal of Earth Sciences*, 49, 1027-1052. doi: 10.1139/e2012-042.
- Greig, C.J., 1992. Fieldwork in the Oweegee and Snowslide ranges and Kinskuch Lake area, northwestern British Columbia. In: *Current Research, Part A*, Geological Survey of Canada, Current Research 92-1A, pp. 145-155.
- Greig, C.J., 2014. Latest Triassic-earliest Jurassic contractional deformation, uplift and erosion in Stikinia, NW B.C. *Geological Society of America Abstracts with Programs*, 46, p. 588.
- Greig, C.J., and Gehrels, G.E., 1995. U-Pb zircon geochronology of Lower Jurassic and Paleozoic Stikinian strata and Tertiary intrusions, northwestern British Columbia. *Canadian Journal of Earth Sciences*, 32, 1155-1171. doi: 10.1139/e95-095.
- Greig, C.J., Anderson, R.G., Daubeny, P.H., and Bull, K.F., 1994. Geology of the Cambria Icefield: Stewart (103P/13), Bear River (104A/4), and parts of Meziadin Lake (104A/3) and Paw Lake (103P/12) map areas, northwestern British Columbia. Geological Survey of Canada Open File, 2931, 1:50,000 scale.
- Hanson, G., 1922. Upper Kitsault Valley, British Columbia. In: *Geological Survey of Canada, Summary Report Part A*, pp. 7-21.
- Higgs, A.A., 2015. 2015 Technical Report for the Dolly Varden Property, Skeena Mining Division (NTS 103P/11, 12, 13, and 14), 133 p. <<https://www.dollyvardensilver.com/site/assets/files/1326/dv-2015-04-16-43-101-technical-report.pdf>> (last accessed December 2019).
- Hunter, R.C., and van Straaten, B.I., 2020. Preliminary stratigraphy and geochronology of the Hazelton Group, Kitsault River area, Stikine terrane, northwest British Columbia. In: *Geological Fieldwork 2019*, British Columbia Ministry of Energy, Mines and Petroleum Resources, British Columbia Geological Survey Paper 2020-02, pp. 101-118.
- Hunter, R.C., Sebert, C.F.B., Friedman, R., and Wall, C., 2022a. Revised stratigraphy and geochronology of the Hazelton Group, host rocks for volcanogenic mineralization in the Kitsault River area, northwest British Columbia. In: *Geological Fieldwork 2021*, British Columbia Ministry of Energy, Mines and Low Carbon Innovation, British Columbia Geological Survey Paper 2022-01, pp. 63-81.
- Hunter, R.C., Sebert, C.F.B., Friedman, R., and Wall, C., 2022b. Geochronologic data from the Kitsault River area, northwest British Columbia. Ministry of Energy, Mines and Low Carbon Innovation, British Columbia Geological Survey GeoFile 2022-13, 4 p.
- Logan, J.M., and Mihalynuk, M.G., 2014. Tectonic controls on Early Mesozoic paired alkaline porphyry deposit belts (Cu-Au+/-Ag-Pt-Pd-Mo) within the Canadian Cordillera. *Economic Geology*, 109, 827-858. doi: 10.2113/econgeo.109.4.827.
- Macdonald, A.J., Lewis, P.D., Thompson, J.F.H., Nadaraju, G., Bartsch, R., Bridge, D.J., Rhys, D.A., Roth, T., Kaip, A., Godwin, C.I., and Sinclair, A.J., 1996. Metallogeny of an Early to Middle Jurassic arc, Iskut River area, northwestern British Columbia. *Economic Geology*, 91, 1098-1114. doi: 10.2113/econgeo.91.6.1098.
- McCuaig, M., and Sebert, C., 2017. 2016 Technical Report for the Dolly Varden Property, Skeena Mining Division. British Columbia Ministry of Energy, Mines and Petroleum Resources, Assessment Report 36934.
- Miller, E.A., Kennedy, L.A., and van Straaten, B.I., 2020. Geology of the Kinskuch Lake area and Big Bulk porphyry prospect: Syndepositional faulting and local basin formation during the Rhaetian (latest Triassic) transition from the Stuhini to the Hazelton Group. In: *Geological Fieldwork 2019*, British Columbia Ministry of Energy, Mines and Petroleum Resources, British Columbia Geological Survey Paper 2020-02, pp. 77-100.
- Mortensen, J.K., and Kirkham, R.V., 1992. A U-Pb zircon age for host rocks of a syngenetic strontium(-zinc) occurrence in the Kitsault Lake area, west-central British Columbia. In: *Radiogenic Age and Isotopic Studies: Report 5*, Geological Survey of Canada Paper 91-2, pp. 181-185.
- Nelson, J.L., and Kyba, J., 2014. Structural and stratigraphic control of porphyry and related mineralization in the Treaty Glacier-KSM-Brucejack-Stewart trend of western Stikinia. In: *Geological Fieldwork 2013*, British Columbia Ministry of Energy and Mines, British Columbia Geological Survey Paper 2014-1, pp. 111-140.
- Nelson, J.L., and van Straaten, B., 2020. Recurrent syn- to post-subduction mineralization along deep crustal corridors in the Iskut-Stewart-Kitsault region of western Stikinia, northwestern British Columbia. In: Sharman, E.R., Lang, J.R., and Chapman, J.B., (Eds.), *Porphyry Deposits of the Northwestern Cordillera of North America: A 25-Year Update*. Canadian Institute of Mining and Metallurgy Special Volume 57, pp. 194-211.
- Nelson, J., Colpron, M., and Israel, S., 2013. The Cordillera of British Columbia, Yukon and Alaska: tectonics and metallogeny. In: Colpron, M., Bissig, T., Rusk, B., and Thompson, J.F.H., (Eds.), *Tectonics, Metallogeny and Discovery: The North American Cordillera and Similar Accretionary Settings*. Society of Economic Geologists, Special Publication 17, pp. 53-109.
- Nelson, J.L., Waldron, J., van Straaten, B.I., Zagorevski, A., and Rees, C., 2018. Revised stratigraphy of the Hazelton Group in the Iskut River region, northwestern British Columbia. In: *Geological Fieldwork 2017*, British Columbia Ministry of Energy, Mines and Petroleum Resources, British Columbia Geological Survey Paper 2018-1, pp. 15-38.
- Nelson, J.L., van Straaten, B., and Friedman, R., 2022. Latest Triassic-Early Jurassic Stikine-Yukon-Tanana terrane collision and the onset of accretion in the Canadian Cordillera: Insights from Hazelton Group detrital zircon provenance and arc-back-arc configuration. *Geosphere*, 18, 670-696. doi: 10.1130/GES02444.1.
- Pinsent, R.H., 2001. Mineral deposits of the upper Kitsault River area, British Columbia. In: *Geological Fieldwork 2000*, British Columbia Ministry of Energy and Mines, British Columbia Geological Survey Paper 2001-1, pp. 313-326.
- Roth, T., Thompson, J.F.H., and Barrett, T.J., 1997. The precious metal-rich Eskay Creek deposit, northwestern British Columbia. In: Barrie, C.T., Hannington, M.D., (Eds.), *Volcanic Associated Massive Sulfide Deposits: Processes and Examples in Modern and Ancient Settings*, *Reviews in Economic Geology* 8, p.0. doi: 10.5382/Rev.08.15.

# Stratigraphy of the Stuhini Group (Upper Triassic) in the Galore Creek area, northwestern British Columbia



Bram I. van Straaten<sup>1</sup>, Richard M. Friedman<sup>2</sup>, and Alfredo Camacho<sup>3</sup>

<sup>1</sup> British Columbia Geological Survey, Ministry of Energy, Mines and Low Carbon Innovation, Victoria, BC, V8W 9N3

<sup>2</sup> Pacific Centre for Isotopic and Geochemical Research, Department of Earth, Ocean and Atmospheric Sciences, The University of British Columbia, 6339 Stores Road, Vancouver, BC, V6T 1Z4

<sup>3</sup> Manitoba Isotope Research Facility, Department of Earth Sciences, University of Manitoba, 125 Dysart Road, Winnipeg, MB, R3T 2N2

<sup>a</sup> corresponding author: Bram.vanStraaten@gov.bc.ca

Recommended citation: van Straaten, B.I., Friedman, R.M., and Camacho, A., 2023. Stratigraphy of the Stuhini Group (Upper Triassic) in the Galore Creek area, northwestern British Columbia. In: Geological Fieldwork 2022, British Columbia Ministry of Energy, Mines and Low Carbon Innovation, British Columbia Geological Survey Paper 2023-01, pp. 33-49.

## Abstract

The 1.4 Bt Galore Creek porphyry Cu-Au-Ag deposit is hosted in, and broadly coeval with, a multi-phase alkalic silica-undersaturated volcano-intrusive complex. Based on stratigraphic studies supplemented by new geochronological data, we subdivide the host Stuhini Group strata (Upper Triassic) into a lower succession and an upper succession. The lower succession (at least ~1.2 km thick) grades upward from reworked intermediate volcanic to sedimentary and mafic volcanic strata. The succession was deposited, at least in part, in a submarine setting, part of the Stuhini arc (~1300 km long) developed along the eastern margin and northern part of Stikinia. The lower succession is abruptly overlain by an upper alkalic volcanic succession (at least ~0.8 km thick). In the eastern part of the study area, the upper succession includes a local biotite-phyric volcanic and reworked volcanic unit, mostly deposited subaqueously. Overlying K-feldspar-phyric volcanic rocks, found throughout the study area, are subaerial deposits as indicated by accretionary lapilli, welded beds, and irregular-shaped bombs. Pseudoleucite-phyric volcanic rocks and pseudoleucite-phyric subvolcanic intrusions are found in the western and central parts of the study area; their depositional setting and relationship to other alkalic units are unclear. We constrain the onset of upper succession alkalic volcanism to 210.26 ± 0.17 Ma using high-precision U-Pb zircon and titanite geochronology. The new age is broadly coeval with published ages for mineralogically, texturally, and compositionally similar alkalic silica-undersaturated Galore intrusions (ca. 210-208 Ma) and suggests a short-lived alkalic magmatic event responsible for porphyry Cu-Au-Ag formation. Regionally, the upper alkalic volcanic succession and alkalic silica-undersaturated Galore intrusions are part of a magmatic belt (~155 km long) of small-volume stocks and rare volcanic rocks that orthogonally transects the earlier Stuhini arc. It reflects post-subduction alkalic magmatism and alkalic silica-undersaturated porphyry Cu-Au-Ag deposit formation during the early stages of collision between the Yukon-Tanana and Stikine terranes.

**Keywords:** Stuhini Group, Late Triassic, stratigraphy, Galore Creek, Copper canyon, porphyry Cu-Au, Galore plutonic suite, silica-undersaturated, alkalic, magmatism, geochronology, Stikinia

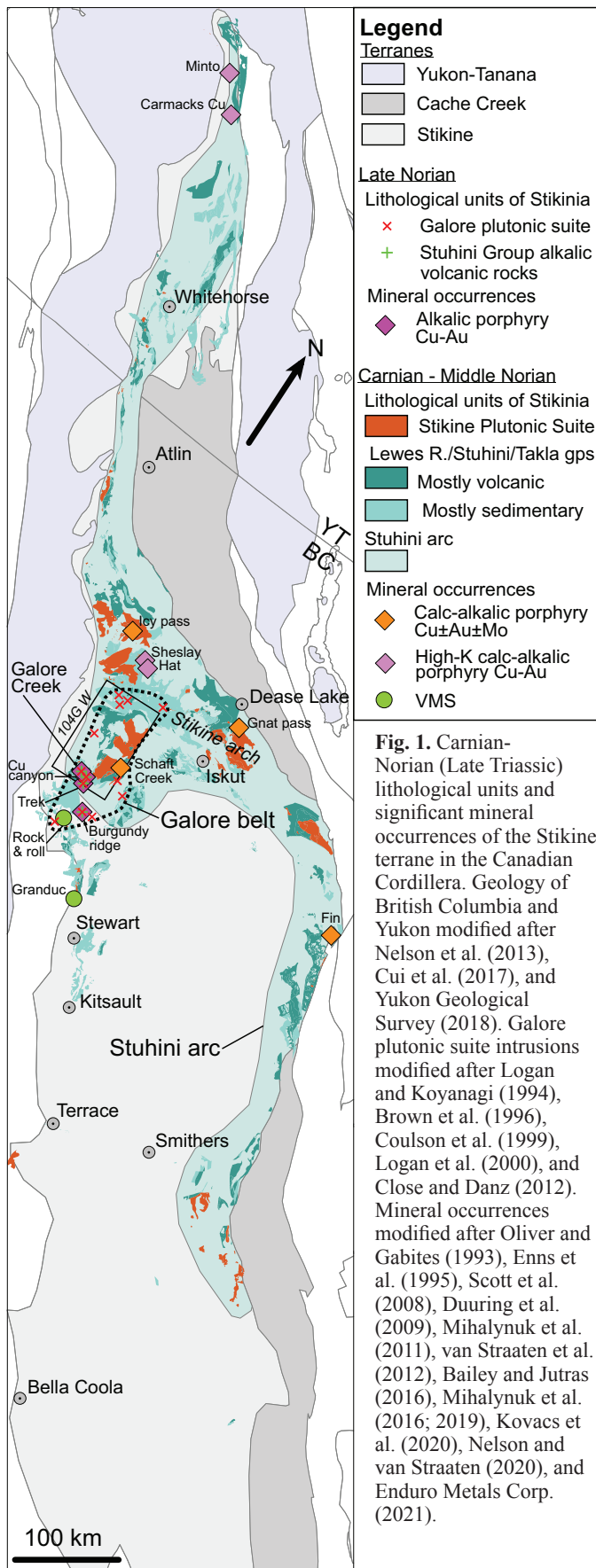
## 1. Introduction

The Galore Creek Cu-Au-Ag deposit is one of several large (>1 Bt) porphyry systems in northwestern British Columbia (Fig. 1) on the traditional lands of the Tahltan First Nation. The deposit is unique with respect to other large deposits in the region in its genetic link to an alkalic silica-undersaturated volcano-intrusive complex, and the presence of silica-deficient hydrothermal alteration (Enns et al., 1995; Logan and Mihalynuk, 2014). The deposit is hosted in the Stuhini Group (Upper Triassic), a volcanic arc succession that is widespread throughout the Stikine terrane (Fig. 1). Herein we present a stratigraphic analysis of the Stuhini Group and show that, in the Galore Creek area, it records an abrupt change from mafic-intermediate arc volcanism to alkalic silica-undersaturated post-arc volcanism. We describe volcano-sedimentary units in the Galore Creek area estimating their thicknesses and lateral variations, provide a preliminary high-precision geochronological determination for the onset of alkalic volcanism, and discuss the tectonic implications.

## 2. Geological setting

### 2.1. Regional geology

The Galore Creek area is in the multi-episodic Stikine island arc terrane (Stikinia), in which volcano-sedimentary rocks of the Stikine assemblage (Devonian to Permian) are overlain by the Stuhini Group (Upper Triassic) and the Hazelton Group (uppermost Triassic to Middle Jurassic). These successions are bounded by regional unconformities that mark significant deformation including: 1) poorly characterized Permo-Triassic deformation that affects Paleozoic rocks (Logan and Koyanagi, 1994); 2) latest Triassic deformation that affects Stuhini Group and older strata throughout northwestern British Columbia, and has been attributed to collision between the Yukon-Tanana and Stikine terranes (e.g., Nelson et al., 2022); and 3) a Middle Jurassic fold-and-thrust belt along the northeastern margin of Stikinia, formed due to accretion of Stikinia and intervening Intermontane terranes to Ancestral North America (Mihalynuk et al., 1994; Nelson et al., 2013).



Accretion of Stikinia to inboard terranes and the Ancestral North American margin is recorded by deposition of Bowser Lake Group siliciclastic rocks (Middle Jurassic to mid-Cretaceous) in a foreland basin atop Stikinia (Evenchick et al., 2007). Bowser Lake Group and older rocks are deformed by Cretaceous Skeena fold-and-thrust belt shortening linked to continued convergence between accreted terranes and Ancestral North America (Evenchick et al., 2007).

The main axis of Late Triassic magmatism in Stikinia (hereafter referred to as the Stuhini arc) is defined by thick accumulations of predominantly mafic volcanic strata assigned to the Lewes River Group in Yukon, Stuhini Group in northwestern and central British Columbia, and Takla Group in north-central British Columbia (Fig. 1). These strata are accompanied by ca. 229-216 Ma Stikine Plutonic Suite intrusions. These volcanic and intrusive rocks extend for at least ~1300 km along the eastern margin and northern part of Stikinia (Fig. 1) and have been interpreted as an east-facing arc (Nelson and van Straaten, 2020). Several porphyry Cu±Au±Mo deposits formed along the Stuhini arc (e.g., Schaft Creek, Fig. 1), with VMS deposits developed in the back arc (e.g., Granduc, Fig. 1). Stuhini arc activity terminated in latest Triassic by a collision between northern Stikinia and the Yukon-Tanana terrane. This collision is expressed by: 1) the latest dated Stuhini arc magmatism at ca. 216 Ma (van Straaten et al., 2022); 2) the latest Triassic shortening of the Stuhini Group and older strata throughout northwestern British Columbia (Henderson et al., 1992; Rhys, 1993; Brown et al., 1996; Rees et al., 2015; Nelson et al., 2018); 3) a regional-scale unconformity between the Stuhini and Hazelton groups (e.g., Nelson et al., 2018; 2022); 4) a ca. 9-12 m.y. magmatic gap in the Kitsault, Stewart to Iskut corridor (ca. 216 to 207-204 Ma; Hollis and Bailey, 2013; Hunter and van Straaten, 2020; Campbell, 2021), extending to ca. 31-41 m.y. along the Stikine arch (ca. 216 to 185-175 Ma; Brown et al., 1996; van Straaten et al., 2022); and 5) crustal thickening and burial of the Yukon-Tanana terrane to amphibolite facies in southern Yukon, and coincident ca. 205-194 Ma mid- to lower-crustal magmatism along the Yukon-Tanana - Stikinia suture in southern Yukon (Colpron et al., 2022).

From ca. 210-208 Ma (Mortensen et al., 1995; Logan and Mihalyuk, 2014; Enduro Metals Corp., 2021), a distinct magmatic belt (~155 km long) developed in northwestern Stikinia, orthogonal to the Stuhini arc axis (Fig. 1). This belt is defined by small-volume Galore plutonic suite intrusions of predominantly alkaline affinity and very rare alkalic volcanic rocks. The orientation of the belt, small volume intrusions, localized volcanic rocks and alkalic chemistry suggest that it is a post-subduction feature generated by partial melting of previously subduction-metasomatized sub-arc lithosphere (Nelson and van Straaten, 2020). Recent studies of the collision (Colpron et al., 2022; Nelson et al., 2022) suggest the alkalic magmatism occurred during the early stages of Yukon-Tanana - Stikinia collision.

## 2.2. Galore Creek area geology

The oldest rocks in the Galore Creek area are in the hanging wall of the west-verging Copper canyon thrust fault and comprise Stikine assemblage limestone (Permian) and fine-grained siliciclastic sedimentary rocks (Lower-Middle Triassic; Logan and Koyanagi, 1994; Fig. 2). Elsewhere, the area is underlain by Stuhini Group volcano-sedimentary rocks (Upper Triassic). Logan and Koyanagi (1994) subdivided the Stuhini Group into: 1) a lower unit of subalkaline hornblende-bearing basaltic andesite and sedimentary equivalent wacke, turbidite, and conglomerate; 2) a middle unit of subalkaline to alkaline augite-porphyritic basalt, and sedimentary and epiclastic rocks

with predominantly pyroxene; and 3) an uppermost unit of alkaline orthoclase- and pseudoleucite-bearing shoshonitic basalt, tuff, and epiclastic rocks. Stuhini Group strata are cut by foid syenite, alkali-feldspar syenite, syenite, monzonite, monzodiorite, and rare quartz syenite of the Galore intrusions (part of the Galore plutonic suite) that are K-feldspar and/or pseudoleucite porphyritic and less commonly equigranular (Enns et al., 1995; Fig. 2). The age range of alkalic silica-undersaturated Galore intrusions has been difficult to establish due to a general lack of zircon and thermal resetting. It is broadly constrained by a  $210 \pm 1$  Ma U-Pb titanite and K-feldspar age for an early syn-mineralization K-feldspar and

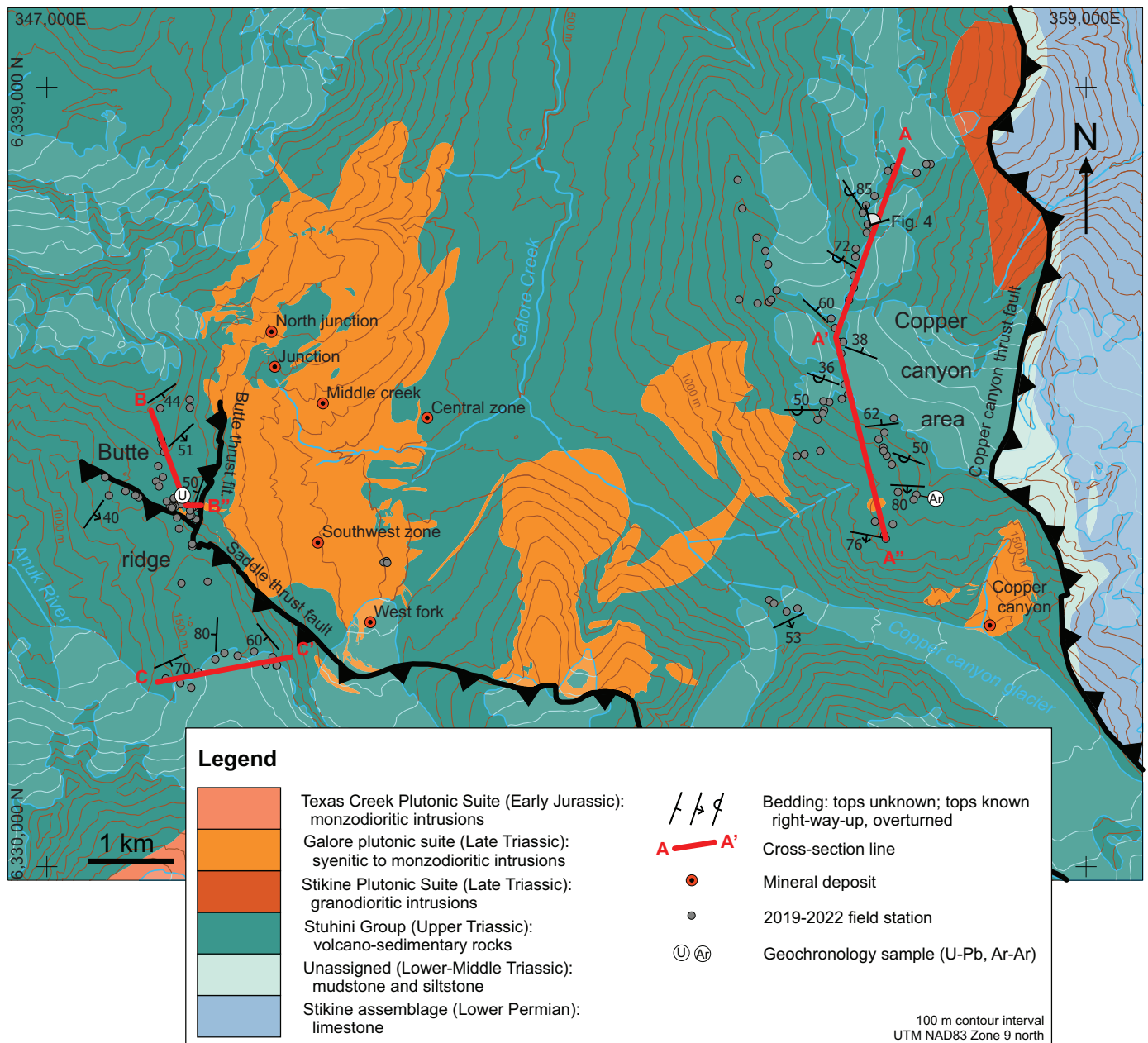


**Fig. 2.** Geology of the Galore Creek area (modified after Logan et al., 1993a, b; Cui et al., 2017). Galore intrusions, Butte and Saddle thrust faults after Prince (2020). UTM coordinates here and throughout this paper are in NAD83 zone 9 north.

pseudoleucite porphyritic syenite intrusion (Mortensen et al., 1995) and a  $208.5 \pm 0.8$  Ma U-Pb titanite age for a K-feldspar porphyritic biotite quartz syenite plug (Logan and Mihalynuk, 2014) interpreted by Enns et al. (1995) as the youngest phase of the Galore intrusions.

Compared to porphyry deposits worldwide, Galore Creek represents a unique alkalic silica-undersaturated endmember (Lang et al., 1995). Chalcopyrite  $\pm$ bornite mineralization is hosted in Stuhini Group strata, breccia bodies, and early- to syn-mineralization Galore intrusions, and is accompanied by silica-deficient hydrothermal alteration including K-feldspar, biotite, garnet and anhydrite (Enns et al., 1995; Byrne and Tosdal, 2014; Micko et al., 2014). At least two mineralizing episodes are interpreted, with large volume orthoclase megacrystic syenite intrusions mostly late- to post-mineral (Enns et al., 1995; Schwab et al., 2008; Byrne and Tosdal, 2014; Micko et al., 2014). The Galore Creek district contains NI 43-101 compliant mineral resources (Measured, Indicated, and Inferred) of 1466 Mt containing 15 Blbs Cu, 13 Moz Au and 205 Moz Ag across six different deposits (Central zone, Southwest zone, Junction/North Junction, West fork, Middle creek and Copper canyon; Table 1, Fig. 2; Hatch Ltd. et al., 2005; Teck Resources Limited, 2019). Mineral resource estimates are currently being updated as part of a prefeasibility study carried out by Galore Creek Mining Corporation, a 50/50 partnership between Teck Resources Limited and Newmont Corporation.

Fig. 4). Consistent southwest younging directions  $<100$  m on either side of the folds imply they are minor parasitic folds (Figs. 3a, 4). Although other unrecognized folds may result in overestimation of the calculated thickness of units, they unlikely affect the interpreted stratigraphic superposition presented below (see Section 4). Two faults, one low angle and the other high angle, are interpreted in recessive zones surrounded by wall rock with a well-developed fault-parallel spaced fracture cleavage. Stratigraphic offsets suggest an apparent reverse south- to southwest-vergent sense for both. The northern half of the cross section displays consistently overturned steeply northeast-dipping strata, except one right-way-up very steeply west-southwest-dipping bedding measurement. Bedding attitudes shallow towards the middle of the cross section. Slightly farther south in a fault-bounded panel, one measurement shows an overturned shallow north-northeast dip. The southern half of the cross-section shows largely overturned moderately north-northeast-dipping strata with rare right-way-up steeply south-southwest dipping strata. Stereonet analysis shows that all poles to overturned and inferred overturned bedding planes cluster in the southwest quadrant, whereas poles to right-way-up bedding planes are in the northeast quadrant (Fig. 5a). The variation in bedding attitudes is attributed to fault rotation, minor asymmetric folds, original non-horizontal deposition of volcanic strata, surface processes such as frost-heave, and measurement errors. Tectonic foliation is absent to weak outside of the fault zones noted above.

**Table 1.** Total NI 43-101 compliant mineral resources in the Galore Creek area. Galore Creek estimates from Teck Resources Limited (2019), Copper canyon estimates from Hatch Ltd. et al. (2005).

Category	Zone	Mt	Cu (%)	Au (g/t)	Ag (g/t)	Cu (Blbs)	Au (Moz)	Ag (Moz)
Measured	Galore	256.8	0.72	0.36	5.8	4.06	3.00	47.80
Indicated	Galore	846.7	0.39	0.23	3.7	7.27	6.26	102.05
Inferred	Galore	198.1	0.27	0.21	2.7	2.95	1.34	16.88
Inferred	Cu canyon	164.8	0.35	0.54	7.2	1.16	2.86	37.91
<b>Total</b>		<b>1466.4</b>	-	-	-	<b>15.43</b>	<b>13.46</b>	<b>204.63</b>

### 3. Study area structure and stratigraphic superposition

In this study we establish the Stuhini Group (Upper Triassic) stratigraphy in the Galore Creek area based on detailed field studies at three locations; one northwest of the Copper canyon deposit and two on Butte ridge (between the headwaters of the Anuk River and Galore Creek; Figs. 2, 3).

#### 3.1. Copper canyon area

Stuhini Group strata throughout the Copper canyon area consistently young towards the southwest and south (Section A-A'-A'', Fig. 3a) although largely coherent mafic volcanic or subvolcanic rocks in the far north lack bedding measurements and younging indicators. Along the entire cross section line, we observed only one 0.5 m-scale tight synform and a nearby several m-scale open asymmetrical z-fold (looking north;

#### 3.2. Butte ridge north

The northwest end of Butte ridge exposes moderately southeast dipping right-way-up Stuhini Group strata (Section B-B'-B'', Fig. 3b) with at least one  $\sim 140$  m-scale asymmetric open s-fold (looking north). The succession steepens towards B'. In the northeast, between B' and B'', steeply west-dipping strata lack way up indicators. Here, the upper part of a volcanic succession (uTrSvc.gal) contains an s-fold (looking north); farther east near the volcanic-sedimentary contact we noted z-folds (looking north; Fig. 3b). Sedimentary clasts in the volcanic rocks immediately above the volcanic-sedimentary contact may suggest this part of the succession is right-way-up. If so, the z- and s-fold geometries suggest the presence of an  $\sim 60$  m-scale isoclinal syncline. The change in attitudes and rock types at B' have been tentatively interpreted to mark a fault.

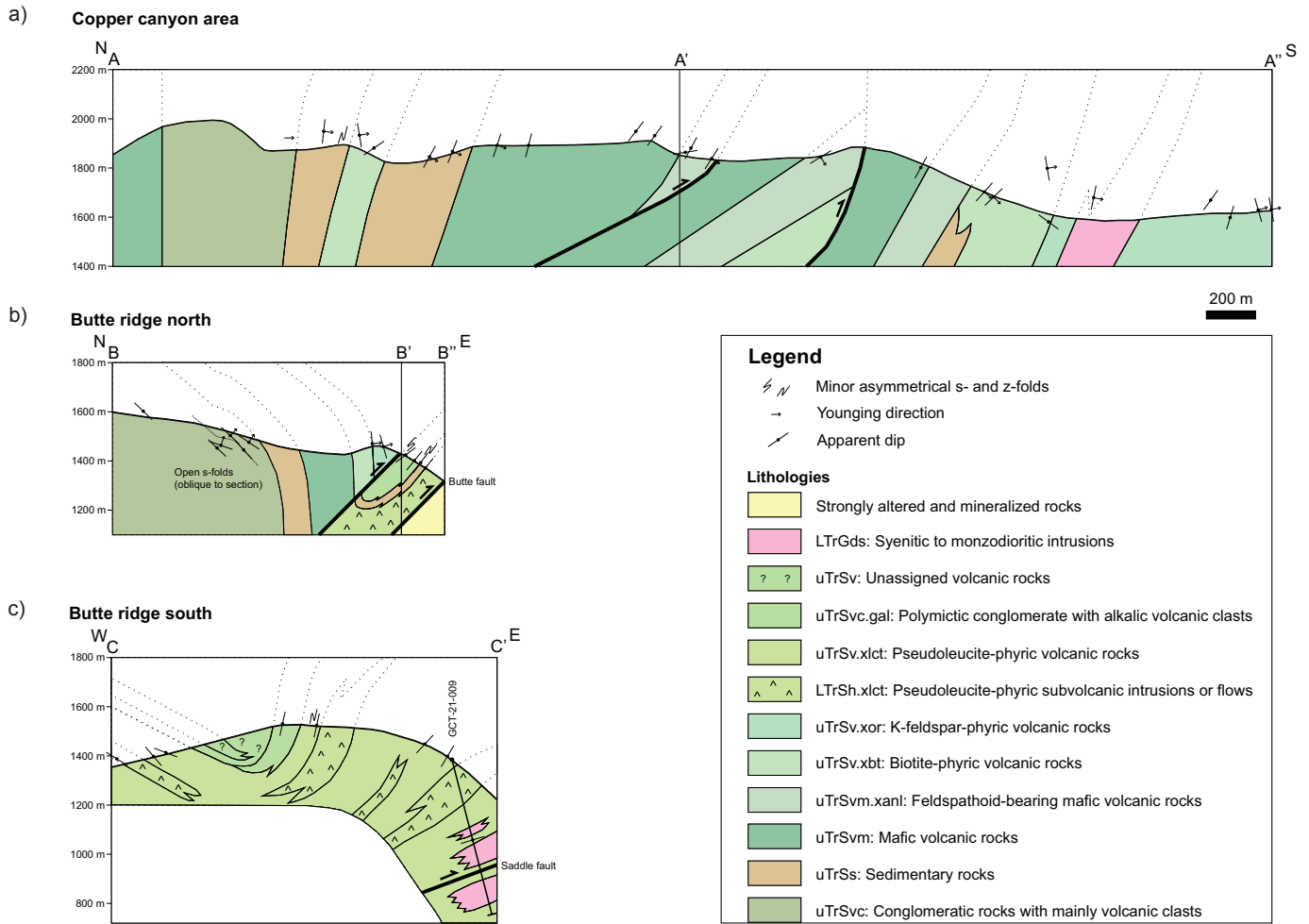


**Fig. 3.** Schematic vertical cross sections. **a)** Copper canyon area. **b)** North end of Butte ridge. **c)** South end of Butte ridge.

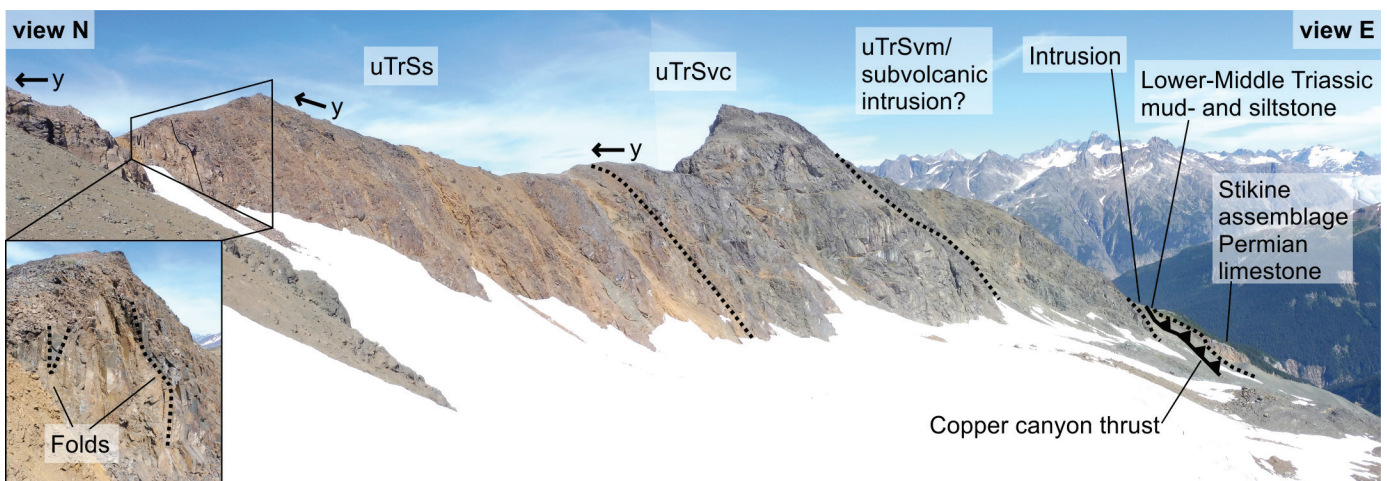


**Fig. 4.** Panoramic view of alpine ridge in Copper canyon area showing Stuhini Group units in the footwall of the Copper canyon thrust fault. Looking north to east (UTM 356478E–6337417N, see Fig. 2 for location). Inset shows 0.5 m-scale tight synform and a several m-scale open asymmetrical z-fold (looking north). y = younging direction.

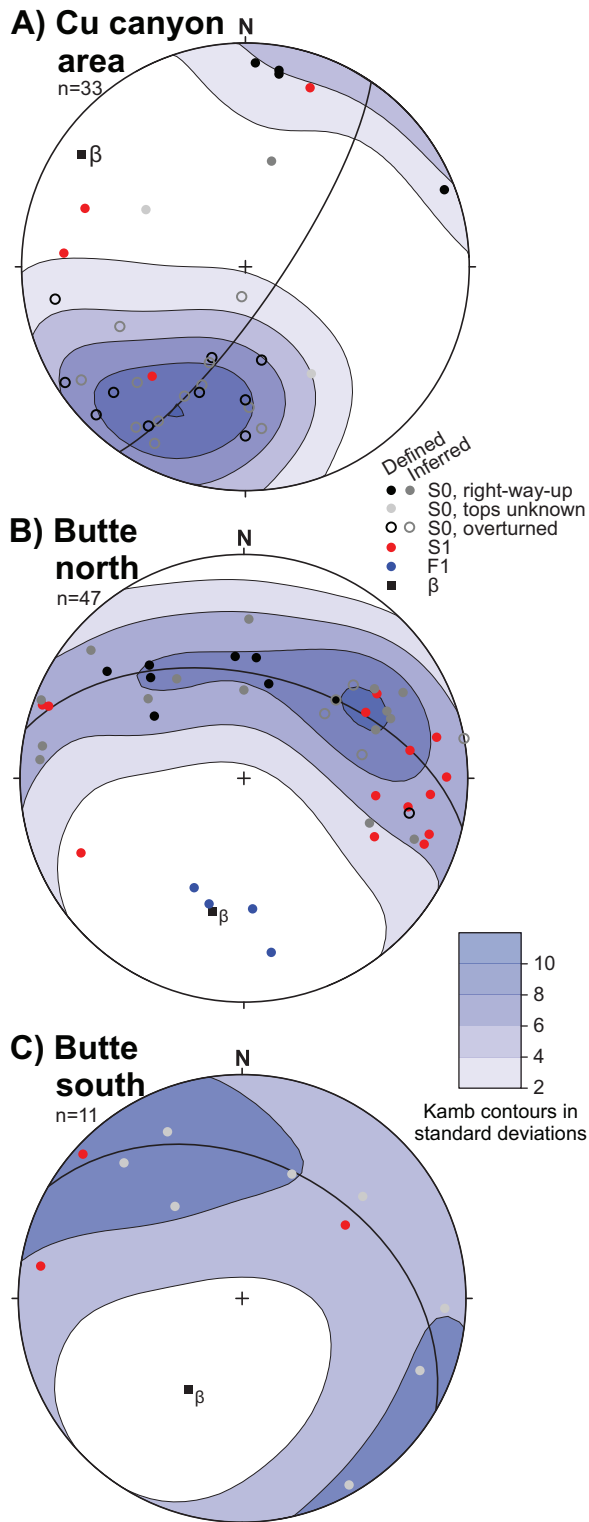


**Fig. 5.** Stereographic projections showing poles to bedding (S0, contoured), poles to foliation (S1) and fold axes (F1) along **a)** cross-section A-A'-A''; **b)** B-B'-B''; and **c)** C-C'. Lower hemisphere equal area projections were produced using Stereonet 11, where known and inferred overturned bedding planes are shown with negative poles (poles to overturned planes point upward into the upper hemisphere and are plotted in the lower hemisphere; Allmendinger et al., 2013; Cardozo and Allmendinger, 2013). Calculated best fit fold axes ( $\beta$ ) are  $304^\circ/13^\circ$  in a),  $193^\circ/39^\circ$  in b), and  $210^\circ/51^\circ$  in c).

The interpreted syncline is in the immediate hanging wall of the Butte thrust fault (Fig. 3b), which juxtaposes largely unaltered rocks with altered and mineralized rocks in the Galore Creek valley (Schwab et al., 2008; Prince, 2020). Stereonet analysis shows a moderately south-southwest plunging fold axis, similar to two measured fold axes and two fold axes calculated from bedding measurements of outcrop-scale folds (Fig. 5b). The entire area displays a steeply west-dipping flattening fabric (Figs. 5b, 6; see Johnston et al., 2023).

### 3.3. Butte ridge south

At the south end of Butte ridge, bedding measurements are limited and younging indicators were not observed. Southeast dipping Stuhini Group strata in the west and broadly west dipping strata in the east define a possible synform (Section C-C', Fig. 3c). One z-fold (looking north), observed in the east, supports this interpretation. At depth towards the east in diamond drill hole GCT-21-009, oriented core data shows that bedding shallows to a gentle southwest dip before intersecting a fault correlated with the Saddle thrust fault (Prince, 2020). Stereonet analysis shows a moderately southwest-plunging fold axis (Fig. 5c). For the purpose of constructing a stratigraphic column we assume the strata in the moderately plunging fold are right-way-up (see Section 4). Given the limited bedding measurements and lack of way-up indicators, more major folds could be in this area, which would result in overestimation of unit thicknesses. The entire area displays a steeply dipping west- to northwest-dipping flattening fabric (see Johnston et al., 2023).

## 4. Geological units

All stratified units and subvolcanic intrusions described below are part of the Stuhini Group (Upper Triassic), which we have subdivided into a lower intermediate to mafic volcano-sedimentary succession, and an upper alkalic volcanic succession (Fig. 7). The vertical arrangement of units, from

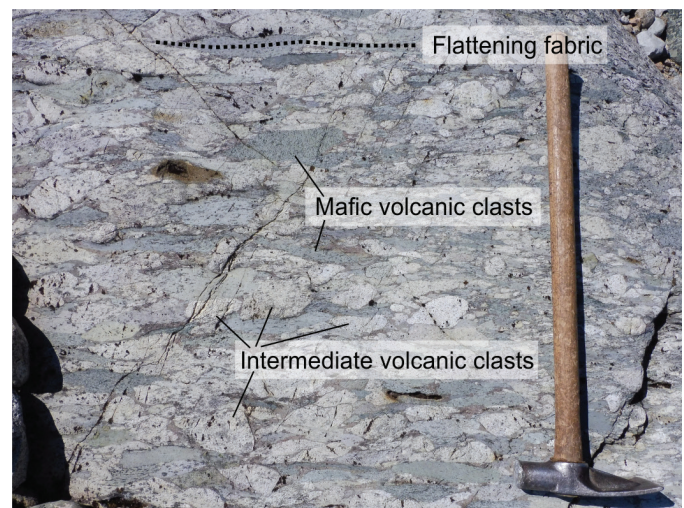


**Fig. 6.** Foliated polymictic conglomerate with light-toned intermediate volcanic clasts and medium green mafic volcanic clasts in a sandy matrix at north end of Butte ridge, unit uTrSvc (UTM 348320E-6334933N).

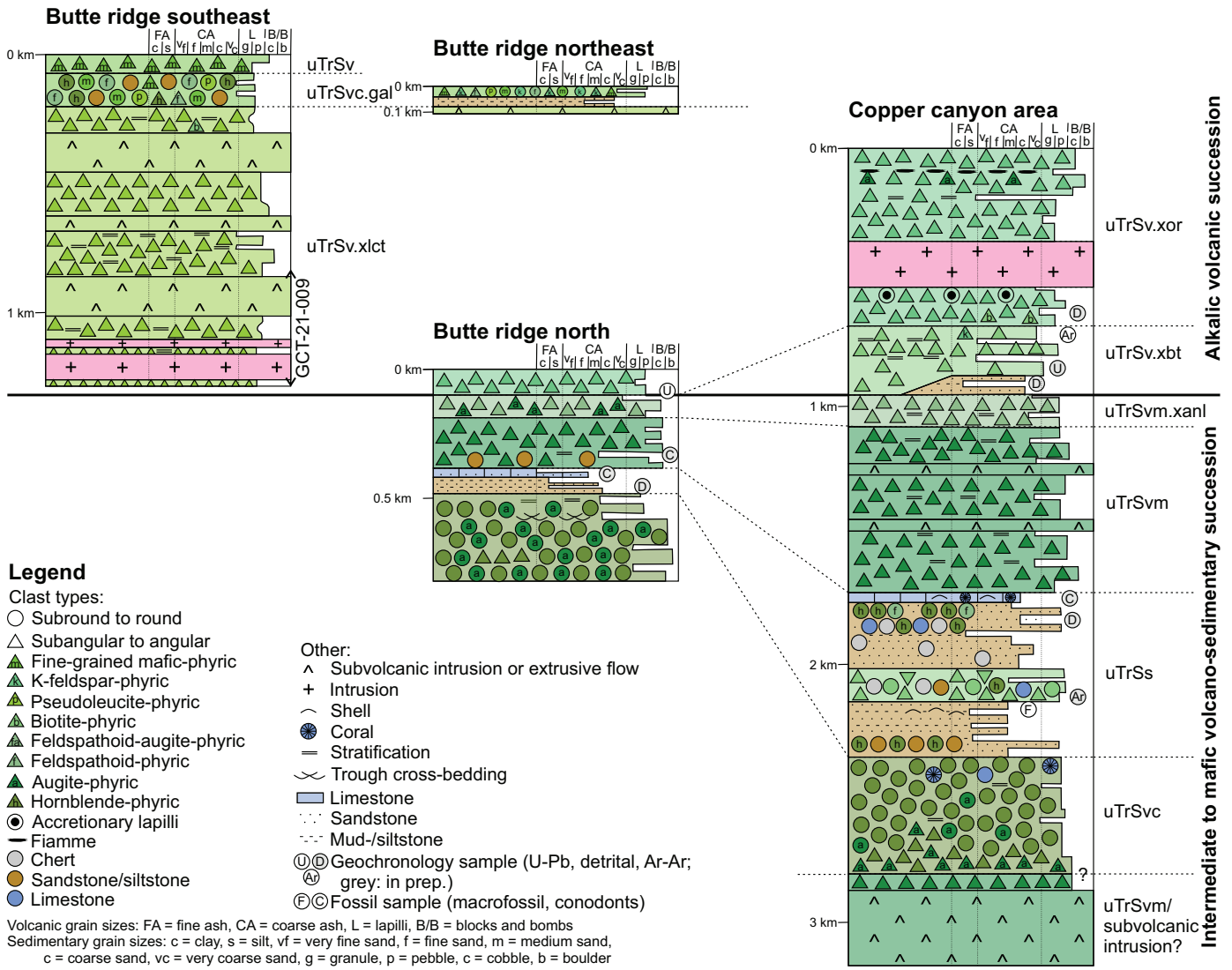


**Fig. 7.** Schematic stratigraphic sections for the southeast end of Butte ridge, northeast end of Butte ridge, north end of Butte ridge, and Copper canyon area. Stratigraphic units labelled on right-hand side of stratigraphic columns. See Figure 3 for colour legend of rock types.

bottom to top, was determined from observations presented above. Unit thicknesses were calculated by measuring the distance perpendicular to strike between stations and correcting for bedding dip, elevation change, and the presence of folds. Stuhini Group units are cut by Galore intrusions, part of the Galore plutonic suite (Late Triassic).

**4.1. Stuhini Group (Upper Triassic)**  
**4.1.1. Lower intermediate to mafic volcano-sedimentary succession**

The lower succession comprises a conglomeratic unit with mainly volcanic clasts, a finer grained sedimentary unit, a mafic volcanic unit, and a feldspathoid-bearing mafic volcanic unit; all units are exposed in the Copper canyon area and at the north end of Butte ridge (Figs. 3a, b, and 7).

At the base of the section is a conglomeratic unit (uTrSvc) with light-toned hornblende-phyric intermediate volcanic

clasts and generally lesser medium green augite-phyric mafic volcanic clasts (Fig. 6). Metre-scale beds of conglomerate are interlayered with dm-scale beds of medium- to very coarse-grained sandstone and pebbly sandstone containing mainly volcanic fragments (Fig. 8). Minor intermediate and mafic volcanic rocks are locally observed. At Butte ridge, the unit fines upward from boulder conglomerate to pebble conglomerate, and the proportion of sandstone increases up section (Fig. 7); trough cross-bedding was observed near the top of the unit. In the Copper canyon area, a succession of mafic coherent rocks and minor mafic fragmental volcanic rocks is northeast of the polymictic conglomerate unit (Figs. 3a, 4 and 7). A lack of bedding measurements, way-up criteria, and the generally coherent nature of these rocks precludes a straightforward interpretation of their stratigraphic position. These rocks could represent a unit of mafic volcanic rocks stratigraphically below uTrSvc, or a relatively thin interbed of mafic volcanic rocks and



**Fig. 8.** Conglomerate and pebbly sandstone with well-rounded predominantly light-toned intermediate volcanic clasts, Copper Canyon area, unit uTrSvc (UTM 356557E–6337744N).

a thick mafic subvolcanic intrusion within uTrSvc. The fining-upward trend observed at Butte ridge continues in overlying unit uTrSs (Fig. 7), suggesting that the upper contact of unit uTrSvc is gradational.

The conglomeratic unit (uTrSvc) is overlain by a sedimentary unit (uTrSs; Figs. 3a, b, 4 and 7) in which interstratified fine- to very coarse-grained sandstone and siltstone predominate (Fig. 9a). Coarser grained sandstone contains abundant angular feldspar crystals, locally common light-toned microphenocrystic (likely intermediate) volcanic clasts, and ~2% quartz crystals. Minor conglomerate interbeds contain hornblende-phyric intermediate volcanic clasts, sedimentary rip-up clasts, chert clasts, limestone clasts and locally fine-grained white feldspathoid-phyric volcanic clasts. Bivalve imprints in the Copper canyon area (Fig. 9b) have been identified as *Monotis (Pacimonotis) subcircularis* Gabb 1864, a key index species of the Upper Norian Gnomohalorites cordilleranus ammonoid zone (C. McRoberts, pers. comm., 2022). Minor lime mudstone, limestone contaminated by siliciclastic sand and rare packstone is at or near the top of the unit. In the Copper canyon area, solitary corals are present in packstone and as reworked clasts in overlying sandstone. Also in the Copper canyon area, the unit contains an interval of biotite-phyric volcanic rocks and polymictic conglomerate with biotite-phyric volcanic clasts, chert clasts, sandstone/siltstone clasts, hornblende-phyric intermediate volcanic clasts and limestone clasts (Fig. 7). Interbedded mafic volcanic rocks, sandstone, siltstone, and lime mudstone at the base of the overlying mafic volcanic unit (uTrSvm) in the Copper canyon area suggest that the contact between uTrSs and uTrSvm is gradational. At Butte ridge, the contact with the overlying mafic volcanic unit (uTrSvm) is sharp.

A mafic volcanic unit (uTrSvm) overlies the sedimentary unit (uTrSs). It consists of lapillistone, tuff breccia, volcanic breccia,



**Fig. 9.** **a)** Laminated to dm-scale bedded sandstone and siltstone, unit uTrSs (UTM 348339E–6334499N). **b)** Bivalve *Monotis (Pacimonotis) subcircularis* Gabb 1864 (C. McRoberts, pers. comm., 2022) in sedimentary unit (22BvS-19-177, UTM 356420E–6337551N).

lesser coarse crystal tuff, and fine tuff. Volcanic clasts contain 15-30% equant augite phenocrysts (0.1-3 mm) and, locally, minor plagioclase phenocrysts and/or amygdules. Volcanic clasts commonly have smooth to lobate edges (Fig. 10) suggesting minimal reworking. At Butte ridge are very rare beds of volcanic-derived sandstone and limestone contaminated by crystal tuff or siliciclastic sand. Augite-phyric amygdaloidal coherent intervals, with up to 30-40% augite phenocrysts (up to 5 mm) and commonly with tubular vesicles represent sills and dikes, although some may be flows. At the north end of Butte ridge, volcanic rocks assigned to the overlying feldspathoid-bearing mafic volcanic unit (uTrSvm.xanl) contain both augite-phyric and feldspathoid-augite-phyric clasts, suggesting that the upward transition from unit uTrSvm is gradational.

A feldspathoid-bearing mafic volcanic unit (uTrSvm.xanl) overlies the mafic volcanic unit (uTrSvm). In the Copper canyon area, lapillistone, crystal tuff and volcanic breccia contain volcanic clasts up to 1 m with 10% white feldspathoid (0.2-2 mm) and 15% augite (1-2 mm) phenocrysts (Fig. 11). Based on the fine-grained nature of the feldspathoid and its occurrence in mafic rocks, it is interpreted as analcime. In the Copper canyon area, a biotite-phyric volcanic unit (uTrSv.

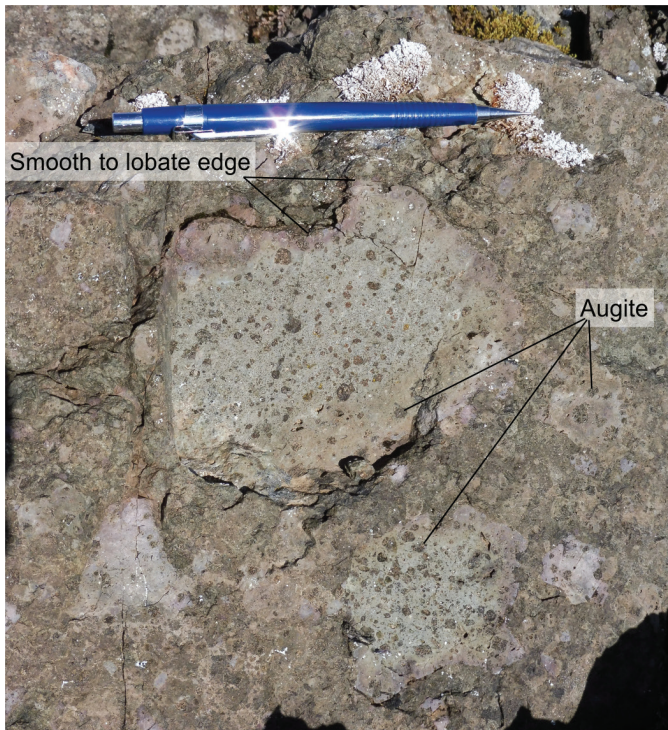


**Fig. 10.** Mafic tuff breccia with augite-phyric volcanic clasts with smooth to lobate edges, unit uTrSvm (UTM 356316E–6336829N).

xbt) of the upper succession overlies the feldspathoid-bearing mafic volcanic unit but is separated by a 2-metre covered interval. In the absence of evidence of a fault, we assume an abrupt stratigraphic contact. At the north end of Butte ridge, the K-feldspar-phyric volcanic unit (uTrSv.xor) of the upper succession overlies unit uTrSvm.xanl. In this case, the contact is exposed and sharp (Fig. 12), which we take as marking an abrupt stratigraphic transition between the lower and upper succession.

#### 4.1.2. Upper alkalic volcanic succession

The upper alkalic volcanic succession can be subdivided into a biotite-phyric volcanic unit (uTrSv.xbt), a K-feldspar-phyric volcanic unit (uTrSv.xor), pseudoleucite-phyric volcanic and subvolcanic units (uTrSv.xlct and LTrSh.xlct), and a polymictic conglomerate unit with alkalic volcanic clasts (uTrSvc.gal; Fig. 7). The biotite-phyric volcanic unit was only observed in the Copper canyon area. The K-feldspar phyric volcanic unit is exposed in the Copper canyon area and at the north end of Butte ridge. The pseudoleucite-phyric units and polymictic conglomerate unit are only found on Butte ridge (Fig. 3). The stratigraphic position of the pseudoleucite-phyric units and polymictic conglomerate unit relative to the other alkalic volcanic units is poorly constrained.

The biotite-phyric volcanic unit (uTrSv.xbt) consist of laminated to m-scale bedded maroon and green coarse crystal tuff, lapilli-tuff, lapillistone and fine tuff with biotite-phyric volcanic clasts and common free biotite crystals (Fig. 13). Interbeds of biotite-rich volcanic sandstone and volcanic

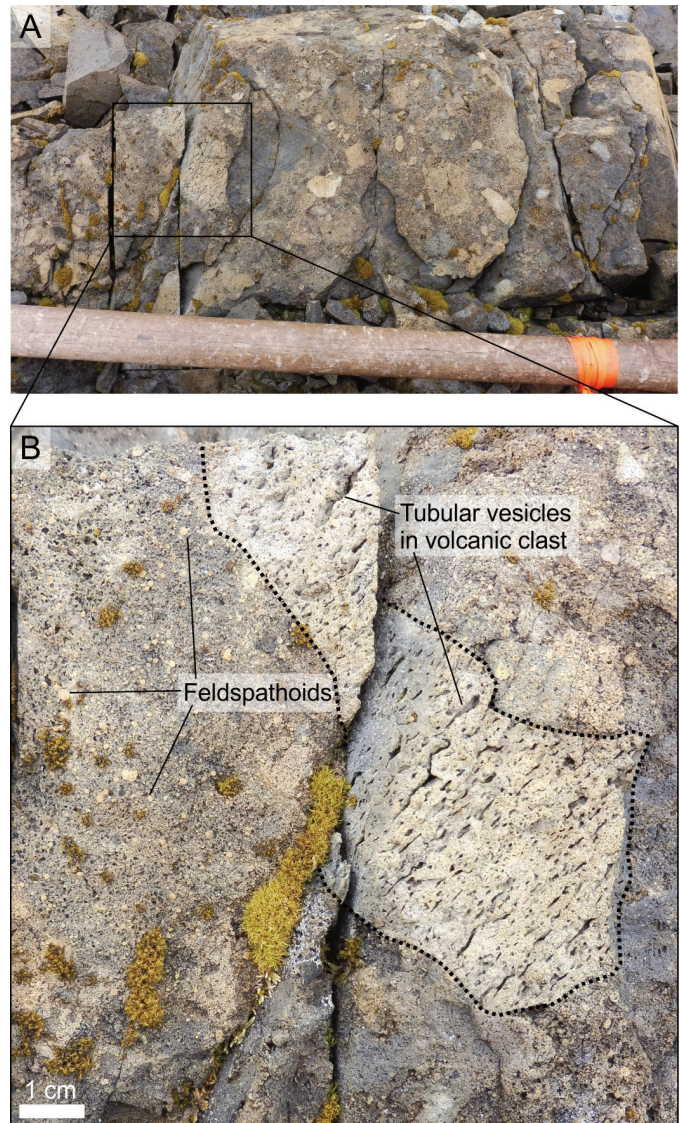


**Fig. 11. a)** Lapillistone. **b)** close up of a) showing subangular volcanic clasts containing fine-grained white feldspathoids, augite, and rare tubular vesicles, unit uTrSvm.xanl (UTM 355296E–6337109N).

siltstone are locally common and contain rare soft-sediment deformation structures. Farther east (shown at depth on Fig. 3a), the base of the unit comprises laminated to dm-scale bedded siltstone, medium- to very coarse-grained sandstone, and lesser m-scale beds of lapillistone. Siliciclastic strata show fining upward sandstone to siltstone couplets with common basal flames, scours, and load casts. A similar maroon tuff to lapillistone unit with biotite-phyric clasts at the toe of the Copper canyon glacier locally contains accretionary lapilli near its top contact. In the Copper canyon area and at the toe of the Copper canyon glacier (Fig. 2), the biotite-phyric volcanic unit is gradationally overlain by a K-feldspar-phyric volcanic unit (uTrSv.xor), with the biotite crystal content decreasing and the K-feldspar crystal content increasing across the contact (Fig. 7).

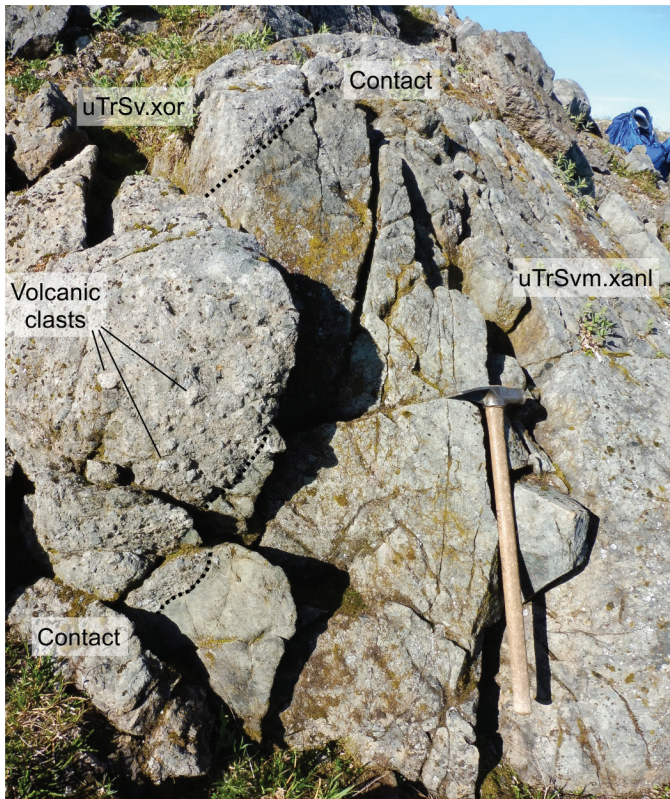


**Fig. 12.** Sharp basal contact of K-feldspar-phyric volcanic unit (uTrSv.xor) with underlying feldspathoid-bearing mafic volcanic unit (uTrSvm.xanl), north end of Butte ridge (UTM 348453E–6334157N).



**Fig. 13.** Laminated to dm-scale bedded crystal tuff and lapilli-tuff with biotite crystals (unit uTrSv.xbt) (UTM 355975E–6335269N).

The K-feldspar-phyric volcanic unit (uTrSv.xor) comprises crudely interstratified lapilli-tuff, tuff, lapillistone, tuff breccia, and volcanic breccia containing predominantly K-feldspar-phyric clasts and free blocky to tabular K-feldspar crystals up to 2-5 cm long (Fig. 14a). Volcanic clasts show a wide range in K-feldspar phenocryst abundance, size, and shape. Accretionary lapilli were locally observed near the bottom of the unit in the Copper canyon area (Fig. 14b). The unit contains minor welded lapilli tuff with sparsely K-feldspar-phyric fiamme in the Copper canyon area and at the north end of Butte ridge (Fig. 14c). In the Copper canyon area, rare tuff breccia

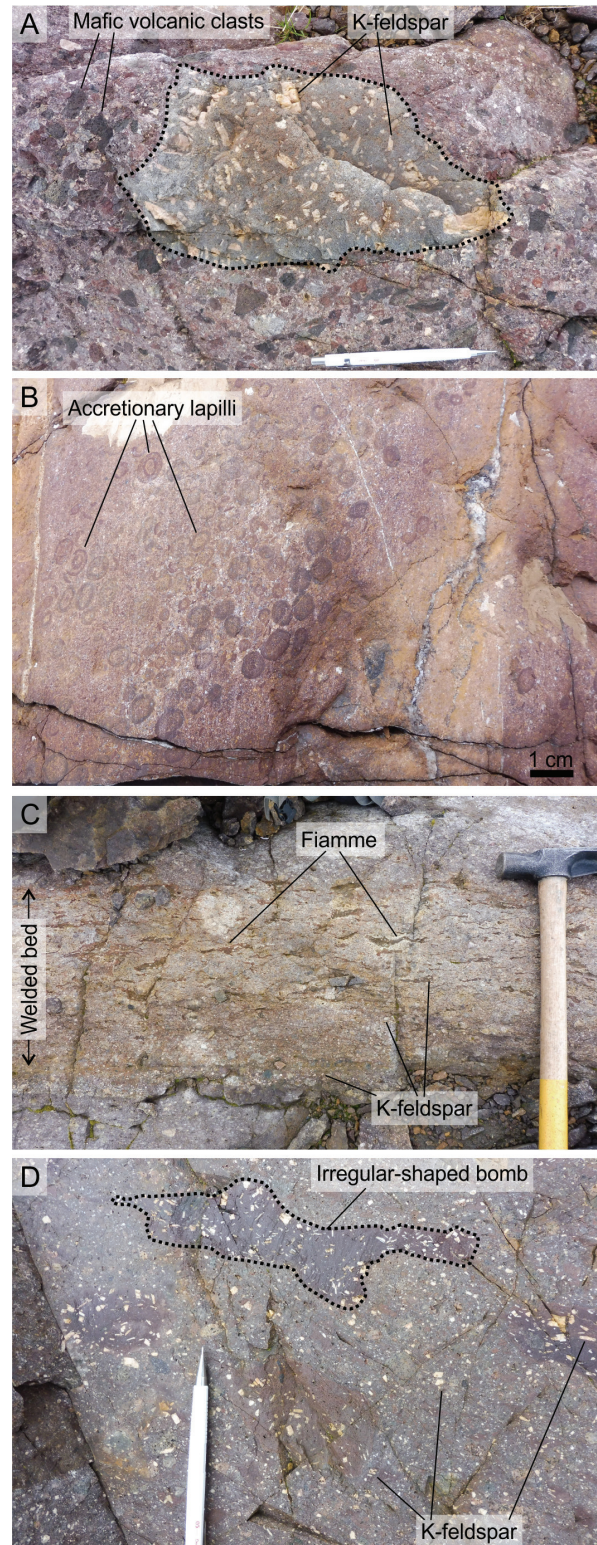


**Fig. 14.** K-feldspar-phyric volcanic unit (uTrSv.xor). **a)** Tuff breccia with K-feldspar-phyric volcanic clasts, dark-toned augite-plagioclase-phyric mafic volcanic clasts and maroon to grey fine-grained volcanic clasts (UTM 356670E–6333826N). **b)** Lapilli-tuff with accretionary lapilli (UTM 356828E–6334325). **c)** Welded lapilli-tuff with sparsely K-feldspar-phyric fiamme (same UTM as a). **d)** Lapillistone with sparsely K-feldspar-phyric volcanic bombs with lobate outlines (same UTM as a).

with K-feldspar-phyric volcanic clasts and augite-plagioclase-phyric clasts, both with subangular shapes to irregular lobate borders, suggests coeval eruption of alkalic and mafic magma. Locally in the Copper canyon area are sparsely K-feldspar-phyric elongate volcanic bombs with irregular lobate borders (Fig. 14d). Welding textures, accretionary lapilli, and irregular-shaped volcanic bombs all suggest primary pyroclastic subaerial deposition.

A pseudoleucite-phyric volcanic unit (uTrSv.xlct) is exposed on the southern and eastern parts of Butte ridge (Figs. 3c, 7), but contact relationships with units described above were not observed. The unit comprises lapillistone to lapilli-tuff, lesser tuff breccia, and minor laminated to cm-scale bedded fine tuff and coarse crystal tuff. The rocks contain clast- to matrix-supported light to medium grey to greenish-grey pseudoleucite-phyric volcanic clasts, light to medium grey to greenish grey aphyric volcanic clasts and common free pseudoleucite crystals in an ash matrix (Fig. 15a). Crude stratification is defined by slight variations in clast size and rare tuff layers. Irregular- to amoeboid-shaped pseudoleucite-phyric clasts are locally common. Massive intervals with abundant broken pseudoleucite crystals (Fig. 15b) are likely fragmental in origin; the uniform appearance of these intervals may be due to welding or alteration of matrix. The unit contains minor pseudoleucite-phyric coherent intervals similar to unit LTrSh.xlct described below.

Pseudoleucite-phyric coherent rocks (unit LTrSh.xlct) are common on the southern, eastern, and northeastern parts of Butte ridge (Figs. 3b, c and 7). They generally contain 15-35% zoned pseudoleucite phenocrysts (1-5 cm; Fig. 15c); crystals are locally flattened and rarely broken. Abrupt contacts, locally sharp and clearly intrusive, suggest these are mostly subvolcanic intrusions cutting units uTrSv.xlct and uTrSvc.gal, although some coherent intervals could also be extrusive lava flows.

A polymictic conglomerate unit with alkalic volcanic clasts (uTrSvc.gal) occurs on the southern and northeastern parts of Butte ridge. At the south end of Butte ridge, polymictic conglomerate is interbedded with lesser sandstone to coarse crystal tuff laminae, beds, and lenses (Fig. 16). The pebble to rare cobble conglomerate contains subangular to subrounded fine-grained feldspathoid-phyric volcanic clasts, hornblende-phyric intermediate volcanic clasts, green fine-grained volcanic clasts, pseudoleucite-phyric volcanic clasts, stratified crystal tuff to sandstone clasts, and very rare chert and limestone clasts. At the northeast end of Butte ridge, green laminated to cm-scale bedded volcanic-derived sandstone transitions gradationally westward into alternating interbeds of: 1) lapillistone to lapilli-tuff with volcanic clasts containing 10-15% mostly equant mafic phenocrysts (0.5-1.5 mm); 2) lapillistone to lapilli-tuff with volcanic clasts containing tabular K-feldspar phenocrysts; 3) polymictic pebble conglomerate containing predominantly volcanic clasts similar to 1) and 2) above and sparser clasts with 15% white feldspathoid (0.2-3 mm) phenocrysts, clasts

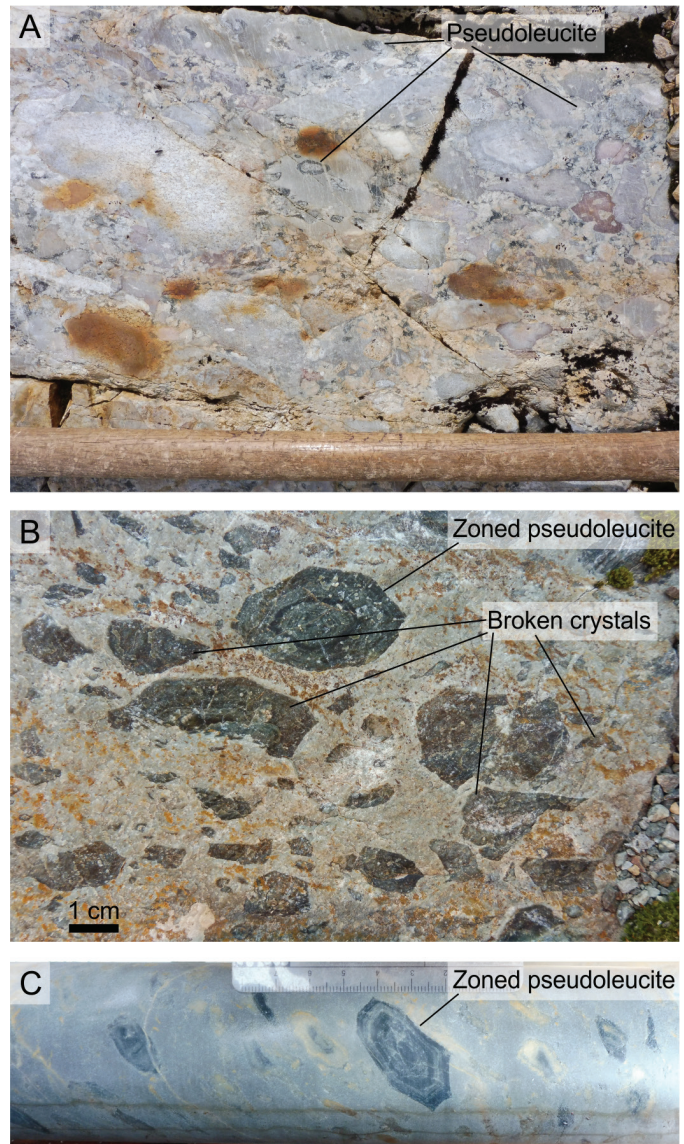


**Fig. 15.** Pseudoleucite-phyric volcanic and subvolcanic units (uTrSv.xlct, LTrSh.xlct). **a)** Tuff breccia with pseudoleucite-phyric and aphyric volcanic clasts (349393E-6332484N). **b)** Massive rock with abundant broken pseudoleucite crystals (349657E-6332326N). **c)** Coherent rock with coarse pseudoleucite phenocrysts (DDH GCT-21-009, UTM 349652E-6332319N).

with pseudoleucite phenocrysts, and clasts with feldspathoid and K-feldspar phenocrysts; and 4) volcanic-derived sandstone to crystal tuff (Figs. 3b, 7). Common stratified green siltstone to sandstone clasts in the basal volcanic rocks suggest the succession is right-way-up.

At the southern end of Butte ridge, a succession of polymictic conglomerate with alkalic volcanic clasts (uTrSvc.gal) transitions westward into unassigned volcanic rocks (uTrSv; Fig. 3c); the contact is not exposed. The unassigned volcanic rocks include medium grey lapillistone to tuff breccia with volcanic clasts that contain 15-20% equant mafic minerals (1 mm). Farther west, across the axial trace of an inferred synform, the lapillistone to tuff breccia succession envelops



**Fig. 16.** Foliated polymictic conglomerate interbedded with sandstone to coarse crystal tuff, south end of Butte ridge, unit uTrSv.gal (UTM 348945E–6332394N).

distinct dark green fragmental volcanic rocks with ~10% mafic minerals (<1 mm, Fig. 3c).

#### 4.2. Galore plutonic suite (Late Triassic)

A multi-phase syenitic to monzodioritic intrusive complex in the Galore Creek valley (Fig. 2) envelopes and partly hosts the mineral deposits in the area. The alkalic intrusions typically contain distinct K-feldspar phenocrysts and/or pseudoleucite phenocrysts. Numerous smaller satellite stocks, sills, and dikes are present throughout the Galore Creek area. The intrusive phases were not studied in detail here, and the reader is referred to Enns et al. (1995) for detailed descriptions.

In the Copper canyon area, common K-feldspar- and pseudoleucite-K-feldspar-phyric intrusions cut all units, including the K-feldspar-phyric volcanic unit (uTrSv.xor). Two distinct pyritic pseudoleucite and K-feldspar porphyritic dikes (up to 1 m wide) were observed cutting unit uTrSv.xor. These dikes may be related to a compositionally similar stock centred on the Copper canyon deposit (Petsel and McConeghy, 2008; Fig. 2). At the southeast end of Butte ridge in drill hole GCT-21-009, several Galore intrusions cut the pseudoleucite-phyric volcanic unit (uTrSv.xlct; Figs. 3c, 7), and include fine-grained equigranular and K-feldspar porphyritic varieties.

#### 5. Geochronology

Herein we present preliminary results for four geochronology samples collected in 2019. Detailed analytical methods and final results will be reported elsewhere. U-Pb zircon and titanite analyses were carried out at the Pacific Centre for Isotopic and Geochemical Research (University of British Columbia), and Ar-Ar biotite analyses at the Manitoba Isotope Research Facility (University of Manitoba). Two samples failed to return zircon or titanite: one sample of the K-feldspar-phyric volcanic unit (19BvS-9-84, UTM 357008E-6334238N); and one sample

of the pseudoleucite-phyric volcanic unit (19BvS-9-80, UTM 348679E-6333727N).

#### 5.1. Biotite-phyric volcanic unit (uTrSv.xbt), upper succession

In the Copper canyon area, near the top of the biotite-phyric volcanic unit (uTrSv.xbt), we sampled a green-weathering well-stratified coarse crystal tuff, lapilli tuff, and volcanic sandstone (Figs. 2, 7; sample 19BvS-9-83, UTM 357039E-6334294N). The rocks contain abundant fresh biotite (0.5-2 mm), common angular K-feldspar crystals, and angular to subangular biotite-phyric and K-feldspar-phyric volcanic clasts. The sample returned a  $209 \pm 1$  Ma Ar-Ar biotite cooling age defined by 86.62% of  $^{39}\text{Ar}$  released (Fig. 17a). Heating steps 3 to 6 define a visual plateau, and because the errors on the dates for these steps are very small (0.2 Ma at  $2\sigma$ , Fig. 17a), we report the two sigma error on the age as the standard deviation of the dates for these steps.

#### 5.2. K-feldspar-phyric volcanic unit (uTrSv.xor), upper succession

At the north end of Butte ridge, from the immediate base of the K-feldspar-phyric volcanic unit (uTrSv.xor), we sampled interstratified coarse crystal tuff, lapilli-tuff, lapillistone, and minor tuff or fine-grained volcanic-derived sandstone (Figs. 2, 7; sample 19BvS-9-82, UTM 348565E-6334285N). The outcrop contains abundant K-feldspar-phyric volcanic clasts set in a K-feldspar crystal-rich matrix, with rare 30-40 cm sandstone clasts. The sample yielded minor zircon and titanite. It returned a U-Pb zircon chemical abrasion thermal ionization mass spectrometry (CA-TIMS) date of  $210.27 \pm 0.19$  Ma, an overlapping U-Pb titanite isotope dilution thermal ionization mass spectrometry (ID TIMS) date of  $210.22 \pm 0.36$  Ma, and a combined  $210.26 \pm 0.17$  Ma date (Fig. 17b) interpreted as the depositional age. It is the first precise age determination for the onset of upper succession alkalic volcanism in northwestern British Columbia.

#### 6. Discussion

Below we present thickness estimates and discuss the general depositional setting, volcanic history, and significance of intermediate volcanic and alkalic volcanic rocks of the Stuhini Group in the Galore Creek area, and the tectonic setting of Stuhini Group volcanism regionally.

##### 6.1. Thickness estimates

In Figure 18 we compare the thickness estimates of the Stuhini Group at Butte ridge and Copper canyon area with those for the Central zone deposit area (L. Bailey, pers. comm., 2022). The Central zone estimates are based on a three-dimensional lithological model generated from extensive drilling of altered and mineralized rocks. Thickness estimates at Butte ridge and the Copper canyon area have been corrected by removing intrusions and subvolcanic sills. Due to strong texturally

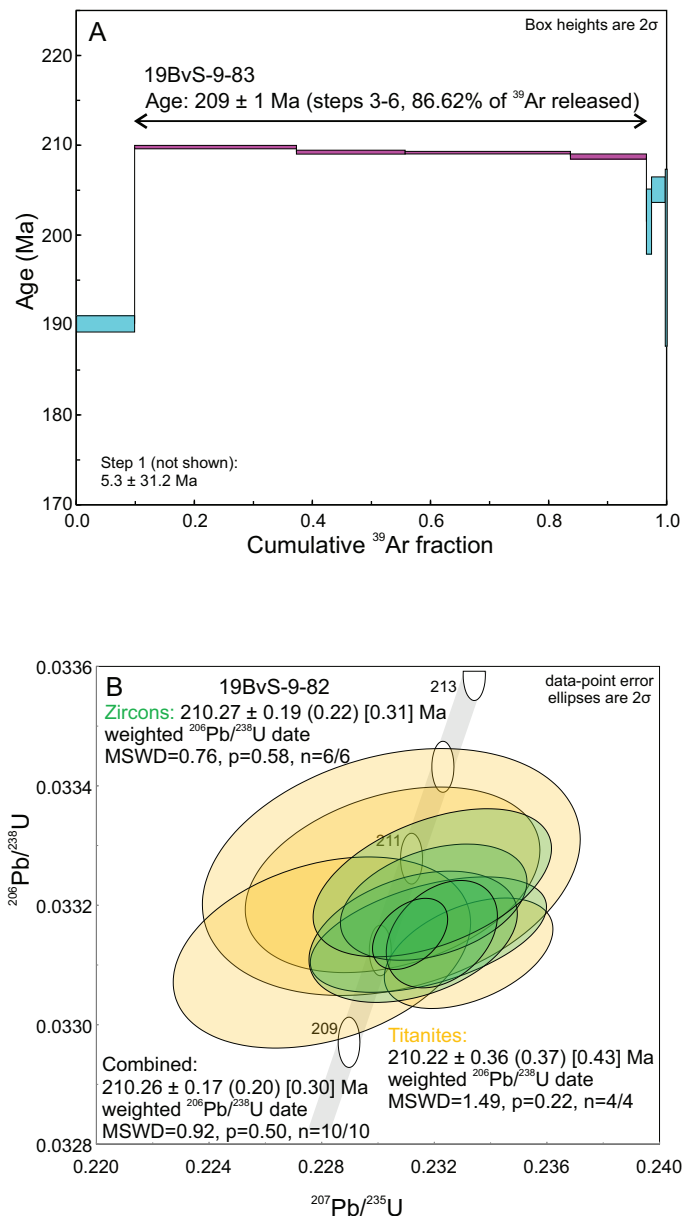


**Fig. 17.** Geochronology plots. **a)** Biotite Ar-Ar step-heating spectrum from biotite-phyric volcanic unit (uTrSv.xbt). **b)** U-Pb concordia diagram showing zircon CA-TIMS and titanite ID-TIMS results from the base of the K-feldspar-phyric volcanic unit (uTrSv.xor). Weighted average  $2\sigma$  errors are reported in the format  $\pm X$  (Y) [Z] of Schoene et al. (2006), where X is based on analytical errors only; Y also includes isotopic tracer errors, and Z also includes analytical, tracer and  $^{238}\text{U}$  decay constant errors. When comparing U-Pb results with dates derived from other isotopic systems (e.g., Ar-Ar), the largest error, Z, should be used.

destructive hydrothermal alteration and mineralization, it is unclear if the pseudoleucite-phyric unit in the Central zone represents a subvolcanic intrusion, an extrusive volcanic unit, or a combination of both (L. Bailey, N. Peterson and W.-S. Lee, pers. comm., 2022).

Precise thickness estimates for Butte ridge and the Copper canyon area are hampered by common massive to poorly

stratified lithological units, tectonic flattening fabrics, folds, and faults. The thickness estimates for the southeast end of Butte ridge may be overestimated due to limited bedding measurements and possible folds. At the north end of Butte ridge, thickness estimates may be underestimated due to the flattening fabric developed throughout the area. Thickness estimates for the Copper canyon area may be overestimated because of unrecognized folds. Minimum thickness estimates for the lower intermediate to mafic volcano-sedimentary succession vary from 0.7 km at Butte ridge, to 1.1 km in the Central zone, to 1.8 km in the Copper canyon area and suggest an eastward thickening trend (Fig. 18). The average of these three measurements, 1.2 km, is probably a realistic minimum for this succession. The upper alkalic volcanic succession shows significant facies changes throughout the Galore Creek area but is at least 0.8 km thick.

## 6.2. Depositional setting and volcanic history

The lower intermediate to mafic volcano-sedimentary succession grades upward from a conglomeratic unit containing hornblende-phyric intermediate volcanic clasts and augite-phyric mafic volcanic clasts, a finer-grained sedimentary unit capped by limestone, a mafic volcanic unit to a feldspathoid-bearing mafic volcanic unit. Abundant coarse volcanic clasts in the lower conglomeratic unit suggests proximity to volcanic centres. The succession was deposited, at least in part, in a submarine setting as shown by the presence of marine bivalves, corals, and limestone. A fining upward trend accompanied by a decrease in volcanic debris in the sedimentary unit (Fig. 7) likely marks the decline of intermediate volcanic activity culminating in limestone deposition. The overlying mafic volcanic and feldspathoid-bearing mafic volcanic units are largely primary volcanic in origin, with limited evidence for reworking and very rare sandy limestone beds suggesting possible continued subaqueous deposition. The presence of monomictic volcanic breccia with feldspathoid-augite-phyric volcanic clasts up to 1 m (unit uTrSv.m.xanl) in the Copper canyon area suggests vent-proximal deposition, and a transition to silica-undersaturated magmatism.

The upper alkalic volcanic succession includes a biotite-phyric volcanic unit, a K-feldspar-phyric volcanic unit, pseudoleucite-phyric volcanic and subvolcanic units and a polymictic conglomerate unit with alkalic volcanic clasts. A sharp basal contact suggests an abrupt change to alkalic volcanism. In the Copper canyon area, initial deposition occurred in a subaqueous setting with common sedimentary rocks and reworked biotite crystal-rich volcanic strata (both containing soft-sediment deformation structures) near the base grading up into biotite-phyric volcanic rocks. Accretionary lapilli near the top of this unit at the toe of the Copper canyon glacier suggest a change to subaerial deposition. This unit has not been observed in the Galore Creek valley and on Butte ridge. Within the overlying K-feldspar-phyric unit, accretionary lapilli, welded beds, and irregular-shaped bombs suggest subaerial primary volcanic deposition. This unit is observed throughout the Galore Creek

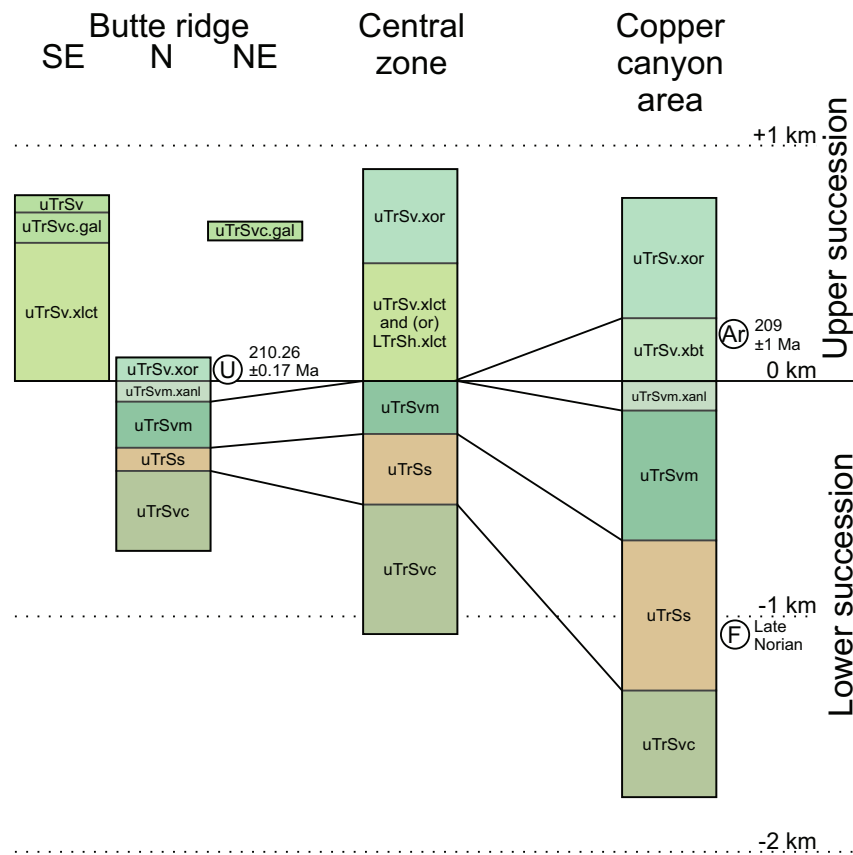


**Fig. 18.** Stratigraphic thickness variations and correlations across the Galore Creek district from west to east. Thicknesses are corrected by removing (subvolcanic) intrusions. Central zone deposit area thicknesses from L. Bailey (pers. comm., 2022).

area, suggesting a paleogeography with an emergent volcanic centre. A pseudoleucite-phyric volcanic unit several 100 m thick is at the south end of Butte ridge, with unknown thicknesses of pseudoleucite-phyric volcanic rocks at the east end of Butte ridge. A thick section of pseudoleucite-phyric rocks also occurs in the Central zone, but their origin as volcanic and/or subvolcanic rocks is uncertain due to a strong alteration and mineralization overprint. Their absence in the eastern part of the study area suggests they formed local volcanic centres. The relative timing of K-feldspar-phyric and pseudoleucite-phyric volcanism is uncertain. They may be temporally coincident but spatially restricted, temporally coincident and interfingering, or superimposed. Polymictic conglomerates from reworking of alkalic volcanic strata on Butte ridge either formed late or in a more distal position that allowed sourcing from different volcanic centres. No strata younger than the alkalic volcanic succession have been observed in the study area, and the lack of a top contact precludes determination of total thicknesses.

### 6.3. Stuhini Group intermediate volcanic rocks

Throughout Stikinia, Lewes River, Stuhini and Takla group (Late Triassic) volcanic strata consist predominantly of augite-phyric mafic volcanic rocks (Monger, 1977; Bradford and Brown, 1993; van Straaten et al., 2022). In contrast, Late Triassic strata in the Galore Creek area and west half

of the Telegraph Creek map sheet (NTS 104G/W, Fig. 1) contain both augite-phyric mafic volcanic and hornblende-phyric intermediate volcanic rocks (Logan and Koyanagi, 1994; Brown et al., 1996; this study). Interestingly, this area also exposes the oldest known rocks within Stikinia (Early to Middle Devonian Stikine assemblage; Logan et al., 2000; Logan, 2004) and the area contains two large (>1 Bt) porphyry Cu±Au deposits. The presence of intermediate volcanic rocks suggests a more mature arc segment, possibly due to a different crustal architecture or distinct magmatic evolution, which may have played a role in the region's significant endowment with magmatic-hydrothermal mineral deposits.

### 6.4. Stuhini Group alkalic volcanic rocks

Our high-precision U-Pb zircon and titanite age of 210.26 ± 0.17 Ma for the onset of upper succession alkalic volcanism is broadly coeval with published ages for mineralogically, texturally, and compositionally similar alkalic silica-undersaturated Galore intrusions (ca. 210-208 Ma, see Section 2.2.) and genetically related porphyry Cu-Au-Ag formation. Regionally, strata similar to the upper alkalic volcanic unit of the Stuhini Group described herein are prospective for Galore Creek-style porphyry systems. In the Burgundy ridge area (Fig. 1) K-feldspar- and biotite-phyric volcanic rocks are surrounded by an apron of detrital biotite-

rich wacke (Mihalynuk et al., 2011; 2012). The Burgundy ridge prospect (MINFILE 104B 325) hosts skarn- and porphyry-style alteration in K-feldspar-porphyrific syenitic rocks, where drilling returned 91.26 m of 0.38% Cu, 0.3 g/t Au and 4.12 g/t Ag (Enduro Metals Corp., 2021). A sample from a megacrystic syenite intrusion returned a  $207.8 \pm 2.7$  Ma LA-ICP-MS U-Pb titanite age (Enduro Metals Corp., 2021). In the Trek area (Fig. 1), pseudoleucite-phyric volcanic rocks and K-feldspar- and pseudoleucite-porphyrific intrusions were reported by Close and Danz (2012). Drilling at the Trek north zone prospect (MINFILE 104G 022) returned 113.64 m of 0.25% Cu, 0.30 g/t Au, and 3.01 g/t Ag (Close and Danz, 2012). The Galore Creek, Copper Canyon, Trek, and Burgundy ridge occurrences may represent a northwest-southeast trending corridor containing Stuhini Group alkalic volcanic rocks, with enhanced prospectivity and increased preservation potential for Galore Creek-type porphyry systems.

### 6.5. Tectonic setting

Our stratigraphic and geochronological studies at Galore Creek confirm that Stuhini arc volcanism, widespread throughout Stikinia, is succeeded by local ca. 210-208 Ma alkalic silica-undersaturated magmatism. Post-subduction alkalic magmatism is coeval with a significant magmatic gap, a regional-scale unconformity and deformation attributed to the onset of collision between the Yukon-Tanana and Stikine terranes (Nelson and van Straaten, 2020; Nelson et al., 2022).

### 7. Conclusions

Our stratigraphic studies in the Galore Creek area show that the Stuhini Group can be subdivided in a lower intermediate to mafic volcano-sedimentary succession and an upper alkalic volcanic succession. The lower succession (at least ~1.2 km thick) shows a fining upward sequence from reworked intermediate  $\pm$  mafic volcanic rocks to sedimentary rocks (Late Norian), which are overlain by mafic volcanic rocks and capped by a relatively thin unit of analcime-bearing mafic volcanic rocks. Deposition of the lower succession was, at least in part, submarine. The lower succession is part of the Stuhini arc found along the eastern margin and northern part of Stikinia.

The contact between the lower succession and the upper alkalic volcanic succession (at least ~0.8 km thick) is abrupt. In the east, a local biotite-phyric volcanic and reworked volcanic unit was largely deposited subaqueously. Overlying K-feldspar-phyric volcanic rocks are found throughout the Galore area and record subaerial deposition. A thick package of pseudoleucite-phyric volcanic rocks and pseudoleucite-phyric subvolcanic intrusions is in the western and central parts of the Galore area; its depositional setting and relationships to other alkalic units are unclear. We constrain the onset of upper succession alkalic volcanism to  $210.26 \pm 0.17$  Ma using high-precision U-Pb zircon and titanite geochronology, broadly coeval with less-precise published ages for mineralogically, texturally, and compositionally similar alkalic silica-undersaturated Galore intrusions (ca. 210-208 Ma) suggesting a short-lived alkalic

magmatic event responsible for porphyry Cu-Au-Ag formation. The upper alkalic volcanic succession and alkalic silica-undersaturated Galore intrusions are part of a magmatic belt of small-volume stocks and rare volcanic rocks that orthogonally transects the earlier Stuhini arc. It reflects post-subduction alkalic magmatism and alkalic silica-undersaturated porphyry Cu-Au-Ag deposit formation during the early stages of Yukon-Tanana-Stikinia collision.

### Acknowledgments

The first author would like to thank Galore Creek Mining Corporation for logistical support, and Leif Bailey, Nils Peterson, Well-Shen Lee and colleagues for discussions and a warm welcome in camp. Thanks to Rebecca Hunter, Meghan Holowath and Emily Miller who assisted with field work in 2019 and 2022, Jim Logan, Gayle Febbo, Lori Kennedy, Russell Johnston, and Terry Poulton for discussions, Christopher McRoberts for bivalve identification, and JoAnne Nelson for a thorough review of the manuscript.

### References cited

- Allmendinger, R.W., Cardozo, N.C., and Fisher, D., 2013. *Structural Geology Algorithms: Vectors and Tensors*. Cambridge University Press, 289 p.
- Bailey, L., and Jutras, G., 2016. 2015 assessment report on the Schaft Creek porphyry copper-gold-molybdenum deposit. British Columbia Ministry of Energy and Mines, British Columbia Geological Survey Assessment Report 35967, 107 p.
- Bradford, J.A., and Brown, D.A., 1993. Geology of the Bearskin Lake and southern Tatsamenie Lake map areas, northwestern British Columbia (104K/1 and 8). In: *Geological Fieldwork 1992*, British Columbia Ministry of Energy and Mines, British Columbia Geological Survey Paper 1993-1, pp. 159-176.
- Brown, D.A., Gunning, M.H., and Greig, C.J., 1996. The Stikine project: Geology of western Telegraph Creek map area, northwestern British Columbia. British Columbia Ministry of Employment and Investment, British Columbia Geological Survey Bulletin 95, 130 p.
- Byrne, K., and Tosdal, R.M., 2014. Genesis of the Late Triassic southwest zone breccia-hosted alkalic porphyry Cu-Au deposit, Galore Creek, British Columbia, Canada. *Economic Geology*, 109, 915-938. Doi: 10.2113/econgeo.109.4.915.
- Campbell, M.E., 2021. The geology and geochemistry of the Sulphurets district porphyry Au-Cu-Mo deposits, British Columbia, Canada: Insights from a long-lived, gold-enriched porphyry district. Ph.D. thesis, Oregon State University, 238 p. Available from <[https://ir.library.oregonstate.edu/concern/graduate\\_thesis\\_or\\_dissertations/jw827k32f](https://ir.library.oregonstate.edu/concern/graduate_thesis_or_dissertations/jw827k32f)>
- Cardozo, N., and Allmendinger, R.W., 2013. Spherical projections with OSXStereonet. *Computers & Geosciences*, 51, 193-205. Doi: 10.1016/j.cageo.2012.07.021.
- Close, S., and Danz, N., 2012. 2011 Geological, geophysical and geochemical report on the Trek property. British Columbia Ministry of Energy and Mines, British Columbia Geological Survey Assessment Report 32866, 53 p.
- Colpron, M., Sack, P.J., Crowley, J.L., Beranek, L.P., and Allan, M.M., 2022. Late Triassic to Jurassic magmatic and tectonic evolution of the intermontane terranes in Yukon, northern Canadian Cordillera: Transition from arc to syn-collisional magmatism and post-collisional lithospheric delamination. *Tectonics*, 41 (2), e2021tc007060. Doi: 10.1029/2021TC007060.
- Coulson, I.M., Russell, J.K., and Dipple, G.M., 1999. Origins of the

- Zippa Mountain pluton: a Late Triassic, arc-derived, ultrapotassic magma from the Canadian Cordillera. *Canadian Journal of Earth Sciences*, 36, 1415-1434. Doi: 10.1139/e99-045.
- Cui, Y., Hickin, A.S., Schiarizza, P., and Diakow, L.J., 2017. British Columbia digital geology. British Columbia Ministry of Energy, Mines and Petroleum Resources, British Columbia Geological Survey Open File 2017-08, 9p. Data version 2019-12-19. <<https://www2.gov.bc.ca/gov/content/industry/mineral-exploration-mining/british-columbia-geological-survey/geology/bcdigitalgeology>>
- Duuring, P., Rowins, S.M., McKinley, B.S.M., Dickinson, J.M., Diakow, L.J., Kim, Y.-S., and Creaser, R.A., 2009. Examining potential genetic links between Jurassic porphyry Cu-Au  $\pm$ Mo and epithermal Au  $\pm$ Ag mineralization in the Toadoggonne district of north-central British Columbia, Canada. *Mineralium Deposita*, 44, 463-496. Doi: 10.1007/s00126-008-0228-9.
- Enduro Metals Corp., 2021. University study pinpoints Enduro's Burgundy system as Galore Creek suite. News release, January 18, 2021. <https://endurometals.com/> (last accessed December 16, 2022).
- Enns, S.G., Thompson, J.F.H., Stanley, C.R., and Yarrow, E.W., 1995. The Galore Creek porphyry copper-gold deposits, northwestern British Columbia. In: Schroeter, T.G., (Ed.), *Porphyry deposits of the northwestern Cordillera of North America*, Canadian Institute of Mining and Metallurgy, Special Volume 46, pp. 630-644.
- Evenchick, C.A., McMechan, M.E., McNicoll, V.J., and Carr, S.D., 2007. A synthesis of the Jurassic-Cretaceous tectonic evolution of the central and southeastern Canadian Cordillera: Exploring links across the orogen. In: Sears, J.W., Harms, T.A., and Evenchick, C.A., (Eds.), *Whence the Mountains? Inquiries into the Evolution of Orogenic Systems: A Volume in Honor of Raymond A. Price*, Geological Society of America Special Paper 433, 117-145. Doi: 10.1130/2007.2433(06).
- Hatch Ltd., GR Technical Services Ltd., and Giroux Consultants Ltd., 2005. Geology and resource potential of the Copper canyon property. NI 43-101 technical report prepared for NovaGold Resources Inc., 74p. Available from <<https://www.sedar.com>>
- Henderson, J.R., Kirkham, R.V., Henderson, M.N., Payne, J.G., Wright, T.O., and Wright, R.L., 1992. Stratigraphy and structure of the Sulphurets area, British Columbia. In: *Current Research, Part A, Cordillera and Pacific Margin*, Geological Survey of Canada, Paper no. 92-1A, pp. 323-332.
- Hollis, L., and Bailey, L., 2013. Assessment report on drilling, geological, geochemical and geophysical work conducted during 2012 at the GJ/Kinaskan copper-gold porphyry project. BC Ministry of Energy and Mines, British Columbia Geological Survey Assessment Report 33815, 60 p.
- Hunter, R.C., and van Straaten, B.I., 2020. Preliminary stratigraphy and geochronology of the Hazelton Group, Kitsault River area, Stikine terrane, northwest British Columbia. In: *Geological Fieldwork 2019*, British Columbia Ministry of Energy, Mines and Petroleum Resources, British Columbia Geological Survey Paper 2020-02, pp. 101-118.
- Johnston, R., Kennedy, L., and van Straaten, B.I., 2023. Preliminary observations of a high-strain zone along the western flank of the Galore Creek deposit area, northwestern British Columbia. In: *Geological Fieldwork 2022*, British Columbia Ministry of Energy, Mines and Low Carbon Innovation, British Columbia Geological Survey Paper 2023-01, pp. 51-63.
- Kovacs, N., Allan, M.M., Crowley, J.L., Colpron, M., Hart, C.J.R., Zagorevski, A., and Creaser, R.A., 2020. Carmacks copper Cu-Au-Ag deposit: Mineralization and postore migmatization of a Stikine arc porphyry copper system in Yukon, Canada. *Economic Geology*, 115, 1413-1442. Doi: 10.5382/econgeo.4756.
- Lang, J.R., Stanley, C.R., and Thompson, J.F.H., 1995. Porphyry copper-gold deposits related to alkaline igneous rocks in the Triassic-Jurassic arc terranes of British Columbia. In: Pierce, F.W., and Bolm, J.G., (Eds.), *Porphyry Deposits of the American Cordillera*, Arizona Geological Society Digest 20, pp. 219-236.
- Logan, J.M., 2004. Geology and geochemistry of the Foremore area. British Columbia Ministry of Energy and Mines, British Columbia Geological Survey Open File 2004-11, 1:50,000 scale.
- Logan, J.M., Drobe, J.R., and McClelland, W.C., 2000. Geology of the Forrest Kerr-Mess Creek area, northwestern British Columbia. British Columbia Ministry of Energy and Mines, British Columbia Geological Survey Bulletin 104, 132 p.
- Logan, J.M., and Koyanagi, V.M., 1994. Geology and mineral deposits of the Galore Creek area. British Columbia Ministry of Energy, Mines and Petroleum Resources, British Columbia Geological Survey Bulletin 92, 102 p.
- Logan, J.M., and Mihalynuk, M.G., 2014. Tectonic controls on Early Mesozoic paired alkaline porphyry deposit belts (Cu-Au  $\pm$ Ag-Pt-Pd-Mo) within the Canadian Cordillera. *Economic Geology*, 109, 827-858. Doi: 10.2113/econgeo.109.4.827.
- Logan, J.M., Koyanagi, V.M., and Rhys, D., 1993a. Geology and mineral occurrences of the Galore Creek area (NTS 104G/3). British Columbia Ministry of Energy, Mines and Petroleum Resources, British Columbia Geological Survey Geoscience Map 1993-01. 1:50,000 scale.
- Logan, J.M., Koyanagi, V.M., and Rhys, D., 1993b. Geology and mineral occurrences of the Galore Creek area (NTS 104G/4). British Columbia Ministry of Energy, Mines and Petroleum Resources, British Columbia Geological Survey Geoscience Map 1993-02. 1:50,000 scale.
- Micko, J., Tosdal, R.M., Bissig, T., Chamberlain, C.M., and Simpson, K.A., 2014. Hydrothermal alteration and mineralization of the Galore Creek alkalic Cu-Au porphyry deposit, northwestern British Columbia, Canada. *Economic Geology*, 109, 891-914. Doi: 10.2113/econgeo.109.4.891.
- Mihalynuk, M.G., Nelson, J., and Diakow, L.J., 1994. Cache Creek terrane entrapment: Oroclinal paradox within the Canadian Cordillera. *Tectonics*, 13, 575-595. Doi: 10.1029/93TC03492.
- Mihalynuk, M.G., Logan, J.M., Zagorevski, A., and Joyce, N., 2011. Geology and mineralization of the Hoodoo Mountain area (NTS 104B/14E). In: *Geological Fieldwork 2010*, British Columbia Ministry of Energy and Mines, British Columbia Geological Survey Paper 2011-1, pp. 37-63.
- Mihalynuk, M.G., Zagorevski, A., and Cordey, F., 2012. Geology of the Hoodoo Mountain area (NTS 104B/14W). In: *Geological Fieldwork 2011*, British Columbia Ministry of Energy and Mines, British Columbia Geological Survey Paper 2012-1, pp. 45-68.
- Mihalynuk, M.G., Zagorevski, A., Joyce, N.L., and Creaser, R.A., 2016. Age of magmatism and mineralization at the Star (Sheslay, Copper Creek) copper porphyry prospect: Inception of the Late Triassic mineralized arc. In: *Geological Fieldwork 2015*, British Columbia Ministry of Energy and Mines, British Columbia Geological Survey Paper 2016-1, pp. 65-75.
- Mihalynuk, M.G., Zagorevski, A., Logan, J.M., Friedman, R.M., and Johnston, S.T., 2019. Age constraints for rocks hosting massive sulphide mineralization at Rock and Roll and Granduc deposits between Iskut and Stewart, British Columbia. In: *Geological Fieldwork 2018*, Ministry of Energy, Mines and Petroleum Resources, British Columbia Geological Survey Paper 2019-01, pp. 97-111.
- Monger, J.W.H., 1977. The Triassic Takla Group in McConnell Creek map-area, north central British Columbia. Geological Survey of Canada, Paper 76-29, 45 p.
- Mortensen, J.K., Ghosh, D., and Ferri, F., 1995. U-Pb age constraints of intrusive rocks associated with copper-gold porphyry deposits in the Canadian Cordillera. In: Schroeter, T.G., (Ed.), *Porphyry Deposits of the Northwestern Cordillera of North America*, Canadian Institute of Mining and Metallurgy Special Volume 46, pp. 142-158.
- Nelson, J.L., Colpron, M., and Israel, S., 2013. The Cordillera of British Columbia, Yukon and Alaska: Tectonics and metallogeny.

- In: Colpron, M., Bissig, T., Rusk, B. G., and Thompson, J., (Eds.), *Tectonics, Metallogeny and Discovery: The North American Cordillera and Similar Accretionary Settings*, Society of Economic Geologists Special Publication 17, pp. 53-110.
- Nelson, J.L., and van Straaten, B.I., 2020. Recurrent syn- to post-subduction mineralization along deep crustal corridors in the Iskut-Stewart-Kitsault region of western Stikinia, northwestern British Columbia. In: Sharman, E.R., Lang, J.R., and Chapman, J.B., (Eds.), *Porphyry Deposits of the Northwestern Cordillera of North America: A 25-Year Update*, Canadian Institute of Mining and Metallurgy Special Volume 57, pp. 149-211.
- Nelson, J.L., van Straaten, B., and Friedman, R., 2022. Latest Triassic-Early Jurassic Stikine-Yukon-Tanana terrane collision and the onset of accretion in the Canadian Cordillera: Insights from Hazelton Group detrital zircon provenance and arc-back-arc configuration. *Geosphere*, 18, 670-696. Doi: 10.1130/GES02444.1.
- Nelson, J.L., Waldron, J., van Straaten, B.I., Zagorevski, A., and Rees, C., 2018. Revised stratigraphy of the Hazelton Group in the Iskut River region, northwestern British Columbia. In: *Geological Fieldwork 2017*, British Columbia Ministry of Energy, Mines and Petroleum Resources, British Columbia Geological Survey Paper 2018-1, pp. 15-38.
- Oliver, J., and Gabites, J., 1993. Geochronology of rocks and polyphase deformation, Bearskin (Muddy) and Tatsamenie lakes district, northwestern British Columbia (104K/8, 1). In: *Geological Fieldwork 1992*, British Columbia Ministry of Energy, Mines and Natural Gas, British Columbia Geological Survey Paper 1993-1, pp. 177-188.
- Petsel, S.A., and McConeghy, C., 2008. 2007 Diamond drilling assessment report on the Copper canyon property. British Columbia Ministry of Energy and Mines, British Columbia Geological Survey Assessment Report 30184, 21 p.
- Prince, J., 2020. 2019 drilling, geological mapping and aerial survey assessment report on the Galore Creek project. British Columbia Ministry of Energy and Mines, British Columbia Geological Survey Assessment Report 39156, 48 p.
- Rees, C., Riedell, K.B., Proffett, J.M., Macpherson, J., and Robertson, S., 2015. The Red Chris porphyry copper-gold deposit, northern British Columbia, Canada: Igneous phases, alteration, and controls of mineralization. *Economic Geology*, 110, 857-888. Doi: 10.2113/econgeo.110.4.857.
- Rhys, D.A., 1993. Geology of the Snip mine, and its relationship to the magmatic and deformational history of the Johnny Mountain area, northwestern British Columbia. M.Sc. thesis, The University of British Columbia, Vancouver, B.C., Canada. <<https://circle.ubc.ca/handle/2429/2173>>
- Schoene, B.A., Crowley, J.L., Condon, D.J., Schmitz, M.D., and Bowring, S.A., 2006. Reassessing the uranium decay constants for geochronology using ID-TIMS U-Pb data. *Geochimica et Cosmochimica Acta*, 70 (2006), 426-445.
- Schwab, D.L., Petsel, S., Otto, B.R., Morris, S.K., Workman, E.E., and Tosdal, R.M., 2008. Overview of the Late Triassic Galore Creek copper-gold-silver porphyry system, northwestern British Columbia, Canada. In: Spencer, J. E., and Titley, S.R., (Eds.), *Ores and Orogenesis: Circum-Pacific Tectonics, Geologic Evolution and Ore Deposits*, Arizona Geological Society Digest 22, pp. 471-484.
- Scott, J.E., Richards, J.P., Heaman, L.M., Creaser, R.A., and Salazar, G.S., 2008. The Schaft Creek porphyry Cu-Mo-(Au) deposit, northwestern British Columbia. *Exploration and Mining Geology*, 17, 163-196. Doi: 10.2113/gsemg.17.3-4.163.
- Teck Resources Limited, 2019. Annual information form. Report by Teck Resources Limited, 121 p. Available from <<https://www.sedar.com/>>
- van Straaten, B.I., Logan, J.M., and Diakow, L.J., 2012. Mesozoic magmatism and metallogeny of the Hotailuh batholith, northwestern British Columbia. British Columbia Ministry of Energy, Mines and Natural Gas, British Columbia Geological Survey Open File 2012-06, 58 p.
- van Straaten, B.I., Logan, J.M., Nelson, J.L., Moynihan, D.P., Diakow, L.J., Gibson, R., Bichlmaier, S.J., Wearmouth, C.D., Friedman, R.M., Golding, M.L., Miller, E.A., and Poulton, T.P., 2022. Bedrock geology of the Dease Lake area. British Columbia Ministry of Energy, Mines and Low Carbon Innovation, British Columbia Geological Survey Geoscience Map 2022-01, 1:100,000 scale.
- Yukon Geological Survey, 2018. Yukon digital bedrock geology. Yukon Geological Survey. Available from <<https://data.geology.gov.yk.ca/Compilation/3>>



# Preliminary observations of a high-strain zone along the western flank of the Galore Creek deposit area, northwestern British Columbia



Russell Johnston<sup>1,a</sup>, Lori Kennedy<sup>1</sup>, and Bram I. van Straaten<sup>2</sup>

<sup>1</sup> Department of Earth, Ocean and Atmospheric Sciences, The University of British Columbia, Vancouver, BC, V6T 1Z4

<sup>2</sup> British Columbia Geological Survey, Ministry of Energy, Mines and Low Carbon Innovation, Victoria, BC, V8W 9N3

<sup>a</sup> corresponding author: rjohnston@eoas.ubc.ca

Recommended citation: Johnston, R., Kennedy, L., and van Straaten, B.I., 2023. Preliminary observations of a high-strain zone along the western flank of the Galore Creek deposit area, northwestern British Columbia. In: *Geological Fieldwork 2022*, British Columbia Ministry of Energy, Mines and Low Carbon Innovation, British Columbia Geological Survey Paper 2023-01, pp. 51-63.

## Abstract

The 1.4 Bt Galore Creek Cu-Au porphyry deposit is hosted in a Late Triassic alkalic silica-undersaturated volcano-intrusive complex. The deposit is bordered to the west by a 2-3 km wide, >6 km long, poorly understood, foliated, and folded zone (here termed the Butte ridge deformation zone) juxtaposed against the deposit by faults. The deformation zone records anomalously high strain in Stuhini Group rocks compared to elsewhere in the Galore Creek area, and its origin is enigmatic. Previous workers have considered the zone as mylonitic or a zone of flattening. Based on three 1:5000-scale transects across Butte ridge, we divide the area into seven fault-bounded structural domains. Our preliminary observations of changes in fold geometry and foliation intensity coupled with consistent southward fold plunges suggest that west-dipping thrust faults juxtaposed rocks in these domains from different structural levels. The lowest apparent strain and presumably shallowest structural level is in domain 7, east of the deformation zone and in the footwall of the Saddle thrust and Butte fault. In the northern domains (1 and 2), folds are typically open and show a well-developed axial planar pressure solution cleavage; beds maintain a constant layer thickness typical of parallel folds, which tend to form under relatively low-temperature conditions. Farther south, in domains 3 and 6, all folds are tight to isoclinal and have the thickened hinges of similar folds that typically form under higher temperatures, and the rocks display a well-developed bedding-parallel cleavage. We consider that deeper structural levels are exposed southward, with rocks in domain 6 having formed at the greatest depth. We interpret that the Butte ridge area records strain by fold and foliation development rather than by non-coaxial strain along discrete shear zones. Local examples of non-coaxial strain were likely produced due to slip as a fold mechanism. Future work will assess the absolute and relative timing of deformation and determine the relationship between deformation and mineralization.

**Keywords:** Alkalic porphyry Cu-Au, Galore Creek, Stuhini Group, deformation, strain

## 1. Introduction

Galore Creek is a large alkalic silica-undersaturated porphyry Cu-Au-Ag deposit in northwestern British Columbia (Fig. 1) on the traditional lands of the Tahltan First Nation. The deposit is bounded to the west by a north-striking deformation zone (here called the Butte ridge deformation zone) that is several km wide and at least 6 km long (Fig. 2). The deformation zone has been described as mylonitic (Enns et al., 1995; Logan, 2005), a folded corridor (Schwab et al., 2008; Micko et al., 2014; Febbo, 2019), and the site of weak metamorphism (Micko et al., 2014). Enns et al. (1995) considered that the zone is cut by alteration and mineralization. If true, deformation must be younger than the age of the host rocks (<210 Ma, van Straaten et al., 2023) and older than the age of mineralization (>210-208.5 Ma; Mortensen et al., 1995; Logan and Mihalynuk, 2014), suggesting broadly syn-mineralization deformation. The Butte ridge deformation zone records higher strain than that observed in the deposit, and the origin of the deformation is not well understood.

Here, we present preliminary field observations on the lithology, structural style, and kinematics of the Butte ridge

deformation zone. Ongoing studies will address the timing and physical conditions (P, T) of deformation in the Galore Creek area, the relationship of deformation to mineralization and to regional deformation events. Our long-term goal is to unravel the latest Triassic to recent deformation history of the Galore Creek area, with a focus on the timing and style of deformation and their relationship to the emplacement and post-emplacement modification of the Galore Creek alkalic porphyry Cu-Au system.

## 2. Geological setting

### 2.1. Regional geology

The Galore Creek area is in the Stikine island arc terrane (Stikinia), which consists of three volcano-sedimentary packages: the Stikine assemblage (Devonian to Permian), the Stuhini Group (Upper Triassic) and the Hazelton Group (uppermost Triassic to Middle Jurassic). These successions are separated by unconformities associated with deformation in the Permo-Triassic (Logan and Koyanagi, 1994), latest Triassic (e.g., Nelson et al., 2022) and Middle Jurassic (Mihalynuk et al., 1994; Nelson et al., 2013). Accretion of

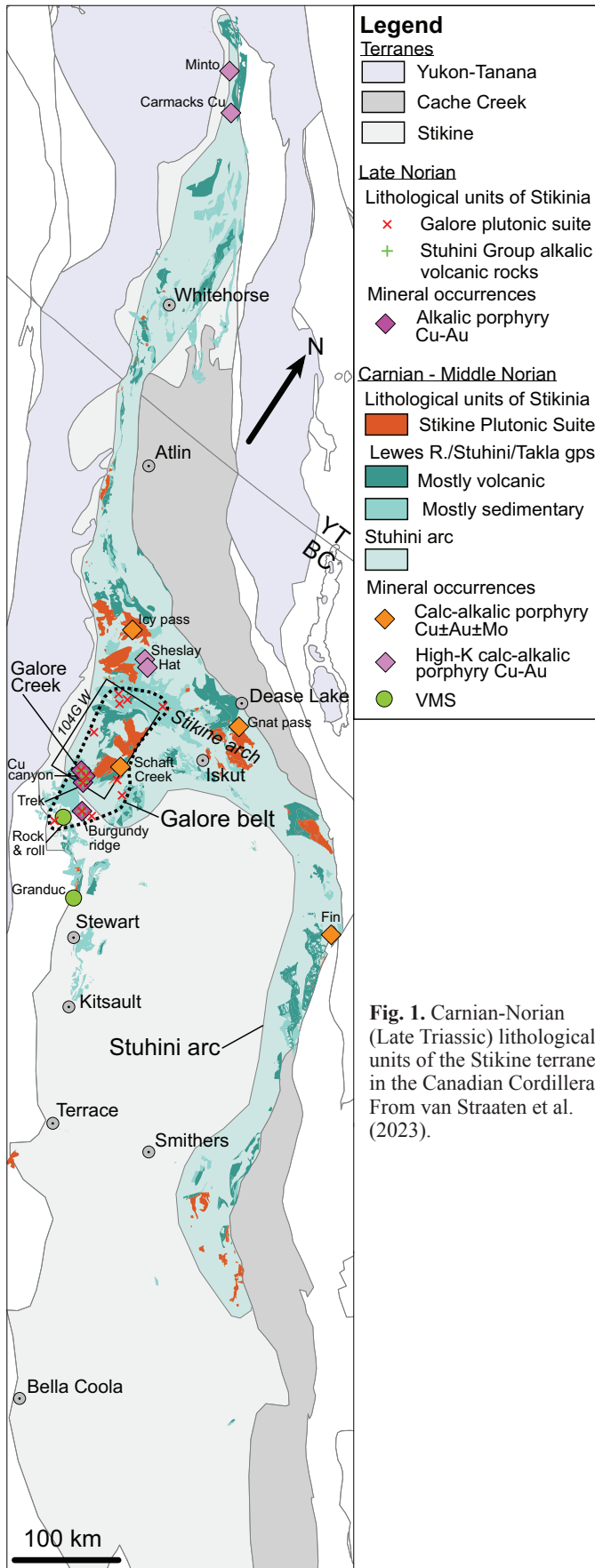


**Fig. 1.** Carnian-Norian (Late Triassic) lithological units of the Stikine terrane in the Canadian Cordillera. From van Straaten et al. (2023).

Stikinia to Ancestral North America is recorded by deposition of Bowser Lake Group siliciclastic rocks (Middle Jurassic to mid-Cretaceous) in a foreland basin atop Stikinia (Evenchick et al., 2007). Bowser Lake Group and older rocks are deformed by Cretaceous Skeena folding and thrusting linked to continued convergence between accreted terranes and Ancestral North America (Evenchick et al., 2007). Bowser basin displays a thin-skinned folding and thrusting structural style. In the older rocks of Stikinia, which are more competent than the sedimentary rocks of the Bowser Basin, strain tends to be partitioned into narrow zones of folding and faulting controlled by pre-existing structures, or local less competent horizons (Febbo et al., 2019; Nelson and van Straaten, 2020). Two generations of folds have been associated with Cretaceous deformation. Northwest-trending, orogen-parallel folds are predominant in the Bowser basin although distinct sets of northeast-trending folds are also present. Northwest-trending folds are thought to have formed from orogen-normal shortening, and northeast-trending folds due to orogen-parallel shortening (Evenchick, 2001; Evenchick et al., 2007). Late Cretaceous dextral faults and Paleocene-Eocene dextral transtensional faults are documented throughout the region. Eocene deformation may have reactivated earlier faults (Nelson et al., 2013).

The Stuhini arc (Late Triassic) contains thick accumulations of predominantly mafic volcanic strata and 229-216 Ma Stikine Plutonic Suite intrusions. These volcanic and intrusive rocks extend for at least 1300 km along the northeastern margin of the Stikine terrane (Fig. 1) and have been interpreted as an east-facing arc (Nelson and van Straaten, 2020). Stuhini arc activity was terminated in latest Triassic by a collision between northern Stikinia and the Yukon-Tanana terrane. This collision is expressed, in part, by latest Triassic shortening of the Stuhini Group and older strata throughout northwestern British Columbia (Henderson et al., 1992; Rhys, 1993; Brown et al., 1996; Rees et al., 2015; Nelson et al., 2018). In addition, recent studies of the collision (Colpron et al., 2022; Nelson et al., 2022) suggest the alkalic magmatism responsible for the Galore plutonic suite occurred during the early stages of Yukon-Tanana - Stikinia collision (van Straaten et al., 2023).

## 2.2. Geology of the Galore Creek area

The oldest rocks in the Galore Creek area are in the hanging wall of the west-verging Copper canyon thrust, and comprise Stikine assemblage limestone (Permian) and fine-grained siliciclastic rocks (Lower-Middle Triassic; Logan and Koyanagi, 1994; Fig. 2). Elsewhere, the study area is underlain by Stuhini Group volcano-sedimentary rocks (Upper Triassic). Stuhini Group strata are cut by the Galore plutonic suite (Enns et al., 1995; Fig. 2). The age range of alkalic silica-undersaturated intrusions is broadly constrained by a  $210 \pm 1$  Ma U-Pb titanite and K-feldspar age for an early syn-mineralization K-feldspar and pseudoleucite porphyritic syenite intrusion (Mortensen et al., 1995) and a  $208.5 \pm 0.8$  Ma U-Pb titanite age for a K-feldspar porphyritic biotite quartz syenite plug (Logan and Mihalynuk, 2014) interpreted by Enns et al. (1995) as the youngest Galore intrusions.

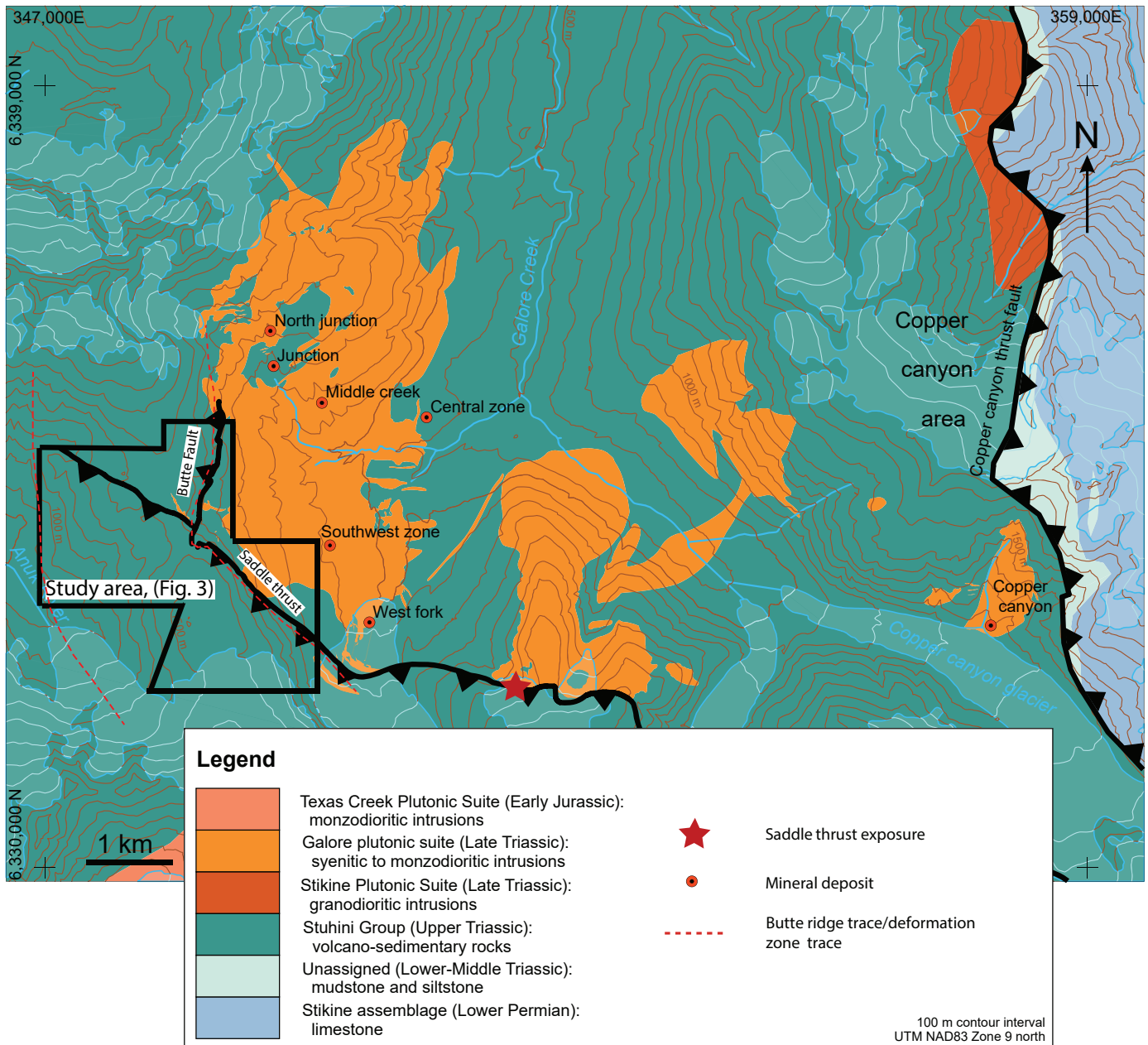


**Fig. 2.** Geology of the Galore Creek area. Modified from van Straaten et al. (2023); location of Saddle and Butte thrusts based on 2022 mapping. UTM coordinates here and throughout this paper are in NAD83 zone 9 north.

Penetrative planar fabrics are common in Paleozoic and Middle Triassic strata. However, penetrative deformation of Upper Triassic and younger rocks is rare, restricted to north-trending zones of foliation, such as the Butte ridge deformation zone (Figs. 2, 3; Febbo, 2019; Micko et al., 2014). Logan and Koyanagi (1994) documented post-Triassic southward-vergent structures that are overprinted by post-Jurassic northerly trending folds and thrusts in the Stuhini Group and younger rocks. Brittle deformation is widespread, including map-scale reverse faults (e.g., east-verging Saddle and Butte thrusts; west-verging Canyon Creek thrust, Fig. 2) and outcrop-scale thrusts. Dextral and sinistral fault zones are common; they crosscut the main foliation and are defined by offset units.

### 3. Butte ridge stratigraphy

We carried out detailed (1:5000 scale) mapping of Butte ridge along three cross-strike transects (Figs. 3, 4) that we refer to as ‘northern’ (section A-A’), central (section B-B’), and southern (section C-C’). Stuhini Group subunits and map unit codes described below mainly follow van Straaten et al. (2023).

#### 3.1. Stuhini Group (Upper Triassic)

van Straaten et al. (2023) subdivided the Stuhini Group in the Galore Creek area into a lower intermediate to mafic volcano-sedimentary succession and an upper alkalic volcanic succession.

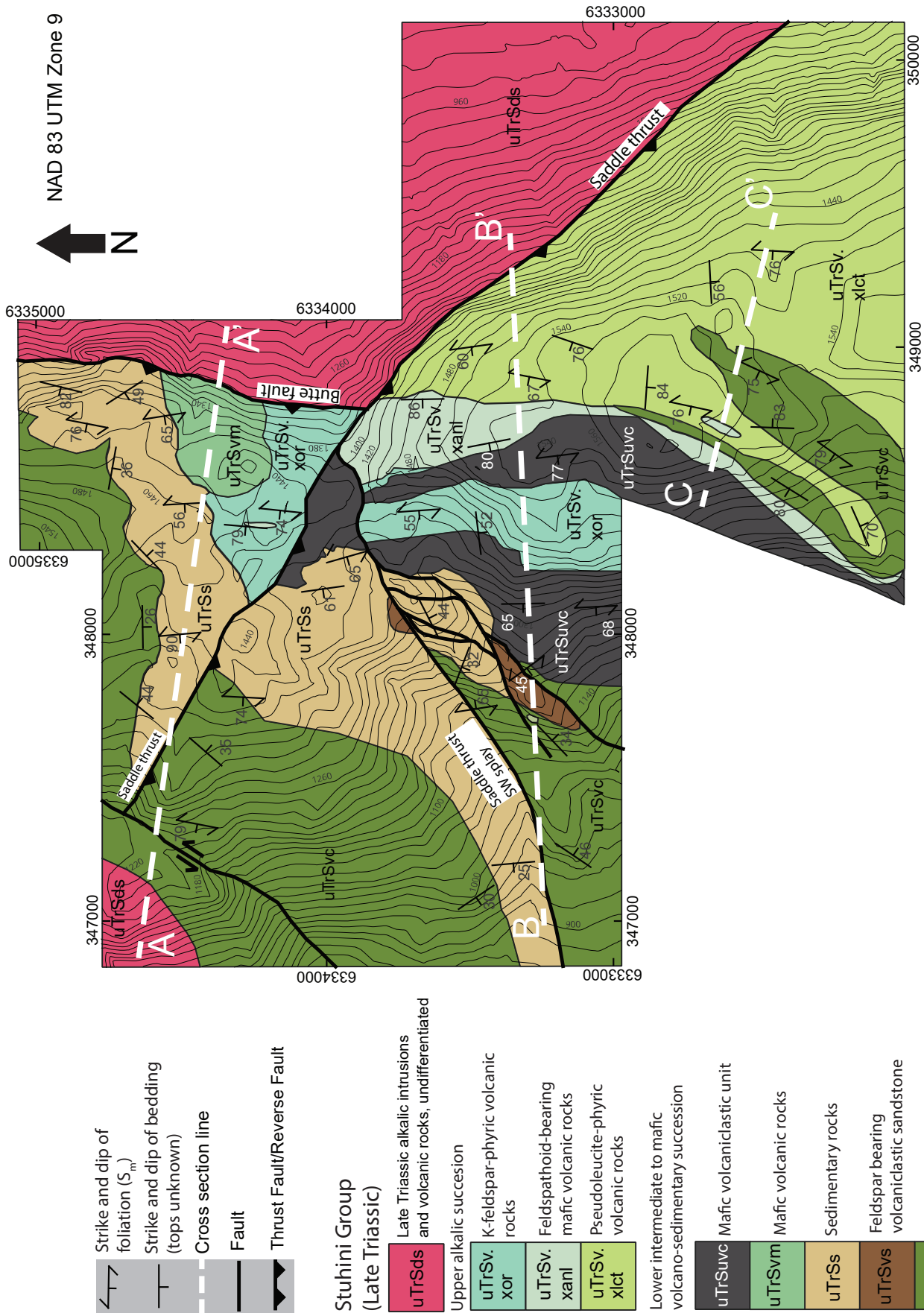


Fig. 3. Geology of the Butte ridge deformation zone. Cross section lines A-A', B-B', C-C' are shown on Figure 4.

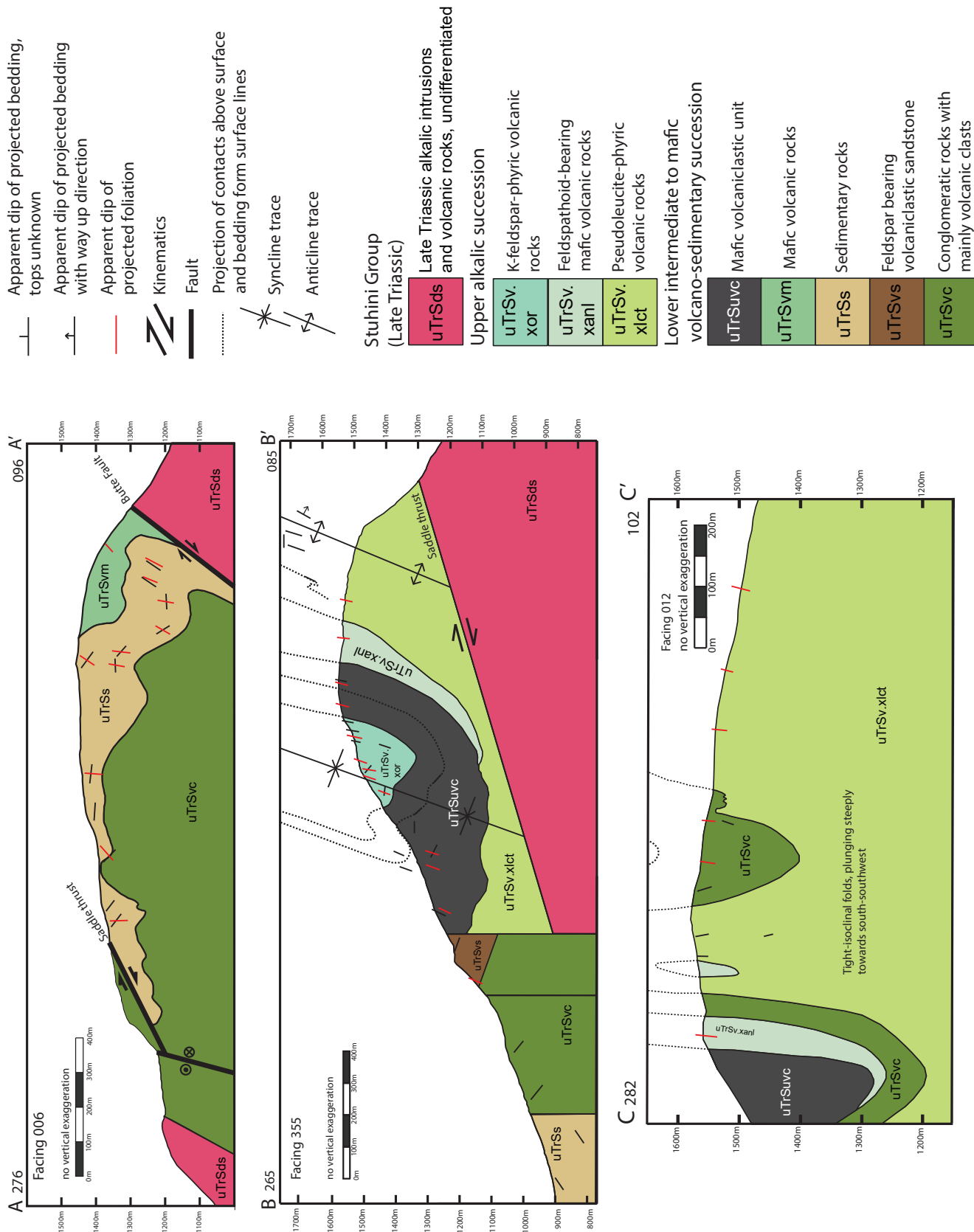


Fig. 4. Cross sections across Butte ridge. a) A-A', b) B-B', c) C-C'. See Figure 3 for locations.

### 3.1.1. Lower intermediate to mafic volcano-sedimentary succession

At the base of the section is a commonly well-bedded (cm-m scale) conglomeratic unit (uTrSvc) containing white-weathering, pebble to cobble amphibole-porphyrific igneous clasts and sparser other volcanic clasts (Fig. 5a). Where a fabric is well-developed, the matrix is generally chloritized. The white-weathering clasts are commonly aligned in the main foliation plane ( $S_m$ ). Some have internal extension fractures perpendicular to  $S_m$ ; some clasts appear broken, with segments displaced along internal fractures oblique to  $S_m$  (Fig. 5a). The unit is exposed on the northern and western margins of the map area and locally on the southern margin (Fig. 3). It is locally interbedded with narrow lenses of augite-phyric mafic volcanic rocks (similar to unit uTrSvm, see below). A well-bedded feldspar (plagioclase?) bearing volcanoclastic sandstone unit (uTrSvs) overlies uTrSvc in two small areas and may be a lateral equivalent of unit uTrSs (see below).

The volcanic clast-bearing conglomerate unit (uTrSvc) is overlain by a sedimentary unit (uTrSs) containing siltstone, sandstone, conglomerate, and limestone. Sandstones and siltstones may define sharp-based fining-upward sequences (Fig. 5b). Sandstones and conglomerates are typically massive and rarely show bedding. This unit is in the northern and western parts of the map area. The lower contact with the volcanic clast-bearing conglomerate unit was not directly observed; the location of the contact is constrained to <30 m in the east, but unconstrained in the west.

A mafic volcanic unit (uTrSvm) contains clasts with 20-40% euhedral-subhedral augite crystals (up to 5 mm) and locally elongate plagioclase crystals (<5 mm) in an aphanitic groundmass (Fig. 5c). This unit is restricted to the northeastern part of the map area (Fig. 3) and was not observed elsewhere.

A distinct feldspathoid-bearing mafic volcanic unit (uTrSvm.xanl) is commonly found as m- to dam-scale lenses in units uTrSv.xor, uTrSv.xlet, and uTrSvm. As much as 150 m is present at the western contact of uTrSv.xlet. The distinctive phenocrysts are white spheroidal minerals, interpreted as feldspathoids. The crystals are typically 0.5-3 mm and range from 15-75% of the rock by volume (Fig. 6a). Augite phenocrysts are locally present. The groundmass is dark grey and aphanitic. This unit is interpreted as transitional between the lower intermediate to mafic volcano-sedimentary succession and the upper alkalic volcanic succession.

The mafic volcanoclastic unit (uTrSuvc) consists of volcanic-derived siltstone, sandstone, and conglomerate (Fig. 6b). The unit was not mapped north of the Saddle thrust fault. Clasts in the conglomerate range from pebbles to cobbles and are typically mafic. The volcanic clasts commonly contain fine augite(?) and feldspar crystals. The unit is similar to uTrSvc but lacks the diagnostic white-weathering amphibole-phyric clasts of uTrSvc. The two volcanoclastic sequences appear to occupy different stratigraphic positions. Although pseudoleucite-bearing clasts seem to be lacking, uTrSuvc appears to be between uTrSvm.xanl and uTrSv.xor (see below).

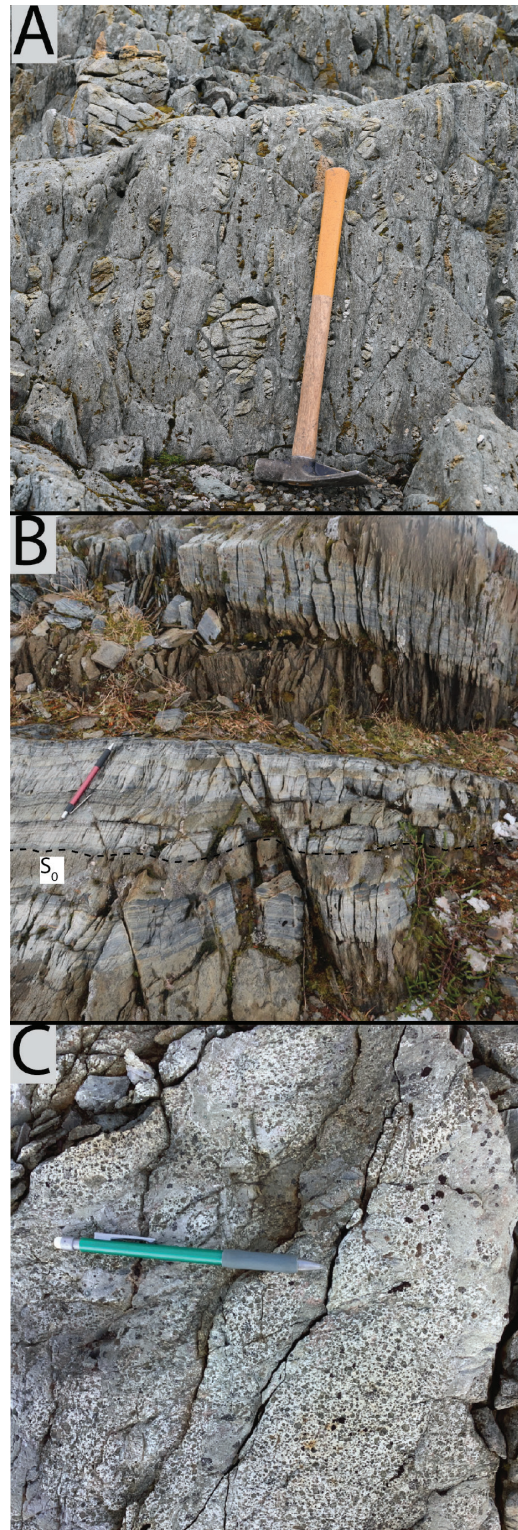


**Fig. 5.** Lower intermediate to mafic volcano-sedimentary succession. **a)** Unit uTrSvc with a well-developed chloritic foliation ( $S_m$ ); some white-weathering clasts have internal extension fractures normal to the foliation, some clasts appear broken, with slip along shear fractures oblique to  $S_m$  (348641E, 6332288N). **b)** Unit uTrSs well-bedded siltstone and sandstone with sharp-based fining upward sequences and a well-developed pressure solution cleavage ( $S_0$ ). Bedding is orthogonal to cleavage, indicating a fold hinge (348009E, 6334548N). **c)** uTrSvm with coarse augite phenocrysts (346430E, 6335567N).

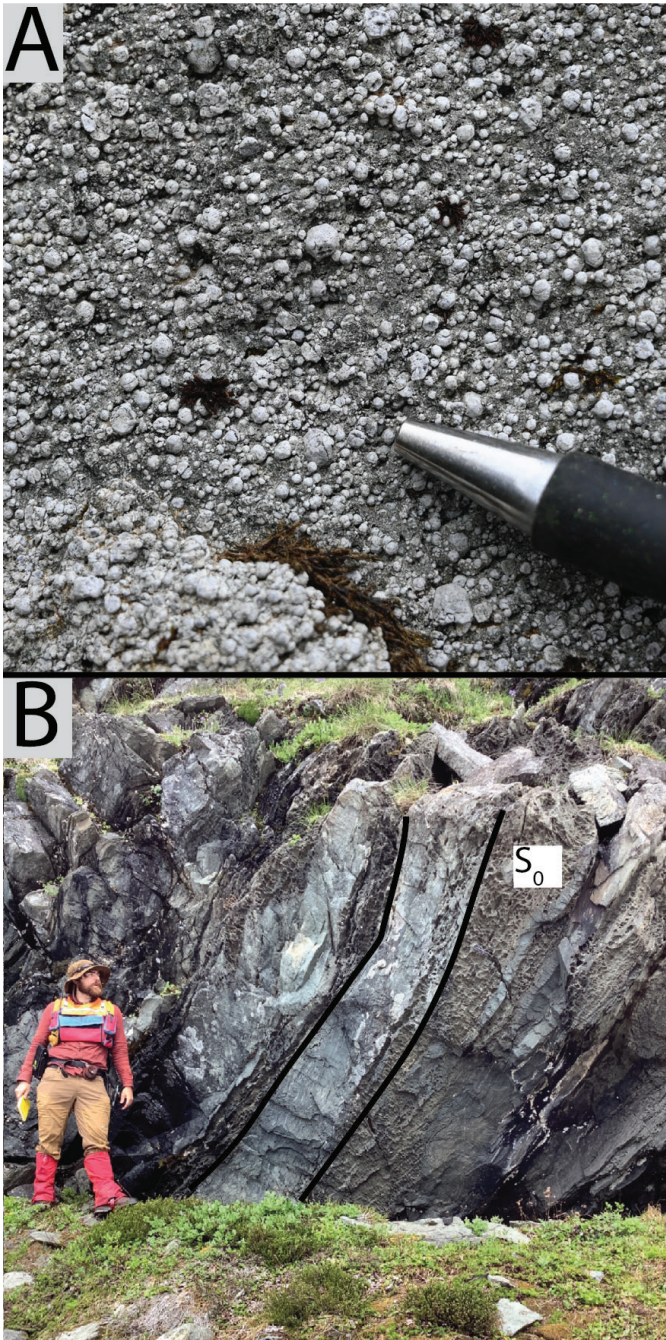


**Fig. 6.** Rock units in the central transect. **a)** uTrSvm.xanl, crystal tuff facies with white-weathering spheroidal feldspathoid crystals (348613E, 6332657N). **b)** Unit uTrSvuc volcaniclastic, siltstone and sandstone facies (348082E, 6333247N).

### 3.1.2. Upper alkalic volcanic succession

Capping the mafic volcaniclastic unit uTrSvuc is a pseudoleucite-phyric volcanic unit (uTrSv.xlct); pseudoleucite phenocrysts are diagnostic of the unit. Here, pseudoleucite refers to any mineral or aggregate of minerals that originated as a leucite crystal. Pseudoleucite crystals may be black and set in a light-toned groundmass (Fig. 7a) or white weathering in a dark grey to black groundmass (Fig. 7b). The unit may contain good bedding, defined by tuffaceous interbeds or variation in

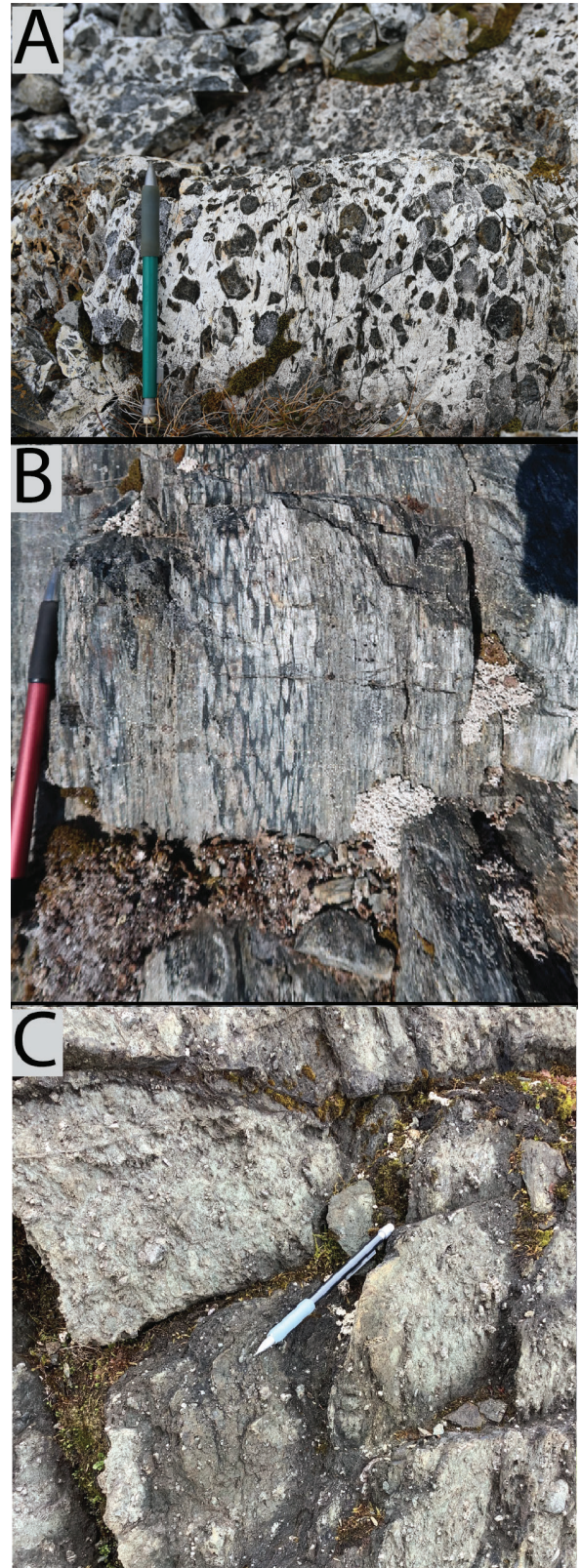


**Fig. 7.** Upper alkalic volcanic succession rocks. **a)** Coarse, zoned, and broken pseudoleucite-bearing uTrSv.xlct (349189E, 6332688N). **b)** Bedded and flattened pseudoleucite-bearing uTrSv.xlct. Foliation is parallel to bedding (348866E, 3333267N). **c)** uTrSvm.xor, crystal tuff facies with coarse (>1 cm) broken euhedral K-feldspar crystals (348472E, 6333298N).

pseudoleucite crystal size and abundance. In some areas, the unit is massive with up to 35% 1-3 cm broken pseudoleucite crystals in a grey uniform groundmass. The pseudoleucite-phyric volcanic unit is the most voluminous lithology at surface in the map area but is spatially restricted to the southeast (Fig. 3).

A K-feldspar-phyric volcanic unit (uTrSv.xor) contains diagnostic tabular, generally euhedral, and broken K-feldspar crystals, <1 mm to >3 cm long (most commonly >0.5 cm; Fig. 7c). A wide range of volcanic facies are observed, with significant variation in crystal abundances and grain size distributions. The unit is most abundant in the central transect but is locally mapped in the northern transect.

### 3.2. Galore plutonic suite and undifferentiated Late Triassic alkalic volcanic rocks

Rocks in the footwall of the Saddle and Butte thrust faults consist of altered and mineralized Late Triassic volcanic rocks and intrusions. The intrusions are Late Triassic and range from syenitic to monzodioritic. The alkalic intrusions typically contain distinct K-feldspar phenocryst and/or pseudoleucite phenocrysts. For detailed descriptions, see Enns et al. (1995).

## 4. Study area deformation

The Butte ridge deformation zone (Fig. 2) contains the most strained Stuhini Group rocks in the area. However, deformation intensity is variable both across and along strike. Folds are common and have a poorly to well-developed axial planar foliation. Crenulation cleavages are common; they are steeply and shallowly dipping, with both steep and shallowly plunging fold axes, and a wide range of orientations. The crenulations fold the main foliation. Crenulation intensity varies with location; rocks in the hanging wall of the Saddle thrust are the most crenulated.

Penetrative folding and cleavage development records coaxial flattening or ‘pure shear’ (Fig. 8); non-coaxial or ‘simple shear’ strain is rare in the Butte ridge deformation zone. Relatively

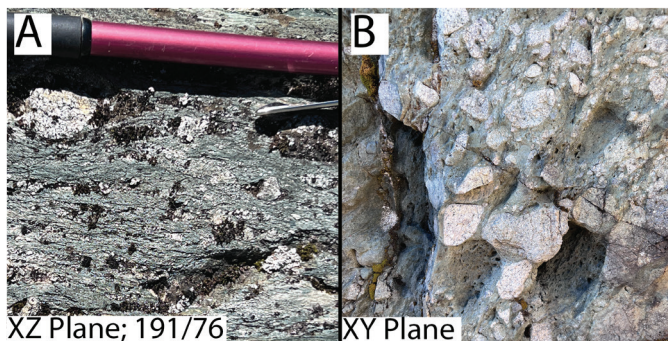


**Fig. 8.** Different views of the  $S_m$  fabric at the same outcrop; unit uTrSvc. **a)** Photo taken perpendicular to the XZ plane of the strain ellipse, showing a well-developed fabric defined by flattened clasts in chlorite-rich matrix. **b)** View looking down on the plane of flattening of the strain ellipse (XY plane). In this plane, the clasts are not elongate, indicating that the foliation is a flattening foliation related to folding, with no evidence of stretching (e.g., shearing) (347399E, 6334542N).

incompetent sedimentary and volcanoclastic rocks typically have a well-developed foliation whereas more competent rocks do not. Pseudoleucite-bearing rocks locally exhibit extreme strain partitioning in texturally homogenous rocks over a m- to dm-scale, with some units strongly flattened and others weakly flattened.

Brittle faults, both outcrop scale and map scale are abundant. Along strike and across strike of the Butte ridge deformation zone, brittle faults separate areas with distinct deformation styles, that we separate into structural domains (Fig. 9). Below, we first describe the faults that bound these domains and then we describe the deformation features within each domain.

### 4.1. Brittle faults

Two major thrust faults (Butte and Saddle, Figs. 3, 4) are in the area; minor thrusts are common throughout the Butte ridge deformation zone (Fig. 10). The Butte fault is a north-trending structure that defines the eastern boundary of the Butte ridge deformation zone in the northern part of the study area. The fault juxtaposes the deformation zone against Galore plutonic suite intrusions and/or strongly hydrothermally altered rocks (Fig. 3). At the surface, the fault is a 5-6 m wide light-toned band, exposed for 100s of m along strike. Due to steep topography, the fault was only accessible in one area, where it is exposed as a zone >10 m wide within which are strips of fault gouge (<0.5 m wide) between bands of more coherent but brecciated rock. Reverse motion is not confirmed by stratigraphic offset or kinematics from within the fault zone. Using drill core intersections, the fault is estimated as moderately to steeply west dipping. It is unclear if  $S_m$  and the Butte fault are cogenetic or if the fault is a later structure.

The Saddle thrust fault ( $118^\circ/34^\circ$ , where measured) trends northwest for a >8 km strike length across the Butte Ridge deformation zone, juxtaposing the volcanic conglomerate unit (uTrSvc) over siltstones, sandstones, and conglomerates of unit (uTrSs). The thrust contains abundant quartz veins in the footwall and a 1-5 m deformation zone consisting of numerous faults splays (Febbo, 2019). At Butte ridge, the Saddle thrust splays into at least two distinct segments. One splay, along a topographic lineament in the southwest part of the map area (‘Saddle thrust southwest splay’, Fig. 3), is defined by an abrupt change in lithology, bedding orientation, and foliation intensity. The main fault extends into the northwestern portion of the map area (‘Saddle thrust northwest’, Fig. 3) and is inferred on the basis of a pronounced topographic lineament, an abrupt change in lithology from uTrSvc to uTrSs, a sharp decrease in foliation intensity from east to west, an abrupt change in bedding orientation, and abundant quartz veins in the footwall. The amount of offset on these fault segments is unclear. The Saddle thrust appears to truncate the Butte thrust.

### 4.2. Structural domains

The Butte fault, the Saddle thrust and two interpreted northeast-trending faults on the western side of the central transect define separate domains of distinct structural style

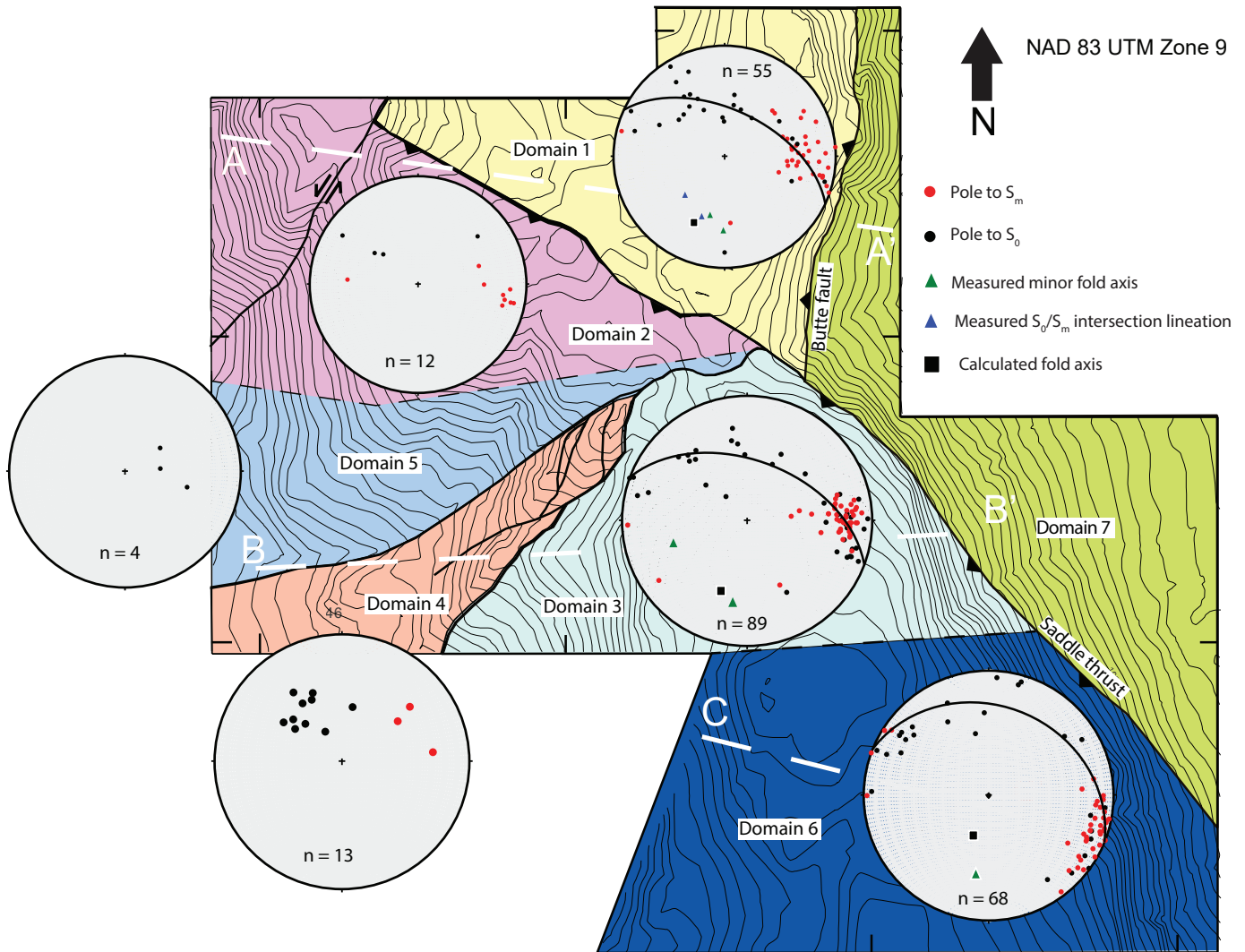


**Fig. 9.** Structural domains and lower hemisphere equal-area stereographic projections of the Butte deformation zone. Calculated  $F_2$  fold axes: domain 1,  $205/35^\circ$ ; domain 3,  $200/40^\circ$ ; domain 6,  $201/62^\circ$ . Stereonets and  $\beta$  calculations were produced using Stereonet 11 (Allmendinger et al., 2013; Cardozo and Allmendinger, 2013). Colours do not imply stratigraphy and are used only to highlight the domains.

and/or structural orientation (domains 1-9, Fig. 9). Below we describe these domains within each transect from east to west across Butte ridge, focussing on penetrative strain and folds. Minor brittle faults and veins are common in all domains but do not change character between domains.

#### 4.2.1. Domain 1

This domain is a fault block bounded by the Butte fault to the east and the Saddle thrust to the west (Figs. 3, 9). Folds with wavelengths ranging from 10 cm to 1 km generally have an open, and rarely close, geometry. Axial surfaces are steeply inclined to the west and fold axes are gently to moderately plunging to the south-southwest ( $\beta$  calculation,  $206^\circ/35^\circ$ ; Fig. 9). Bedding thicknesses are generally constant indicating that these are parallel folds (Class 1B of Ramsay, 1967). Sedimentary rocks can have a strong axial planar pressure solution cleavage ( $S_m$ , Fig. 5b); volcanoclastic rocks have

moderately developed axial planar cleavage defined by chlorite (Fig. 5b). Cleavage orientations show significant variation, with an average orientation of  $180^\circ/64^\circ$ . Rare intrafolial folds have smaller wavelengths ( $<10$  cm) than described above. The folds have a tight to isoclinal geometry and have a similar fold profile with thickened hinges (Fig. 11; Class 2 of Ramsay, 1967).

Map scale folds on the eastern side of this fault block are gentle to open and asymmetric, with long limbs dipping steeply to the east (northern transect, Fig. 4a) and record an easterly vergence. Bedding orientation shallows towards the center of the fault block and is interpreted as a hinge zone to a km-scale fold. Foliation intensity in this domain is greatest on the eastern margin, near the Butte fault, and gradually weakens to the west. Near the Saddle thrust, the rocks are weakly to non-foliated. From west to east there is a progressive decrease in the angles between the fold axial surfaces and  $S_m$  and the Butte fault (Fig. 4a).



**Fig. 10.** Minor thrust fault in the Butte deformation zone showing top-to-east kinematics. It is unclear if  $S_m$  formed before the fault or if the fault and  $S_m$  are cogenetic (348850E, 6334768N).



**Fig. 11.** Tight to isoclinal similar intrafolial folds in domain 1 tuffs (348449E, 6334484N).

#### 4.2.2. Domain 2

Most of this fault-bounded domain consists of the volcanic clast-bearing conglomerate unit (uTrSvc). Rocks in the hanging wall of the Saddle thrust are highly strained relative to those in the immediate footwall. Unit uTrSvc has a well-developed north-trending steeply dipping cleavage defined by chlorite; more competent igneous clasts display internal

fractures (Fig. 5a). Foliation intensity is strongest close to the Saddle thrust, but has the same general orientation as in domain 1 across the fault.

#### 4.2.3. Domain 3

Domain 3 is bounded by the Saddle thrust to the east and an unnamed inferred fault to the west (Fig. 9). The domain shows a different style of folds than observed in domain 1 to the north. Folds are close to tight, with steeply inclined west-dipping axial surfaces, and have gentle to moderate south-southwest plunges ( $\beta$  calculation,  $200^\circ/40^\circ$ ; Figs. 9, 12). Folds have wavelengths of <1 m to 500 m and verge to the east. A map-scale east-vergent synform-antiform pair is on the eastern side of domain 3 (Fig. 4b).

The eastern portion of this domain is mainly underlain by pseudoleucite-bearing rocks (uTrSv.xlct). A strong fabric ( $S_m$ ) is present throughout, typically defined by chlorite and by alignment of clasts and pseudoleucite crystals. Flattened pseudoleucite grains can have aspect ratios of 2:1 to 10:1 (Fig. 7b). However, adjacent pseudoleucite-phyric coherent rocks can be largely undeformed, illustrating extreme strain gradients. The  $S_m$  fabric is commonly parallel to bedding and, similar to the northern transect, dips steeply to the west.



**Fig. 12.** Close folds in unit uTrSv.xlct (348997E, 6333035N).

#### 4.2.4. Domain 4

This domain is separated from domain 3 by a northeast-trending fault across which bedding orientation and foliation intensity changes abruptly. Bedding in this fault block consistently dips  $35-50^\circ$  to the southeast (Fig. 9). Foliation intensity is weaker than in domain 3 and decreases to the west. In the easternmost part of the fault block, weak foliations were

mapped in two locations, dipping moderately to the southeast. On western edge of the fault block, a fabric is locally developed in carbonate-bearing clasts (lenses?), but the host rock is not foliated (Fig. 13).

#### 4.2.5. Domain 5

Domain 5 is separated from domain 4 by an interpreted splay off the Saddle thrust. Bedding in domain 5 dips gently-moderately to the west and this fault is interpreted based on the sharp change in bedding orientation and lithology. Siltstones and volcanoclastic rocks in this domain are not foliated.

#### 4.2.6. Domain 6

Tight to isoclinal south-plunging ( $\beta$  calculation,  $201^\circ/66^\circ$ ; Fig. 9) folds are common throughout this area and are well-exposed at the m- to dm-scale (Fig. 14). Unlike the northern domains, where folds verge to the east, the isoclinal folds do not show vergence (Fig. 4c). Rocks generally have a well-defined  $S_m$  foliation defined by chlorite alignment, aligned clasts, and local pressure solution cleavage. In this domain, pseudoleucite-phyric volcanic rocks are locally strongly foliated, with the foliation defined by flattened pseudoleucite crystals that locally display a stretching lineation; aspect ratio 1:8). Rock types with black pseudoleucite crystals in a light-toned groundmass display significantly less flattening strain (aspect ratios of 1:1 to 1:4) than rock types with white pseudoleucite crystals in a dark-toned groundmass (aspect ratio 1:2).

An outcrop displaying dm-scale type 3 fold interference pattern is exposed at the southern edge of this domain in a volcanic tuff, where isoclinal  $F_1$  folds with the  $S_m$  foliation are

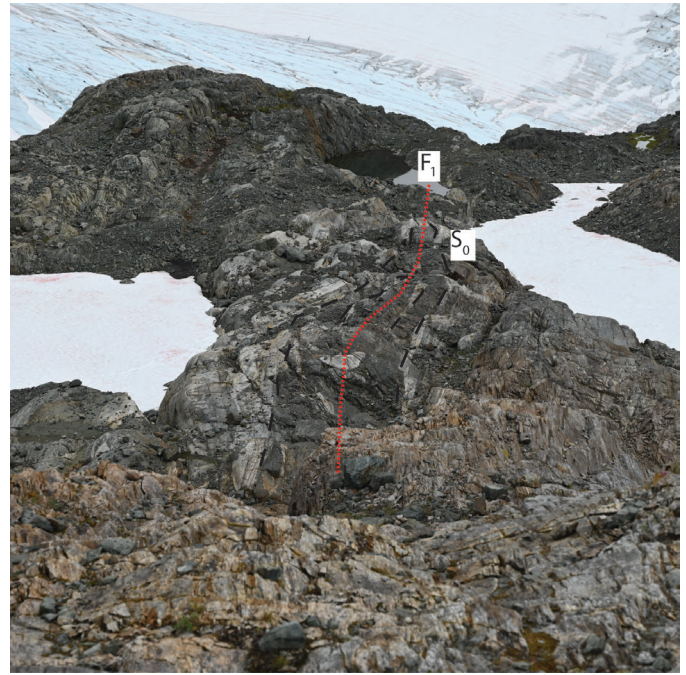


**Fig. 14.** Decametre-scale isoclinal fold in domain 6. The light-toned unit(s) are tuffaceous beds. View to the south (348483E, 6332228N).

overprinted by later tight folds lacking a foliation (Fig. 15). The hinge of the tight later fold is thickened relative to the limbs. This type of refolding was not observed elsewhere on Butte ridge but was observed 8 km along strike to the north. In the southern part of the domain  $S_m$  foliation is oriented  $233^\circ/86^\circ$ , in the northern part of the domain, foliation is oriented  $188^\circ/83^\circ$ .

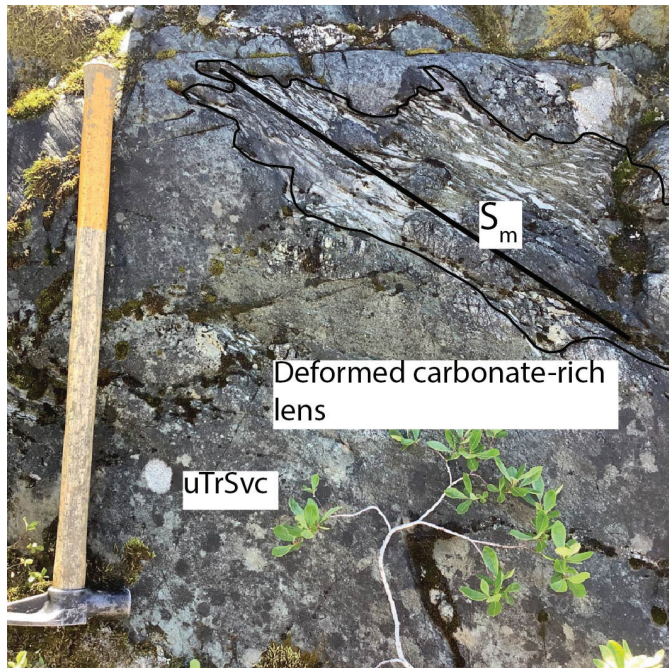


**Fig. 13.** Flattening fabric in carbonate-bearing clast (lens?) in otherwise unfoliated uTrSmv (347234E, 6333134N).

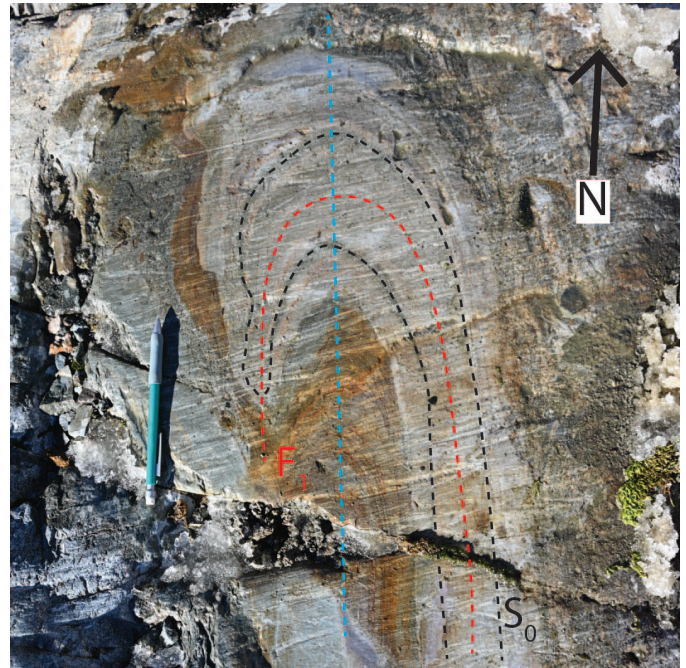


**Fig. 15.** Type 3 fold interference pattern in volcanic tuff. Early folds are isoclinal and have a layer-parallel foliation, later folds are tight (348405E, 6332151N).

#### 4.2.7. Domain 7

The easternmost domain is in the footwall of the Saddle thrust and Butte faults. The domain is underlain by the Galore plutonic suite intrusive rocks and highly altered and locally mineralized volcanic rocks. Rocks in this fault block are generally unfoliated but are strongly faulted and locally folded (Febbo, 2019).

#### 5. Discussion

The Butte ridge area consists of a series of fault-bounded folded domains, where fold geometry and orientation change from north to south. In the northern domains, folds are typically open and, more rarely, close and show a well-developed axial planar cleavage. Fold axial surfaces generally dip steeply to the west and the folds plunge gently to moderately south-southwest. A pressure solution cleavage is typical, and beds maintain a constant layer thickness, typical of parallel folds (class 1B of Ramsay, 1967). Such folds tend to form under relatively low temperatures typical of thin-skinned fold and thrust belts. We interpret that the area records strain by fold and foliation development rather than by non-coaxial strain along discrete shear zones. Local examples of non-coaxial strain were likely produced due to slip as a fold mechanism.

In the central domains, map-scale folds are generally steeply inclined, east verging, and plunge gently to moderately to the south-southwest. Although most folds are tight, open to close profiles were observed. Bedding and cleavage are parallel except at fold hinges. In domain 6, all folds are tight to isoclinal. The folds have the thickened hinges of similar folds (class 2 of Ramsay, 1967) typically associated with higher temperature deformation. Rocks display a well-developed bedding-parallel cleavage, and a stretching lineation was noted at one locality. Locally, outcrop-scale coaxial fold interference was observed, with an isoclinal fold containing a bedding-parallel foliation being tightly refolded into a type 3 (Ramsay, 1967) hook displaying a similar fold profile. We interpret the southern domain to represent the highest strain on the ridge.

Preliminary observations suggest that changes in deformation style and strain intensity are a result of faulting that has juxtaposed rocks from different structural levels, presumably along west- or southwest-dipping faults. We interpret that the shallowest structural level in the area is in the footwall of the Saddle and Butte faults (domain 7, Fig. 9). Based on fold geometry, foliation intensity, and consistent southward fold plunges, we consider that deeper structural levels are exposed between the Saddle and Butte faults (domain 1) and still deeper levels farther south, with rocks in domain 6 recording the deepest structural level.

We are uncertain how folds and fabrics in the study area relate to the regional geology, and the absolute timing of the Saddle and Butte thrusts is unclear. The structures may be related to latest Triassic regional shortening or Cretaceous development of the Skeena fold and thrust belt, or both. Future work will aim to establish both the absolute and relative timing

of the structures and to place the area into a regional structural framework.

Enns et al. (1995) considered that the deformation zone is cut by alteration and mineralization. If true, deformation must be younger than the age of the host rocks (<210 Ma, van Straaten et al., 2023) and older than the age of Galore Creek porphyry Cu-Au-Ag mineralization (>210-208.5 Ma; Mortensen et al., 1995; Logan and Koyanagi, 1994; Logan, 2004), suggesting a broadly syn-mineralization deformation event. We did not see with confidence cross-cutting relationships between alteration/mineralization and deformation that would constrain the relative timing.

#### 6. Summary

Galore Creek is a large alkalic silica-undersaturated porphyry Cu-Au-Ag deposit in northwestern British Columbia. The deposit area is bounded to the west by a north-striking deformation zone (here called the Butte ridge deformation zone) that is several km wide and at least 6 km long. The deformation zone contains the most strained Stuhini Group rocks in the Galore area (Logan and Koyanagi, 1994; Micko et al., 2014; Febbo, 2019) consisting of folded rocks with moderately to strongly developed axial planar cleavage. We propose that progressively deeper structural levels, separated by faults, are exposed from north to south along the Butte ridge.

#### Acknowledgments

Funding for this research was provided by a Department of Natural Resources Geoscience Targeted GeoSciences Initiative grant to Lori Kennedy and Bram van Straaten. We thank Galore Creek Mining Corporation for their generous logistical support; Leif Bailey, Nils Peterson, Well-Shen Lee, and other colleagues for discussions and camaraderie at camp. Thanks to Gayle Febbo and Jim Logan for sharing with us their knowledge and insight of the (complicated) Galore Creek geology. An internal report and geological maps of the area by Gayle Febbo, Jim Logan and Esther Bordet were valuable resources. We thank Jim Logan for a helpful review of the manuscript. Thanks to William Raleigh-Smith for providing capable and cheerful field assistance.

#### References cited

- Allmendinger, R.W., Cardozo, N., and Fisher, D., 2012. Structural geology algorithms: Vectors and tensors in structural geology. Cambridge University Press, 289 p.
- Brown, D.A., Gunning, M.H., and Greig, C.J., 1996. The Stikine project: Geology of western Telegraph Creek map area, northwestern British Columbia. British Columbia Ministry of Employment and Investment, British Columbia Geological Survey Bulletin 95, 130 p.
- Cardozo, N., and Allmendinger, R.W., 2013. Spherical projections with OSXStereonet. *Computers & Geosciences*, 51, 193-205.
- Colpron, M., Sack, P.J., Crowley, J.L., Beranek, L.P., and Allan, M.M., 2022. Late Triassic to Jurassic magmatic and tectonic evolution of the Intermontane terranes in Yukon, northern Canadian Cordillera: Transition from arc to syn-collisional magmatism and post-collisional lithospheric delamination. *Tectonics*, 41, article e2021tc007060, doi:10.1029/2021TC007060.

- Enns, S.G., Thompson, J.F.H., Stanley, C.R., and Yarrow, E.W., 1995. The Galore Creek porphyry copper-gold deposits, northwestern British Columbia. In: Schroeter, T.G., (Ed.), *Porphyry Deposits of the Northern Cordillera*. Canadian Institute of Mining and Metallurgy Special Volume 46, pp. 630-644.
- Evenchick, C.A., 2001. Northeast-trending folds in the western Skeena Fold Belt, northern Canadian Cordillera: A record of Early Cretaceous sinistral plate convergence. *Journal of Structural Geology*, 23, 1123-1140.
- Evenchick, C.A., McMechan, M.E., McNicoll, V.J., and Carr, S.D., 2007. A synthesis of the Jurassic-Cretaceous tectonic evolution of the central and southeastern Canadian Cordillera: Exploring links across the orogen. In: Sears, J.W., Harms, T.A., and Evenchick, C.A., (Eds.), *Whence the Mountains? Inquiries into the Evolution of Orogenic Systems: A Volume in Honor of Raymond A. Price*. Geological Society of America Special Paper 443, pp. 117-145.
- Febbo, G., 2019. Galore Creek geology map. In: Prince, J., 2019, *Drilling, Geological Mapping, and Aerial Survey Assessment Report on the Galore Creek Project*. British Columbia Geological Survey Assessment Report number 39156, Appendix XIV.
- Febbo, G.E., Kennedy, L.A., Nelson, J.L., Savell, M.J., Campbell, M.E., Creaser, R.A., Friedman, R.M., van Straaten, B.I., and Stein, H.J., 2019. The evolution and structural modification of the supergiant Mitchell Au-Cu porphyry, northwestern British Columbia. *Economic Geology*, 114, 303-324.
- Henderson, J.R., Kirkham, R.V., Henderson, M.N., Payne, J.G., Wright, T.O., and Wright, R.L., 1992. Stratigraphy and structure of the Sulphurets area, British Columbia. In: *Current Research Part A, Cordillera and Pacific Margin*, Geological Survey of Canada, Paper 92-1A, pp. 323-332.
- Lang, J.R., Lueck, B., Mortensen, J.K., Russell, J.K., Stanley, C.R., and Thompson, J.F.H., 2005. Triassic-Jurassic silica-undersaturated and silica-saturated alkalic intrusions in the Cordillera of British Columbia: Implications for arc magmatism. *Geology*, 23, 451-454.
- Logan, J.M., 2005. Alkaline magmatism and porphyry Cu-Au deposits at Galore Creek, northwestern British Columbia. In: *Geological Fieldwork 2004*, British Columbia Ministry of Energy, Mines and Petroleum Resources, British Columbia Geological Survey Paper 2005-01, pp. 237-248.
- Logan, J.M., and Koyanagi, V.M., 1994. Geology and mineral deposits of the Galore Creek area. British Columbia Ministry of Energy, Mines and Petroleum Resources, British Columbia Geological Survey, Bulletin 92, 102 p.
- Logan, J.M., and Mihalynuk, M.G., 2014. Tectonic controls on Early Mesozoic paired alkaline porphyry deposit belts (Cu-Au ±Ag-Pt-Pd-Mo) within the Canadian Cordillera. *Economic Geology*, 109, 827-858.
- Micko, J., Tosdal, R.M., Bissig, T., Chamberlain, C.M., and Simpson, K.A., 2014. Hydrothermal alteration and mineralization of the Galore Creek alkalic Cu-Au porphyry deposit, northwestern British Columbia, Canada. *Economic Geology*, 109, 891-914.
- Mihalynuk, M.G., Nelson, J., and Diakow, L.J., 1994. Cache Creek terrane entrapment: Oroclinal paradox within the Canadian Cordillera. *Tectonics*, 13, 575-595.
- Mortensen, J.K., Ghosh, D.K., and Ferri, F., 1995. U-Pb geochronology of intrusive rocks associated with copper-gold porphyry deposits in the Canadian Cordillera. In: Schroeter, T.G., (Ed.), *Porphyry Deposits of the Northwestern Cordillera of North America*. Canadian Institute of Mining, Metallurgy and Petroleum, Special Volume 46, pp. 142-158.
- Nelson, J., and Kyba, J., 2014. Structural and stratigraphic control of porphyry and related mineralization in the Treaty Glacier-KSM-Brucejack-Stewart trend of western Stikinia. In: *Geological Fieldwork 2013*, British Columbia Ministry of Energy, Mines and Petroleum Resources, British Columbia Geological Survey Paper 2014-1, pp. 111-140.
- Nelson, J., Waldron, J., van Straaten, B., Zagoresvski, A., and Rees, C., 2018. Revised stratigraphy of the Hazelton Group in the Iskut River region, northwestern British Columbia. In: *Geological Fieldwork 2017*, British Columbia Ministry of Energy, Mines and Petroleum Resources, British Columbia Geological Survey Paper 2018-1, pp. 15-38.
- Nelson, J.L., and van Straaten, B., 2020. Recurrent syn- to post-subduction mineralization along deep crustal corridors in the Iskut-Stewart-Kitsault region of western Stikinia, northwestern British Columbia. In: Sharman, E.R., Lang, J.R., and Chapman, J.B., (Eds.), *Porphyry Deposits of the Northwestern Cordillera of North America: A 25-Year Update*. Canadian Institute of Mining and Metallurgy Special Volume 57, pp. 194-211.
- Nelson, J.L., van Straaten, B., and Friedman, R., 2022. Latest Triassic-Early Jurassic Stikine-Yukon-Tanana terrane collision and the onset of accretion in the Canadian Cordillera: Insights from Hazelton Group detrital zircon provenance and arc-back-arc configuration. *Geosphere*, 18, 670-696.
- Nelson, J.L., Colpron, M., and Israel, S., 2013. The Cordillera of British Columbia, Yukon and Alaska: Tectonics and metallogeny. In: Colpron, M., Bissig, T., Rusk, B.G., and Thompson, J., (Eds.), *Tectonics, Metallogeny and Discovery: The North American Cordillera and Similar Accretionary Settings*, Society of Economic Geologists Special Publication 17, pp. 53-110.
- Ramsay, J.G., 1967. *Folding and fracturing of rocks*: McGraw-Hill Book Company, New York, 560 p.
- Rees, C., Riedell, K.B., Proffett, J.M., Macpherson, J., and Robertson, S., 2015. The Red Chris porphyry copper-gold deposit, northern British Columbia, Canada: Igneous phases, alteration, and controls of mineralization. *Economic Geology*, 110, 857-888.
- Rhys, D.A., 1993. Geology of the Snip Mine, and its relationship to the magmatic and deformational history of the Johnny Mountain area, northwestern British Columbia. M.Sc. thesis, The University of British Columbia, Vancouver, B.C., Canada. Available from <<https://circle.ubc.ca/handle/2429/2173>> accessed April 12, 2012.
- Schwab, D.L., Petsel, S., Otto, B.R., Morris, S.K., Workman, E., and Tosdal, R.M., 2008. Overview of the Late Triassic Galore Creek copper-gold-silver porphyry system. In: Spencer, J.E., and Tittle, S.R., (Eds.), *Arizona Geological Society Digest 22*, pp. 1-14.
- van Straaten, B.I., Friedman, R.M., and Camacho, A., 2023. Stratigraphy of the Stuhini Group (Upper Triassic) in the Galore Creek area, northwestern British Columbia. In: *Geological Fieldwork 2022*, British Columbia Ministry of Energy, Mines and Low Carbon Innovation, British Columbia Geological Survey Paper 2023-01, pp. 33-49.





# U-Pb zircon dates for rhyolite and sandstone of Cadwallader terrane, lower Chilcotin River area, south-central British Columbia

Paul Schiarizza<sup>1, a</sup>, and Richard M. Friedman<sup>2</sup>

<sup>1</sup> British Columbia Geological Survey, Ministry of Energy, Mines and Low Carbon Innovation, 300-865 Hornby Street, Vancouver, BC, V6Z 2G3

<sup>2</sup> Retired, formerly at Pacific Centre for Isotopic and Geochemical Research, Department of Earth, Ocean and Atmospheric Sciences, The University of British Columbia, Vancouver, BC, V6T 1Z4

<sup>a</sup> corresponding author: Paul.Schiarizza@gov.bc.ca

Recommended citation: Schiarizza, P., and Friedman, R.M., 2023. U-Pb zircon dates for rhyolite and sandstone of Cadwallader terrane, lower Chilcotin River area, south-central British Columbia. In: Geological Fieldwork 2022, British Columbia Ministry of Energy, Mines and Low Carbon Innovation, British Columbia Geological Survey Paper 2023-01, pp. 65-84.

## Abstract

Cadwallader terrane, exposed in a structural window beneath overthrust Cache Creek terrane along the Chilcotin River, 50 km southwest of Williams Lake, comprises: 1) basalt, rhyolite and tonalite of the Wineglass assemblage (Late Permian); 2) conglomerates and sandstones (Tyaughton Formation, Late Triassic) that rest unconformably above the Wineglass assemblage; and 3) siltstones and sandstones (Ladner Group, Early and Middle Jurassic) that are disconformably above the Tyaughton Formation. Rhyolite from near the top of the Wineglass assemblage, dated using the U-Pb zircon chemical abrasion thermal ionization mass spectrometry method (CA-TIMS), crystallized at  $260.8 \pm 0.3$  Ma. Detrital zircons from red sandstone in the lower part of the Tyaughton Formation, dated with Laser Ablation Inductively Coupled Plasma Mass Spectrometry (LA-ICP-MS), include a population of Late Permian to Middle Triassic grains, probably derived from the underlying Wineglass assemblage and/or related rocks, and a population of Late Triassic grains that are inferred to have been derived from Late Triassic volcanic and plutonic rocks exposed elsewhere in Cadwallader terrane. Green sandstone from a higher stratigraphic level in the Tyaughton Formation contains only Late Triassic zircons, and these have a range that is very similar to that of detrital zircons analyzed from a sample of Hurley Formation (Late Triassic) in a separate fault panel north of the Chilcotin River window. The Permian to Jurassic rocks exposed in the Chilcotin River window represent the Tyaughton Creek facies of Cadwallader terrane, which contrasts with other parts of the terrane (Camelsfoot facies) represented mainly by the Pioneer and Hurley formations of the Cadwallader Group (Middle to Late Triassic). The Permian to Jurassic rocks of the Tyaughton Creek facies correlate with rocks in central British Columbia (Sitlika assemblage) and northern British Columbia (Kutcho assemblage and overlying rocks), forming a fragmented belt that can be traced the full south to north length of British Columbia.

**Keywords:** Cadwallader terrane, Wineglass assemblage, Tyaughton Formation, Hurley Formation, Late Permian, Late Triassic, U-Pb, zircon, CA-TIMS, LA-ICP-MS

## 1. Introduction

Read (1992, 1993) identified Late Permian volcanic and intrusive rocks along the lower reaches of the Chilcotin River southwest of Williams Lake. These rocks were in part mapped by Schiarizza (2013), who referred to them as the Wineglass assemblage and correlated them with the Sitlika and Kutcho assemblages of central and northern British Columbia. Schiarizza (2013) also correlated undated conglomerates and sandstones that rest unconformably above the Permian rocks with the Tyaughton Formation (Late Triassic) of Cadwallader terrane, thus inferring that the Wineglass assemblage is also part of that terrane. Four samples collected during this mapping were submitted for U-Pb zircon isotopic dating at the Pacific Centre for Isotopic and Geochemical Research (PCIGR), Department of Earth, Ocean and Atmospheric Sciences, the University of British Columbia. Herein we present the geochronologic data and age interpretations for these samples. One sample of rhyolite was dated using the U-Pb zircon chemical abrasion

thermal ionization mass spectrometry method (CA-TIMS), confirming the Late Permian age for at least the upper part of the Wineglass assemblage. The other three samples are sandstones, submitted for U-Pb detrital zircon analysis using Laser Ablation Inductively Coupled Plasma Mass Spectrometry (LA-ICP-MS). Two sandstone samples are from the sedimentary succession that is unconformably above the Wineglass assemblage, and the data corroborate its correlation with the Tyaughton Formation. The third sandstone sample is from the Hurley Formation in an adjacent fault panel; these zircons are very similar to those from the Tyaughton Formation, confirming that the Hurley and Tyaughton formations are part of the same terrane.

## 2. Setting

The lower Chilcotin River area is on the Fraser Plateau, along and west of the Fraser River, within the traditional territories of the Tsilhqot'in and Secwepemc First Nations (Figs. 1, 2). It is underlain, in large part, by late Paleozoic and early Mesozoic

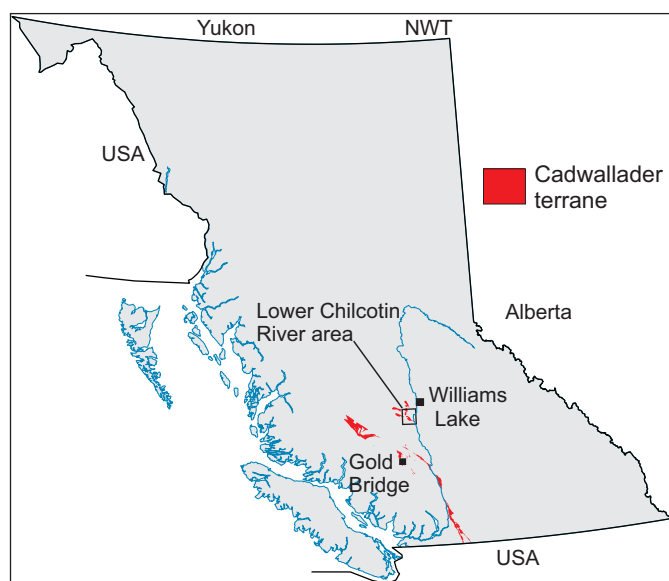


**Fig. 1.** Location of the lower Chilcotin River area and distribution of Cadwallader terrane (after Schiarizza, 2013) in southern British Columbia.

rocks assigned to Cache Creek terrane, Cadwallader terrane, and Thaddeus assemblage, the latter comprising Carboniferous greenstone and limestone of uncertain correlation or terrane affinity (Read, 1993). These units are separated from one another by thrust faults, of uncertain Middle Jurassic to mid-Cretaceous age, that are commonly marked by serpentinite melange (Fig. 2; Read, 1993). Younger rocks exposed in the area include small Middle to Late Jurassic diorite and quartz diorite intrusions, Eocene volcanic and sedimentary rocks, and flat-lying Neogene basalts of the Chilcotin Group.

The Cache Creek complex (Cache Creek terrane) is subdivided into three composite units: one comprising chert, siliceous phyllite, and limestone; another of basalt and limestone; and a third of mainly siltstone and sandstone (Fig. 2). Biochronologic data come mainly from the chert-siliceous phyllite-limestone unit, which has yielded Early Permian, Middle Triassic, and Late Triassic radiolarians (Cordey and Read, 1992). A large body of diorite and gabbro that is also included in Cache Creek terrane (Fig. 2) has yielded a U-Pb zircon age of  $241.5 \pm 0.5$  Ma (Middle Triassic; Mahoney et al., 2013).

Cadwallader terrane is represented, in part, by Upper Triassic sandstone, conglomerate and limestone of the Hurley Formation, which occurs west of Cache Creek terrane along and north of the Chilcotin River, and also forms a folded thrust panel that encompasses Bald Mountain (Fig. 2). A much different group of rocks (Late Permian to Early Jurassic) that are also part of Cadwallader terrane are exposed in a structural window beneath Cache Creek terrane (Chilcotin River window) southeast of the Hurley exposures (Fig. 2).

## 2.1. Geology of the Chilcotin River window

The Chilcotin River window, 22 km long and up to 6.5 km wide, is an inlier of Late Permian to Early Jurassic rocks that

are structurally beneath rocks of Cache Creek terrane along and southwest of the Chilcotin River (Fig. 2). It is mainly underlain by Late Permian volcanic and intrusive rocks assigned to the Wineglass assemblage, but also includes conglomerates and sandstones that are unconformably above the Permian rocks, and a younger unit of finer grained siliciclastic rocks that contain Early Jurassic fossils. Schiarizza (2013) correlated the conglomerate-sandstone unit with the Tyaughton Formation (Late Triassic), and assigned the overlying Jurassic rocks to the Ladner Group.

The Wineglass assemblage is in large part represented by the Wineglass pluton, a body of tonalite, quartz diorite and granodiorite that has yielded U-Pb crystallization ages of  $258 \pm 5$  Ma (Friedman and van der Heyden, 1992) and  $254 \pm 1.2$  Ma (Read, 1993). Volcanic and volcanoclastic rocks of the assemblage are best exposed on the southwest margin of the Wineglass pluton (Fig. 3) where they were mapped and subdivided into two units by Schiarizza (2013). The oldest unit (Wv1) is mainly basalt and basalt-derived chlorite schist, but also includes narrow units of felsic volcanic rock (dikes, sills, or flows) and small bodies of diorite. These rocks are overlain by a more heterogeneous unit (Wv2) that includes basalt and pillowed basalt, rhyolite and dacite flows, and volcanoclastic rocks containing quartz, feldspar and felsic to mafic volcanic lithic fragments. Read (1993) reported a U-Pb zircon age of  $259 \pm 2$  Ma from dacite of unit Wv2. This Late Permian age is confirmed by the CA-TIMS age ( $260.8 \pm 0.3$  Ma) reported here.

The Tyaughton Formation comprises a southwest-dipping succession of siliciclastic sedimentary rocks that rests unconformably above the Wineglass assemblage near the southwest margin of the Chilcotin River window (Figs. 2, 3). It includes a basal unit of mainly red pebble conglomerates, and an overlying unit of massive, blue-green to olive green sandstones (Schiarizza, 2013). The conglomerates of the basal unit consist mainly of felsic volcanic fragments, but also include clasts of tonalite, mafic volcanic rock, chert, and microdiorite.

The youngest rocks exposed in the Chilcotin River window are assigned to the Ladner Group (Early to Middle Jurassic). They comprise grey, thin-bedded siltstones and fine- to medium-grained sandstones that overlie the Tyaughton Formation across a sharp, probably disconformable contact (Fig. 3). Hickson (1990) reported that fossils collected from the lower part of this unit are Early Jurassic (Toarcian).

## 3. CA-TIMS geochronology

Here we present U-Pb zircon isotopic dating results obtained by the chemical abrasion thermal ionization mass spectrometry method (CA-TIMS) for one rhyolite sample collected from the Wineglass assemblage.

### 3.1. Analytical procedures

CA-TIMS procedures described here are modified from Mundil et al. (2004), Mattinson (2005) and Scoates and Friedman (2008). After rock samples underwent standard mineral separation procedures, zircons were handpicked



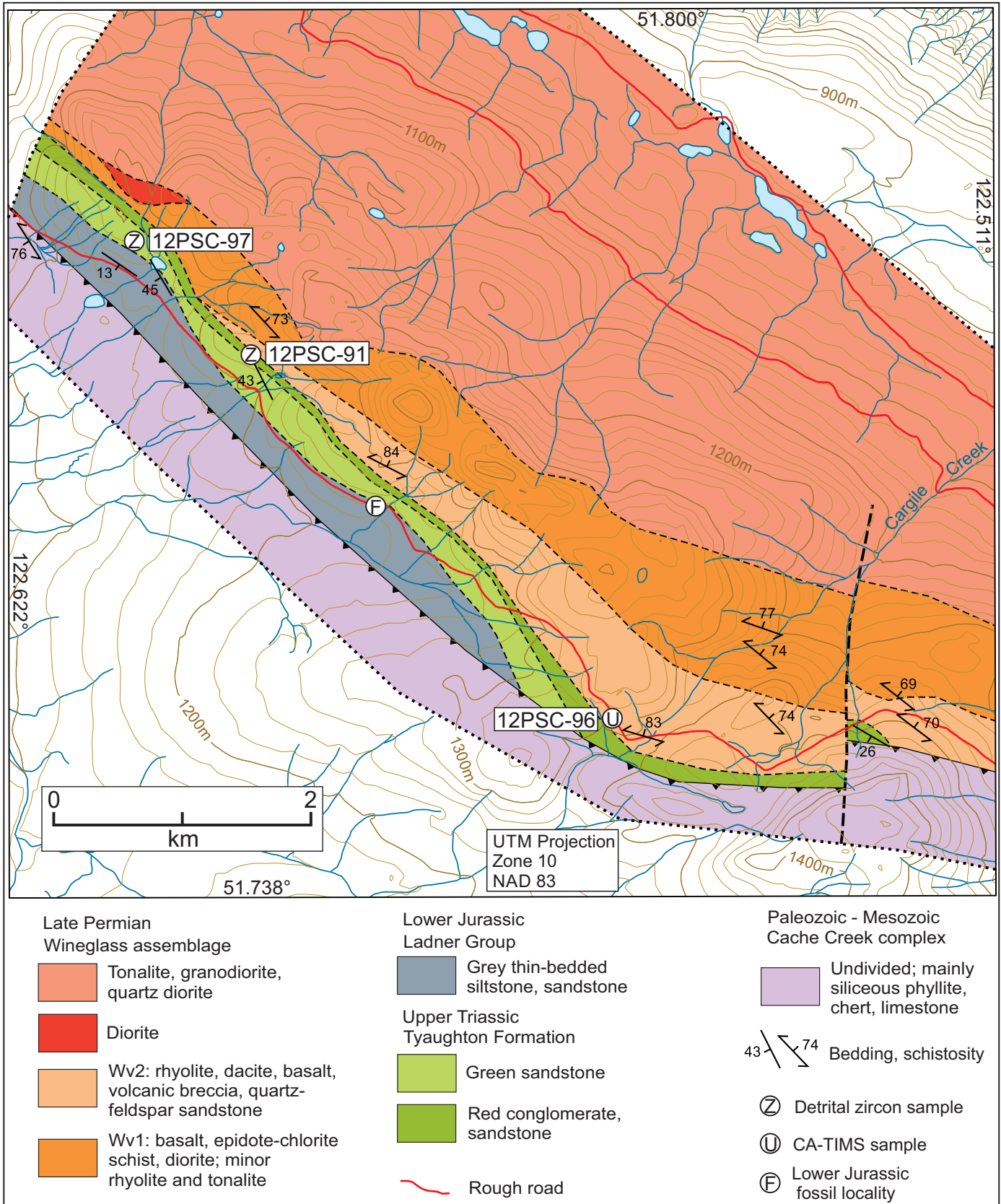


Fig. 3. Geology of the southwestern part of the Chilcotin River window, after Schiarizza (2013).

in alcohol. The clearest, crack- and inclusion-free grains were selected, photographed, and then annealed in quartz glass crucibles at 900°C for 60 hours. Annealed grains were transferred into 3.5 mL PFA screwtop beakers, ultrapure HF (up to 50% strength, 500  $\mu$ L) and HNO<sub>3</sub> (up to 14 N, 50  $\mu$ L) were added and caps were closed finger tight. The beakers were placed in 125 mL PTFE liners (up to four per liner) and about 2 mL HF and 0.2 mL HNO<sub>3</sub>, of the same strength as the acid in the beakers containing the samples, were added to the liners. The liners were then slid into stainless steel Parr™ high-pressure dissolution devices, which were sealed and brought to a maximum of 200°C for 8-16 hours (typically 175°C for 12 hours). Beakers were removed from the liners and zircon was separated from the leachate. Zircons were rinsed with >18 M $\Omega$ .cm water and subboiled acetone. Then 2 mL of subboiled 6N HCl was added and beakers were set on a hotplate at 80-130°C for 30 minutes and again rinsed with water and acetone. Masses were estimated from the dimensions (volumes) of grains. Single grains were transferred into clean 300  $\mu$ L PFA microcapsules (crucibles), and 50  $\mu$ L 50% HF and 5  $\mu$ L 14 N HNO<sub>3</sub> were added. Each was spiked with a <sup>233-235</sup>U-<sup>205</sup>Pb tracer solution (EARTHTIME ET535), capped and again placed in a Parr liner (8-15 microcapsules per liner). HF and nitric acids, in a 10:1 ratio, were added to the liner, which was then placed in a Parr high-pressure device and dissolution was achieved at 240°C for 40 hours. The resulting solutions were dried on a hotplate at 130°C, 50  $\mu$ L 6N HCl was added to microcapsules and fluorides were dissolved in high-pressure Parr devices for 12 hours at 210°C. HCl solutions were transferred into clean 7 mL PFA beakers and dried with 2  $\mu$ L of 0.5 N H<sub>3</sub>PO<sub>4</sub>. Samples were loaded onto degassed, zone-refined Re filaments in 2  $\mu$ L of silicic acid emitter (Gerstenberger and Haase, 1997).

Isotopic ratios were measured by a modified single collector

VG-54R or 354S (with Sector 54 electronics) thermal ionization mass spectrometer equipped with analogue Daly photomultipliers. Analytical blanks were 0.2 pg for U and up to 1 pg for Pb. U fractionation was determined directly on individual runs using the EARTHTIME ET535 mixed <sup>233-235</sup>U-<sup>205</sup>Pb isotopic tracer. Pb isotopic ratios were corrected for fractionation of 0.25  $\pm$  0.03%/amu, based on replicate analyses of NBS-982 reference material and the values recommended by Thirlwall (2000). Data reduction employed the Excel-based program of Schmitz and Schoene (2007). Standard concordia diagrams were constructed and weighted averages calculated with Isoplot (Ludwig, 2003). Interpreted ages for all samples are based on weighted <sup>206</sup>Pb/<sup>238</sup>U dates reported at the 2 sigma confidence level in the three error,  $\pm X (Y) [Z]$  format of Schoene et al. (2006), where X includes internal errors only, largely comprised of analytical (counting statistics), mass fractionation and common lead composition uncertainties. The (Y) error includes X plus isotopic tracer calibration uncertainty and [Z] additionally includes uranium decay constant errors. Isotopic dates are calculated with the decay constants  $\lambda_{U238}=1.55125E^{-10}$  and  $\lambda_{U235}=9.8485E^{-10}$  (Jaffey et al., 1971). EARTHTIME U-Pb synthetic solutions were analyzed on an on-going basis to monitor the accuracy of results.

### 3.2. Sample 12PSC-96, rhyolite, Wineglass assemblage

Sample 12PSC-96 was collected from the upper part of the upper volcanic unit of the Wineglass assemblage, about 75 m northeast of the (unexposed) contact with the overlying Tyaughton Formation (Figs. 3, 4; 530786E, 5733372N, UTM Zone 10, NAD83). It is a pale green to grey metarhyolite with abundant 1-2 mm plagioclase and quartz phenocrysts in a very fine-grained groundmass of mainly quartz, feldspar and secondary sericite (Fig. 5).

Four of the six zircon grains analyzed (Table 1) are mutually

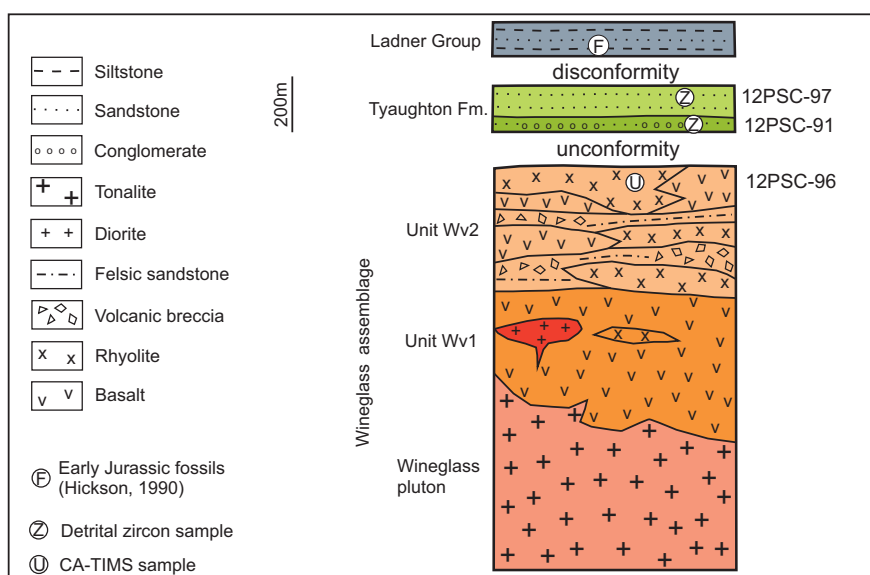


**Fig. 4.** Schematic stratigraphy of the Wineglass assemblage and overlying Tyaughton Formation and Ladner Group, showing stratigraphic context of geochronology samples. Vertical scale very approximate, based on bedding dips and mapped contacts of Tyaughton Formation.



**Fig. 5.** Quartz and plagioclase-phyric metarhyolite, Wineglass assemblage, sample site 12PSC-96.

overlapping on or near concordia, with a weighted mean  $^{206}\text{Pb}/^{238}\text{U}$  date of  $260.8 \pm 0.3$  (0.4) [0.5] Ma (MSWD=1.04), interpreted as the crystallization age of the rhyolite (Fig. 6). The other two grains give slightly younger dates (259.86 and 259.68 Ma), possibly due to minor Pb loss.

#### 4. Detrital zircon geochronology

Here we present the results from isotopic analyses of detrital zircons extracted from three samples, two from the Tyaughton Formation where it overlies the Wineglass assemblage, and one from the Hurley Formation in an adjacent fault panel.

##### 4.1. Analytical procedures

Zircons were analyzed using laser ablation (LA) ICP-MS methods, as described by Tafti et al. (2009). Instrumentation comprised a New Wave UP-213 laser ablation system and a ThermoFinnigan Element2 single collector, double-focusing, magnetic sector ICP-MS. All zircons greater than about 50 microns in diameter were picked from the mineral separates and mounted in an epoxy puck along with several grains of the Plešovice ( $337.13 \pm 0.13$  Ma, Sláma et al., 2007) and Temora2 ( $416.78 \pm 0.33$  Ma) zircon standards, and brought to a very high polish. The surface of the mount was washed for 10 minutes with dilute nitric acid and rinsed in ultraclean water before analysis. The highest quality portions of each grain, free of alteration, inclusions, or possible inherited cores, were selected for analysis. Line scans rather than spot analyses were employed in order to minimize elemental fractionation during the analyses. A laser power level of 38% was used, with a spot size of 30 micrometres. Backgrounds were measured with the laser shutter closed for ten seconds, followed by data collection with the laser firing for approximately 35 seconds. The time-integrated signals were analyzed using GLITTER software (Griffin et al., 2008), which automatically subtracts background

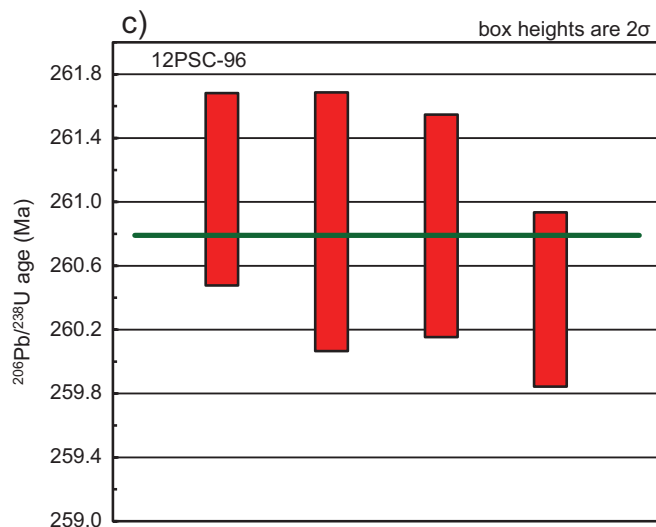
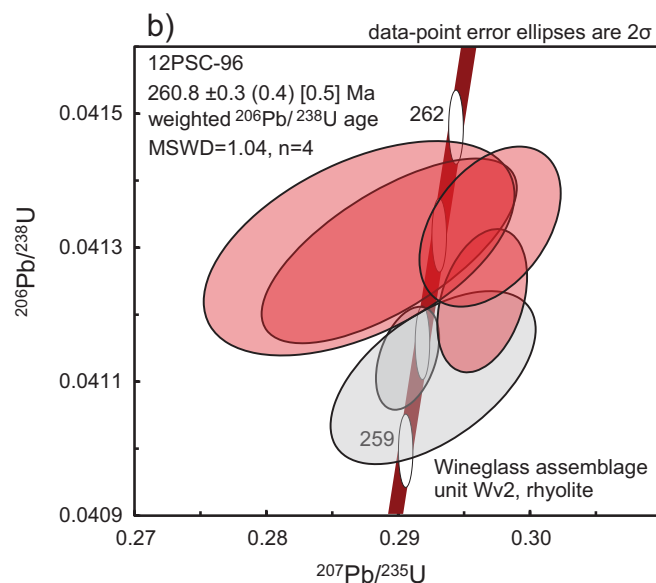
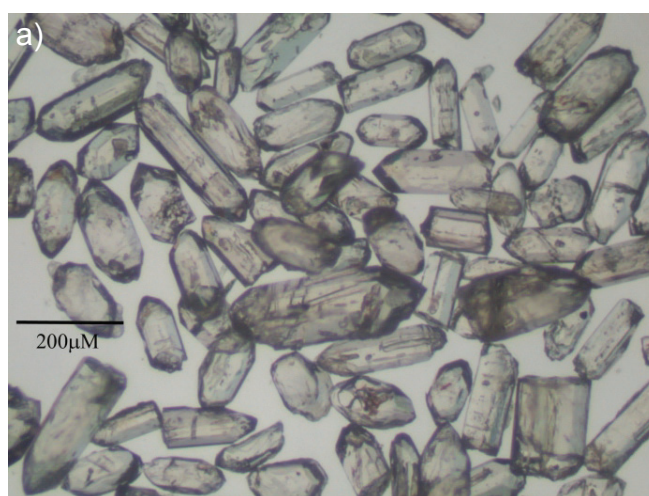


**Fig. 6.** U-Pb data for zircons from sample 12PSC-96. **a)** Photomicrograph of zircons. **b)** Concordia plot. **c)**  $^{206}\text{Pb}/^{238}\text{U}$  ages and calculated weighted mean age, based on four of the six analyses.

**Table 1.** Zircon U-Th-Pb CA-TIMS analytical results for sample 12PSC-96, Wineglass assemblage rhyolite.

Sample	Compositional Parameters										Radiogenic Isotope Ratios						Isotopic Ages						
	Wt.	U	Th	Pb	$^{206}\text{Pb}^*$	mol %	Pb*	$^{206}\text{Pb}$	$^{208}\text{Pb}$	$^{206}\text{Pb}$	$^{207}\text{Pb}$	$^{206}\text{Pb}$	$^{207}\text{Pb}$	$^{206}\text{Pb}$	$^{238}\text{U}$	$^{206}\text{Pb}$	$^{235}\text{U}$	$^{207}\text{Pb}$	$^{238}\text{U}$	$^{206}\text{Pb}$			
	mg	ppm	ppm	ppm	pg	mol	pg	pg	pg	pg	pg	pg	pg	pg	pg	pg	pg	pg	pg	pg	pg		
12PSC96																							
A	0.0041	36	0.424	1.6	0.2553	98.60%	21	0.30	1323	0.133	0.050813	2.555	0.289310	2.734	0.041294	0.273	0.682	232.34	58.98	258.02	6.23	260.85	0.70
B	0.0034	69	0.496	3.0	0.4003	98.96%	29	0.35	1779	0.157	0.051257	0.630	0.290703	0.674	0.041134	0.153	0.391	252.40	14.49	259.11	1.54	259.86	0.39
C	0.0041	45	0.494	2.0	0.3166	98.83%	26	0.31	1578	0.157	0.051633	2.038	0.292633	2.170	0.041105	0.257	0.557	269.21	46.73	260.63	4.99	259.68	0.65
D	0.0026	141	0.604	6.5	0.6297	98.85%	27	0.60	1603	0.194	0.052143	0.895	0.296348	0.943	0.041220	0.214	0.335	291.69	20.44	263.54	2.19	260.39	0.54
E	0.0029	25	0.387	1.2	0.1251	96.03%	7	0.42	464	0.121	0.050405	3.208	0.287018	3.354	0.041298	0.317	0.498	213.73	74.29	256.21	7.59	260.88	0.81
F	0.0029	46	0.425	2.0	0.2319	98.66%	22	0.26	1379	0.136	0.052114	1.379	0.296982	1.460	0.041331	0.236	0.415	290.39	31.49	264.04	3.39	261.08	0.60

(a) A, B etc. are labels for fractions composed of single zircon grains or fragments; all fractions annealed and chemically abraded after Mattinson (2005) and Scoates and Friedman (2008).

(b) Nominal fraction weights estimated from photomicrographic grain dimensions, adjusted for partial dissolution during chemical abrasion.

(c) Nominal U and total Pb concentrations subject to uncertainty in photomicrographic estimation of weight and partial dissolution during chemical abrasion.

(d) Model Th/U ratio calculated from radiogenic  $^{208}\text{Pb}/^{206}\text{Pb}$  ratio and  $^{207}\text{Pb}/^{235}\text{U}$  age.

(e) Pb\* and Pb represent radiogenic and common Pb, respectively; mol %  $^{206}\text{Pb}^*$  with respect to radiogenic, blank and initial common Pb.

(f) Measured ratio corrected for spike and fractionation only. Mass discrimination of 0.25% ± 0.03 per amu based on analysis of NBS-982; all Daly analyses.

(g) Corrected for fractionation, spike, and common Pb; up to 0.3 pg of common Pb was assumed to be procedural blank:  $^{206}\text{Pb}/^{204}\text{Pb} = 18.50 \pm 1.0\%$ ;  $^{207}\text{Pb}/^{204}\text{Pb} = 15.50 \pm 1.0\%$ ;  $^{208}\text{Pb}/^{206}\text{Pb} = 38.40 \pm 1.0\%$  (all uncertainties 1-sigma). Excess over blank was assigned to initial common Pb with Stacey and Kramers (1975) model Pb composition at 260 Ma.

(h) Errors are 2-sigma, propagated using the algorithms of Schmitz and Schoene (2007) and Crowley et al. (2007).

(i) Calculations are based on the decay constants of Jaffey et al. (1971),  $^{206}\text{Pb}/^{238}\text{U}$  and  $^{207}\text{Pb}/^{235}\text{U}$  ages corrected for initial disequilibrium in  $^{230}\text{Th}/^{238}\text{U}$  using  $\text{Th/U} [\text{magma}] = 3$ .



**Fig. 7.** Red sandstone, Tyaughton Formation, sample site 12PSC-91.

measurements, propagates all analytical errors, and calculates isotopic ratios and ages. Corrections for mass and elemental fractionation were made by bracketing analyses of unknown grains with replicate analyses of the Plešovice zircon standard. A typical analytical session consisted of four analyses of the Plešovice standard zircon, followed by two analyses of the Temora2 zircon standard, five analyses of unknown zircons, two standard analyses, then five unknown analyses. Each session was completed with two Temora2 and four Plešovice standard analyses. The Temora2 reference zircon was analyzed as an unknown in order to monitor the reproducibility of the age determinations on a run-to-run basis. Final interpretation and plotting of the analytical results employed the ISOPLOT software of Ludwig (2003).

**4.2. Sample 12PSC-91, Tyaughton Formation, red sandstone**

Sample 12PSC-91 was collected from the basal unit of the Tyaughton Formation a few 10s of m southeast of its (unexposed) contact with the Wineglass assemblage (Figs. 3, 4; 527964E, 5736192N, UTM Zone 10 NAD 83). The exposure at this locality is predominantly red and grey-green, fine- to coarse-grained sandstone, intercalated with red siltstone and red pebble conglomerate. The sample is from a red, coarse-grained sandstone bed that includes about 10% secondary calcite as small patches and veins (Fig. 7). It is composed mainly of feldspathic, felsic to mafic volcanic lithic grains, but also includes saussuritic plagioclase, quartz (including some grains with embayed margins), epidote-altered aggregates derived from mafic mineral or lithic grains, siltstone, quartzite, and tonalite. The tonalite grains (equigranular intergrowths of plagioclase and quartz) are uncommon but tend to be larger (2 mm) than the other detrital grains (≤1.5 mm).

Sixty-four detrital zircon grains were analyzed from sample 12PSC-91, yielding  $^{206}\text{Pb}/^{238}\text{U}$  ages ranging from 271.9 Ma to 212.7 Ma (Table 2). Two strong peaks and an intervening trough on the probability density curve (Fig. 8) permit subdivision into two populations. The older population (n=39) consists mainly

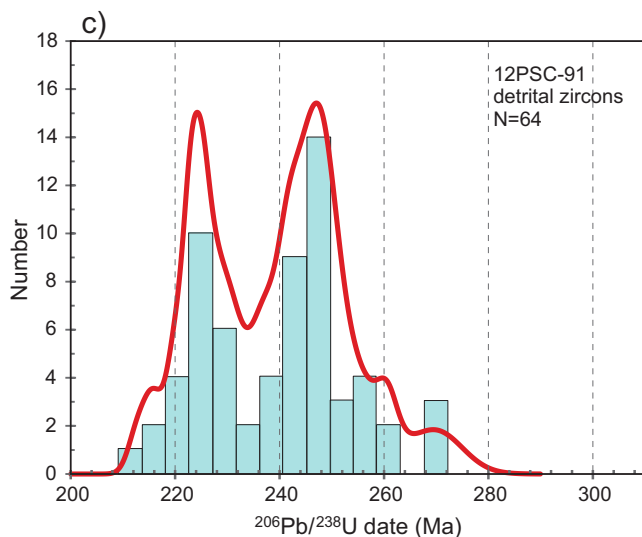
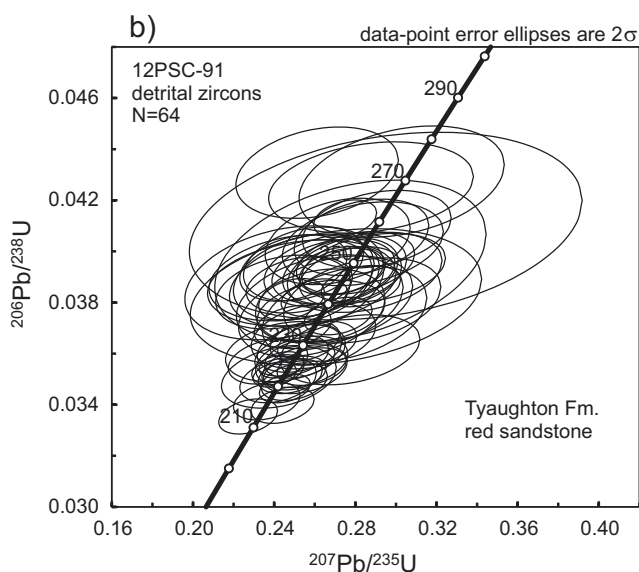
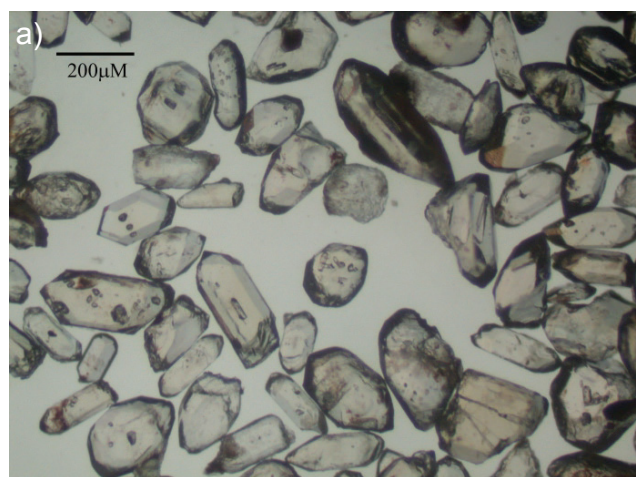


**Fig. 8.** U-Pb data for detrital zircons from sample 12PSC-91. **a)** Photomicrograph of zircons. **b)** Concordia plot of all grains. **c)** Histogram of detrital zircon ages and superimposed probability density curve.

of Late Permian to Middle Triassic grains (260.7 to 237.1 Ma) with a peak at 247 Ma on the probability density curve, but also includes an outlier of three grains with early Middle Permian ages (271.9, 269.7, 268.3 Ma). The younger population ( $n=25$ ) comprises Late Triassic grains (234.6 to 212.7 Ma) with a peak at 224 Ma on the probability density curve. The youngest grains (212.7, 215.4, 216.4 Ma) suggest a middle to late Norian maximum depositional age.

#### 4.3. Sample 12PSC-97, Tyaughton Formation, green sandstone

Sample 12PSC-97 was collected from the upper part of the Tyaughton Formation, 1300 m northwest of sample 12PSC-91 (Figs. 3, 4; 527054E, 5737072N, UTM Zone 10 NAD 83). It comes from an outcrop of green medium- to coarse-grained sandstone that weathers greenish-brown and shows no discernible bedding (Fig. 9). The sandstone consists mainly of very-fine-grained lithic grains that are variably altered to sericite±epidote. Some of these grains contain microphenocrysts of feldspar and/or quartz and were derived from felsic volcanic rock, but others may have been derived from siltstone. The sandstone also contains grains of sericite±epidote-altered plagioclase, quartz (most markedly angular, some rounded with embayed margins), and mafic mineral or lithic grains altered to epidote and chlorite.

The  $^{206}\text{Pb}/^{238}\text{U}$  ages for the analyzed zircons ( $n=64$ ) range from 237.7 to 205.6 Ma, with a peak at 219 Ma on the probability density curve (Table 3; Fig. 10). The oldest grain (237.7 Ma) is near the Middle Triassic/Late Triassic boundary, and the other grains span most of the Late Triassic. The youngest grains (205.6, 205.7, 208.5, 208.7, 208.9 Ma) suggest a late Norian or Rhaetian maximum depositional age.

#### 4.4. Sample 12PSC-98, Hurley Formation, green sandstone

Sample 12PSC-98 was collected from an outcrop on the south side of Highway 20 (527054E, 5737072N, UTM Zone 10, NAD 83), 8 km west-northwest of Riske Creek (Fig. 2). These rocks are part of a package of siliciclastic rocks and limestones that were identified as Hurley Formation (Cadwallader Group) by Rusmore and Woodsworth (1991) and mapped as a folded thrust panel (Bald Mountain slice) by Read (1992, 1993) and Mahoney et al. (2013). Limestone units in this fault panel, of unknown stratigraphic relationship to the siliciclastic rocks sampled along the highway, have yielded late Carnian and early Norian conodonts (Mahoney et al., 2013). The outcrop along Highway 20 comprises green gritty to pebbly sandstone (Fig. 11) intercalated with medium to thick beds of pebble conglomerate. Aphanitic and quartz-feldspar-phyric felsic volcanic clasts predominate, but the conglomerates and pebbly sandstones also contain angular to subrounded clasts of limestone, aphanitic and plagioclase-phyric mafic volcanic rock, red and green chert, cherty argillite, diabase, and tonalite. Sample 12PSC-98, from the central part of the outcrop, is a green coarse-grained sandstone with scattered lithic granules. Detrital grains are mainly felsic volcanic rock (some with



**Fig. 9.** Massive green sandstone, Tyaughton Formation, sample site 12PSC-97.

quartz and/or feldspar phenocrysts) but also include quartz, plagioclase, pyroxene, and chlorite-epidote-altered mafic volcanic rock.

Sixty-two detrital zircon grains were analyzed from sample 12PSC-98, yielding late Middle Triassic and Late Triassic  $^{206}\text{Pb}/^{238}\text{U}$  ages ranging from 239.8 Ma to 210 Ma (Table 4). The probability density curve shows a strong peak at 223 Ma, and subsidiary peaks at 219 Ma, 230 Ma and 239 Ma (Fig. 12). The youngest grains (210, 210.6, 212.5, 212.5, 213.6 Ma) suggest a late Norian maximum depositional age.

## 5. Discussion

Read (1993) mapped Mesozoic siliciclastic rocks that rest unconformably above Late Permian rocks of the Wineglass assemblage as a single unit, which he considered Early Jurassic because it included an exposure of siltstone with Toarcian fossils (Hickson, 1990). Schiarizza (2013), on lithologic grounds, assigned the lower part of this Mesozoic succession to the Tyaughton Formation (Late Triassic), and the upper part, including the fossiliferous siltstones, to the Ladner Group (Early to Middle Jurassic). Detrital zircons from samples 12PSC-91 and 12PSC-97 (Figs. 3 and 4) corroborate the interpretation of Schiarizza (2013) by providing maximum depositional ages consistent with the late Norian to Rhaetian age of the Tyaughton Formation in its type area (Tozer, 1979; Umhoefer, 1990; Umhoefer and Tipper, 1998). The very strong similarity between the detrital zircon populations of samples 12PSC-97 (Tyaughton Formation) and 12PSC-98 (Hurley Formation in a different fault panel) also corroborate the interpretation that both samples are from Triassic rocks of the same terrane, and support the long-held view that the Late Triassic siliciclastic rocks of Cadwallader terrane (Hurley and Tyaughton formations) were sourced from an associated Late Triassic magmatic arc (Rusmore, 1987; Rusmore et al., 1988; Umhoefer, 1990).

Sample 12PSC-91 (lower part of the Tyaughton formation near its contact with underlying Wineglass assemblage) yielded,

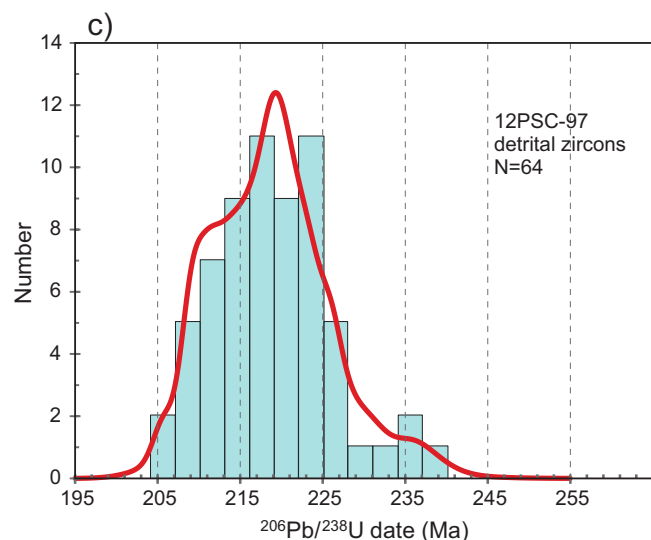
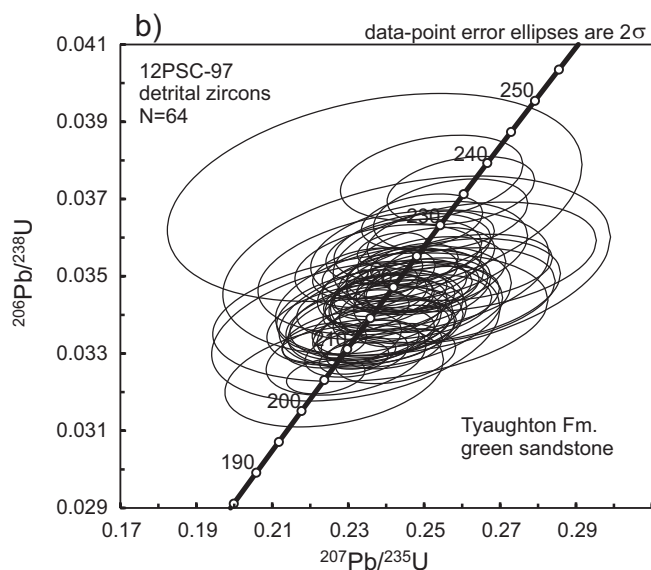
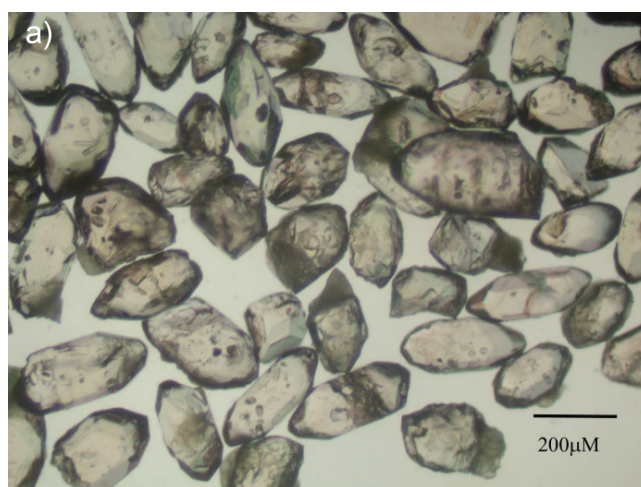


**Fig. 10.** U-Pb data for detrital zircons from sample 12PSC-97. **a)** Photomicrograph of zircons. **b)** Concordia plot of all grains. **c)** Histogram of detrital zircon ages and superimposed probability density curve.

**Table 2.** Zircon U-Pb laser ablation analytical data for sample 12PSC-91, Tyaughton Formation red sandstone.

Sample no. Analysis ID	Isotopic Ratios					Isotopic Ages							
	$^{207}\text{Pb}/^{235}\text{U}$	$1\sigma$	$^{206}\text{Pb}/^{238}\text{U}$	$1\sigma$	$\rho$	$^{207}\text{Pb}/^{206}\text{Pb}$	$1\sigma$	$^{207}\text{Pb}/^{235}\text{U}$	$1\sigma$	$^{206}\text{Pb}/^{238}\text{U}$	$1\sigma$	$^{207}\text{Pb}/^{206}\text{Pb}$	$1\sigma$
	(abs)	(abs)	(abs)	(abs)		(abs)	(abs)	(Ma)	(Ma)	(Ma)	(Ma)	(Ma)	(Ma)
12PSC91-1	0.2586	0.0148	0.0376	0.0007	0.33	0.0546	0.0028	233.5	11.9	237.9	4.37	395.4	109
12PSC91-2	0.2837	0.0162	0.0403	0.0007	0.29	0.0520	0.0027	253.6	12.8	254.7	4.13	283.7	113
12PSC91-3	0.3028	0.0207	0.0427	0.0009	0.31	0.0515	0.0030	268.6	16.1	269.7	5.51	261.5	130
12PSC91-4	0.2594	0.0125	0.0367	0.0005	0.30	0.0533	0.0023	234.2	10.1	232.4	3.27	339.7	96.1
12PSC91-5	0.2950	0.0396	0.0410	0.0015	0.27	0.0490	0.0059	262.5	31	259	9.26	149.2	260
12PSC91-6	0.2776	0.0273	0.0396	0.0013	0.33	0.0617	0.0054	248.8	21.7	250.6	7.98	664.9	178
12PSC91-7	0.2420	0.0077	0.0350	0.0004	0.32	0.0504	0.0014	220	6.31	221.5	2.24	212.2	64.1
12PSC91-8	0.2721	0.0093	0.0392	0.0004	0.29	0.0501	0.0015	244.4	7.45	248.1	2.44	200.4	69.3
12PSC91-9	0.2830	0.0136	0.0406	0.0006	0.31	0.0525	0.0022	253.1	10.7	256.3	3.76	308.8	92.7
12PSC91-10	0.2716	0.0068	0.0375	0.0003	0.32	0.0541	0.0012	244	5.45	237.1	1.88	376.9	48.6
12PSC91-11	0.2423	0.0116	0.0351	0.0005	0.30	0.0521	0.0023	220.3	9.45	222.3	3.13	290.8	95.9
12PSC91-12	0.2546	0.0142	0.0390	0.0007	0.32	0.0497	0.0024	230.3	11.5	246.6	4.3	179.2	110
12PSC91-13	0.2545	0.0121	0.0395	0.0006	0.31	0.0511	0.0022	230.2	9.8	249.8	3.65	244	95
12PSC91-14	0.2727	0.0116	0.0392	0.0005	0.32	0.0527	0.0020	244.8	9.27	248.1	3.31	315.8	82.9
12PSC91-15	0.2696	0.0158	0.0381	0.0007	0.31	0.0524	0.0027	242.4	12.7	241.1	4.35	302.6	114
12PSC91-16	0.2479	0.0064	0.0351	0.0003	0.31	0.0510	0.0012	224.9	5.24	222.5	1.77	242.6	52.4
12PSC91-17	0.2702	0.0144	0.0393	0.0006	0.28	0.0527	0.0026	242.8	11.5	248.3	3.64	317	106
12PSC91-18	0.2890	0.0145	0.0394	0.0006	0.28	0.0516	0.0023	257.8	11.4	248.9	3.42	267.2	100
12PSC91-19	0.2437	0.0046	0.0356	0.0002	0.32	0.0496	0.0008	221.4	3.71	225.3	1.29	176.9	38.3
12PSC91-20	0.2442	0.0064	0.0340	0.0003	0.33	0.0518	0.0012	221.8	5.19	215.4	1.78	274.5	52.2
12PSC91-21	0.2612	0.0080	0.0364	0.0004	0.32	0.0551	0.0015	235.7	6.41	230.5	2.2	415.1	59
12PSC91-22	0.2847	0.0156	0.0392	0.0006	0.30	0.0543	0.0027	254.3	12.3	247.7	3.95	382.5	106
12PSC91-23	0.2500	0.0172	0.0390	0.0007	0.26	0.0464	0.0029	226.5	14	246.4	4.27	18.4	145
12PSC91-24	0.2451	0.0201	0.0388	0.0009	0.29	0.0538	0.0041	222.6	16.4	245.2	5.63	363.9	162
12PSC91-25	0.2419	0.0053	0.0354	0.0002	0.31	0.0497	0.0010	219.9	4.31	224.1	1.5	181.5	44.7
12PSC91-26	0.2524	0.0107	0.0387	0.0005	0.27	0.0481	0.0019	228.6	8.66	244.7	2.8	104.2	88.5
12PSC91-27	0.2444	0.0136	0.0384	0.0006	0.28	0.0484	0.0025	222	11.1	243	3.64	118	117
12PSC91-28	0.2598	0.0067	0.0382	0.0003	0.31	0.0502	0.0012	234.5	5.39	241.6	1.84	204.9	52.3
12PSC91-29	0.2502	0.0063	0.0352	0.0003	0.30	0.0507	0.0011	226.7	5.11	223.3	1.69	226.4	51.1
12PSC91-30	0.2834	0.0158	0.0381	0.0007	0.32	0.0536	0.0026	253.4	12.5	240.9	4.22	353.9	106
12PSC91-31	0.2456	0.0121	0.0361	0.0005	0.27	0.0504	0.0023	223	9.85	228.5	3.01	212	102
12PSC91-32	0.2487	0.0074	0.0359	0.0003	0.31	0.0514	0.0014	225.5	6.04	227.5	2.06	257.7	60.6
12PSC91-33	0.2801	0.0119	0.0396	0.0005	0.30	0.0541	0.0021	250.8	9.43	250.1	3.11	375.9	82.9
12PSC91-34	0.2713	0.0146	0.0404	0.0007	0.32	0.0508	0.0024	243.7	11.7	255.2	4.29	232.1	104
12PSC91-35	0.2550	0.0086	0.0354	0.0004	0.33	0.0546	0.0017	230.7	6.96	224.2	2.42	394	65.6
12PSC91-36	0.2747	0.0166	0.0376	0.0008	0.34	0.0556	0.0029	246.4	13.2	237.7	4.69	435.3	113
12PSC91-37	0.2705	0.0293	0.0382	0.0011	0.26	0.0504	0.0050	243.1	23.4	241.8	6.75	213.3	215
12PSC91-38	0.2532	0.0144	0.0388	0.0007	0.31	0.0507	0.0026	229.2	11.7	245.2	4.27	227.7	112
12PSC91-39	0.2750	0.0063	0.0413	0.0003	0.32	0.0512	0.0010	246.7	5.05	260.7	1.84	250.5	45.9
12PSC91-40	0.2827	0.0080	0.0386	0.0003	0.30	0.0520	0.0013	252.8	6.32	244.4	2.08	286.2	55.9
12PSC91-41	0.2906	0.0150	0.0409	0.0006	0.29	0.0539	0.0025	259	11.8	258.2	3.83	368.4	101
12PSC91-42	0.2612	0.0164	0.0431	0.0007	0.27	0.0469	0.0027	235.6	13.2	271.9	4.49	45	131
12PSC91-43	0.2878	0.0206	0.0425	0.0007	0.24	0.0502	0.0033	256.8	16.3	268.3	4.53	204	147
12PSC91-44	0.2495	0.0108	0.0394	0.0005	0.31	0.0507	0.0020	226.2	8.78	248.8	3.28	225.4	86.8
12PSC91-45	0.2486	0.0066	0.0381	0.0003	0.32	0.0501	0.0012	225.5	5.4	241.2	2.03	197.3	53.6
12PSC91-46	0.2551	0.0070	0.0365	0.0003	0.32	0.0523	0.0013	230.7	5.67	231	1.99	298.9	54.5
12PSC91-47	0.2693	0.0124	0.0392	0.0005	0.29	0.0509	0.0021	242.1	9.92	247.9	3.21	238.2	93.6
12PSC91-48	0.2625	0.0168	0.0380	0.0008	0.31	0.0495	0.0028	236.7	13.5	240.6	4.63	170.5	126
12PSC91-49	0.2585	0.0070	0.0355	0.0003	0.31	0.0526	0.0013	233.5	5.62	224.8	1.84	312.6	53.8
12PSC91-50	0.2453	0.0051	0.0346	0.0002	0.32	0.0517	0.0010	222.7	4.17	219.5	1.44	270.2	42
12PSC91-52	0.2631	0.0129	0.0377	0.0005	0.27	0.0513	0.0023	237.2	10.3	238.2	3.14	252.4	99.4
12PSC91-53	0.2773	0.0141	0.0362	0.0006	0.30	0.0560	0.0026	248.5	11.2	228.9	3.49	453.6	99.2
12PSC91-54	0.2364	0.0067	0.0341	0.0003	0.31	0.0515	0.0013	215.4	5.5	216.4	1.85	262.3	57.8
12PSC91-55	0.2272	0.0059	0.0335	0.0003	0.32	0.0509	0.0012	207.9	4.9	212.7	1.74	236.6	53.1
12PSC91-56	0.2492	0.0078	0.0371	0.0003	0.29	0.0491	0.0014	225.9	6.33	234.6	2.11	151	64.8
12PSC91-57	0.2526	0.0071	0.0358	0.0003	0.31	0.0493	0.0012	228.7	5.74	226.8	1.92	164	56.9
12PSC91-58	0.2526	0.0086	0.0362	0.0004	0.31	0.0513	0.0015	228.7	6.93	229.2	2.38	251.9	67.6
12PSC91-59	0.2370	0.0080	0.0357	0.0004	0.30	0.0493	0.0015	216	6.58	226.1	2.26	164	69.7
12PSC91-60	0.2500	0.0067	0.0349	0.0003	0.32	0.0531	0.0013	226.5	5.41	221.1	1.85	334.6	53.1
12PSC91-61	0.2537	0.0190	0.0388	0.0007	0.24	0.0453	0.0032	229.6	15.4	245.2	4.28	0.1	124
12PSC91-62	0.2777	0.0103	0.0390	0.0005	0.33	0.0549	0.0018	248.8	8.16	246.8	2.94	407.1	70.7
12PSC91-63	0.2536	0.0093	0.0357	0.0004	0.31	0.0536	0.0018	229.5	7.52	226	2.56	354.8	71.9
12PSC91-64	0.2403	0.0044	0.0352	0.0002	0.31	0.0503	0.0008	218.7	3.57	222.9	1.27	208.8	36.7
12PSC91-65	0.2732	0.0084	0.0392	0.0004	0.31	0.0522	0.0014	245.2	6.73	248	2.3	293.6	61.3

**Table 3.** Zircon U-Pb laser ablation analytical data for sample 12PSC-97, Tyaughton Formation green sandstone.

Sample no. Analysis ID	Isotopic Ratios						Isotopic Ages						
	$^{207}\text{Pb}/^{235}\text{U}$	$1\sigma$ (abs)	$^{206}\text{Pb}/^{238}\text{U}$	$1\sigma$ (abs)	$\rho$	$^{207}\text{Pb}/^{206}\text{Pb}$	$1\sigma$ (abs)	$^{207}\text{Pb}/^{235}\text{U}$	$1\sigma$ (Ma)	$^{206}\text{Pb}/^{238}\text{U}$	$1\sigma$ (Ma)	$^{207}\text{Pb}/^{206}\text{Pb}$	$1\sigma$ (Ma)
12PSC97-1	0.2372	0.0094	0.0337	0.0004	0.31	0.0492	0.0018	216.1	7.73	213.7	2.6	158.8	81.5
12PSC97-2	0.2241	0.0042	0.0324	0.0002	0.31	0.0486	0.0008	205.3	3.51	205.6	1.2	126	39.5
12PSC97-3	0.2412	0.0120	0.0340	0.0006	0.33	0.0527	0.0023	219.4	9.84	215.5	3.52	314.9	97.4
12PSC97-4	0.2322	0.0056	0.0330	0.0003	0.32	0.0491	0.0011	212	4.58	209.3	1.57	150.3	49.2
12PSC97-5	0.2607	0.0142	0.0355	0.0006	0.30	0.0540	0.0027	235.2	11.4	224.8	3.59	369	106
12PSC97-6	0.2363	0.0081	0.0342	0.0003	0.29	0.0505	0.0016	215.3	6.64	216.8	2.13	216.1	70.8
12PSC97-7	0.2400	0.0057	0.0339	0.0003	0.31	0.0505	0.0011	218.4	4.66	214.8	1.57	216.8	48.5
12PSC97-8	0.2507	0.0078	0.0344	0.0004	0.33	0.0528	0.0015	227.1	6.36	218	2.18	319.9	61.8
12PSC97-9	0.2478	0.0082	0.0342	0.0003	0.30	0.0500	0.0015	224.8	6.67	216.8	2.1	195.4	68.1
12PSC97-10	0.2465	0.0078	0.0349	0.0003	0.30	0.0504	0.0015	223.8	6.39	221.1	2.06	212.2	65.7
12PSC97-12	0.2447	0.0084	0.0356	0.0004	0.29	0.0493	0.0015	222.2	6.83	225.6	2.21	161.4	70.9
12PSC97-13	0.2385	0.0050	0.0345	0.0002	0.32	0.0508	0.0010	217.2	4.11	218.8	1.41	231.4	43
12PSC97-14	0.2385	0.0180	0.0339	0.0007	0.26	0.0537	0.0039	217.2	14.8	215.2	4.24	358	154
12PSC97-15	0.2474	0.0047	0.0353	0.0002	0.33	0.0526	0.0009	224.5	3.84	223.7	1.36	312.3	37.9
12PSC97-16	0.2410	0.0070	0.0343	0.0003	0.31	0.0515	0.0013	219.2	5.71	217.6	1.92	261.4	58.5
12PSC97-17	0.2406	0.0101	0.0353	0.0004	0.30	0.0507	0.0020	218.9	8.23	223.4	2.72	225.3	86.4
12PSC97-18	0.2381	0.0060	0.0344	0.0003	0.31	0.0502	0.0011	216.9	4.88	217.9	1.68	203.7	50.9
12PSC97-19	0.2358	0.0052	0.0347	0.0003	0.33	0.0505	0.0010	215	4.26	220.1	1.54	217.1	44.7
12PSC97-20	0.2597	0.0079	0.0372	0.0004	0.32	0.0519	0.0014	234.4	6.4	235.6	2.22	280.6	60.7
12PSC97-21	0.2442	0.0060	0.0351	0.0003	0.31	0.0505	0.0011	221.9	4.88	222.3	1.65	218.7	49.8
12PSC97-22	0.2334	0.0037	0.0330	0.0002	0.32	0.0507	0.0007	213	3.07	209.3	1.06	225.1	32.4
12PSC97-23	0.2438	0.0050	0.0346	0.0002	0.32	0.0524	0.0010	221.5	4.1	219.2	1.45	304.5	41.1
12PSC97-24	0.2295	0.0086	0.0329	0.0004	0.32	0.0503	0.0017	209.8	7.11	208.7	2.51	207	75.6
12PSC97-25	0.2347	0.0046	0.0341	0.0002	0.33	0.0511	0.0009	214.1	3.81	216.2	1.36	246	40
12PSC97-26	0.2367	0.0066	0.0335	0.0003	0.31	0.0508	0.0013	215.7	5.38	212.3	1.78	230.8	56.7
12PSC97-27	0.2263	0.0118	0.0324	0.0005	0.32	0.0480	0.0022	207.2	9.73	205.7	3.37	98	107
12PSC97-28	0.2316	0.0037	0.0329	0.0002	0.32	0.0511	0.0007	211.5	3.09	208.5	1.09	245.5	32.7
12PSC97-29	0.2487	0.0117	0.0356	0.0005	0.32	0.0495	0.0021	225.5	9.49	225.7	3.3	173.2	93.7
12PSC97-30	0.2356	0.0090	0.0338	0.0004	0.31	0.0512	0.0018	214.8	7.38	214.2	2.48	249.6	77.2
12PSC97-31	0.2446	0.0157	0.0351	0.0007	0.29	0.0500	0.0029	222.2	12.8	222.4	4.13	194.4	129
12PSC97-32	0.2321	0.0155	0.0336	0.0007	0.33	0.0516	0.0031	211.9	12.8	212.9	4.6	265.5	131
12PSC97-33	0.2358	0.0101	0.0341	0.0005	0.31	0.0481	0.0018	214.9	8.25	216.1	2.82	102.7	87.2
12PSC97-34	0.2284	0.0064	0.0334	0.0003	0.32	0.0488	0.0012	208.9	5.3	211.6	1.88	137.1	57.5
12PSC97-35a	0.2487	0.0057	0.0347	0.0003	0.31	0.0508	0.0010	225.5	4.64	219.8	1.57	230.1	46.3
12PSC97-36	0.2493	0.0062	0.0347	0.0003	0.31	0.0505	0.0011	226	5.02	220	1.66	216.9	50
12PSC97-37	0.2419	0.0127	0.0344	0.0006	0.32	0.0499	0.0023	220	10.4	217.9	3.63	188.1	104
12PSC97-38	0.2395	0.0078	0.0337	0.0003	0.28	0.0498	0.0015	218	6.35	213.4	1.95	184.7	67.2
12PSC97-39a	0.2399	0.0074	0.0336	0.0003	0.33	0.0520	0.0014	218.4	6.06	212.8	2.13	284.8	61
12PSC97-40	0.2455	0.0065	0.0348	0.0003	0.31	0.0505	0.0012	222.9	5.27	220.3	1.76	218.2	53.4
12PSC97-41	0.2447	0.0093	0.0347	0.0004	0.32	0.0494	0.0017	222.3	7.61	219.6	2.63	164.8	76.6
12PSC97-42	0.2316	0.0094	0.0338	0.0004	0.31	0.0494	0.0018	211.5	7.75	214	2.68	166.5	82.5
12PSC97-43	0.2425	0.0065	0.0329	0.0003	0.33	0.0523	0.0012	220.4	5.3	208.9	1.78	298.2	52.9
12PSC97-44	0.2380	0.0095	0.0339	0.0004	0.31	0.0506	0.0018	216.7	7.8	214.8	2.59	223.6	81
12PSC97-45	0.2548	0.0122	0.0345	0.0005	0.31	0.0516	0.0022	230.4	9.85	218.6	3.19	265.3	94.7
12PSC97-46	0.2570	0.0083	0.0366	0.0004	0.32	0.0530	0.0015	232.3	6.7	231.7	2.39	330.5	63
12PSC97-47	0.2520	0.0098	0.0376	0.0005	0.31	0.0490	0.0017	228.2	7.97	237.7	2.8	149.1	78.9
12PSC97-48	0.2506	0.0074	0.0355	0.0003	0.31	0.0526	0.0014	227	6	224.8	1.97	312.6	59
12PSC97-49	0.2494	0.0071	0.0347	0.0003	0.30	0.0522	0.0013	226.1	5.77	220.2	1.88	294.4	57
12PSC97-50	0.2358	0.0053	0.0333	0.0002	0.31	0.0510	0.0010	215	4.32	211.2	1.46	239.4	45
12PSC97-51	0.2518	0.0069	0.0359	0.0003	0.32	0.0506	0.0012	228	5.56	227.6	1.91	221.1	54.5
12PSC97-52	0.2370	0.0223	0.0370	0.0011	0.32	0.0511	0.0043	215.9	18.3	234.4	6.86	244.8	183
12PSC97-53	0.2415	0.0055	0.0332	0.0002	0.32	0.0520	0.0010	219.6	4.47	210.5	1.48	284.8	45.3
12PSC97-54	0.2556	0.0124	0.0346	0.0006	0.33	0.0515	0.0022	231.1	10	219.5	3.44	263.8	93.8
12PSC97-55	0.2480	0.0209	0.0353	0.0010	0.32	0.0508	0.0038	225	17	223.4	5.91	232.3	163
12PSC97-56	0.2613	0.0092	0.0352	0.0004	0.28	0.0518	0.0015	235.7	7.39	223.2	2.19	274.7	66.6
12PSC97-57	0.2495	0.0065	0.0364	0.0003	0.30	0.0498	0.0012	226.1	5.31	230.6	1.81	184	52.9
12PSC97-58	0.2380	0.0061	0.0351	0.0003	0.30	0.0497	0.0011	216.8	4.99	222.2	1.7	181.8	52.2
12PSC97-59	0.2352	0.0059	0.0351	0.0003	0.31	0.0482	0.0011	214.4	4.87	222.2	1.71	111.2	51.8
12PSC97-60	0.2505	0.0086	0.0351	0.0004	0.32	0.0522	0.0016	227	6.98	222.2	2.46	294.8	67.4
12PSC97-61	0.2391	0.0054	0.0345	0.0002	0.31	0.0505	0.0010	217.7	4.43	218.4	1.5	219.3	45.8
12PSC97-62	0.2416	0.0038	0.0357	0.0002	0.32	0.0511	0.0007	219.8	3.08	226.1	1.13	243.9	30.7
12PSC97-63	0.2469	0.0084	0.0357	0.0004	0.30	0.0504	0.0015	224.1	6.86	226.4	2.26	211.3	69.6
12PSC97-64	0.2237	0.0046	0.0333	0.0002	0.31	0.0493	0.0009	205	3.79	211.1	1.34	163.3	41.8
12PSC97-65	0.2444	0.0050	0.0337	0.0002	0.32	0.0520	0.0009	222.1	4.08	213.7	1.39	285.5	40.3

**Table 4.** Zircon U-Pb laser ablation analytical data for sample 12PSC-98, Hurley Formation sandstone.

Sample no. Analysis ID	Isotopic Ratios					Isotopic Ages							
	$^{207}\text{Pb}/^{235}\text{U}$	$1\sigma$ (abs)	$^{206}\text{Pb}/^{238}\text{U}$	$1\sigma$ (abs)	$\rho$	$^{207}\text{Pb}/^{206}\text{Pb}$	$1\sigma$ (abs)	$^{207}\text{Pb}/^{235}\text{U}$	$1\sigma$ (Ma)	$^{206}\text{Pb}/^{238}\text{U}$	$1\sigma$ (Ma)	$^{207}\text{Pb}/^{206}\text{Pb}$	$1\sigma$ (Ma)
12PSC98-2	0.2523	0.0079	0.0376	0.0004	0.31	0.0495	0.0014	228.5	6.4	237.9	2.28	173.2	64.1
12PSC98-3	0.2470	0.0145	0.0350	0.0006	0.30	0.0502	0.0027	224.1	11.8	221.9	3.89	204.6	119
12PSC98-4	0.2601	0.0086	0.0354	0.0004	0.34	0.0536	0.0016	234.7	6.89	224.2	2.43	355.4	64.2
12PSC98-5	0.2463	0.0061	0.0352	0.0003	0.30	0.0508	0.0012	223.6	4.99	222.8	1.63	231.6	51.6
12PSC98-6	0.2389	0.0048	0.0344	0.0002	0.30	0.0499	0.0009	217.5	3.94	218	1.34	191.1	41.9
12PSC98-7	0.2512	0.0062	0.0353	0.0003	0.32	0.0521	0.0012	227.5	5.05	223.4	1.75	287.7	50.2
12PSC98-8	0.2292	0.0070	0.0332	0.0003	0.30	0.0503	0.0014	209.5	5.75	210.6	1.88	206.5	63.7
12PSC98-9	0.2485	0.0087	0.0343	0.0004	0.32	0.0516	0.0016	225.4	7.08	217.6	2.45	266.6	70
12PSC98-10	0.2451	0.0060	0.0344	0.0003	0.31	0.0502	0.0011	222.6	4.87	218.2	1.59	204.4	50.7
12PSC98-11	0.2503	0.0097	0.0354	0.0004	0.32	0.0519	0.0018	226.8	7.85	224.1	2.73	279.2	77.4
12PSC98-12	0.2409	0.0057	0.0349	0.0003	0.31	0.0503	0.0011	219.2	4.62	221.2	1.58	207.3	48.7
12PSC98-13	0.2427	0.0058	0.0341	0.0003	0.31	0.0502	0.0011	220.6	4.73	215.9	1.57	202.5	49.2
12PSC98-14	0.2383	0.0056	0.0335	0.0002	0.29	0.0482	0.0010	217	4.57	212.5	1.45	111.2	49.4
12PSC98-15	0.2428	0.0057	0.0339	0.0002	0.30	0.0498	0.0011	220.7	4.62	215	1.51	185.1	48.5
12PSC98-16	0.2423	0.0076	0.0338	0.0003	0.30	0.0482	0.0014	220.3	6.24	214.4	1.99	110	66
12PSC98-17	0.2333	0.0084	0.0331	0.0004	0.32	0.0513	0.0017	212.9	6.89	210	2.35	255	73.5
12PSC98-18	0.2474	0.0049	0.0345	0.0002	0.32	0.0499	0.0009	224.5	4.01	218.4	1.34	191.9	41.1
12PSC98-19	0.2514	0.0063	0.0346	0.0003	0.31	0.0526	0.0012	227.7	5.07	218.9	1.66	312.7	50.4
12PSC98-20	0.2341	0.0071	0.0335	0.0003	0.29	0.0494	0.0014	213.6	5.82	212.5	1.82	168.4	63.7
12PSC98-21	0.2478	0.0061	0.0341	0.0003	0.32	0.0492	0.0011	224.8	4.94	216	1.68	157	50.1
12PSC98-22	0.2526	0.0078	0.0349	0.0004	0.33	0.0522	0.0014	228.7	6.32	220.9	2.17	295.3	61.6
12PSC98-23	0.2466	0.0116	0.0347	0.0005	0.33	0.0521	0.0022	223.8	9.42	219.8	3.36	289.4	92.8
12PSC98-24	0.2501	0.0060	0.0343	0.0003	0.30	0.0503	0.0011	226.6	4.89	217.1	1.57	207.7	49.8
12PSC98-25	0.2495	0.0043	0.0345	0.0002	0.32	0.0514	0.0008	226.1	3.52	218.3	1.2	257.8	35.4
12PSC98-26	0.2472	0.0048	0.0354	0.0002	0.32	0.0516	0.0009	224.3	3.87	224.2	1.4	269.7	38.9
12PSC98-27	0.2573	0.0116	0.0350	0.0005	0.32	0.0534	0.0022	232.5	9.36	222	3.15	343.8	88.4
12PSC98-28	0.2396	0.0062	0.0357	0.0003	0.30	0.0496	0.0012	218.1	5.09	226	1.75	178	54.1
12PSC98-29	0.2478	0.0164	0.0362	0.0008	0.32	0.0504	0.0030	224.8	13.3	229.3	4.79	213.6	130
12PSC98-30	0.2380	0.0042	0.0350	0.0002	0.32	0.0503	0.0008	216.8	3.48	221.7	1.25	207.3	36.7
12PSC98-31	0.2610	0.0118	0.0367	0.0005	0.31	0.0520	0.0021	235.4	9.51	232.2	3.23	287	90.1
12PSC98-32	0.2606	0.0123	0.0371	0.0006	0.33	0.0526	0.0022	235.2	9.89	234.7	3.57	311.7	92.3
12PSC98-33	0.2446	0.0060	0.0363	0.0003	0.32	0.0512	0.0011	222.1	4.88	229.6	1.76	247.8	50
12PSC98-34	0.2502	0.0056	0.0366	0.0003	0.31	0.0502	0.0010	226.7	4.55	231.6	1.57	202.2	46.2
12PSC98-35	0.2444	0.0067	0.0364	0.0003	0.30	0.0486	0.0012	222	5.44	230.5	1.89	127	56.9
12PSC98-36	0.2478	0.0074	0.0379	0.0003	0.30	0.0491	0.0013	224.8	6.01	239.8	2.13	153	61.8
12PSC98-37	0.2623	0.0223	0.0377	0.0010	0.32	0.0551	0.0042	236.5	17.9	238.7	6.37	416.3	162
12PSC98-38	0.2567	0.0080	0.0379	0.0004	0.30	0.0485	0.0014	232	6.49	239.7	2.18	123.4	65.5
12PSC98-39	0.2578	0.0064	0.0354	0.0003	0.31	0.0506	0.0011	232.9	5.15	224.4	1.7	224.4	50.4
12PSC98-40	0.2535	0.0059	0.0354	0.0003	0.33	0.0518	0.0011	229.4	4.77	224.3	1.66	274.7	46.9
12PSC98-41	0.2477	0.0060	0.0371	0.0003	0.30	0.0493	0.0011	224.7	4.85	234.8	1.69	160	50
12PSC98-42	0.2591	0.0067	0.0378	0.0003	0.32	0.0518	0.0012	233.9	5.41	239.5	1.91	276.3	52.3
12PSC98-43	0.2572	0.0058	0.0364	0.0003	0.33	0.0515	0.0010	232.4	4.72	230.4	1.68	262.4	45.5
12PSC98-44	0.2616	0.0060	0.0363	0.0003	0.32	0.0535	0.0011	235.9	4.84	230	1.68	348.4	45.8
12PSC98-45	0.2350	0.0071	0.0357	0.0004	0.32	0.0515	0.0014	214.3	5.86	225.9	2.19	263.4	61.5
12PSC98-46	0.2434	0.0085	0.0349	0.0004	0.29	0.0506	0.0016	221.2	6.96	221.3	2.22	222.9	72.8
12PSC98-47	0.2577	0.0055	0.0364	0.0003	0.32	0.0508	0.0010	232.8	4.45	230.4	1.55	230.8	43.2
12PSC98-48	0.2384	0.0098	0.0350	0.0004	0.29	0.0510	0.0019	217.1	8	221.6	2.6	240	84.5
12PSC98-49	0.2498	0.0047	0.0346	0.0002	0.32	0.0516	0.0009	226.4	3.85	219.5	1.33	267.1	38.3
12PSC98-50	0.2507	0.0077	0.0352	0.0003	0.31	0.0515	0.0014	227.1	6.24	223.1	2.11	263.9	62.2
12PSC98-51	0.2382	0.0055	0.0352	0.0003	0.32	0.0497	0.0010	217	4.53	223	1.61	180.3	47.9
12PSC98-52	0.2597	0.0084	0.0356	0.0004	0.33	0.0521	0.0015	234.4	6.73	225.7	2.37	291.7	63.2
12PSC98-53	0.2356	0.0185	0.0369	0.0009	0.32	0.0489	0.0035	214.8	15.2	233.6	5.75	144.7	157
12PSC98-54	0.2640	0.0070	0.0356	0.0003	0.33	0.0536	0.0013	237.9	5.6	225.7	1.91	353.4	52.3
12PSC98-55	0.2508	0.0055	0.0359	0.0003	0.32	0.0506	0.0010	227.2	4.46	227.3	1.55	223.2	44.5
12PSC98-58	0.2438	0.0051	0.0364	0.0002	0.32	0.0507	0.0009	221.5	4.13	230.3	1.51	225.8	42.3
12PSC98-59	0.2435	0.0064	0.0352	0.0003	0.34	0.0532	0.0013	221.3	5.22	222.9	1.91	336.7	52.6
12PSC98-60	0.2517	0.0066	0.0363	0.0003	0.33	0.0524	0.0012	228	5.35	229.6	1.91	304.5	52.3
12PSC98-61	0.2404	0.0164	0.0370	0.0008	0.32	0.0486	0.0030	218.7	13.4	234.2	4.98	126.1	138
12PSC98-62	0.2334	0.0116	0.0337	0.0005	0.32	0.0503	0.0023	213	9.55	213.6	3.35	209.3	100
12PSC98-63	0.2471	0.0044	0.0368	0.0002	0.34	0.0502	0.0008	224.2	3.57	233	1.34	203.3	36
12PSC98-64	0.2521	0.0069	0.0367	0.0003	0.32	0.0525	0.0013	228.3	5.55	232	2.02	308.4	54.2
12PSC98-65	0.2453	0.0108	0.0348	0.0005	0.31	0.0516	0.0021	222.8	8.84	220.6	3.01	266.9	88.7



**Fig. 11.** Pebbly sandstone, Hurley Formation, near sample site 12PSC-98.

in addition to Late Triassic detrital zircons, a predominant population of Late Permian to Middle Triassic zircons not seen in the younger sample from the Tyaughton Formation (12PSC-97) or in the sample from the Hurley Formation (12PSC-98). This population of zircons is inferred to have been derived from the Wineglass assemblage and/or related rocks that form the older component of Cadwallader terrane in this region. The oldest zircons in this population are the same age as the dated volcanic and plutonic rocks of the Wineglass assemblage, and it is suspected that the Lower and Middle Triassic grains are from younger, eroded and/or covered components of the assemblage. A Late Permian to Middle Triassic age range thus inferred for the Wineglass assemblage is consistent with its correlation with the Sitlika volcanic unit and the Kutcho assemblage (Schiarizza, 2013), because each of these units contains volcanic and intrusive rocks with an age range from Late Permian to Middle Triassic (Fig. 15 of Schiarizza, 2013).

**5.1. Tyaughton Creek facies of Cadwallader terrane**

Cadwallader terrane in south-central British Columbia comprises Late Permian to Middle Jurassic rocks that are exposed in numerous small and large outcrop belts that have been dispersed by major dextral strike-slip faults of the Yalakom and Fraser systems, and are commonly separated from one another by large areas of younger rock (Fig. 13). The terrane was originally defined for exposures near Gold Bridge (Fig. 13; Rusmore et al., 1988) where it includes two distinct stratigraphic successions, referred to as the Camelsfoot facies and the Tyaughton Creek facies (Schiarizza et al., 1997). Both of these facies also occur in the other major outcrop belts of Cadwallader terrane, near Tatlayoko and Chilko lakes, and along the lower reaches of the Chilcotin River (Fig. 13). Their original paleogeographic relationship is unknown, although the Camelsfoot facies most commonly occurs west of the Tyaughton Creek facies. The Camelsfoot facies consists of the Cadwallader Group, including Middle to Late Triassic basalt of

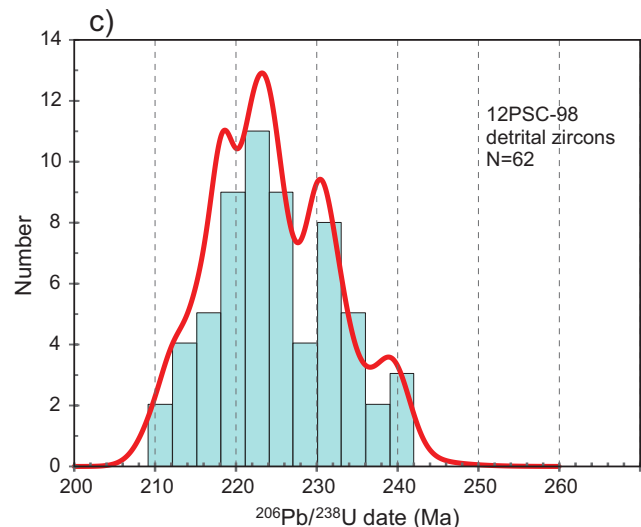
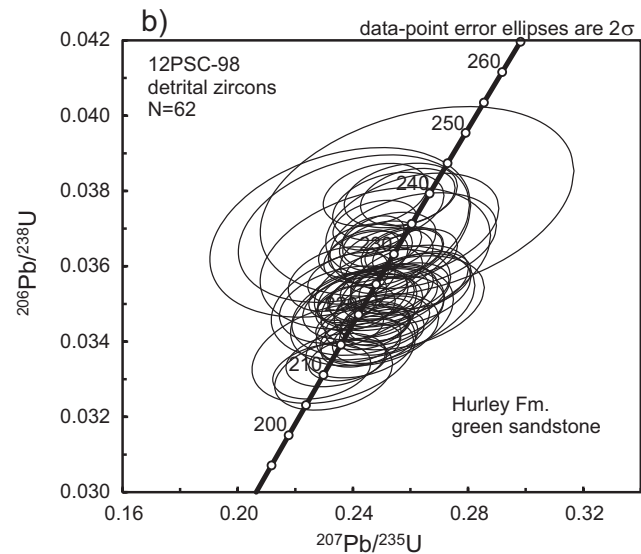
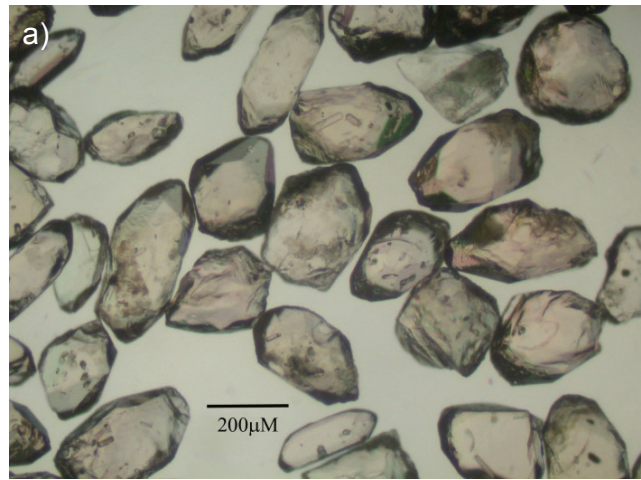


**Fig. 12.** U-Pb data for detrital zircons from sample 12PSC-98. **a)** Photomicrograph of zircons. **b)** Concordia plot of all grains. **c)** Histogram of detrital zircon ages and superimposed probability density curve.

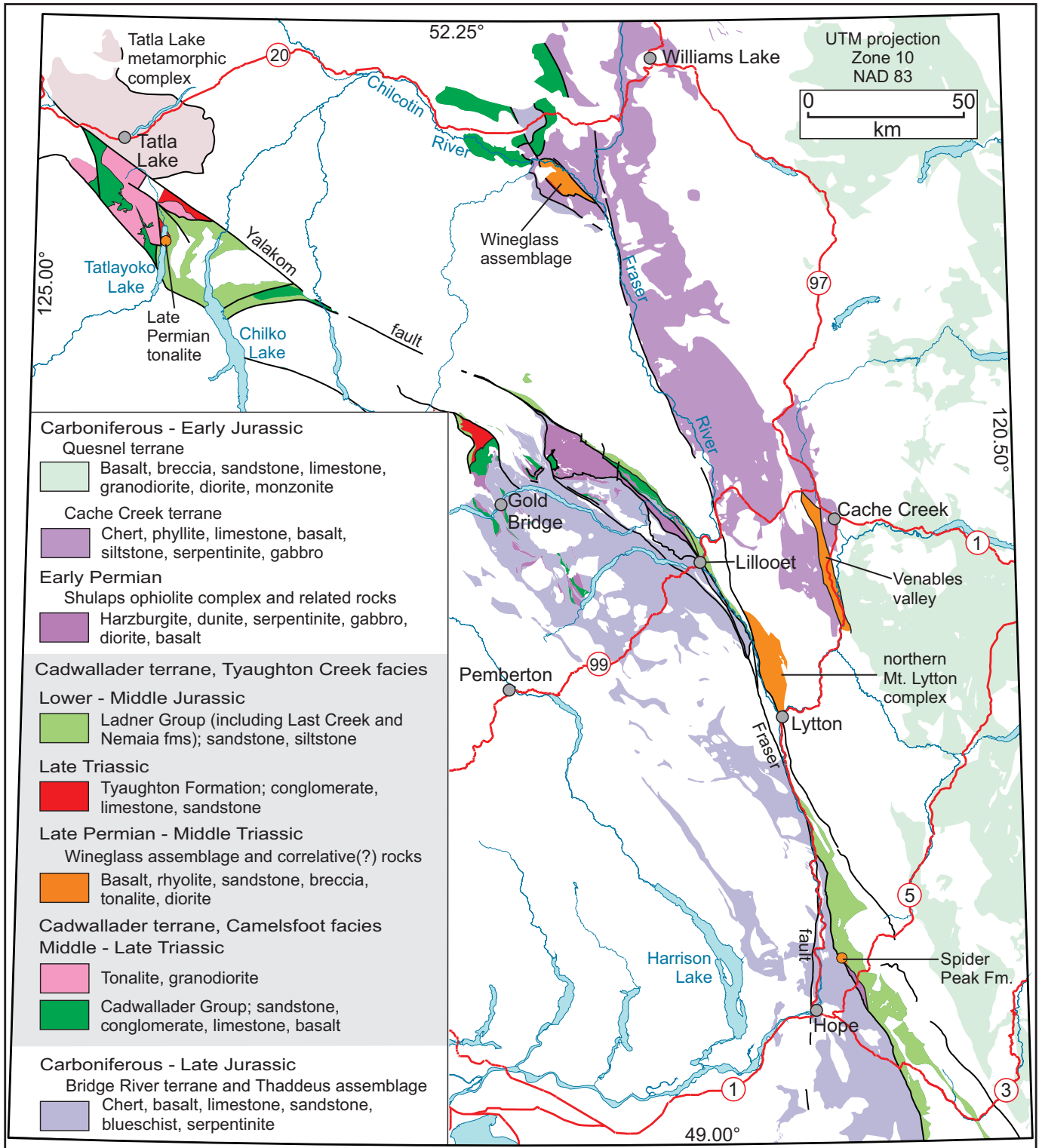


**Fig. 13.** Map of south-central British Columbia highlighting Cadwallader terrane and adjacent Paleozoic to mid-Mesozoic terranes. Geology from Cui et al. (2017). Uncoloured areas are mainly younger rocks, including Late Jurassic to Cretaceous siliciclastic rocks of the Tyaughton-Methow basin and Late Jurassic to Eocene granitoid intrusions.

the Pioneer Formation and overlying Late Triassic (Carnian to Norian) sandstone, conglomerate and limestone of the Hurley Formation (Rusmore, 1987). The Tyaughton Creek facies, which includes rocks in the Chilcotin River window, has three components separated by unconformities or disconformities: Late Permian (and younger?) volcanic and intrusive rocks; latest Triassic sedimentary rocks of the Tyaughton Formation; and Early to Middle Jurassic sedimentary rocks (Ladner Group and correlatives).

The lower part of the Tyaughton Creek facies is represented by basalt, rhyolite and tonalite of the Wineglass assemblage (Late Permian), which underlies the Tyaughton Formation in the Chilcotin River window (Schiarizza, 2013; this study), and also by Late Permian tonalite that underlies the Tyaughton Formation on the east shore of Tatlayoko Lake (Fig. 13; Schiarizza et al., 1995, 2002). It may also be represented by the northern part of the Mount Lytton complex (Fig. 13), which includes Late Permian or Early Triassic tonalite that Friedman and van der Heyden (1992) correlate with the Wineglass pluton, and by basalt of the Spider Peak Formation, which underlies the Ladner Group (upper part of the Tyaughton Creek facies) in a small area north-northeast of Hope (Fig. 13; Ray, 1990).

The middle part of the Tyaughton Creek facies comprises sedimentary rocks of the Tyaughton Formation (Late Triassic). The most complete section of the formation is in its type area, north-northwest of Gold Bridge (Fig. 13), where it includes a lower unit of red conglomerates and sandstones, ('Lower red beds' of Umhoefer, 1990) a middle unit of massive and bedded limestones ('Massive limestone' and 'Monotis limestone' of Umhoefer, 1990), and an upper unit of green sandstones, pebble conglomerates and calcarenites ('Lower green clastics', 'Cassianella beds', and 'Upper green clastics' of Umhoefer, 1990). Conglomerates in the lower unit contain clasts of felsic to mafic volcanic rock, limestone, and granitoid plutonic rock. The middle and upper units, dated with macrofossils, are late Norian and Rhaetian (Tozer, 1979; Umhoefer, 1990; Umhoefer and Tipper, 1998). The base of the Tyaughton Formation does not occur in its type area, but the formation also occurs 120 km to the northwest (Umhoefer and Tipper, 1998), where exposures at the north end of Tatlayoko Lake rest nonconformably above Late Permian tonalite (Fig. 13; Schiarizza et al., 1995, 2002). Likewise, the Tyaughton Formation in the Chilcotin River window, correlated with the lower and upper units of the type area (limestone unit missing), rests unconformably above Permian volcanic rocks of the Wineglass assemblage.

The upper part of the Tyaughton Creek facies comprises Lower to Middle Jurassic sedimentary rocks, mainly grey siltstones and sandstones, with local pebble conglomerates. North of Gold Bridge they are represented by upper Hettangian to Middle Bajocian rocks of the Last Creek Formation, which overlie the Tyaughton Formation disconformably (Umhoefer, 1990; Umhoefer and Tipper, 1998). Correlative rocks to the northwest, near Tatlayoko and Chilko lakes (Fig. 13), are assigned to the Nemaia Formation (Sinemurian to Bajocian; Umhoefer and Tipper, 1998; Schiarizza et al., 2002), which

apparently overlies the Tyaughton Formation near the north end of Tatlayoko Lake, although the contact is not exposed. The Nemaia Formation can be traced southeastward, with significant dextral offsets along the Yalakom and Fraser faults, into identical rocks of the Lower to Middle Jurassic Ladner Group, which forms a linear belt extending from near Lytton to the international boundary (Fig. 13; Mahoney, 1993; Schiarizza et al., 1997). The base of the Ladner Group is exposed locally northeast of Hope where it rests unconformably above basalts of the Spider Peak Formation (Ray, 1990), which may belong in the lower part of the Tyaughton Creek facies. The middle part, the Tyaughton Formation, is apparently missing, although it may be present as polymictic conglomerates, up to 70 m thick, that occur at the Spider Peak-Ladner contact (Ray, 1990).

## 5.2. Cadwallader terrane correlatives in central and northern British Columbia

Schiarizza (2013) correlated the Wineglass assemblage with the volcanic unit of the Sitlika assemblage in central British Columbia and the Kutcho assemblage in northern British Columbia (Fig. 14). These units have traditionally been included in Cache Creek terrane, although Mihalynuk et al. (2017) suggest they should be treated as a separate terrane. Schiarizza (2013) included the Wineglass assemblage in Cadwallader terrane, implying that the correlative rocks in central and northern British Columbia are also part of Cadwallader terrane. Here, we support this terrane assignment by pointing out that the rocks that overlie both the volcanic unit of the Sitlika assemblage and the Kutcho assemblage are very similar to the middle and upper parts of the Tyaughton Creek facies (Tyaughton Formation and Ladner Group) in southern British Columbia.

In central British Columbia the Wineglass-correlative Sitlika volcanic unit is unconformably(?) overlain by siliciclastic rocks and limestones of the Sitlika clastic unit, which is best exposed in a continuous belt, almost 100 km long, east of the volcanic unit (Figs. 14, 15; Schiarizza, 2000; Schiarizza et al., 2000). The clastic unit, as described by Schiarizza and Payie (1997) and Schiarizza et al. (1998), consists of sandstone, slate, and siltstone, with less common conglomerate, limestone, and calcarenite. Conglomerate commonly forms the base of the unit, and has a clast composition (mainly felsic volcanic plus limestone, mafic volcanic rock, and granitic rock) very similar to conglomerates in the lower part of the Tyaughton Formation. Limestones are mainly in the lower part of the unit, directly above the basal conglomerate where it is present, and therefore have a stratigraphic position similar to the main limestone occurrences in the Tyaughton Formation. The only biochronologic constraint for the unit comes from conodonts extracted from a calcarenite bed in the central part of the main belt of exposures, which are assigned a late Norian to Rhaetian age (M.J. Orchard in Struik et al., 2007, sample 97-PSC-19-2), showing that it is, at least in part, the same age as the Tyaughton Formation. In addition, a small population of detrital zircons (n=6) analyzed from a sample of sandstone collected from the

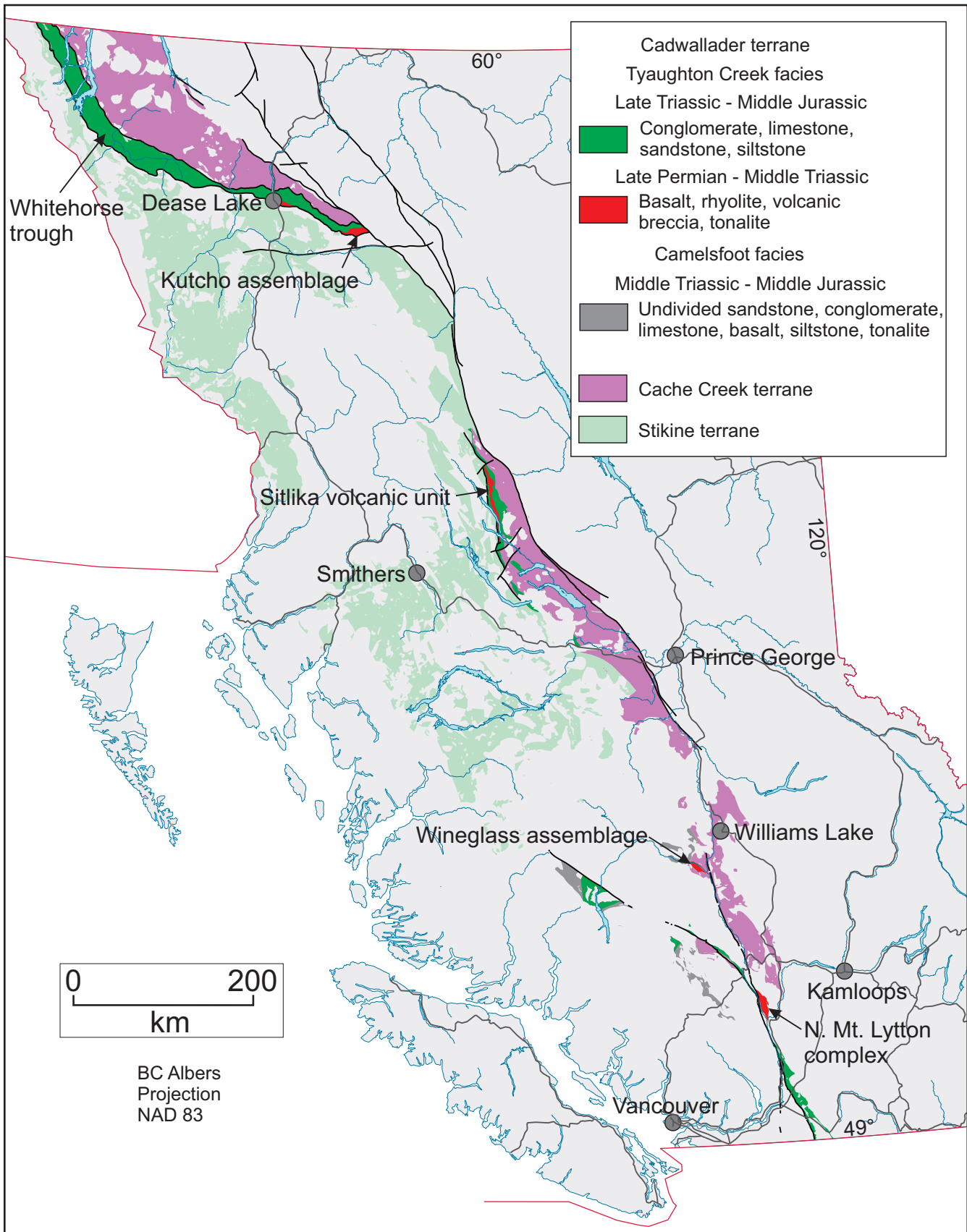


**Fig. 14.** Map highlighting Permian-Jurassic rocks comprising the Tyauhton Creek facies of Cadwallader terrane in southern British Columbia and correlative rocks in central and northern British Columbia. Geology from Cui et al. (2017).

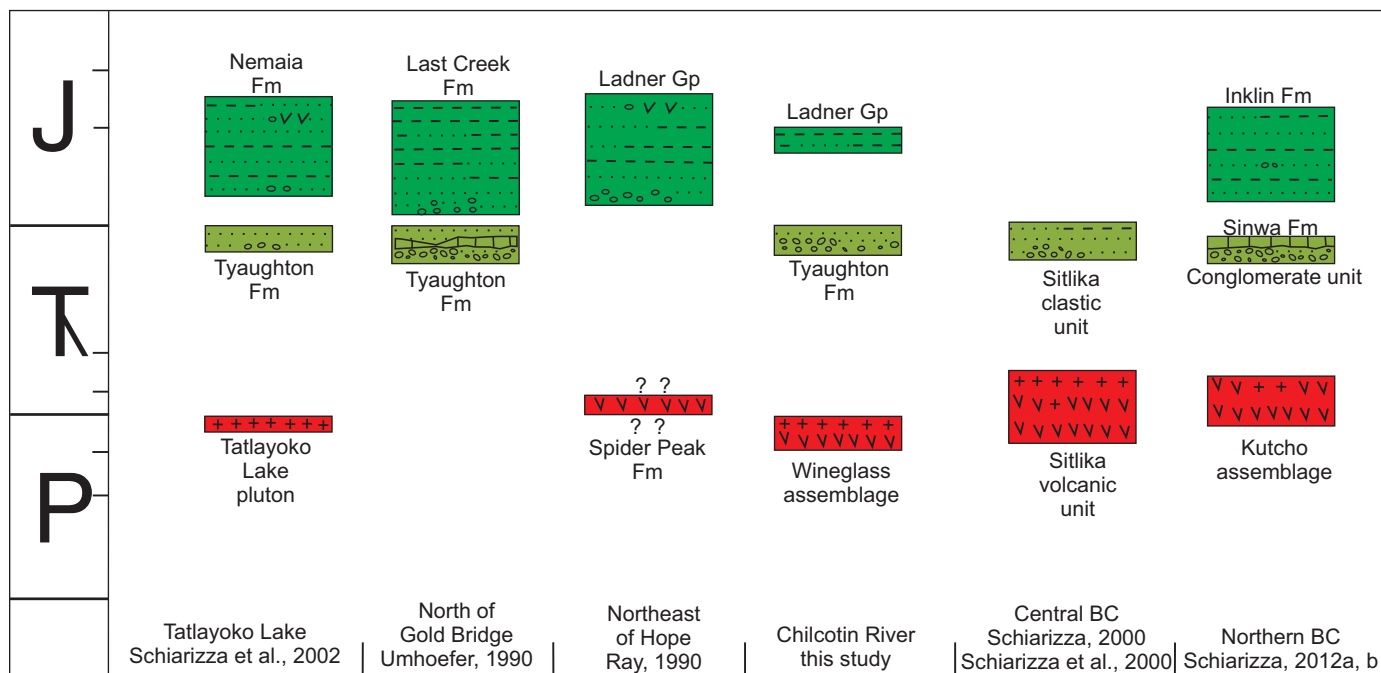


**Fig. 15.** Schematic stratigraphic sections for the Tyaughton Creek facies of Cadwallader terrane in southern British Columbia, and correlative rocks in central and northern British Columbia.

northern part of the main exposure belt contained only Late Triassic grains ranging from 226 to 201.7 Ma (M. Villeneuve, in Struik et al., 2007, sample 97-PSC-22). Despite the very small sample size this is very similar to the age range of detrital zircons from the upper part of the Tyaughton Formation in the Chilcotin River window (Fig. 10).

In northern British Columbia, the Kutcho assemblage is in a narrow belt of mainly Lower to Middle Jurassic siliciclastic rocks (Whitehorse trough, represented by the Inklin Formation) that forms the boundary between the main exposures of Cache Creek terrane to the northeast and Stikine terrane to the southwest (Fig. 14). The Kutcho assemblage is best exposed at the east end of the belt, adjacent to Kutcho Creek where it and overlying rocks were mapped by Schiarizza (2012a, b). Here, the Kutcho assemblage is unconformably overlain by upper Triassic rocks herein correlated with the Tyaughton Formation, which are in turn unconformably or disconformably overlain by Lower Jurassic siliciclastic rocks of the Inklin Formation, herein correlated with the Ladner Group (Fig. 15). The upper Triassic rocks include a lower conglomerate unit (with clasts of felsic volcanic rock, mafic volcanic rock, limestone and tonalite) and overlying massive to well-bedded limestone (Sinwa Formation) which together are very similar to the lower and middle parts of the Tyaughton Formation in its type area. The Sinwa limestone is not dated at Kutcho Creek, but exposures 180 km west-northwest of Dease Lake, near the type area of the formation, contain the ammonoid *Halorites* cf. *H. americanus* Hyatt and Smith and the bivalve *Monotis subcircularis* Gabb (E.T. Tozer in Souther, 1971), both of which characterize the Late Norian fauna of the *Monotis* limestone member of the Tyaughton Formation (Umhoefer and

Tipper, 1978). The Inklin Formation in the Kutcho Creek area comprises metasandstone, metasiltstone, and slate, with local intercalations of pebble conglomerate and rare narrow lenses of limestone (Schiarizza, 2012a). It typically overlies the Sinwa Formation but in places, where the Sinwa and conglomerate unit are missing, it is directly above the Kutcho assemblage. No fossils have been extracted from the formation in this area, but detrital zircons from the base of the formation at one locality indicate an Early Jurassic maximum depositional age (Schiarizza, 2012b), and rocks included in, or correlated with, the formation to the northwest contain Early and early Middle Jurassic fossils (Mihalynuk, 1999; Colpron, 2011). The Inklin Formation is correlated with the Ladner Group on the basis of lithology, inferred Early to Middle Jurassic age, and unconformable or disconformable relationship with underlying rocks correlated with the Tyaughton Formation.

The Inklin Formation forms a continuous narrow belt, deformed by southwest-verging folds and thrust faults, that extends from Kutcho Creek to the northern border of British Columbia (Fig. 14; Christie, 1957; Aitken, 1959; Souther, 1971; Gabrielse, 1988; Mihalynuk, 1999), and from there into southern Yukon where it is mapped as the Richthofen Formation of the Laberge Group (Colpron, 2011). The Richthofen Formation, like the Inklin Formation and Ladner Group, is predominantly lithic sandstone, siltstone and mudstone, and it contains fossils ranging from early Sinemurian to Aalenian (Colpron, 2011), very similar to the fossil ages from the Ladner Group and correlatives in southern British Columbia (Tipper and Umhoefer, 1998). The Richthofen Formation, in southern Yukon, is underlain by the Aksala Formation (Late Triassic), which comprises three members (Colpron, 2011): Mandanna

member, mainly maroon to red weathering sandstone and polymictic conglomerate; Hancock member, mainly massive to thick bedded limestone, dated at many localities as late Norian; and Casca member, mudstone, siltstone and calcareous sandstone, with interbedded bioclastic limestone and igneous or limestone-clast conglomerate. This stratigraphy is remarkably similar to that of the Tyaughton Formation in its type area (Umhoefer, 1990; Umhoefer and Tipper, 1998); a similarity that is even more pronounced when the overlying Jurassic rocks are also compared. The Aksala Formation is part of the Lewes River Group, a Triassic arc-derived succession in Yukon that is typically considered part of Stikine terrane (Colpron, 2011). The correlations proposed here (Aksala with Tyaughton, Richthofen with Ladner) suggest that the Lewes River Group might, at least in part, be part of Cadwallader terrane.

## 6. Summary

Along the Chilcotin River, 50 km southwest of Williams Lake, late Paleozoic and Mesozoic rocks of Cadwallader terrane are exposed in a structural window beneath overthrust Cache Creek terrane. These Cadwallader terrane rocks include Late Permian volcanic and plutonic rocks of the Wineglass assemblage, unconformably overlying sandstones and conglomerates correlated with the Tyaughton Formation (latest Triassic) and Early to Middle Jurassic siltstones and sandstones assigned to the Ladner Group. Rhyolite from the top of the Wineglass assemblage, dated by U-Pb zircon chemical abrasion thermal ionization mass spectrometry (CA-TIMS), crystallized at  $260.8 \pm 0.3$  Ma, confirming a Late Permian age reported by Read (1993). Detrital zircons from red sandstone in the lower part of the Tyaughton Formation, dated by Laser Ablation Inductively Coupled Plasma Mass Spectrometry (LA-ICP-MS), include a population of mainly Late Permian to Middle Triassic grains (260.7 to 237.1 Ma), probably derived from the underlying Wineglass assemblage, and a population of Late Triassic grains (234.6 to 212.7 Ma) inferred to have been derived from Late Triassic volcanic and plutonic rocks exposed elsewhere in Cadwallader terrane. Detrital zircons were also analyzed from a sample of green sandstone in the upper part of the Tyaughton Formation, yielding only Late Triassic grains (237.7 to 205.6 Ma). The youngest zircons from the two samples indicate middle to late Norian and late Norian to Rhaetian maximum depositional ages, respectively, corroborating their correlation with the lower and upper parts of the Tyaughton Formation in its type area.

The Hurley Formation (Late Triassic, Carnian to Norian), a common component of Cadwallader terrane in southern British Columbia, occurs in two fault panels northwest of the Chilcotin River window. Detrital zircons from a Hurley sandstone sample, collected from the Bald Mountain fault panel, comprise latest Middle Triassic to Late Triassic grains (239.8 to 210 Ma) with a range very similar to that of the upper Tyaughton sample (green sandstone), and to the Late Triassic population of the lower Tyaughton sample (red sandstone). These similarities support the interpretation that the Hurley Formation and the

Tyaughton Formation are different parts of the same terrane. The predominance of Late Triassic grains also supports the long-held view that the Late Triassic siliciclastic rocks of Cadwallader terrane (Hurley and Tyaughton formations) were sourced from an associated Late Triassic magmatic arc (Rusmore et al., 1988).

The rocks exposed in the Chilcotin River window are part of a Late Permian to Middle Jurassic succession (Tyaughton Creek facies) that forms a significant part of Cadwallader terrane, but differs from other parts (Camelsfoot facies) comprised mainly of the Cadwallader Group, including Middle to Late Triassic basalts of the Pioneer Formation, and overlying Late Triassic sandstones, conglomerates, and limestones of the Hurley Formation. The Permian to Jurassic rocks of the Tyaughton Creek facies correlate with rocks in central British Columbia (Sitlika assemblage) and northern British Columbia (Kutcho assemblage, Sinwa Formation, Inklin Formation).

## Acknowledgments

Robin Chu assisted with fieldwork and the collection of samples for U-Pb dating. Lawrence Aspler (British Columbia Geological Survey) and Jeffery Chiarenzelli (St. Lawrence University) reviewed the paper and offered suggestions that improved it.

## References cited

- Aitken, J.D., 1959. Atlin map-area, British Columbia. Geological Survey of Canada, Memoir 307, 89 p.
- Christie, R.L., 1957. Bennett, Cassiar District, British Columbia. Geological Survey of Canada, Map 19-1957; scale 1:253,440.
- Colpron, M., 2011. Geological compilation of Whitehorse trough-Whitehorse (105D), Lake Laberge (105E), and part of Carmacks (115I), Glenlyon (105L), Aishihik Lake (115H), Quiet Lake (105F), and Teslin (105C). Yukon Geological Survey, Geoscience Map 2011-1; scale 1:250,000.
- Cordey, F., and Read, P.B., 1992. Permian and Triassic radiolarian ages from the Cache Creek Complex, Dog Creek and Alkali Lake areas, southwestern British Columbia. In: Current Research, Part E, Geological Survey of Canada Paper 92-1E, pp. 41-51.
- Crowley, J.L., Schoene, B., and Bowring, S.A., 2007. U-Pb dating of zircon in the Bishop Tuff at the millennial scale. *Geology*, 35, 1123-1126.
- Cui, Y., Miller, D., Schiarizza, P., and Diakow, L.J., 2017. British Columbia digital geology. British Columbia Ministry of Energy, Mines and Petroleum Resources, British Columbia Geological Survey Open File 2017-8, 9 p.
- Friedman, R.M., and van der Heyden, P., 1992. Late Permian U-Pb dates for the Farwell and northern Mt. Lytton plutonic bodies, Intermontane Belt, British Columbia. In: Current Research, Part A, Geological Survey of Canada Paper 92-1A, pp. 137-144.
- Gabrielse, H., 1998. Geology of Cry Lake and Dease Lake map areas, north-central British Columbia. Geological Survey of Canada, Bulletin 504, 147 p.
- Gerstenberger, H., and Haase, G., 1997. A highly effective emitter substance for mass spectrometric Pb isotopic ratio determinations. *Chemical Geology*, 136, 309-312.
- Griffin, W.L., Powell, W.J., Pearson, N.J., and O'Reilly, S.Y., 2008. Glitter: Data reduction software for laser ablation ICP-MS. In: Sylvester, P.J., (Ed.), *Laser Ablation ICP-MS in the Earth Sciences: Current Practices and Outstanding Issues*, Mineralogical Association of Canada, Short Course 40, pp. 308-311.

- Hickson, C.J., 1990. A new Frontier Geoscience Project: Chilcotin-Nechako region, central British Columbia. In: Current Research, Part F, Geological Survey of Canada Paper 90-1F, pp. 115-120.
- Jaffey, A.H., Flynn, K.F., Glendenin, L.E., Bentley, W.C., and Essling, A.M., 1971. Precision measurement of half-lives and specific activities of  $^{235}\text{U}$  and  $^{238}\text{U}$ . *Physics Review*, C4, 1889-1906.
- Ludwig, K.R., 2003. Isoplot 3.09-A geochronological toolkit for Microsoft Excel. Berkley Geochronology Center, The University of California at Berkeley, Special Publication No. 4.
- Mahoney, J.B., 1993. Facies reconstructions in the Lower to Middle Jurassic Ladner Group, southern British Columbia. In: Current Research, Part A, Geological Survey of Canada Paper 93-1A, pp. 173-182.
- Mahoney, J.B., Hickson, C.J., Haggart, J.W., Schiarizza, P., Read, P.B., Enkin, R.J., van der Heyden, P., and Israel, S., 2013. Geology, Taseko Lakes, British Columbia. Geological Survey of Canada, Open File 6150; scale 1:250,000.
- Mattinson, J.M., 2005. Zircon U-Pb chemical abrasion ("CA-TIMS") method: Combined annealing and multi-step partial dissolution analysis for improved precision and accuracy of zircon ages. *Chemical Geology*, 220, 47-66.
- Mihalynuk, M.G., 1999. Geology and mineral resources of the Tagish Lake area (NTS 104M/8, 9, 10E, 15 and 104N/12W) northwestern British Columbia. British Columbia Ministry of Energy and Mines, British Columbia Geological Survey Bulletin 105, 217 p.
- Mihalynuk, M.G., and Harker, L.L., 2007. Riske Creek Geology (92O/16W). British Columbia Ministry of Energy, Mines and Petroleum Resources, British Columbia Geological Survey Open File 2007-6; scale 1:50,000.
- Mihalynuk, M.G., Zagorevski, A., English, J.M., Orchard, M.J., Bidgood, A.K., Joyce, N., and Friedman, R.M., 2017. Geology of the Sinwa Creek area, northwest BC (104K/14). In: Geological Fieldwork 2016, British Columbia Ministry of Energy and Mines, British Columbia Geological Survey Paper 2017-1, pp. 153-178.
- Mundil, R., Ludwig, K.R., Metcalfe, I., and Renne, P.R., 2004. Age and timing of the Permian Mass Extinctions: U/Pb Dating of Closed-System Zircons. *Science*, 305, 1760-1763.
- Ray, G.E., 1990. The geology and mineralization of the Coquihalla gold belt and Hozameen fault system, southwestern British Columbia. British Columbia Ministry of Energy, Mines and Petroleum Resources, British Columbia Geological Survey Bulletin 79, 97 p.
- Read, P.B., 1992. Geology of parts of Riske Creek and Alkali Lake areas, British Columbia. In Current Research, Part A, Geological Survey of Canada Paper 92-1A, pp. 105-112.
- Read, P.B., 1993. Geology of northeast Taseko Lakes map area, southwestern British Columbia. In: Current Research, Part A, Geological Survey of Canada Paper 93-1A, pp. 159-166.
- Rusmore, M.E., 1987. Geology of the Cadwallader Group and the Intermontane-Insular superterrane boundary, southwestern British Columbia. *Canadian Journal of Earth Sciences*, 24, 2279-2291.
- Rusmore, M.E., and Woodsworth, G.J., 1991. Distribution and tectonic significance of Upper Triassic terranes in the eastern Coast Mountains and adjacent Intermontane Belt, British Columbia. *Canadian Journal of Earth Sciences*, 28, 532-541.
- Rusmore, M.E., Potter, C.J., and Umhoefer, P.J., 1988. Middle Jurassic terrane accretion along the western edge of the Intermontane superterrane, southwestern British Columbia. *Geology*, 16, 891-894.
- Schiarizza, P., 2000. Bedrock geology, Old Hogem (western part) (93N/11, 12, 13). British Columbia Ministry of Energy and Mines, British Columbia Geological Survey Open File 2000-33; scale 1:100,000.
- Schiarizza, P., 2012a. Geology of the Kutcho assemblage between the Kehlechoa and Tucho rivers, northern British Columbia (NTS 104I/01, 02). In: Geological Fieldwork 2011, British Columbia Ministry of Energy and Mines, British Columbia Geological Survey Paper 2012-1, pp. 75-98.
- Schiarizza, P., 2012b. Bedrock geology of the upper Kutcho Creek area, parts of NTS 104I/01, 02. British Columbia Ministry of Energy and Mines, British Columbia Geological Survey, Open File 2012-08; scale 1:40,000. Also published as Geological Survey of Canada, Open File 7234.
- Schiarizza, P., 2013. The Wineglass assemblage, lower Chilcotin River, south-central British Columbia: Late Permian volcanic and plutonic rocks that correlate with the Kutcho assemblage of northern British Columbia. In: Geological Fieldwork 2012, British Columbia Ministry of Energy, Mines and Natural Gas, British Columbia Geological Survey Paper 2013-1, pp. 53-70.
- Schiarizza, P., and Payie, G., 1997. Geology of the Sitlika assemblage in the Kenny Creek-Mount Olson area (93N/12, 13), central British Columbia. In: Geological Fieldwork 1996, British Columbia Ministry of Employment and Investment, British Columbia Geological Survey Paper 1997-1, pp. 79-100.
- Schiarizza, P., Melville, D.M., Riddell, J., Jennings, B.K., Umhoefer, P.J., and Robinson, M.J., 1995. Geology and mineral occurrences of the Tatlayoko Lake map area (92N/8, 9 and 10). In: Geological Fieldwork 1994, British Columbia Ministry of Energy, Mines and Petroleum Resources, British Columbia Geological Survey Paper 1995-1, pp. 297-320.
- Schiarizza, P., Gaba, R.G., Glover, J.K., Garver, J.I., and Umhoefer, P.J., 1997. Geology and mineral occurrences of the Taseko-Bridge River area. British Columbia Ministry of Employment and Investment, British Columbia Geological Survey Bulletin 100, 291 p.
- Schiarizza, P., Massey, N., and MacIntyre, D., 1998. Geology of the Sitlika assemblage in the Takla Lake area (93N/3, 4, 5, 6, 12), central British Columbia. In: Geological Fieldwork 1997, British Columbia Ministry of Employment and Investment, British Columbia Geological Survey Paper 1998-1, pp. 4-1 - 4-19.
- Schiarizza, P., Massey, N., and MacIntyre, D.M., 2000. Bedrock geology, Tsayta Lake (93N/3, 4, 5, 6). British Columbia Ministry of Energy and Mines, British Columbia Geological Survey Open File 2000-19; scale 1:100,000.
- Schiarizza, P., Riddell, J., Gaba, R.G., Melville, D.M., Umhoefer, P.J., Robinson, M.J., Jennings, B.K., and Hick, D., 2002. Geology of the Beece Creek-Niut Mountain area, British Columbia (NTS 92N/8, 9, 10; 92O/5, 6, 12). British Columbia Ministry of Energy and Mines, British Columbia Geological Survey Geoscience Map 2002-3; scale 1:100,000.
- Schmitz, M.D., and Schoene, B., 2007. Derivation of isotope ratios, errors, and error correlations for U-Pb geochronology using  $^{205}\text{Pb}$ - $^{235}\text{U}$ -( $^{233}\text{U}$ )-spiked isotope dilution thermal ionization mass spectrometric data. *Geochemistry, Geophysics, Geosystems*, 8, Q08006, doi:10.1029/2006GC001492.
- Schoene, B.A., Crowley, J.L., Condon, D.J., Schmitz, M.D., and Bowring, S.A., 2006. Reassessing the uranium decay constants for geochronology using ID-TIMS U-Pb data. *Geochimica et Cosmochimica Acta*, 70, 426-445.
- Scoates, J.S., and Friedman, R.M., 2008. Precise age of the platinumiferous Merensky Reef, Bushveld Complex, South Africa, by the U-Pb zircon chemical abrasion ID-TIMS technique. *Economic Geology*, 103, 465-471.
- Sláma, J., Košler, J., Condon, D.J., Crowley, J.L., Gerdes, A., Hanchar, J.M., Horstwood, M.S.A., Morris, G.A., Nasdala, L., Norberg, N., Schaltegger, U., Xchoene, B., Tubrett, M.N., and Whitehouse, M.J., 2007. Plešovice zircon-A new natural reference material for U-Pb and Hf isotopic microanalysis. *Chemical Geology*, 249, 1-35.
- Souther, J.G., 1971. Geology and mineral deposits of Tulsequah map-area, British Columbia. Geological Survey of Canada, Memoir 362, 84 p.

- Stacey, J.S., and Kramers, J.D., 1975. Approximation of terrestrial lead isotopic evolution by a two-stage model. *Earth and Planetary Science Letters*, 26, 207-221.
- Struik, L.C., MacIntyre, D.G., and Williams, S.P., 2007. Nechako NATMAP project: a digital suite of geoscience information for central British Columbia (NTS map sheets 093N, 093K, 093F, 093G/W, 093L/9, 16, and 093M/1, 2, 7, 8). British Columbia Ministry of Energy, Mines and Petroleum Resources, British Columbia Geological Survey Open File 2007-10. Also published as Geological Survey of Canada, Open File 5623.
- Tafti, R., Mortensen, J.K., Lang, J.R., Rebagliati, M., and Oliver, J.L., 2009. Jurassic U-Pb and Re-Os ages for newly discovered Xietongmen Cu-Au porphyry district, Tibet: Implications for metallogenic epochs in the southern Gangdese Belt. *Economic Geology*, 104, 127-136.
- Thirlwall, M.F., 2000. Inter-laboratory and other errors in Pb isotope analyses investigated using a  $^{207}\text{Pb}$ - $^{204}\text{Pb}$  double spike. *Chemical Geology*, 163, 299-322.
- Tipper, H.W., 1978. Taseko Lakes (92O) map area. Geological Survey of Canada Open File 534; scale 1:125,000.
- Tozer, E.T., (1979). Latest Triassic ammonoid faunas and biochronology, western Canada. In: *Current Research, Part B*, Geological Survey of Canada Paper 79-1B, pp. 127-135.
- Umhoefer, P.J., 1990. Stratigraphy and tectonic setting of the upper part of the Cadwallader terrane, southwestern British Columbia. *Canadian Journal of Earth Sciences*, 27, 702-711.
- Umhoefer, P.J., and Tipper, H.W., 1998. Stratigraphy, depositional environment, and tectonic setting of the Upper Triassic to Middle Jurassic rocks of the Chilcotin Ranges, southwestern British Columbia. *Geological Survey of Canada Bulletin* 519, 58 p.

# British Columbia Geological Survey Sample Archive: An emerging resource for public geoscience



Alexei S. Rukhlov<sup>1, a</sup>, Ben Coats<sup>1</sup>, Jackie Van der Vlugt<sup>1</sup>, Isabelle J. Beaupre-Olsen<sup>1</sup>, and Katya Zaborniak<sup>1</sup>

<sup>1</sup>British Columbia Geological Survey, Ministry of Energy, Mines and Low Carbon Innovation, Victoria, BC, V8W 9N3

<sup>a</sup>corresponding author: Alexei.Rukhlov@gov.bc.ca

Recommended citation: Rukhlov, A.S., Coats, B., Van der Vlugt, J., Beaupre-Olsen, I.J., and Zaborniak, K., 2023. British Columbia Geological Survey Sample Archive: An emerging resource for public geoscience. In: *Geological Fieldwork 2022*, British Columbia Ministry of Energy, Mines and Low Carbon Innovation, British Columbia Geological Survey Paper 2023-01, pp. 85-90.

## Abstract

The British Columbia Geological Survey (BCGS) Sample Archive is home to rock, mineral, and geochemical samples collected from across the province in the last several decades by BCGS staff and partner organizations. These collections represent a valuable resource for public geoscience, supporting quality control of published data, re-analysis using modern comprehensive and high-precision analytical methods, and new geoscience initiatives. Following a notice to vacate the historic BCGS storage facility at 254 Belleville Street in downtown Victoria, a systematic sorting, rationalizing, and cataloguing of archived samples was undertaken in anticipation of moving the collection to a new site at 1810 Blanshard Street, Victoria. We have catalogued about 30,000 rock and 91,000 geochemical samples thus far. This inventory includes about 25,400 sediment samples from modern drainages collected as part of the Uranium Reconnaissance and Regional Geochemical Survey programs since 1976. Work will continue to make the Archive a modern and reliable resource supporting Cordilleran geoscience with enhanced and accessible digital cataloging.

**Keywords:** Archived sample, hand specimen, drill core, pulp, sediment, till, sieved fraction, heavy mineral concentrate (HMC), indicator mineral, mineralization, MINFILE, Regional Geochemical Survey (RGS), Uranium Reconnaissance Program (URP)

## 1. Introduction

The British Columbia Geological Survey (BCGS) Sample Archive is home to rock, mineral, and geochemical samples collected by BCGS staff and partner geoscience organizations from many locations throughout the province in the last several decades. These samples include rock or sediment pulps, coarsely crushed rock, bulk sediment and sieved fractions, and heavy mineral concentrates and other mineral separates. Some samples come from reclaimed mines or from sites no longer accessible due to flooding, landslides, or land use status (Ramdeen, 2015). Others may require significant resources to re-sample. Catalogued and georeferenced, a physical sample library represents a valuable resource for public geoscience. The archived samples supply material for quality control of published data by replicate analysis, for re-analysis using new, more comprehensive and precise analytical methods, and for new geoscience initiatives.

Geological surveys routinely re-analyze archived samples using modern methods to test for a wider range of analytes with lower detection limits and improved precision (e.g., McMartin et al., 2008; Werdon et al., 2014; Golding et al., 2016). The Uranium Reconnaissance Program and later Regional Geochemical Surveys (RGS) systematically collected modern drainage sediments (stream- and lake-bottom and moss-trapped) and water from across the province since 1976. Early analyses determined concentrations of a few metals in the <0.177 mm fraction of sediments by flame atomic absorption

spectrometry (AAS) following a Lefort aqua regia digestion. Uranium determinations were by instrumental neutron activation analysis (INAA) and delayed neutron counting (e.g., Ballantyne et al., 1977). Most of the archived RGS samples (tens of thousands) stored mainly at the Geological Survey of Canada in Ottawa and at BCGS Sample Archive in Victoria have been reanalyzed using multi-element techniques such as modified aqua regia digestion with a combination of inductively coupled plasma atomic emission spectroscopy (ICP-AES) and inductively coupled plasma mass spectrometry (ICP-MS), and INAA (see Lett and Rukhlov, 2017 for an overview). BCGS archive samples have been also extensively used in multidisciplinary studies (e.g., Lett and Jackaman, 2002; Canil and Lacourse, 2011; Mao et al., 2016, 2017; van Geffen and Bluemel, 2017; Johnson and Goldblatt, 2018; Simandl et al., 2021; Paradis et al., 2022a, b; Van der Vlugt et al., 2022).

For almost ten years, the BCGS Sample Archive was housed in the heritage 'Stores Building' (ca. 1912) at 254 Belleville Street in downtown Victoria (Fig. 1). Following notice to vacate this facility, we undertook a systematic sorting, rationalizing, and cataloguing of archived samples in anticipation of moving the collection to the Ministry building at 1810 Blanshard Street. This paper reports our progress updating the Archive activities, highlights key examples where archived materials were used in geoscience initiatives, and describes our next steps in creating digital resources for the Archive to support future research.



**Fig. 1.** Heritage 'Stores Building' (ca. 1912) at 254 Belleville Street, Victoria.

## 2. Archive materials

The BCGS Sample Archive comprises a physical library of rock, mineral, and solid geochemical samples. Rock samples include raw hand specimens, sawn slabs, drill core, and thin sections. Collected mainly during mapping projects, the samples are representative of rock units, alteration, and mineralization and provide a physical record of past studies that can be referred to many years after the original work. The samples also support other Ministry initiatives such as prospector training. Individually catalogued rock samples are stored in indexed banks (Fig. 2).

Geochemical materials include pulverized rock or sediment, coarsely crushed rock, bulk sediment (stream, lake, moss-trapped, till, soil) and sieved fractions, heavy mineral concentrates and other mineral separates, and vegetation (Fig. 3). The mass of archived bulk samples such as till is typically up to 2 kg, whereas the upper mass limit for processed sample media such as pulp and various fractions is 200 g. In contrast to rock samples, a catalogue of archived geochemical materials captures sequences of unique, five-digit laboratory identifiers (ID) or other sample identifiers along with the corresponding archive box, type of sample media, and other sample metadata (Fig. 4). Sample identifiers are traceable to records in a publicly available source such as a government report or online databases.

## 3. Ongoing activities and current archive inventory

Recognizing the value of the archived samples for future initiatives and the need to accommodate new samples, a decision was made to consolidate the BCGS laboratory facilities and Sample Archive to one site in the basement of the Ministry building at 1810 Blanshard Street. The initial stage of the project involved designing, permitting, and constructing the new facility. To facilitate the move, which has been completed, and improve the Archive, we undertook a systematic rationalizing of samples housed at the heritage 'Stores Building' on Belleville Street. This work included removing waste such as plastic bags, disposing compromised, unlabelled, or redundant materials, sorting materials into indexed cabinets (rocks) or boxes (geochemical samples),



**Fig. 2.** Indexed banks of rock samples at the BCGS Sample Archive.

splitting oversized samples, and logging sample identifiers and other available metadata (Fig. 5). At the time this report was prepared, we have catalogued 29,698 rock samples, 862 bulk till samples, and about 91,000 geochemical samples contained in 1634 catalogued boxes. The latter inventory includes about 25,400 samples (<0.18 mm and >0.18 mm fractions of stream, lake, and moss-trapped sediment) collected by the Regional Geochemical Survey program since 1976 (Fig. 6).

## 4. Examples of using BCGS Sample Archive

Drainage geochemical surveys are rapid and efficient for prospecting large areas for mineral resources. However, lake sediment, till, and vegetation are more commonly sampled in low-relief regions with extensive transported overburden. Starting in 1976, government-managed uranium and regional



**Fig. 3.** Examples of pulverized rock samples (pulps) at the BCGS Sample Archive. A unique, five-digit laboratory identifier (ID) links the original sample ID, analytical, and other metadata captured in the provincial rock litho-geochemistry database. A geochemical sample catalogue captures sequences of sample IDs per tray, along with the corresponding archive box number, type of sample medium, and other sample metadata.

geochemical programs collected drainage sediment samples in British Columbia. Typically, hundreds to ca. 1500 samples were collected per 1:250,000-scale map sheet. As analytical methods evolved over time from relatively simple colorimetry and AAS to multi-element techniques (INAA, ICP-AES, and ICP-MS), most of the archived RGS and till samples have been re-analyzed (Lett and Rukhlov, 2017 and references therein).

Lett and Jackaman (2002) examined the platinum geochemical response in different drainage sample media, supplementing new surveys with archived RGS samples from different parts of the province. Re-analysis of archived materials revealed new Au anomalies in the McBride and Prince George areas. Canil and Lacourse (2011) re-analyzed Archive till samples to estimate the composition of juvenile upper continental crust in the Cordillera of British Columbia, and Johnson and Goldblatt (2018) re-analyzed till samples for ammonium, which was used as a proxy for the nitrogen content of the upper continental crust to model the cycling of nitrogen in the Earth system.

Mao et al. (2016) used archived rock samples representing different mineral deposit types and unmineralized rocks to



**Fig. 4.** Shelving racks of indexed boxes storing geochemical materials at the BCGS Sample Archive.

investigate apatite trace-element compositions (Fig. 7). Based on electron probe microanalysis (EPMA), laser ablation (LA)-ICP-MS, and multivariate statistics, they demonstrated that apatite compositions can be used to identify different types of mineral deposits. Follow-up orientation studies by Rukhlov et al. (2016) and Mao et al. (2017) applied the discriminant approach to apatite grains recovered from archived till samples both down-ice from known mineral occurrences and in underexplored ‘greenfield’ areas with little or no known mineralization in central British Columbia. Detrital apatite grains in till down-ice from known mineral deposits were correctly identified by the discriminant method. The work by Mao et al. (2017) study also helped generate new exploration targets in greenfield areas lacking known mineralization or hosting only minor mineral occurrences. These studies validated the apatite discriminant method and demonstrated its usefulness as a practical exploration tool in grassroots programs. Simandl et al. (2021) and Paradis et al. (2022a, b) studied archived samples of carbonate-hosted sulfide deposits in B.C.

Recently, Van der Vlugt et al. (2022) retrieved a suite of about 1000 archived samples, predominantly Triassic to Jurassic igneous rocks but including a range from Devonian to Quaternary, mainly from Stikine terrane in northwestern

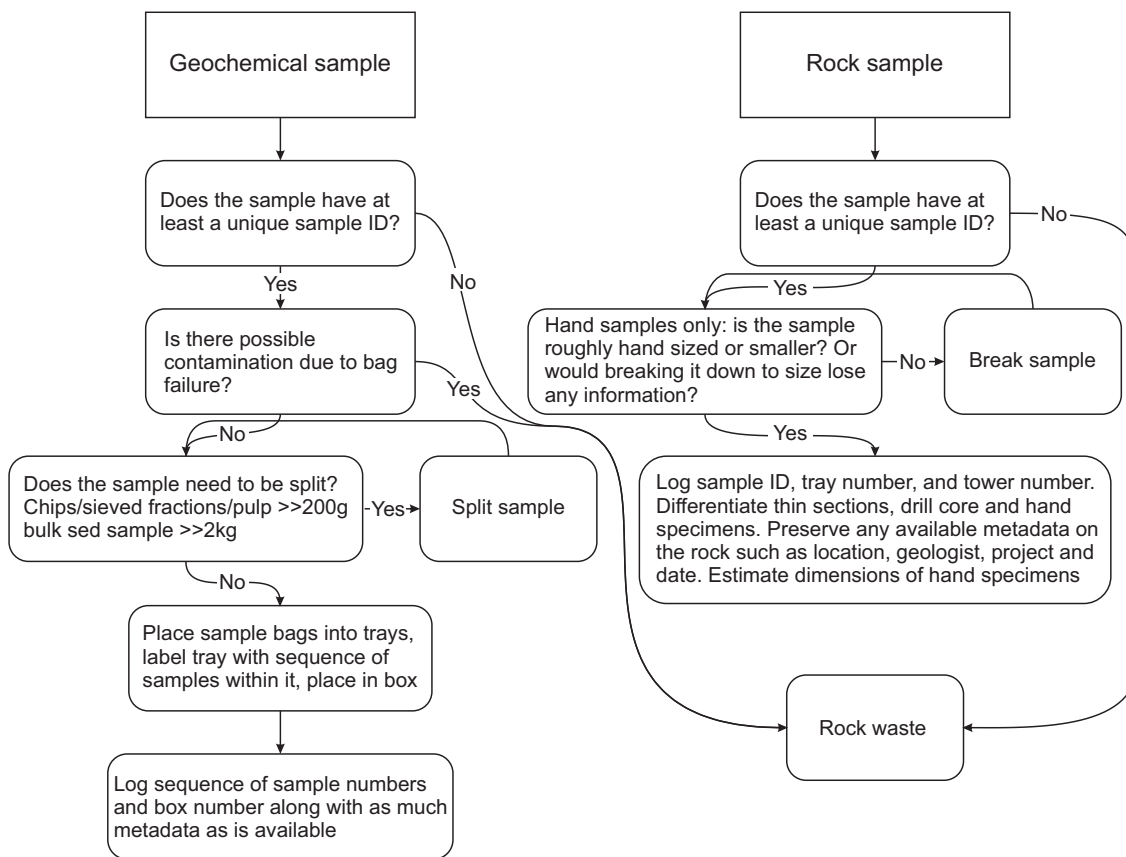


Fig. 5. Flow chart for sorting samples of the BCGS Sample Archive.

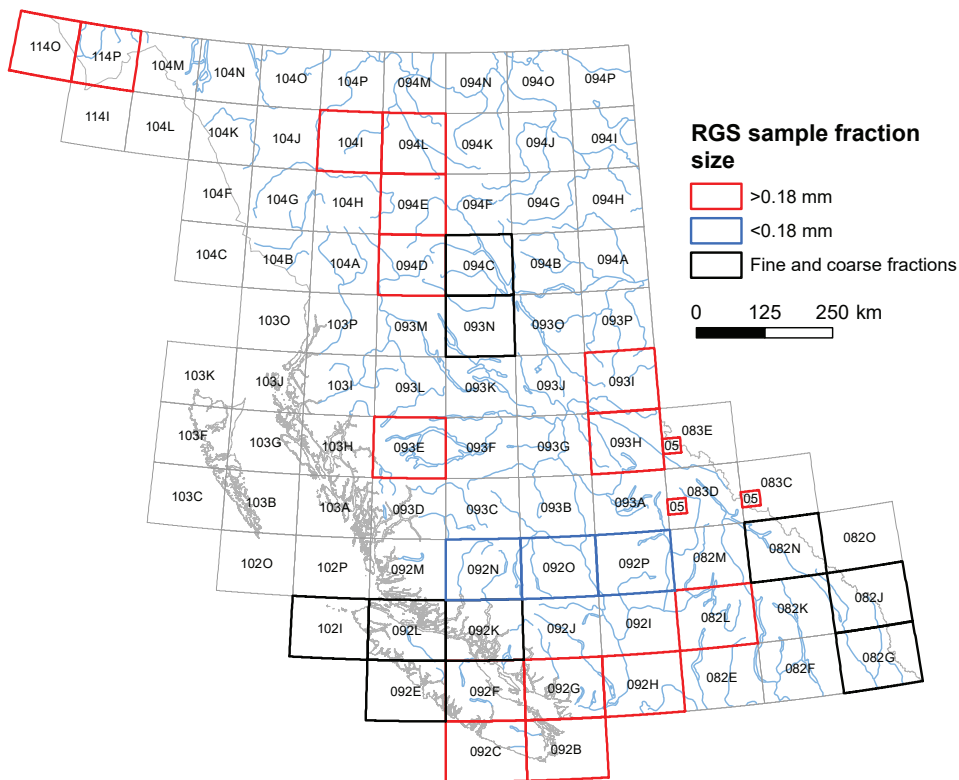


Fig. 6. Footprint of Regional Geochemical Surveys (RGS) with materials available in the BCGS Sample Archive.

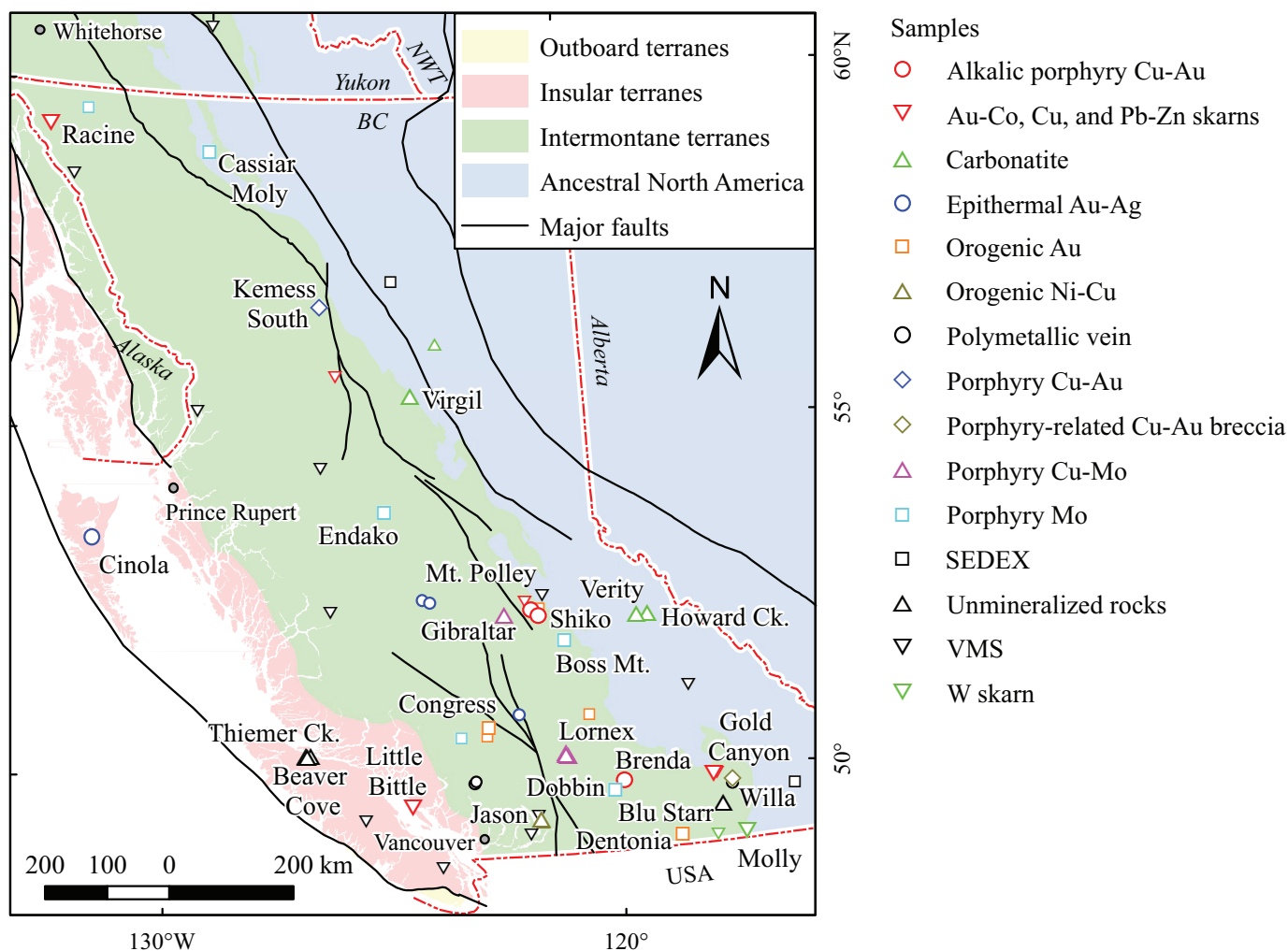


Fig. 7. Sample location map from Mao et al. (2016). Larger symbols represent samples that yielded apatites investigated.

British Columbia. Financially supported by Newcrest Mining Ltd., re-analysis of these samples involved determinations for up to 60 analytes using four-acid digestion with a combination of ICP-AES and ICP-MS for ultra-low minimum detection limits. In addition, about 500 samples that lacked modern ‘total’ determinations were re-analyzed for 56 analytes using lithium-borate fusion with ICP-AES or ICP-MS finish with ultra-low minimum detection limits, and for loss on ignition. Rigorous QA/QC of the new data was achieved using 87 blind quality controls. The study also developed a new, comprehensive metadata structure that captured full bedrock geological unit and sample information from the original sources.

### 5. Next steps and conclusion

The BCGS Sample Archive is the most comprehensive collection of geological samples in the province. Following the initial cataloguing of the archived materials, this project further aims to integrate the digital inventory with other provincial datasets such as litho geochemistry, geochronology, rock

physical properties, MINFILE, archived Ministry laboratory records, and BC Digital Geology in an interoperable database environment. Linked via sample identifiers, querying these datasets will facilitate efficient retrieval of archived materials suitable for specific studies. New protocols will set specific requirements and procedures to archive new samples and to access BCGS archived materials.

The digital database for the Archive, to be integrated with the MapPlace interface, will capture material availability, type (e.g., hand specimen, pulp, specific fraction, indicator minerals), indexed storage box or tray, and images (field and indoor photographs, 3D, hyperspectral, UV-light, transmitted- and reflected-light photomicrographs, X-ray maps, cathodoluminescence, back-scatter electron) for a given georeferenced location. Additional sample attributes populated from related datasets will include measured properties (e.g., assay results, absolute age), preparation and analytical methods, sample and rock unit descriptions, published source(s), and other metadata.

## Acknowledgments

We thank Purple Rock Inc. for cataloguing and photographing more than 1650 rock samples that were previously part of the Mineral Development Office collection and that represent many mineral occurrences in the province. We also thank Nicole Barlow and James Barlow (Purple Rock Inc.) and Luke Ootes (British Columbia Geological Survey) for discussions of future steps to transform the rock inventory into a useful geoscience resource. Summer students Shannon Murtonen and Cameron Fielding provided help as we rationalized the Archive. We appreciate review and comments by Lawrence B. Aspler (British Columbia Geological Survey).

## References cited

- Ballantyne, S.B., Hornbrook, E.H.W., and Lynch, J.J., 1977. National geochemical reconnaissance release NGR 5-76 regional stream sediment-water geochemical reconnaissance data southeastern BC (NTS 82/E), Geological Survey of Canada Open File 409, 13 maps, 1:250,000 scale.
- Canil, D., and Lacourse, T., 2011. An estimate for the bulk composition of juvenile upper continental crust derived from glacial till in the North American Cordillera. *Chemical Geology* 284, 229-239.
- Golding, M.L., Orchard, M.J., and Zagorevski, A., 2016. Microfossils from the Cache Creek Complex in northern British Columbia and southern Yukon. Geological Survey of Canada, Open File 8033, 25 p. <<https://doi.org/10.4095/298696>>
- Johnson, B., and Goldblatt, C., 2018. EarthN: A new Earth system nitrogen model. *Geochemistry, Geophysics, Geosystems* 19, 2516-2542. <<https://doi.org/10.1029/2017GC007392>>
- Lett, R.E., and Jackaman, W., 2002. PGE stream sediment geochemistry in British Columbia. In: Geological Fieldwork 2001, British Columbia Ministry of Energy and Mines, British Columbia Geological Survey Paper 2002-01, pp. 365-376.
- Lett, R., and Rukhlov, A.S., 2018. A review of analytical methods for regional geochemical survey (RGS) programs in the Canadian Cordillera. In: Ferbey, T., Plouffe, A., and Hickin, A.S., (Eds.), Indicator Minerals in Till and Stream Sediments of the Canadian Cordillera. Geological Association of Canada Special Paper Volume 50, and Mineralogical Association of Canada Topics in Mineral Sciences Volume 47, pp. 53-108.
- Mao, M., Rukhlov, A.S., Rowins, S.M., Spence, J., and Coogan, L.A., 2016. Apatite trace element compositions: A robust new tool for mineral exploration. *Economic Geology* 111, 1187-1222.
- Mao, M., Rukhlov, A.S., Rowins, S.M., Hickin, A.S., Ferbey, T., Bustard, A., Spence, J., and Coogan, L.A., 2017. A novel approach using detrital apatite and till geochemistry to identify covered mineralization in the TREK area of the Nechako Plateau, British Columbia. In: Ferbey, T., Plouffe, A., and Hickin, A.S., (Eds.), Indicator Minerals in Till and Stream Sediments of the Canadian Cordillera. Geological Association of Canada Special Paper Volume 50, and Mineralogical Association of Canada Topics in Mineral Sciences Volume 47, pp. 191-243.
- McMartin, I., Campbell, J.E., and Dredge, L.A., 2008. Till geochemistry from archived samples collected over the La Ronge and Rottenstone domains, central Saskatchewan. Geological Survey of Canada, Open File 5799, and Saskatchewan Ministry of Energy and Resources Open File 2008-1, 30 p.
- Paradis, S., Jackson, S.E., Petts, D., Simandl, G.J., D'Souza, R.J., and Hamilton, T., 2022a. Distribution of trace elements in pyrite from carbonate-hosted sulphide deposits of southern British Columbia, Canada. In: Peter, J.M., and Gadd, M.G., (Eds.), Targeted Geoscience Initiative 5: Volcanic- and Sediment-Hosted Massive Sulphide Deposit Genesis and Ore Systems. Geological Survey of Canada Bulletin 617, pp. 129-163. <<https://doi.org/10.4095/328002>>
- Paradis, S., Simandl, G.J., Drage, N., D'Souza, R.J., Kontak, D.J., and Waller, Z., 2022b. Carbonate-hosted deposits (Mississippi Valley-type, magnesite, and REE-F-Ba) of the southeastern Canadian Cordillera: A review and isotopic data comparison. In: Peter, J.M., and Gadd, M.G., (Eds.), Targeted Geoscience Initiative 5: Volcanic- and Sediment-Hosted Massive Sulphide Deposit Genesis and Ore Systems. Geological Survey of Canada Bulletin 617, pp. 39-87. <<https://doi.org/10.4095/327995>>
- Ramdeen, S., 2015. Preservation challenges for geological data at state geological surveys. *GeoResJ* 6, 213-220. <<https://doi.org/10.1016/j.grj.2015.04.002>>
- Rukhlov, A.S., Plouffe, A., Ferbey, T., Mao, M., and Spence, J., 2016. Application of trace-element compositions of detrital apatite to explore for porphyry deposits in central British Columbia. In: Geological Fieldwork 2015, British Columbia Ministry of Energy and Mines, British Columbia Geological Survey, Paper 2016-1, pp. 145-179.
- Simandl, G.J., D'Souza, R.J., Paradis, S., and Spence, J., 2021. Rare-earth content of carbonate minerals in sediment-hosted Pb-Zn deposits, southern Canadian Rocky Mountains. In: Peter, J.M., and Gadd, M.G., (Eds.), Targeted Geoscience Initiative 5: Volcanic- and Sediment-Hosted Massive Sulphide Deposit Genesis and Ore Systems. Geological Survey of Canada Bulletin 617, pp. 165-201. <<https://doi.org/10.4095/328001>>
- Van der Vlugt, J., Rukhlov, A.S., and van Straaten, B.I., 2022. Lithochemical re-analysis of British Columbia Geological Survey archived rock samples from northwestern British Columbia. British Columbia Ministry of Energy, Mines and Low Carbon Innovation, British Columbia Geological Survey GeoFile 2022-14, 15 p.
- van Geffen, P.W.G., and Bluemel, E.B., 2017. Clay-fraction till geochemistry of the TREK project area, central British Columbia (parts of NTS 093B, C, F, G): Progress report. In: Geoscience BC Summary of Activities 2016, Geoscience BC Report 2017-01, pp. 113-114.
- Werdon, M.B., Azain, J.S., and Granitto, M., 2014. Reanalysis of historical U.S. geological survey sediment samples for geochemical data from the western part of the Wrangellia terrane, Anchorage, Gulkana, Healy, Mt. Hayes, Nabesna, and Talkeetna mountains quadrangles, Alaska. State of Alaska Department of Natural Resources, Division of Geological and Geophysical Surveys, Raw Data File 2014-5. <<https://doi.org/10.14509/27287>>

# British Columbia Geological Survey Publications 2022 including peer-reviewed external papers co-authored by BCGS staff

All BCGS publications are available for download, free of charge, from  
[www.BCGeologicalSurvey.ca](http://www.BCGeologicalSurvey.ca)

To receive notification of our latest releases email  
[Geological.Survey@gov.bc.ca](mailto:Geological.Survey@gov.bc.ca)



## Papers

### Paper 2022-01

Geological Fieldwork 2021, a summary of field activities and current research. British Columbia Ministry of Energy, Mines and Low Carbon Innovation, British Columbia Geological Survey Paper 2022-01, 141 p.

Wildgust, N., Cui, Y., Clarke, G., and Hickin, A.S., 2022. British Columbia Geological Survey annual program review 2021-2022. In: Geological Fieldwork 2021, Ministry of Energy, Mines and Low Carbon Innovation, British Columbia Geological Survey Paper 2022-01, pp. 1-15.

Schiarizza, P., Orchard, M.J., and Friedman, R.M., 2022. Conodonts and detrital zircons from Triassic and Jurassic rocks above the Salmon River unconformity, Thompson Plateau, south-central British Columbia. In: Geological Fieldwork 2021, British Columbia Ministry of Energy, Mines and Low Carbon Innovation, British Columbia Geological Survey Paper 2022-01, pp. 17-30.

Ootes, L., Ferri, F., Milidragovic, D., and Wall, C., 2022. The age and provenance of the Lay Range assemblage provides an indirect record of basement to north-central Quesnellia, British Columbia. In: Geological Fieldwork 2021, British Columbia Ministry of Energy, Mines and Low Carbon Innovation, British Columbia Geological Survey Paper 2022-01, pp. 31-44.

Van Wagoner, N., and Ootes, L., 2022. Geology and geochemistry of the Kamloops Group (Eocene) in its type area, Kamloops, British Columbia. In: Geological Fieldwork 2021, British Columbia Ministry of Energy, Mines and Low Carbon Innovation, British Columbia Geological Survey Paper 2022-01, pp. 45-62.

Hunter, R.C., Sebert, C.F.B., Friedman, R., and Wall, C., 2022. Revised stratigraphy and geochronology of the Hazelton Group, host rocks for volcanogenic mineralization in the Kitsault River area, northwest British Columbia. In: Geological Fieldwork 2021, British Columbia Ministry of Energy, Mines and Low Carbon Innovation, British Columbia Geological Survey Paper 2022-01, pp. 63-81.

Stanley, B., and Nelson, J., 2022. Revised stratigraphy of the Stuhini and Hazelton groups and LA-ICP MS zircon geochronology of the Scottie gold mine area, northwestern British Columbia. In: Geological Fieldwork 2021, British Columbia Ministry of Energy, Mines and Low Carbon Innovation, British Columbia Geological Survey Paper 2022-01, pp. 83-102.

Spence, D.W., Crawford, H., Scoates, J.S., Nott, J.A., Nixon, G.T., and Milidragovic, D., 2022. Mapping ultramafic cumulates at the Tulameen ultramafic-mafic Alaskan-type intrusion, south-central British Columbia, aided by remotely piloted aircraft system photogrammetry. In: Geological Fieldwork 2021, British Columbia Ministry of Energy, Mines and Low Carbon Innovation, British Columbia Geological Survey Paper 2022-01, pp. 103-122.

Rukhlov, A.S., Mashyanov, N.R., Pitirimov, P.V., Hickin, A.S., Golovetsky, M., and Coats, B., 2022. Gaseous elemental mercury (GEM) response from sediment-covered, volcanogenic massive sulphide mineralization on southern Vancouver Island. In: Geological Fieldwork 2021, British Columbia Ministry of Energy, Mines and Low Carbon Innovation, British Columbia Geological Survey Paper 2022-01, pp. 123-135.

Appendix: British Columbia Geological Survey Publications 2021, including peer-reviewed external papers co-authored by BCGS staff, pp. 137-141.

## **Geoscience Map**

van Straaten, B.I., Logan, J.M., Nelson, J.L., Moynihan, D.P., Diakow, L.J., Gibson, R., Bichlmaier, S.J., Wearmouth, C.D., Friedman, R.M., Golding, M.L., Miller, E.A., and Poulton, T.P., 2022. Bedrock geology of the Dease Lake area. British Columbia Ministry of Energy, Mines and Low Carbon Innovation, British Columbia Geological Survey, Geoscience Map 2022-01, 1:100,000 scale.

## **Open Files**

OF 2019-09

Angen, J.J., Hart, C.J.R., Nelson, J., and Rahimi, M., 2022. Geology and mineral potential of the western Skeena arch: Evolution of an arc-transverse structural corridor, west-central British Columbia. British Columbia Ministry of Energy, Mines and Low Carbon Innovation, British Columbia Geological Survey Open File 2019-09, Geoscience BC Report 2022-09, MDRU Publication 458, 47 p.

OF 2022-01

Clarke, G., Northcote, B., Corcoran, N.L., and Hancock, K., 2022. Mines, mine development, selected proposed mines, and selected exploration projects in British Columbia, 2021. British Columbia Ministry of Energy, Mines and Low Carbon Innovation, British Columbia Geological Survey Open File 2022-01.

OF 2022-02

Mihalynuk, M.G., Milidragovic, D., Tsekhmistrenko, M., and Zagorevski, A., 2022. Turtle Lake area geology (NTS 104M/16). British Columbia Ministry of Energy, Mines and Low Carbon Innovation, British Columbia Geological Survey Open File 2022-02, Geological Survey of Canada Open File 8757, 1:50,000 scale.

OF 2022-03

Schiarizza, P., 2022. Bedrock geology, Stump Lake-Salmon River, parts of NTS 82L/05 and 92/I/08. British Columbia Ministry of Energy, Mines and Low Carbon Innovation, British Columbia Geological Survey Open File 2022-03, 1:50,000 scale.

## **GeoFiles**

GF 2020-11 (updated)

Lefebvre, D.V., and Jones, L.D., (compilers) 2022. British Columbia Geological Survey mineral deposit profiles, 1995 to 2012; updated with new profiles for VMS, porphyry, and nickel deposits. British Columbia Ministry of Energy, Mines and Low Carbon Innovation, British Columbia Geological Survey GeoFile 2020-11, 635 p.

GF 2022-01

Clarke, G., Northcote, B., Corcoran, N.L., and Hancock, K., 2022. Exploration and mining in British Columbia, 2021. British Columbia Ministry of Energy, Mines and Low Carbon Innovation, British Columbia Geological Survey GeoFile 2021-01 (poster).

GF 2022-02

Clarke, G., 2022. Exploration and mining highlights, Northwest Region, 2021. British Columbia Ministry of Energy, Mines and Low Carbon Innovation, British Columbia Geological Survey GeoFile 2022-02 (poster).

GF 2022-03

Corcoran, N.L., 2022. Exploration and mining highlights, North Central and Northeast regions, 2021. British Columbia Ministry of Energy, Mines and Low Carbon Innovation, British Columbia Geological Survey GeoFile 2022-03 (poster).

GF 2022-04

Northcote, B., 2022. Exploration and mining highlights, Southwest and South Central regions, 2021. British Columbia Ministry of Energy, Mines and Low Carbon Innovation, British Columbia Geological Survey GeoFile 2022-04 (poster).

GF 2022-05

Hancock, K., 2022. Exploration and mining highlights, Southeast Region, 2021. British Columbia Ministry of Energy, Mines and Low Carbon Innovation, British Columbia Geological Survey GeoFile 2022-05 (poster).

GF 2022-06

Norris, J., and Wallace, B., 2022. Assessment report summary: Expenditures and activities 2020. British Columbia Ministry of Energy, Mines and Low Carbon Innovation, British Columbia Geological Survey GeoFile 2022-06 (poster).

GF 2022-07

Rukhlov, A.S., Mashyanov, N.R., Pitirimov, P.V., Hickin, A.S., Golovetsky, M., and Coats, B., 2022. Real-time air mercury guide to discovery. British Columbia Ministry of Energy, Mines and Low Carbon Innovation, British Columbia Geological Survey GeoFile 2022-07 (poster).

GF 2022-08

Stanley, B., Nelson, J.L., and Friedman, R., 2022. LA-ICP-MS U-Pb data files, detrital zircon geochronology, and geochemistry of the Stuhini and Hazelton groups, Scottie gold mine area, northwestern British Columbia. British Columbia Ministry of Energy, Mines and Low Carbon Innovation, British Columbia Geological Survey GeoFile 2022-08, 5 p.

GF 2022-09

Jones, G., Ootes, L., Luo, Y., Stern, R., Vezinet, A., and Pearson, D.G., 2022. In situ zircon U-Pb, Lu-Hf,  $\delta^{18}\text{O}$ , and trace elements from intrusive units in northern Hagem batholith, Quesnel terrane, north-central British Columbia. British Columbia Ministry of Energy, Mines and Low Carbon Innovation, British Columbia Geological Survey GeoFile 2022-09, 19 p.

GF 2022-10

Lett, R.E., Friske, P.W.B., and McClenaghan, M.B., 2022. Heavy mineral and geochemical data from detailed stream-sediment, stream-water, and moss-mat sampling in northwestern British Columbia. British Columbia Ministry of Energy, Mines and Low Carbon Innovation, British Columbia Geological Survey GeoFile 2022-10, 7 p.

GF 2022-11

Northcote, B., 2022. Volcanogenic massive sulphide (VMS) deposits in British Columbia: A review. British Columbia Ministry of Energy, Mines and Low Carbon Innovation, British Columbia Geological Survey GeoFile 2022-11, 30 p.

GF 2022-12

van Straaten, B.I., Logan, J.M., Hunter, R.C., Nelson, J.L., and Miller, E.A., 2022. Igneous lithogeochemistry data for the Dease Lake, Kitsault River, Galore Creek, Telegraph Creek, Foremore, and other areas in northwestern British Columbia. British Columbia Ministry of Energy, Mines and Low Carbon Innovation, British Columbia Geological Survey GeoFile 2022-12, 14 p.

GF 2022-13

Hunter, R.C., Sebert, C.F.B., Friedman, R., and Wall, C., 2022. Geochronologic data from the Kitsault River area, northwest British Columbia. Ministry of Energy, Mines and Low Carbon Innovation, British Columbia Geological Survey GeoFile 2022-13, 4 p.

GF 2022-14

Van der Vlugt, J., Rukhlov, A.S., and van Straaten, B.I., 2022. Lithogeochemical re-analysis of British Columbia Geological Survey archived rock samples from northwestern British Columbia. British Columbia Ministry of Energy, Mines and Low Carbon Innovation, British Columbia Geological Survey GeoFile 2022-14, 15 p.

## **Information Circulars**

IC 2022-01

Provincial Overview of Exploration and Mining in British Columbia, 2021. British Columbia Ministry of Energy, Mines and Low Carbon Innovation, British Columbia Geological Survey, Information Circular 2022-01, 129 p.

Clarke, G., Northcote, B., Corcoran, N.L., and Hancock, K., 2022. Exploration and Mining in British Columbia, 2021: A summary. In: Provincial Overview of Exploration and Mining in British Columbia, 2021. British Columbia Ministry of Energy, Mines and Low Carbon Innovation, British Columbia Geological Survey, Information Circular 2022-01, pp. 1-42.

Clarke, G., 2022. Exploration and mining in the Northwest Region, British Columbia. In: Provincial Overview of Exploration and Mining in British Columbia, 2021. British Columbia Ministry of Energy, Mines and Low Carbon Innovation, British Columbia Geological Survey, Information Circular 2022-01, pp. 43-65.

Corcoran, N.L., 2022. Exploration and mining in the North Central and Northeast regions, British Columbia. In: Provincial Overview of Exploration and Mining in British Columbia, 2021. British Columbia Ministry of Energy, Mines and Low Carbon Innovation, British Columbia Geological Survey, Information Circular 2022-01, pp. 67-83.

Northcote, B., 2022. Exploration and mining in the South Central Region, British Columbia. In: Provincial Overview of Exploration and Mining in British Columbia, 2021. British Columbia Ministry of Energy, Mines and Low Carbon Innovation, British Columbia Geological Survey, Information Circular 2022-01, pp. 85-104.

Hancock, K., 2022. Exploration and mining in the Southeast Region, British Columbia. In: Provincial Overview of Exploration and Mining in British Columbia, 2021. British Columbia Ministry of Energy, Mines and Low Carbon Innovation, British Columbia Geological Survey, Information Circular 2022-01, pp. 105-116.

Northcote, B., 2022. Exploration and mining in the Southwest Region, British Columbia. In: Provincial Overview of Exploration and Mining in British Columbia, 2021. British Columbia Ministry of Energy, Mines and Low Carbon Innovation, British Columbia Geological Survey, Information Circular 2022-01, pp. 117-129.

#### IC 2022-02

British Columbia Geological Survey, 2022. British Columbia Geological Survey. British Columbia Ministry of Energy, Mines and Low Carbon Innovation, British Columbia Geological Survey, Information Circular 2022-02, 14 p. (brochure)

#### IC 2022-03

British Columbia Geological Survey, 2022. Mineral Development Office. British Columbia Ministry of Energy, Mines and Low Carbon Innovation, British Columbia Geological Survey, Information Circular 2022-03, 4 p. (brochure)

#### IC 2022-04

British Columbia Geological Survey, 2022. Online databases at the British Columbia Geological Survey. British Columbia Ministry of Energy, Mines and Low Carbon Innovation, British Columbia Geological Survey, Information Circular 2020-04, 14 p. (brochure)

#### IC 2022-05

British Columbia Geological Survey, 2022. The Golden Triangle of northwestern British Columbia. British Columbia Ministry of Energy, Mines and Low Carbon Innovation, British Columbia Geological Survey, Information Circular 2022-05, 6 p. (brochure)

### **Contributions to partner publications**

Paradis, S., Simandl, G.J., Drage, N., D'Souza, R.J., Kontak, D.J., and Waller, Z., 2022. Carbonate-hosted deposits (Mississippi Valley-type, magnesite, and REE-F-Ba) of the southeastern Canadian Cordillera: A review and isotopic data comparison. In: Peter, J.M., and Gadd, M.G., (Eds.), Targeted Geoscience Initiative 5: Volcanic- and Sediment-Hosted Massive Sulphide Deposit Genesis and Ore Systems. Geological Survey of Canada Bulletin 617, pp. 39-87. <<https://doi.org/10.4095/327995>>

Paradis, S., Jackson, S.E., Petts, D., Simandl, G.J., D'Souza, R.J., and Hamilton, T., 2022. Distribution of trace elements in pyrite from carbonate-hosted sulfide deposits of southern British Columbia, Canada. In: Peter, J.M., and Gadd, M.G., (Eds.), Targeted Geoscience Initiative 5: Volcanic- and Sediment-Hosted Massive Sulphide Deposit Genesis and Ore Systems. Geological Survey of Canada Bulletin 617, pp. 129-163. <<https://doi.org/10.4095/328002>>

Simandl, G.J., D'Souza, R.J., Paradis, S., and Spence, J., 2022. Rare-earth content of carbonate minerals in sediment-hosted Pb-Zn deposits, southern Canadian Rocky Mountains. In: Peter, J.M., and Gadd, M.G., (Eds.), Targeted Geoscience Initiative 5: Volcanic- and Sediment-Hosted Massive Sulphide Deposit Genesis and Ore Systems. Geological Survey of Canada Bulletin 617, pp. 165-201. <<https://doi.org/10.4095/328001>>

### **External peer-reviewed journal and volume publications (access may be limited by publisher)**

Araoka, D., Simandl, G.J., Suzanne Paradis, S., Yoshimura, T., Hoshino, M., and Kon, Y., 2022. Formation of the Rock Canyon Creek carbonate-hosted REE-F-Ba deposit, British Columbia, Canada: Constraints from Mg-Sr isotopes of dolomite, calcite, and fluorite. *Journal of Geochemical Exploration*, 240, 107045. <<https://doi.org/10.1016/j.gexplo.2022.107045>>

Cerpa, N., Sigloch, K., Garel, F., Heuret, A., Rhodri Davies, D., and Mihalyuk, M.G., 2022. The effect of a weak asthenospheric layer on surface kinematics, subduction dynamics and slab morphology in the lower mantle. *Journal of Geophysical Research: Solid Earth*. <<https://doi.org/10.1029/2022JB024494>>

Jones, C.L., Orovan, E.A., Meffre, S., Thompson, J., Belousova, E.A., Cracknell, M.J., Everard, J., Bottrill, R., Bodorkos, S., and Cooke, D.R., 2022. Zircon O and Lu-Hf isotope evidence of mantle and supracrustal origins of Tasmanian Devonian granites. *Gondwana Research*, 110. <<https://doi.org/10.1016/j.gr.2022.06.004>>

Nelson, J.L., van Straaten, B., and Friedman, R., 2022. Latest Triassic-Early Jurassic Stikine-Yukon-Tanana terrane collision and the onset of accretion in the Canadian Cordillera: Insights from Hazelton Group detrital zircon provenance and arc-back-arc configuration. *Geosphere*, 18. <<https://doi.org/10.1130/GES02444.1>>

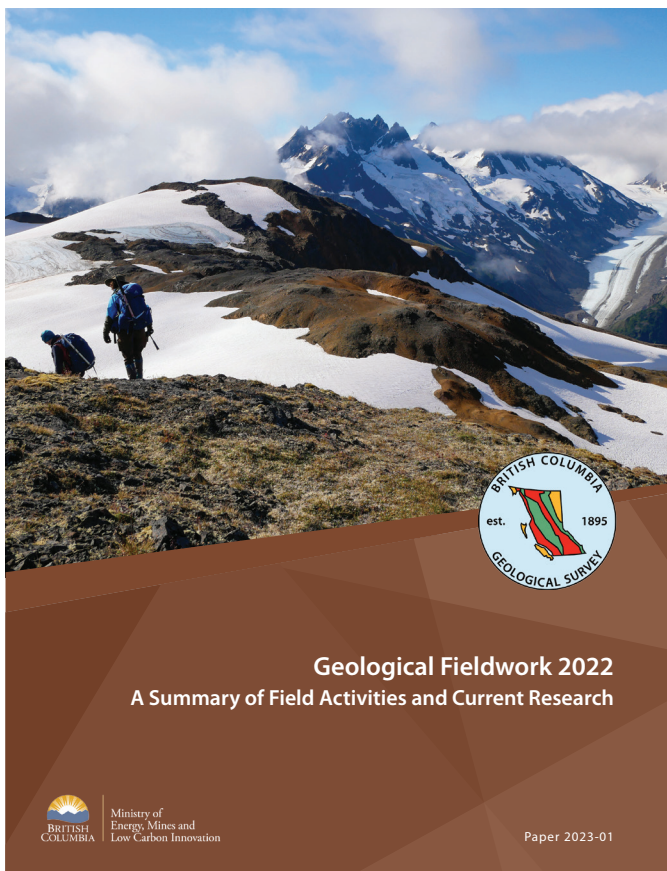
Ootes, L., Milidragovic, D., Friedman, R., Wall, C., Cordey, F., Luo, Y., Jones, G., Pearson, D.G., and Bergen, A., 2022. A juvenile Paleozoic ocean floor origin for eastern Stikinia, Canadian Cordillera. *Geosphere*, 18. <<https://doi.org/10.1130/GES02459.1>>

Plouffe, A., Kjarsgaard, I.M., Ferbey, T., Wilton, D.H.C., Petts, D.C., Percival, J.B., Kobylinski, C.H., and R. McNeil, R., 2022. Detecting buried porphyry Cu mineralization in a glaciated landscape: A case study from the Gibraltar Cu-Mo deposit, British Columbia, Canada. *Economic Geology*, 117, 777-799. <<https://doi.org/10.5382/econgeo.4891>>

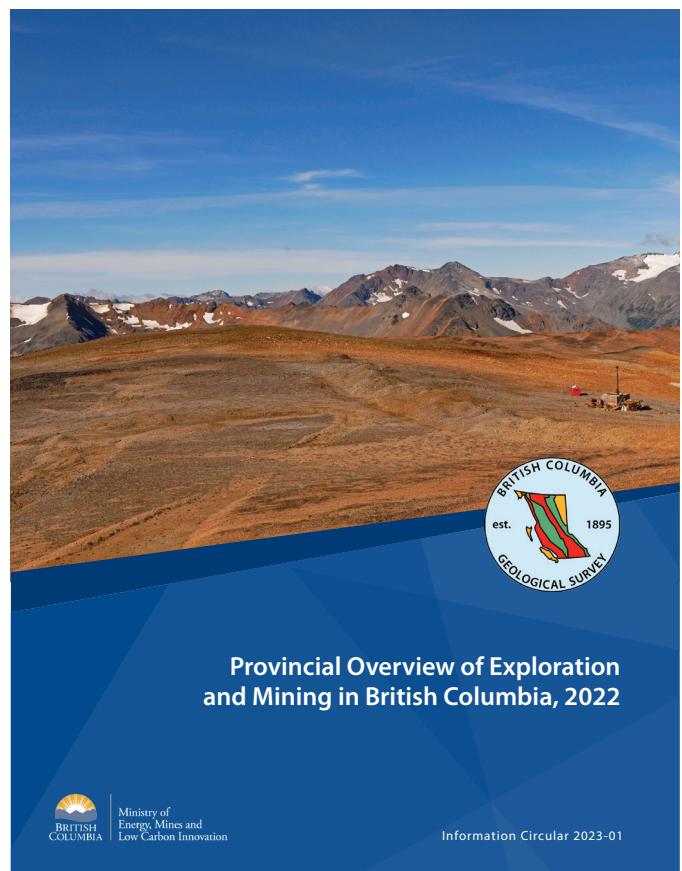
Simandl, G.J., and Paradis, S., 2022. Vanadium as a critical material: economic geology with emphasis on market and the main deposit types. *Applied Earth Science*. <<https://doi.org/10.1080/25726838.2022.2102883>>

---

Each year, the British Columbia Geological Survey publishes *Geological Fieldwork*, a *Summary of Fieldwork and Current Research* (this volume), and the *Provincial Overview of Mining and Exploration in British Columbia*. All British Columbia Geological Survey publications can be downloaded, at no cost, from [www.BCGeologicalSurvey.ca](http://www.BCGeologicalSurvey.ca)



Geological Fieldwork volume, British Columbia Geological Survey Paper 2023-01



Provincial Overview of Mining and Exploration in British Columbia volume, Information Circular 2023-01

